DESIGN AND OPERATION OF MULTISTAGE FLASH (MSF) DESALINATION: ADVANCED CONTROL STRATEGIES AND IMPACT OF FOULING

Design operation and control of multistage flash desalination processes: dynamic modelling of fouling, effect of non-condensable gases on venting system design and implementation of GMC and fuzzy control

Salih Makhlouf Musbah ALSADAIE

Submitted for the Degree of

Doctor of Philosophy

Faculty of Engineering and Informatics

School of Engineering

University of Bradford

2017

ABSTRACT

Salih Makhlouf Musbah ALSADAIE

Design operation and control of multistage flash desalination processes: dynamic modelling of fouling, effect of non-condensable gases on venting system design and implementation of GMC and fuzzy control.

Keyword: MSF, dynamic model, non-condensable gases, fouling model, calcium carbonate, magnesium hydroxide, GMC control, hybrid fuzzy-GMC, gPROMS.

The rapid increase in the demand on fresh water due the increase in the world population and scarcity of natural water puts more stress on the desalination industrial sector to install more desalination plants around the world. Among these desalination plants, multistage flash desalination process (MSF) is considered to be the most reliable technique of producing potable water from saline water. In recent years, however, the MSF process is confronting many problems to cut off the cost and increase its performance. Among these problems are the non-condensable gases (NCGs) and the accumulation of fouling which they work as heat insulation materials. As a result, the MSF pumps and the heat transfer equipment are overdesigned and consequently increase the capital cost and decrease the performance of the plants. Moreover, improved process control is a cost effective approach to energy conservation and increased process profitability. Thus, this study is motivated by the real absence of detailed kinetic fouling model and implementation of advance process control (APC). To accomplish the above tasks, commercial modelling tools can be utilized to model and simulate MSF process taking into account the NCGs and fouling effect, and optimum control strategy.

In this research, gPROMS (**g**eneral **PRO**cess **M**odeling **S**ystem) model builder has been used to develop the MSF process model. First, a dynamic mathematical model of MSF is developed based on the basic laws of mass balance, energy balance and heat transfer. Physical and thermodynamic properties of brine, distillate and water vapour are included to support the model. The model simulation results are validated against actual plant data published in the literature and good agreement with these data is obtained.

Second, the design of venting system in MSF plant and the effect of NCGs on the overall heat transfer coefficient (OHTC) are studied. The release rate of NCGs is studied using Henry's law and the locations of venting points are optimised. The results reveal that high concentration of NCGs heavily affects the OHTC.

Furthermore, advance control strategy namely: generic model control (GMC) is designed and introduced to the MSF process to control and track the set points of the two most important variables in the MSF plant; namely the Top Brine Temperature (TBT) which is the output temperature of the brine heater and the Brine Level (BL) in the last stage. The results are compared to conventional Proportional Integral Derivative Controller (PID) and show that GMC controller provides better performance over conventional PID controller to handle a nonlinear system. In addition, a new control strategy called hybrid Fuzzy-GMC is developed and implemented to control the same aforementioned loops. Its results reveal that the new control outperforms the pure GMC in some areas.

Finally, a dynamic fouling model is developed and incorporated into the MSF dynamic process model to predict fouling at high temperature and high velocity. The proposed dynamic model considers the attachment and removal mechanisms of calcium carbonate and magnesium hydroxide with more relaxation of the assumptions. Since the MSF plant stages work as a series of heat exchangers, there is a continuous change of temperature, heat flux and salinity of the seawater. The proposed model predicts the behaviour of fouling based on the physical and thermal conditions of every single stage of the plant.

Acknowledgement

Dedications

I would like to dedicate this thesis to all my teachers, from those at my first primary school in 1980s to the chemical engineering department staff at Bradford University

Table of Contents

List of Figures

List of Tables

Nomenclature

A_D	Distillate tray area (m^2)
A_{DH}	Debye-Huckel constant
A_h	Heat transfer surface area of the brine heater (m^2)
A_{pipe}	Cross section area of the distillate discharge pipe (m^2)
A_P	Stage area (m^2)
As	Heat transfer surface area of a stage (m^2)
B_{out}	Brine outlet flow rate from a stage (kg/s)
BPE	Boiling point elevation (^{o}C)
B_{vel}	Brine velocity (m/s)
C_1	Correction factor for the number of tubes in vertical direction
C_2	Correction factor for the NCGs
C_b	Concentration of ions in the fluid (kg/m^3)
C_{BHout}	Mass fraction of NCGs in brine leaving brine heater (ppm)
C_{Be}	Equilibrium mass fraction of NCGs in the brine (ppm)
C_{Bin}	Mass fraction of NCGs in the brine entering a stage (ppm)
C_{Bout}	Mass fraction of NCGs in the brine leaving a stage (ppm)
C_{Fin}	Mass fraction of NCGs entering the HRJ (ppm)
C_{Fout}	Mass fraction of NCGs in the make-up stream (ppm)
C_i	Concentration of ions at the solid-liquid surface (kg/m^3)
C_d	Coefficient discharge of the brine
C_c	Coefficient discharge of the distillate
C_{MOLEQ}	Mole fraction of NCGs in the brine
C_{NCGS}	Mass fraction of NCGs in seawater
C_p	Specific heat at constant pressure (kJ/kg ^{o}C)

Nomenclature

C_{rec}	Mass fraction of NCGs of the recycle brine (ppm)
C_R	Mass fraction of NCGs in the recycle brine
C_s	Saturation concentration (kg/m^3)
C_{pw}	Specific heat of seawater at constant pressure (kJ/kg ^{o}C)
C_{VD}	Total condensate flow in a stage (kg/s)
d_i	Inside diameter of tube (m)
d_o	Outside diameter of tube (m)
d_P	Crystal size (m)
D	Diffusion coefficient (m^2/s)
D_h	Hydraulic diameter (m)
D_{out}	Distillate flow rate to a stage (kg/s)
D_{total}	Total distillate product flow rate (kg/s)
E_a	Reaction activation energy (kJ/mole)
f	Friction factor
FF	Fouling factor (m^2 ^{o}C/kW)
F_{last}	Sea water makeup entering the last stage (kg/s)
g	Gravity acceleration (m/s^2)
h_b	Height of the brine (m)
h_i	The brine side heat transfer coefficient (kW/m^2 ^{o}C)
h_o	The vapour side heat transfer coefficient (kW/m^2 ^{o}C)
H_{BHin}	Enthalpy of the brine entering the brine heater (kJ/kg)
H_{BHout}	Enthalpy of the brine leaving the brine heater (kJ/kg)
H_{Bin}	Enthalpy of flashing brine entering a stage (kJ/kg)
H_{Bout}	Enthalpy of flashing brine leaving a stage (kJ/kg)
H_{Dout}	Enthalpy of distillate leaving a stage (kJ/kg)
He	Henry's constant

H_g	Height of a stage gate (m)
H_{NCGs}	Enthalpy of NCGs leaving the flashing brine in a stage (kJ/kg)
H_{NCGsin}	Enthalpy of NCGs entering from previous stage (kJ/kg)
$H_{NCGsout}$	Enthalpy of NCGs leaving in a stage (kJ/kg)
H_{VB}	Enthalpy of vapour below demister in a stage (kJ/kg)
H_{VD}	Enthalpy of vapour released from the distillate tray (kJ/kg)
H_{Vin}	Enthalpy of vapour entering from previous stage (kJ/kg)
H_{Vout}	Enthalpy of vapour leaving a stage (kJ/kg)
I	Ionic strength (mole/kg)
i	Inner
k_b	Brine thermal conductivity (kW/m ^{o}C
k_D	Pre-exponent coefficient (m^4/s.kg)
k_L	Liquid condensate thermal conductivity (kW/m ^{o}C
k_r	Reaction rate constant (m^4/s.kg)
k'_r	Reaction rate coefficient (for magnesium kg/s.m^2, for calcium m^4/kg.s^2)
k_{rem}	Removal rate constant (m^3/s.kg)
k'_{r0}	Pre-exponential constant (for magnesium kg/s.m^2, for calcium m^4/kg.s^2)
k_{sp}	Solubility product (mole^2/kg^2)
k_t	Conductivity of the tube material (kW/m^o.K)
k_v	Venting line orifice discharge coefficient
K_w	Dissociation constant for water (mole/kg)
K	Proportional constant
K_1	First dissociation constant (mole/kg)
K_2	Second dissociation constant (mole/kg)

L_B	Height of the brine (m)
L_D	Height of the distillate (m)
LMTD	Logarithmic mean different temperature of the tube condenser (°C)
$LMTD_h$	Logarithmic mean different temperature of the brine heater (°C)
L_s	Height of a stage (m)
L_t	Tube length of a stage (m)
m_d	Deposit mass rate (kg/s.m^2)
m_f	Net deposit mass rate (kg/s.m^2)
m_i	Molality of ion i (mole/kg)
m_r	Removal mass rate (kg/s.m^2)
M_{BH}	Holdup of the brine in the brine heater (kg)
M_V	Holdup of vapour in a stage (kg)
MV	Manipulated variable
M_W	Holdup of flashing brine in a stage (kg)
MW	Molecular weight (kg/kmole)
n	Reaction order
NEA	Non-equilibrium allowance (°C)
N	Number of tubes in vertical direction in the tube bundle
N_f	Number of defects in the fouling layer
N_t	Number of tubes in the tube bundle
NCGs	Non-condensable gases
o	Outer
OHTC	Overall heat transfer coefficient (kW/m^2 °C)
P	Pressure in a stage (Pa)
P_f	Intercrystalline adhesion force (N)

PR	Performance ratio (kg Distillate/kg steam)
PV	Process variable
Q	Heat transferred to cooling brine in a stage (kW)
Q_h	Heat transferred to heating brine in the brine heater (kW)
R	Universal gas constant (J/mole. K)
Re	Reynolds number
Rec	Recycle brine flow rate (kg/s)
$R_{f,i}$	Internal fouling resistance (m^2 ^{o}C/kW)
$R_{f,o}$	External fouling resistance (m^2 ^{o}C/kW)
S	Salt concentration (g/l)
Sc	Schmidt number
Sh	Sherwood number
TA	Total alkaline (mole/kg)
TBT	Top brine temperature (^{o}C)
T_{Bin}	Temperature of flashing brine entering a stage (^{o}C)
T_{Bout}	Temperature of flashing brine leaving a stage (^{o}C)
TC	Total carbon dioxide (mole/kg)
T_D	Temperature of distillate tray (^{o}C)
T_{Dout}	Temperature of distillate leaving a stage (^{o}C)
T_{F1}	Temperature of cooling brine entering the brine heater (^{o}C)
T_{Fin}	Temperature of cooling brine entering a stage (^{o}C)
T_{Fout}	Temperature of cooling brine leaving a stage (^{o}C)
T_s	Surface temperature inside the tubes (^{o}C)
T_{VB}	Temperature of flashed vapour below demister (^{o}C)
T_V	Temperature of flashed vapour in the vapour space (^{o}C)
T_{steam}	Steam temperature (^{o}C)

Tw	Temperature of external tube wall (°C)
U_h	Overall heat transfer coefficient in the brine heater (kW/m^2 °C)
U_o	Overall heat transfer coefficient in a stage (kW/m^2 °C)
V	Friction velocity (m/s)
V_b	Brine volume (m^3)
V_B	Vapour release flow rate from brine in a stage (kg/s)
V_D	Vapour release flow rate from the distillate tray (kg/s)
V_{in}	Vapour flow rate entering a stage (kg/s)
V_{out}	Vapour flow rate leaving a stage (next stage or vent) (kg/s)
V_{tube}	Volume of the cooling water inside the tube bundle (m^3)
V_v	Vapour volume (m^3)
v_{vel}	Vapour velocity (m/s)
W_{cw}	Rejected cooling brine to the sea (kg/s)
W_{HBout}	Brine mass flow rate leaving brine heater (kg/s)
W_{HBin}	Brine mass flow rate entering brine heater (kg/s)
W_{Rin}	Cooling brine flow entering a stage in the HRS (kg/s)
W_{Rout}	Cooling brine flow leaving a stage in the HRS (kg/s)
W_{Fin}	Cooling seawater flow entering a stage in the HRJ (kg/s)
W_{Fout}	Cooling seawater flow leaving a stage in the HRJ (kg/s)
W_{st}	Width of a stage (m)
W_{steam}	Steam flow rate (kg/s)
x_f	Layer thickness (m)
X_{Bin}	Salt concentration in the brine entering a stage (ppm)
X_{HBout}	Salt concentration in the brine leaving brine heater (ppm)
X_{Bout}	Salt concentration in the brine leaving a stage (ppm)
X_{rec}	Salt concentration of the recycle brine (ppm)

X_{Rout}	Salt concentration in the cooling brine in the HRS (ppm)
X_{Fout}	Salt concentration in the cooling brine in the HRJ (ppm)
Y_{in}	Mass fraction of NCGs in the vapour entering a stage (wt. %)
Y_{mole}	Mole fraction of NCGs in the vapour space in a stage (wt. %)
Y_{out}	Mass fraction of NCGs in the vapour leaving a stage (wt. %)
z_i	Charge of the ion i

Greek letters

ΔT_B	Brine temperature difference (°C)
ΔT_D	Distillate temperature difference (°C)
ΔT_{Dem}	Temperature drop through demister (°C)
ΔP	Pressure difference (Pa)
ρ_B	Brine density (kg/m³)
ρ_L	Distillate density (kg/m³)
ρ_V	Vapour density (kg/m³)
β	Mass transfer coefficient (m/s)
γ	Activity coefficients.
γ	Efficiency of degassing process
λ	Latent heat of vapour in a stage (kJ/kg)
λ_{steam}	Latent heat of steam (kJ/kg)
λf	Conductivity of the fouling layer (kW/m.K)
λ_{solid}	Conductivity of the compact solid (kW/m.K)
λ_{water}	Conductivity of pore medium (kW/m.K)
μ_w	Viscosity of the fluid (N.s/m²)
ρ_f	Density of the fouling layer (kg/m³)

ρ_{solid}	Density of the compact solid of fouling layer (kg/m^3)
ρ_w	Density of the fluid (kg/m^3)
σ_f	Shear strength of the fouling layer (N/m^2)
δ	Linear expansion coefficient (1/K)
τ_f	Surface shear stress of the bulk flow (N/m^2)
ω	Porosity

CHAPTER ONE

Introduction

1.1. Introduction

"and we made every living thing of water"(Quran Kareem, Sorah al-Anbiya, Chapter 21, Verse 30)

Indeed, water is the most precious compound in the world and it is essential to humans and other lifeforms despite the fact that it provides no calories or organic nutrients. Although access to safe drinking water has improved over the last few decades in almost every part of the world, almost 780 million people still lack access to safe drinking water and around 36% of the world's population (2.5 billion people) lack access to improved sanitation Bennett (2013). However, with the rapid increase in the world's population and improved standards of living, some observers have estimated that by 2030, the global needs of water would be 6900 billion m^3 compared to 4500 billion m^3 required in 2009 (Addams et al., 2009). A United Nations report (UN, 2015) estimated that the world population is expected to reach 9.7 billion by 2050, thus the worldwide demand of fresh water will increase; putting a serious strain on the quantity of naturally available freshwater. With most of the accessible water around us being saline (97 percent of the world's water) and 2.5 percent is frozen (Fry and Martin, 2005), desalination technology has been recognized as one of the most sustainable water resource.

Desalination markets have grown significantly in the last few decades. Currently there are more than 16,000 desalination plants in operation worldwide producing around 74.8 million m^3/day. Between 40% and 50% of the world's desalinated water is produced in the Gulf countries (Bennett, 2013). Reverse osmosis (RO) and multi stage flash (MSF) processes account for more than 86% of the total installed desalination capacity (Energy, 2012). Due to the low cost of fossil fuels in Gulf region and North African countries, MSF is the preferred choice while in other parts of the world, where the fossil fuels cost is high, other desalination technologies such as RO are preferred.

Despite its higher cost compared to the RO, the MSF desalting method is by far the most robust technology and does not require intensive pre-treatment as in RO (AlTaee and Sharif, 2011). However, the MSF process is sensitive to increase in energy prices and nowadays is facing many challenges to reduce costs and improve the market shares (profitability).

Numerous researches have been conducted in the past decades on the improvement of the performance of MSF plants to produce desalted water at a lower cost. By utilizing many available commercial process modelling (and optimization) tools, most of these studies used mathematical models in design, operation and control of desalination process due to the fact that mathematical models are less expensive compared to experimental investigation. The benefit of designing a piece of equipment on a computer is that it can be tested before it is bought or constructed. As a result, significant development and progress have been achieved over the past few decades in cost reduction and increase the overall unit capacity. However, despite this considerable progress, it is believed that still more work can be realized through simulation, optimization and design improvement.

In this chapter, an overview of the water crisis, the need for desalination and also the types of desalination processes are presented. A description of the process and different configuration of the MSF plant will be introduced. The aspects of the main parameters affecting the performance of MSF process will be discussed as well. Finally, a definition of the project problem, a scope of the research and the aims and objectives are presented.

1.2 Water Crisis

The exponential growth in the world population and the scarcity of natural water resources has raised a major global challenge to overcome the water crisis. Moreover, the resources of natural fresh water are not distributed equally around the world. While the world as a whole may have sufficient water to support its residents, it is not well distributed and thus some countries are suffering water shortage. In addition, with the increase in the industrial development and introduction of powerful pumps, the ground water is already being depleted and the MAN MADE RIVER in Libya is a good example where 6 million cubic meters

per day of ground water is pumped from the south of the country to the north. Surface waters on the other hand are prone to pollution and are no longer being able to provide pure water and becomes a source of disease in some developing countries.

While the natural water resources remain constant across the world, global water consumption increased by over six times from 1900 to 1995, which is more than double the growth rate of the population (Bassett and Brinkman, 2000) and the United Nations expects the situation to become considerably worse over the next few years. At present, more than 20% of the world's population (1.2 billion people) live in areas of physical scarcity and a half billion people are approaching this situation. Moreover, around one quarter of the world's population (1.6 billion people) face economic water shortage where their countries lack the appropriate infrastructure to take water from available sources such as rivers and aquifers (UN, 2007). The united nation report (UN, 2007) continues to expect that almost 1.8 billion people will be living in countries with absolute water shortage and two thirds of the world's population could be living under water stressed conditions by 2025. Moreover, between 80% to 90% of all disease and around one third of all deaths in developing countries are related to the use of unhealthy water (Prüss-Üstün and Corvalán, 2006).

In the Middle East and North African countries (MENA region), the population was doubled between 1970 and 2001, increasing from 173.4 million people to 385.6 million people and is expected to reach 568 million by 2025. In contrast, the average amount of fresh water available per capita decreased from 3645 cubic meters per person per year to 1,640 cubic meters per person per year for the same period (Roudi-Fahimi et al., 2002). According to Hinrichsen et al. (1998), over 2.8 billion people in 48 countries will suffer from water shortage by 2025 compared to nearly half billion in 31 countries in 1995. Among these 48 countries, 40 are located in the Middle East and North Africa.

Among these countries, Libya is considered to be very arid country where the annual rainfall is very low with less than 5% of the country receiving more than 100 mm/y (Figure 1.1) (Wheida and Verhoeven, 2007). The average annual evaporation rates, in contrast, are generally much higher than the average annual

rainfall, increasing from the north to the south to be 1700 mm towards the east and 6000 mm in the oases in the south part of the country (Salem, 1992).
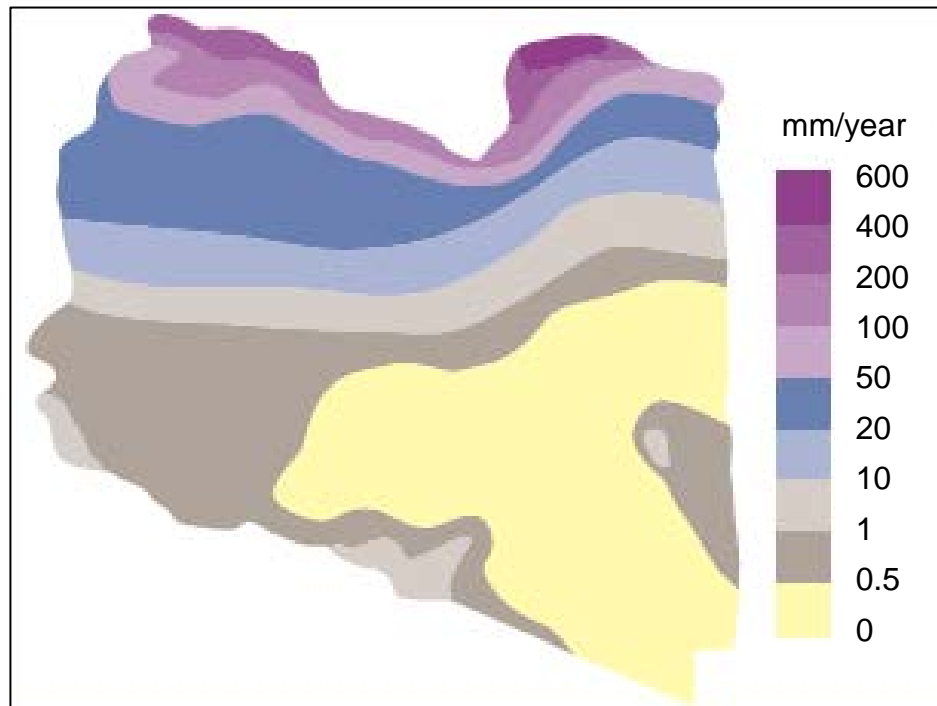
Figure 1.1: Annual average precipitation in Libya (Kuwairi, 2006).

The evaporation rates are considered to be the highest in the world due to the dry climate with temperatures exceeding 40°C in some parts of the country (Abufayed and El-Ghuel, 2001). Libya has a total surface area of 1,775,500 km^2 (Salem, 1992). More than ninety percent of the country is considered to be dry (Al-Hengari et al., 2007). Its water resources are very poor and depend only on rainfall in the coastal area and some ground resources in the south.

With the increase in water demand, serious effort has been made to counteract the country's water deficit problems through locating, developing and managing new resources. Among these efforts is transporting a large quantity of water from the heart of desert through huge project called the Man-Made River Project (MMRP) which is considered to be one of the world's largest water supply project. In this project, over 6 million m³ of water is transported daily from the country's southern regions; where huge quantities of fossil water are available with negligible population density, to the northern coast where it is urgently needed due to high concentrated of population (Salem, 1992). Although the estimated cost of water from MMRP is about US$ 0.28/m³ (Kuwairi, 2006), much less than

from other technologies, the ground water resource is non-renewable and depletion of the water level with time is expected due to over exploitation of groundwater resource to meet the irrigation demands. In fact, the country relies almost completely on its groundwater supply (98% of the whole water consumption) (Salem, 1992, Bremere et al., 2001). However, increasing the demand for freshwater as a result of population growth and improving standard of living cannot be satisfied by just mining groundwater.

Although it is considered as an expensive last possibility solution to provide fresh water for municipal domestic and industrial use, desalination technology is becoming increasingly affordable for the whole world and Libya in particular.

1.3 Need for Desalination

Notwithstanding 71% of the plant's surface is covered by water, the vast majority of water on the earth is too salty for human use. On Earth, about 97% of the planet's water is either salty or undrinkable. Over 2.5% of the rest 3% is frozen and found in Antarctica, the Arctic and glaciers and are not easily accessible for human use. Thus the only available water for humanity to use is around 0.5% of the Earth's water, which is found in lakes, rivers and aquifers (Figure 1.2) (Fry and Martin, 2005). However, the rapid reduction of the groundwater resources and the increasing pollution of the surface waters has forced mankind to search for other source of water to meet the increasing world demand for fresh water. With most of the accessible water around us being saline, it is essential to provide fresh water from seawater through desalination technology.

Desalination is a water treatment process that removes dissolved salts from saline water, thus producing freshwater from seawater or brackish water. According to World Health Organization (WHO) guidelines, the permissible limit of salinity in drinking water is 500 ppm and up to 1000 ppm for special cases. Most of the water available on earth has the salinity up to 10,000 ppm and seawater normally has salinity in the range of 35,000–45,000 ppm in the form of total dissolved salts (Tiwari et al., 2003).
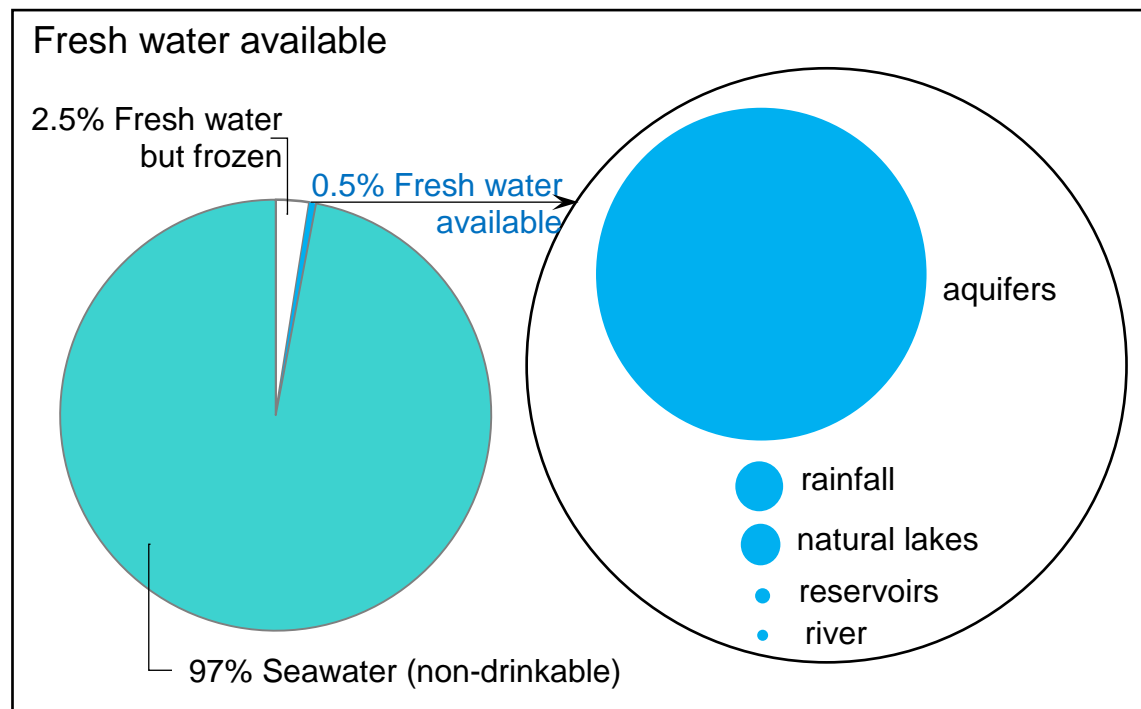
Figure 1.2: Distribution of global water on the planet's surface (Fry and Martin, 2005).

Under these conditions, desalination of seawater and brackish water has become the only available solution to rely on as a new resource of supply fresh water in the region where severe water shortages exist. Other alternative solutions of transporting water from different zones have proved to be more expensive, inadequate and less reliable (Al-bahou et al., 2007). More interestingly, 42 large cities out of 71 that do not have access to new fresh water resources are located along the coasts and around 39% of world population live at distance of less than 100 km from the sea, making the seawater desalination technique the only available option for some countries (Ghaffour et al., 2013). In addition, being independent of climatic conditions and rainfall, desalination technology has become more favourable than other resources. In fact, an adoption of this type of technique has resulted in an increase in the fresh water supply worldwide and bridge the safe drinking water gap.

Desalination markets have grown dramatically in the last few decades as many countries search for solutions to water scarcity caused by population growth and worldwide demand of freshwater. Currently there are more than 16,000 desalination plants in operation worldwide and the total global capacity of all plants is around 74.8 million cubic meters per day (Bennett, 2013). Countries in

Gulf region produce around 40% of the world's desalinated water and some of these countries rely on desalination for more than 90% of their potable water (Mabrouk, 2013). Among the MENA region countries, Libya has adopted the desalination technology since the early seventies and has grown markedly ever since making Libya the largest operator of desalination plants in North Africa and Mediterranean Sea and was ranked the sixth country in the world to use desalination as a resource of water (Kershman, 2001). However, Due to its dependent on the groundwater resource for satisfying its ever increasing demand of freshwater, Libya has registered the lowest contracted capacity during the period of 2001-2005 among all other countries which are in need of desalination despite the fact that the largest growth market is expected to be in the Mediterranean region (Elhassadi, 2008).

1.4 Desalination Technology

Desalination is a process of producing potable water from saline water or brackish water. In nature, desalination is natural process that plays an important role in the water life cycle. Rainwater falls to the ground and flows to the sea through rivers and water streams. During its journey to the sea or oceans, people use the water for different purpose before becoming increasingly salty as results of dissolving process of earth's minerals and other materials. A part of the water is evaporated through the sun's energy, leaving the salts behind and the resulting water vapour forms clouds that produce rain, thus continuing the cycle (Buros, 2000). Moreover, some water flows through the earth to ground. In this case, the earth works as a membrane and the result is ground fresh water. Desalination can be divided into two types; thermal and membrane separation.

Historically, the thermal method was the most ancient way of desalting brackish and salty water. One of the first mentioned methods was described by Aristotle in the fourth century B.C. when he described a method of seawater distillation (Tiwari et al., 2003). Although, the first commercial multi effect desalination plant with overall capacity of 75 m^3/day was installed in Egypt in 1912 (Fiorenza et al., 2003), the major step in the development of desalination was around 1940 during the World War II. Later by the end of 1960s, several commercial desalination plants were installed in various parts of the world and by the 1980s, desalination

technology was a fully commercial enterprise (Buros, 2000). In the preceding years, rapid development of the desalination technology has been observed and is to be continued in the near future. This dramatic increase is due to the reduction of energy requirements to produce fresh water. The energy consumed by best available desalination technology has been reduced from more than 20 kWh/m^3 during the year 1970 to less than 5 kWh/m^3 as shown in Figure 1.3 (Fiorenza et al., 2003). Fiorenza et al. (2003) attributed this reduction to the development of RO technology.
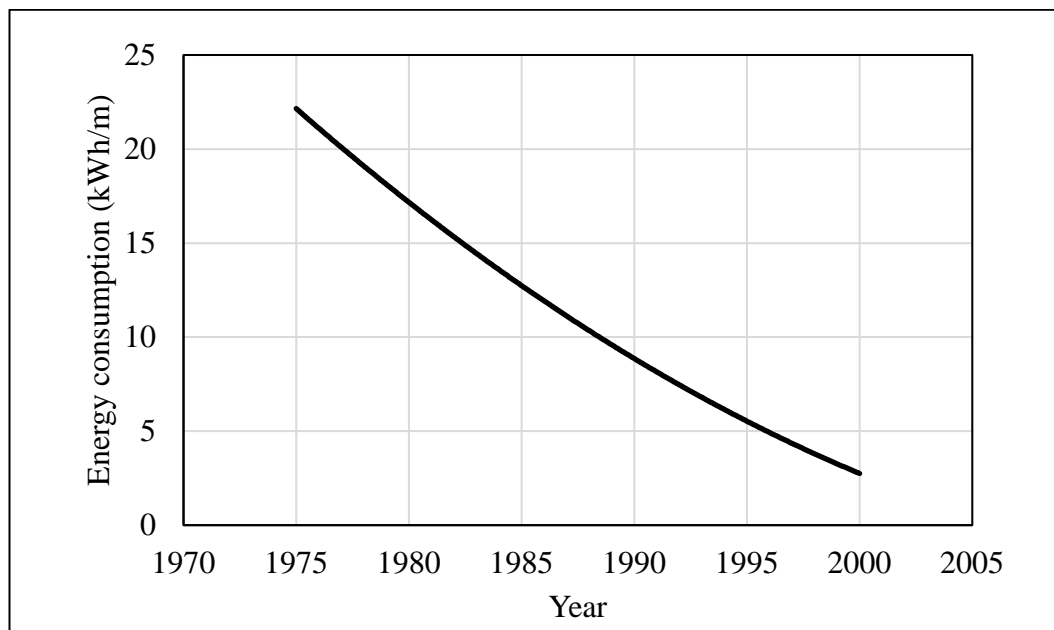
Figure 1.3: Energy required to desalt 1 m^3 water using the best available technology (Fiorenza et al., 2003).

This remarkable progress in cost reduction has been made through design improvement and developing less costly construction materials which in turn significantly reduce the energy requirements. Currently there are more than 16,000 desalination plants in operation worldwide producing around 74.8 million m^3/day in 2012 compared to 47.6 million m^3/day in 2007 (Bennett, 2013). About 38% of the total world capacity is produced in the MENA region, where desalination has become the most important source of water for drinking and agriculture, with Saudi Arabia being the largest desalinating country (Energy, 2012). It is to note that the market share of the desalination industry in the MENA region was more that 50% of the total world capacity (Al-Fulaij, 2011) when the thermal desalination was the main source of fresh water in the MENA region due

to low cost of fossil fuel (until 2005). However, this drop in the market share was not due to decrease in the MENA region's desalination capacity but instead due to the increase of the investment in membrane desalination in other parts of the world. Asia will become a fast growing market in the long run, due to its enormous population and economic growth leading to a water demand that cannot be fulfilled with conventional water sources. In Sep 2013, Prime Minister of Singapore (Lee Hsien Loong) opened Singapore's second and largest desalination plant which can supply about a 318,500 m³/day of fresh water to meet up to a quarter of the country's total water needs (Hyflux, 2013). Moreover, in Australia, a large membrane desalination plant was built with capacity of 444,000 m³/d and started on operation in 2012 (Bennett, 2013).

The growth of desalination capacity in the MENA region is expected to increase rapidly from 21 million m³/d in 2007 to nearly 110 million m³/d by 2030. Around 70% of this growth is expected to be in Saudi Arabia, the United Arab Emirates, Kuwait, Algeria and Libya (Energy, 2012).

1.4.1 Classification of Desalination Process

The commonly used industrial desalination processes can be classified broadly into two groups: (a) thermal processes (b) membrane processes. Although thermal process (mainly MSF) is the oldest and still dominating for large-scale production of freshwater, RO process has been continuously increasing its market share. RO desalination capacity reached 53% of worldwide desalination capacity in 2008 (Al-Karaghouli and Kazmerski, 2011), and in 2013, RO desalination represented 65 % of desalination plants capacity while MSF accounts for 22 % (Miller et al., 2015).

This continuous increase in the capacity of RO is contributed to the advancement of the RO membrane technology and design of high pressure centrifugal pumps efficiency. The new high productivity membrane elements consisting of higher surface area, enhanced permeability and denser membrane packing yield more quantity of fresh water per membrane element (Singh, 2008). The enhancement of membrane technologies is due to the fact that this technology is involved in different separation sciences rather than water desalination.

The cost of fresh water produced by membrane treatment has shown dramatic reduction trend over many years. This remarkable progress has been made mainly through two aspects, huge improvements in membrane material and incorporation of the energy recovery devices in RO systems (Greenleea et al., 2009) which significantly reduce the energy requirements. Khawaji et al. (2008) reported that the unit energy consumption for seawater desalination has been reduced to as low as 2 kWh/m^3 compared to 4 kWh/m^3 consumed in a thermal process such as Multi-stage flash distillation (MSF).

Although thermal desalination is more energy intensive and costly compared to membrane based desalination, it can better deal with high feed salinity water and delivers even higher permeate quality in terms of freshwater salinity (Fritzmann et al., 2007, Misdan et al., 2012). For example, desalination of seawater with salinity higher than 36000 ppm, the thermal desalination is the optimum choice (Ettouney et al., 2002). Another factor is the production capacity; while the thermal desalination is used mainly in medium and large capacity systems, membrane desalination is used by medium and small size systems (Karagiannis and Soldatos, 2008). Despite the several advantages of thermal desalination technology, there are other drawbacks rather than the high cost of the fuels such as the environmental impact of high temperature and salinity of the brine discharge. Table 1.1 summarises the advantages and disadvantages of thermal desalination technology.

1.4.1.1 Thermal Desalination

The fundamental concept of thermal desalination relies on phase change separation technique where saline water is heated to boiling point to produce water vapour. The freshwater is then formed through condensation of the water vapour (UNEP, 2001). As mentioned before, the low cost of fossil fuels in Gulf region and North African countries is the main reason of adopting the thermal desalination technology in these countries. The thermal technology represents 70% of the total capacity in the Gulf Cooperation Council (GCC) countries, while Reverse Osmosis presents only 30% (Sharif, 2016). In other countries, where the fossil fuels cost is high; other desalination technologies such as RO are preferred. Moreover, the features of coupling the thermal plants with power plants to

produce water and electricity is another reason for thermal process to hold strong position in water desalination market (Baig et al., 2011).

Table 1.1: Advantages and disadvantages of thermal desalination technology.

Advantages	Disadvantages
Very good water quality	High cost due large amount of energy.
High production capacity	High tendency of fouling and corrosion
Can better deal with high feed salinity water	High level of carbon dioxide emissions
High reliability performance and low degradation over time	Harmful impact to the marine ecology due to high temperature and salinity of the water discharge.
Ease of operation	

The most known types of thermal processes are multistage flash (MSF) and multiple effects (MED). Although, MSF has been the most frequently used technique in large scale commercial until the late 1980s, the MED process has been requested during the past few years by many clients (De Gunzbourg and Larger, 1999).

1.4.1.1.1 Multistage Flash Desalination (MSF)

Despite its higher cost compared to the RO and other thermal desalination technologies, the MSF desalting method is by far the most robust and reliable technology for the production of desalted water at large capacities due to enormous field experience that has been accumulating in process technology over the last 50 years. The MSF process represents more than 93% of the thermal process production (Garcia-Rodriguez, 2003) and 26% of the total world desalination production.

The MSF process is similar to multicomponent distillation, but there is no exchange of material between the counter current streams. The MSF process is

evaporation of saline water and condensation of the generating vapour in vacuum, where the vacuum changes from one stage to the next and the evaporation temperature decreases from the first to the last stage. The process itself is well known and can be found in the specialized literature. The MSF unit can be divided into two sections in once-through MSF process (MSF-OT); a brine heater section (BR) and heat recovery section (HRS). For brine recirculation MSF process (MSF-BR), however, an extra section is added called heat reject section (HRJ). The recovery and reject sections are made up of a series of stages where each stage has a flash chamber and a condenser. The sequence has a cold end and a hot end while intermediate stages have intermediate temperatures. A MSF plant can contain from 4 to about 40 stages and usually operate with top brine temperatures (TBT) in the range of 90 - 110 °C to produce 6-11 kg of distillate per kg of steam applied (Mayere, 2011).

The MSF plants have been operating without problems for many years and have the highest capacity units (Darwish and Alsairafi, 2004). This success of the process has resulted in dramatic increase in the unit production capacity from 6 MIGD during 80s and 90s to 16.9 MIGD in 2004 when a MSF unit was built in UAE (Al-bahou et al., 2007); allowing in turn significant reduction in the capital cost and operating cost as well (Borsani and Rebagliati, 2005). More details on MSF process will be presented in section 1.5.

1.4.1.1.2 Multi Effects Distillation (MED)

The multi effect distillation (MED) process (also known as multi effect evaporation MEE or multi effect boiling MEB), is the oldest method for seawater desalination (Bruggen and Vandecasteele, 2002) and has been used for industrial distillation for a long time. However, despite its small unit capacity compared to MSF, recently, the MED process becomes a strong competitor to the MSF process due to its low specific energy consumption (Darwish and Abdulrahim, 2008) and the low top brine temperature which ranges between 60 – 70 ºC (Al-Sahali and Ettouney, 2007).

The MED process, as shown in Figure 1.4 takes place in a series of stages known as effects and uses the concept of condensation and evaporation at reduced pressure and decreased temperature from one effect to another. Hence, the feed

seawater undergoes boiling in series of effect without the need to supply additional heat after the first effect. The extracted steam from low and medium pressure turbine lines is fed to the first effect, releasing its latent heat for evaporation of preheated seawater and results in formation of a small amount of water vapour, which is used to generate heat to the second effect. The vapour from the first effect releases its latent heat in the second effect and condensate inside the tubes. The released latent heat results in formation a smaller amount of vapour in the second effect and is used to gives heat to the third effect. This process continues for several effects with gradually decreasing temperature and pressure until the vapour temperature becomes close to the feed seawater temperature (Al-Sahali and Ettouney, 2007). The seawater evaporates outside the tubes and the formed vapour is transferred to flow inside the tubes of the next effect, which are lower in pressure and boiling point temperature. The vapour then condenses and vaporizes more seawater (Zak, 2012). The feed seawater is either sprayed, or distributed in a thin film on the surface of evaporator tubes where it boils and partially evaporates, producing more vapour.
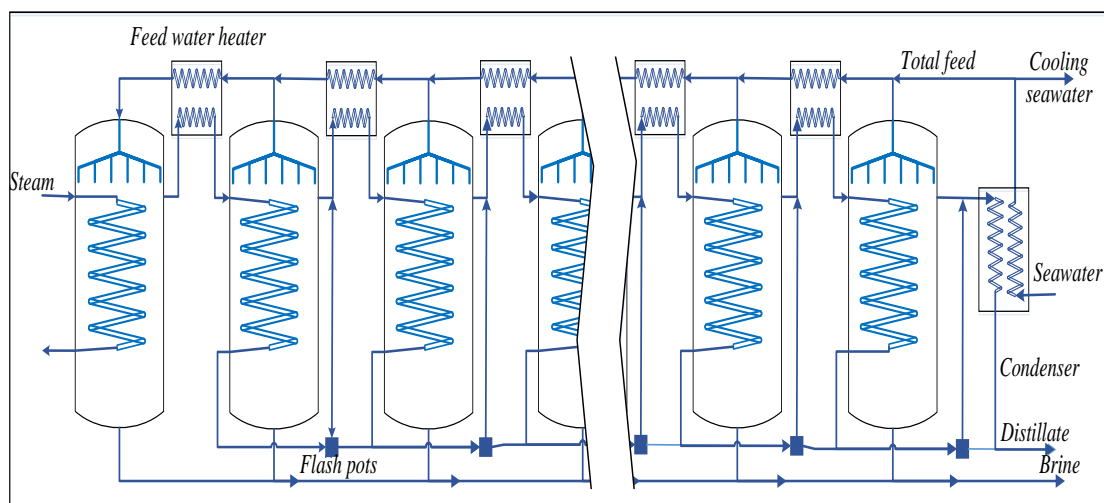
Figure 1.4: Schematic diagram of MED process (Zak, 2012)

1.4.1.2 Membrane Desalination

Since the 1960s (Loeb and Sourirajan, 1963) membrane processes have been rapidly developing and are now surpassing thermal desalination processes. In industrial applications, membranes are used in two commercially important desalting processes: Reverse Osmosis (RO) and Electrodialysis (ED). Each process uses the ability of the membranes to differentiate and selectively

separate salts and water. However, membranes are used differently in each of these processes. While the RO uses the pressure driven force to allow fresh water to move through a permeable membrane and leaving the salt behind, the ED uses electrical driven force to move salts through the membrane and leaving fresh water behind as product (Figure 1.5) (Buros, 2000). However, RO is more preferred over ED due to the high hands-on experience and operation skills requirement for the ED (Altaee and Sharif, 2015c).
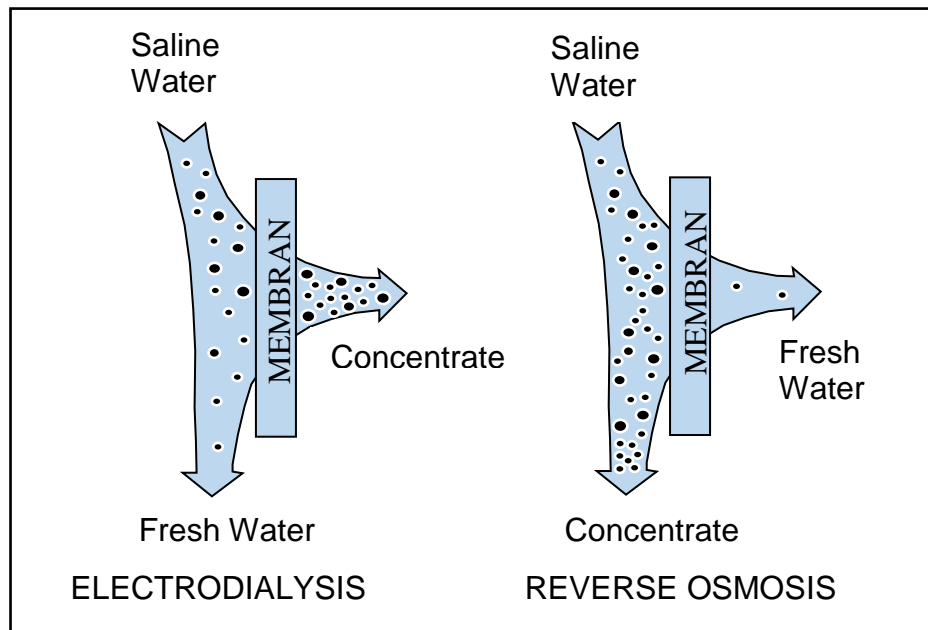
Figure 1.5: The mechanism of ED and RO membrane process (Buros, 2000)

1.4.1.2.1 Reverse Osmosis

Reverse osmosis (RO) is a type of membrane process commonly used for seawater and brackish water desalination. RO is believed to be the most efficient desalination technology with highest number of installations worldwide (Altaee and Sharif, 2015b). The process concept is simple yet effective and uses a membrane as filter and osmosis phenomenon to filter out salt from seawater by applying pressure larger than osmosis pressure of the seawater. After pre-treatment, seawater is pressurized by a high pressure pumps and passes through special membranes into closed vessel where most dissolved solids are blocked and retained for disposal while pure water goes through and collected as a product (Figure 1.6). The amount of fresh water produced can be vary between 30% and 85% of the volume of the input water and it is dependent on the salt content of the sea water and the technology and types of membranes (Cooley et

al., 2006). Since no heating or phase change is required for this separation, the only energy requirement is for pressurizing the feed water. The amount of pressure required depends on the salts concentration of the feed water; the higher salt concentration, the higher pressure is required. For brackish water, the pump pressure ranges from 15 to 25 bar and for seawater the pump may need to generate between 54 and 80 bar due to higher concentration of salt in seawater (Buros, 2000).

The present design of the MSF and MED processes consume more energy in the form of electricity and heating steam than is required by RO. In some cases, this value is close to four times that required by the RO process. However, the membrane replacement cost and extensive feed treatment for the RO process offset this large difference in energy consumption (Al-bahou et al., 2007).
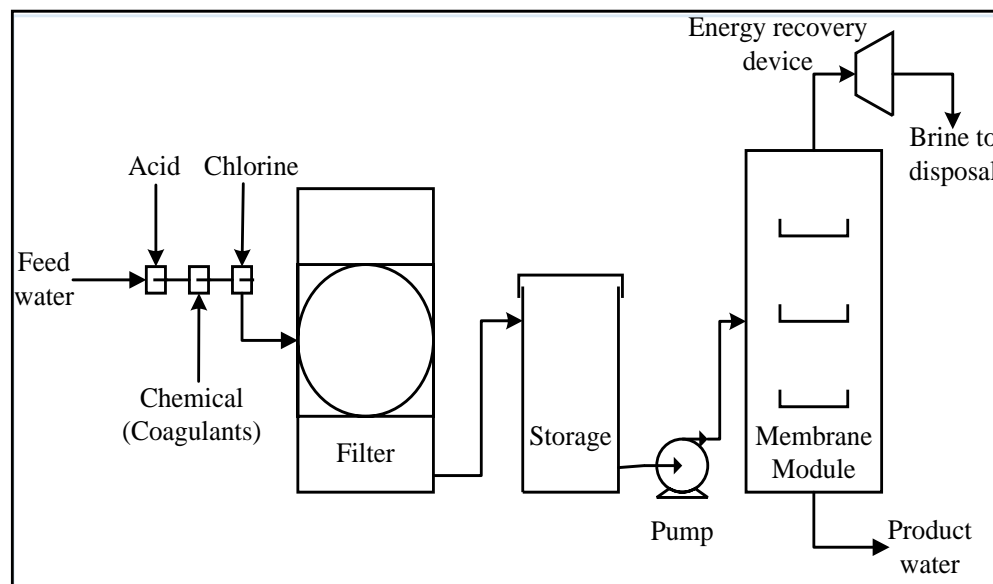
Figure 1.6: A Typical RO Desalination Process

Integration of a seawater RO unit with an MSF distiller provides the opportunity to blend the products of the two processes. Such arrangement allows operating the RO unit with relatively high total dissolved solids and thus reduces the replacement rate of the membranes (Hamed, 2005b). Also this integration can improve the performance of MSF and reduce the cost of desalted water (Calì et al., 2008).

1.4.1.2.2 Electrodialysis

Electrodialysis (ED) is an electrochemical separation process that uses voltage driven force to allow salts to move through a stack of cationic and anionic membranes and leaving pure water behind. The process was commercially introduced in the early 1950s and considered to be a cost effective way to desalinate brackish water (Buros, 2000). The process, as shown in Figure 1.7, occurs in individual membrane units called cell pairs. Each cell pair consists of two types of membrane; a cation membrane, an anion membrane and two spacers. The whole assembly of cell pairs and electrodes is called the membrane stack (Younos and Tulou, 2005). When electrodes are connected to an external source of electricity, electrical current is carried through the saline solution. The cation membrane allows only positive ions such as sodium to migrate to the cathode while anion membrane allows only negative ions such as chloride to migrate to the anode. Therefore, water passing between membranes is split into two streams, one is pure water and another is concentrated water (Al-Shayji, 1998).
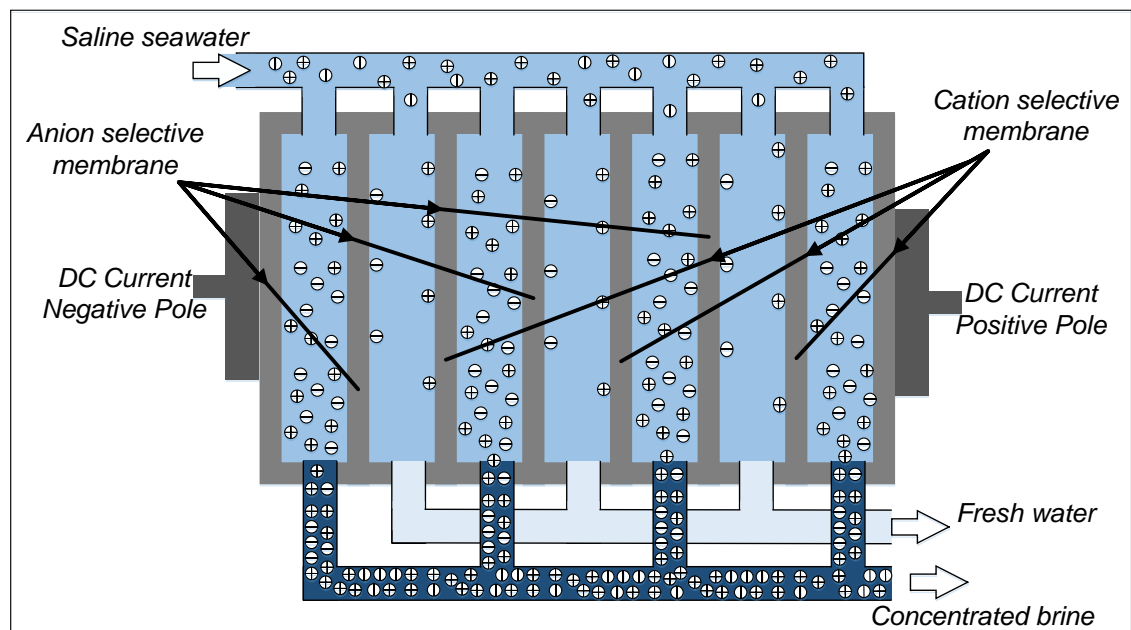
Figure 1.7: A Schematic Electrodialysis Process

1.5 MSF Desalination Process Description

As described in section (1.4.1.1.1), there are two types of MSF plants that can be found in the literature which are developed over the years: once-through MSF

unit (MSF-OT) and recirculation brine MSF unit (MSF-BR). The selection of a specific type depends mainly on economic and operational considerations

1.5.1 Once-Through MSF Process (MSF-OT)

The MSF-OT process, which is illustrated in Figure 1.8, is an applied desalination method particularly known for its simplicity and a small number of components. As shown, in the MSF-OT there is no specific heat rejection section (HRJ). The intake seawater at the cold inlet temperature is pumped into the inside of condenser tubes of the last flashing stage in the heat recovery section (HRS). The cooling seawater gradually gets heated as it passes through the tubes from one stage to another by exchanging the thermal energy from the flashing vapour in each stage. Passing through the first stage, the preheated brine (first stage outlet seawater) enters the brine heater, where its temperature is raised to the maximum allowable value of saturation temperature for the greater operational economy of the plant, but avoiding the scale formation in the brine heater tubes. The heat energy required to increase the brine temperature to the top brine temperature (TBT) is supplied by surplus superheated steam that coming from an electrical power plant. Hence, water production and electricity are normally constructed together in the same region. The saturated or supersaturated heating steam with temperature range of 97 – 117 $^{\circ}$C flows on the outside of the brine heater tubes and the brine stream flows on the inside of the tubes. As the heating steam condenses, the brine stream gains the latent heat of condensation and reaches the desirable temperature (El-Dessouky et al., 1999).

At this point, the flashing brine enters the first stage of the heat recovery section (HRS), through an orifice or weir, where the pressure inside the stage is reduced in such a way that the water will become superheated and flashed off to give pure vapour. The vapour generated from the brine rises and passes through the demisters, where the entrained brine droplets are removed and it condenses on the outside surface of the cooling tubes bundle located at the top of the stage. Since the cooling brine going to the brine heater flows through the interior of this tube bundle, the vapour releases its latent heat and condenses whereas the cooling brine gains the latent heat and it is preheated further. The heat exchange between the cooling brine and the vapour increase the heat recovery as the

cooling brine temperature is increased incrementally to its maximum value so that the thermal energy required in the brine heater is reduced. The condensate is then collected in the distillate trays and pumped out as the desalination product. Due to the large amount of latent heat required for vaporization only a small fraction of brine is evaporated before the brine temperature drops below the boiling point (Gambier et al., 2002). As the flashing brine would still be hot enough to boil again at a slightly lower pressure, the brine flows through orifice into the next stage with lower pressure and another small fraction of the brine is flashed off to produce vapour. The flashing process is then repeated as the brine flows in a number of consecutive stages where pressure is decreased to allow the water to further boil at lower temperature (Abdul-Wahab et al., 2012). The process is repeated until the last stage where the blowdown brine is discharged back to the sea. Figure 1.9 shows the cross-section of a single stage. The distillate trays are connected to each other by a channel where all the accumulated distillate flows through and finally collected in a distillate box at the last stage of the HRS and then is extracted by a distillate pump to the product storage.
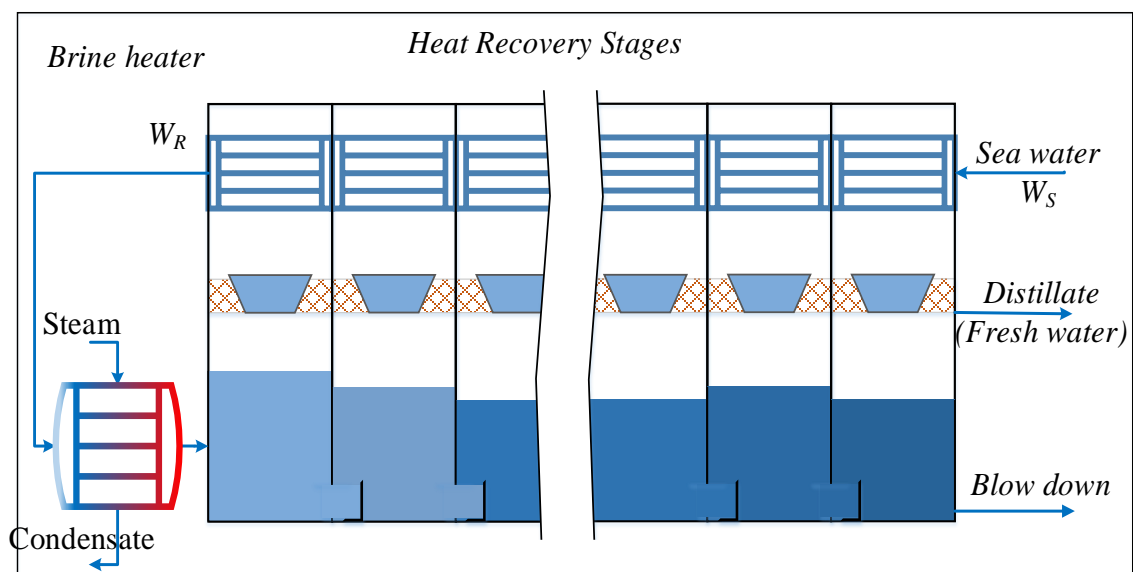
Figure 1.8: Schematic of Once through MSF desalination process (MSF-OT)

The objective of the MSF-OT system is to overcome the main drawback of the single stage flash unit which is the low value of the performance ratio (kg of distillate per kg of steam). This can be done by increasing the number of stages. Indeed, increasing the number of stages for the same flashing range would result in a reduction of the temperature drop per stage and in turn would reduce the

driving force for heat transfer and consequently increases the total heat transfer area (El-Dessouky and Ettouney, 2002). Though the once-through MSF process (MSF-OT) is simple and requires less capital investment compared to MSF-BR, it consumes large amount of chemical additives due to the large amount of intake seawater (Helal and Odeh, 2004).
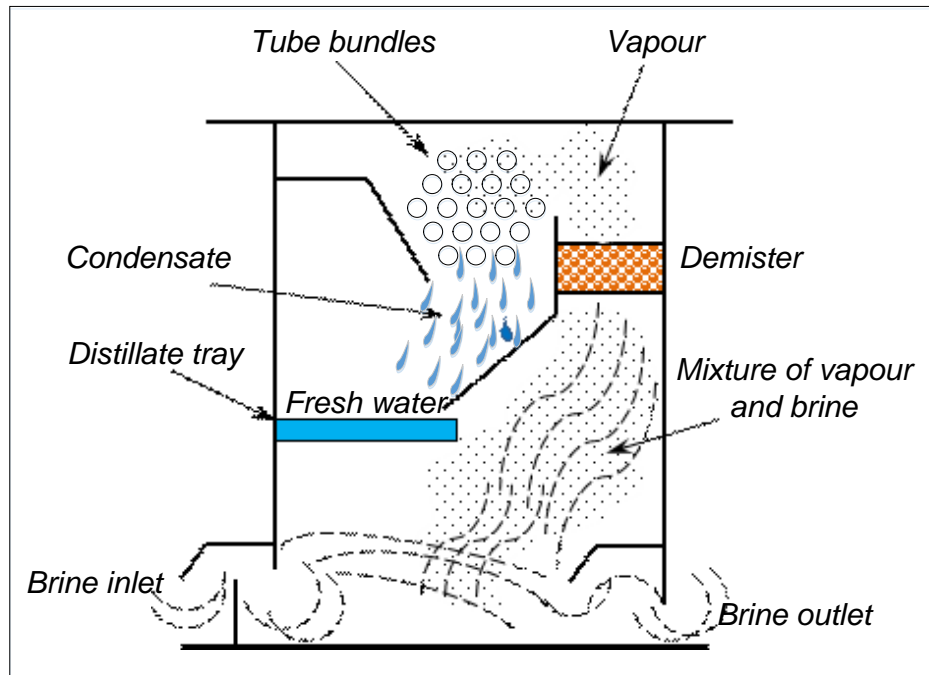
Figure 1.9: A single stage in the MSF desalination plant (Al-shayji et al., 2005)

1.5.2 Brine Recirculation MSF Process (MSF-BR)

The MSF-BR process, also called conventional MSF process, is illustrated in Figure 1.10. Normally this process involves recycle of brine from the reject section to the recovery section. In the MSF-OT process, the whole seawater flow being heated to high temperature, it has to be treated with anti-scale which increases the operating costs. Moreover, the size of the stages must be designed for winter operation, leading to an increased evaporator volume and thus increased investment costs. These two points have led to the idea of separating the flashing stage into two parts (HRS and HRJ) and introducing the brine recycle MSF-BR. The flashing stages are divided into a large number of heat recovery stages and a smaller number of heat rejection stages, commonly three. Although the heat rejection and recovery sections are drawn separately, the two sections are integrated.

In the MSF-BR process, the intake seawater is fed into the condenser tubes of the HRJ. Then, after leaving the HRJ, the seawater feed stream is split into two parts; one part is firstly entered through the deaerator unit to strip its dissolved air by using steam and then it is added to the flash chamber of the last stage as make-up. The second part is rejected back to the sea in summer season while in winter season this can be divided into two parts; one is rejected back to the sea, thus rejecting part of the heat supplied and another part of the second stream is mixed with the cold seawater to preheat it.

After the make-up enters the last stage of the HRJ, The recirculating brine is drawn from the last stage and then introduced to the last stage of the HRS where the recycle brine gradually gets heat in the HRS as it passes through the tubes from one stage to another as described in the previous section.
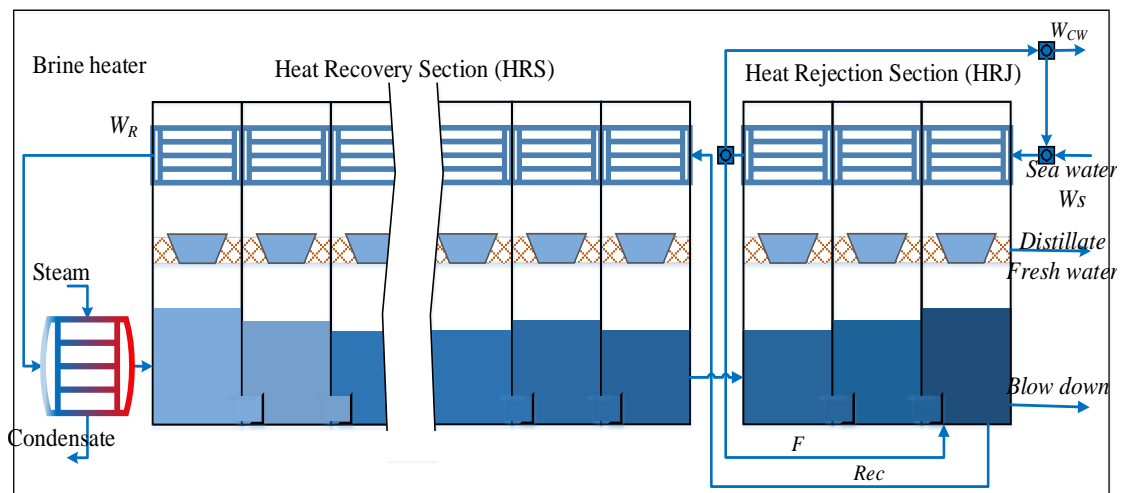
Figure 1.10: Schematic of brine recirculation MSF Desalination Process (MSF-BR)

The remaining part of the concentrated brine is withdrawn from the brine pool and rejected to the sea as blow-down. It is worth noting that the temperature of the last stage of HRJ should be the same as the temperature of the last stage of HRS to avoid thermal shocking (El-Dessouky et al., 1995, Maniar and Deshpande, 1996, El-Dessouky et al., 1999, Gambier and Badreddin, 2004, Al-Hengari et al., 2005, Al-shayji et al., 2005, Abdel-Jabbar et al., 2007, Bodalal et al., 2010, Abdul-Wahab et al., 2012)

The majority of MSF plants are of the brine circulation type, which are more superior to the once through design. The brine recirculation results in decrease

of the flow rate of the feed seawater. As a result, this lowers the chemical additive consumption rate because only the make-up water is treated instead of the whole amount of cooling water. In fact, the MSF-OT requires about 70% more chemicals than needed for the traditional MSF-BR design when the two plants are operated under the same conditions (Helal, 2004). Also, the recycle in MSF-BR gives good control on the temperature of the feed seawater. In addition, the recycled brine contains higher energy than the feed seawater, as a result, the process thermal efficiency will be improved (El-Dessouky and Ettouney, 2002).

According to El-Dessouky and Ettouney (2002), the major features of the MSF-BR process include the following:

- ➢ The flashing stages are divided into two heat sections, (heat recovery section HRS and heat rejection section HRJ).
- ➢ The excess heat added to the system by the heating steam is rejected to the seawater in the heat rejection system. The coolant seawater leaving the heat reject section may be used in winter to warm up the cooling seawater, thus enabling the evaporator volume to be designed for a reasonably high temperature.
- ➢ The remaining part of the intake seawater is used as make-up to replace the portion of the recirculating brine lost to vapour formation and mixed with the brine entered the heat recovery section.
- ➢ A portion of the brine from the last stage of the heat rejection section is mixed with the makeup stream and then is recirculated through the tube side of the condensers to the brine heater.
- ➢ The blowdown stream from the last stage of the heat rejection section can be mixed with the rejected part of the cooling seawater before rejecting them to the sea to decrease the salinity and the temperature of the blow-downstream before it is rejected to the sea.

Although the MSF-OT is characterized by its simplicity over the conventional BR design, the latter has dominated the thermal desalination market. Due to high consumption of chemical additives and the difficulty of the intake seawater temperature control, the MSF-OT process is preferred for small plants and in areas where the temperature of the seawater remains approximately constant

throughout the year. It is important at this stage to confirm that this study will focus on this type of MSF plant.

1.6 MSF Cost

Although the MSF process is considered to be very expensive and energy intensive compared to RO, the number of plants installed worldwide is still increasing. In recent years, despite a cost increase in the raw materials by 40%, the installation cost of water desalination plants is decreasing due to the significant developments in desalination technologies (Borsani and Rebagliati, 2005, Reddy and Ghaffour, 2007). The cost of water depends on the installation and operating cost. The cost of water produced from MSF can vary between 0.52 $/m^3 and 1.044 $/m^3 depending on plant location, feed water properties and energy cost (Reddy and Ghaffour, 2007). Karagiannis and Soldatos (2008) carried out very comprehensive cost review for most of types of desalination processes and reported that for MSF capacity from 23000 m^3/day to 528000 m^3/day, the cost can vary between 0.52 $/m^3 and 1.75 $/m^3.

Hawaidi (2013) carried out a simulation study to estimate the capital and operating costs of a medium sized MSF plant. For fixed water demand and fixed plant configuration, it has been found that the operating cost varies between 0.66 $/m^3 and 0.8 $/m^3 at TBT = 90 ^{o}C and with variation of the water production and number of stages, it was found that the total capital cost varied between 1.55 $/m^3 in summer and 1.84 $/m^3 in winter. Although results indicated high cost in the summer, the MSF plant in his study produced larger amounts in summer to meet the high demand for fresh water and thus per cubic metre of product, the total cost is less in summer. Hawaidi and Mujtaba (2011a) found that the total operating cost may vary between 0.83 $/m^3 and 0.865 $/m^3 by varying the number of stages from 16 to 14 stages respectively. At the same TBT (90 ^{o}C) but different number of stages to meet the variation of fresh water demand based on the climate change during the year, Hawaidi and Mujtaba (2011b) found that the total capital cost of water can vary from 1.67 $/m^3 in winter to 1.77 $/m^3 in summer.

One way of cost reduction is by integration of a seawater RO unit with an MSF distiller (Hybrid MSF/RO). Such integration can improve the performance of MSF and reduce the cost of desalted water. Moreover, blending the products of the two processes allows the RO unit to operate with relatively high salinity seawater and as result the cost of the membranes replacement rate can be reduced (Hamed, 2005a). Helal et al. (2003), (Helal et al., 2004a, Helal et al., 2004b, Marcovecchio et al., 2005, Marcovecchio et al., 2009, Skiborowski et al., 2012) studied the feasibility of hybrid MSF/RO desalination process to minimize the production cost of freshwater. Helal et al. (2004b) concluded that the cost of fresh water from MSF plant could be reduced by up to 24% through hybridization with RO technology. Tian et al. (2005) studied several MSF plants of different sizes and configuration and showed that for one particular MSF plant of 528000 m^3/day capacity, the cost per water unit can be decreased from 1.75 $/$m^3$ to 1.49 $/$m^3$ when combined with a RO desalination unit. Also, pairing MSF plant with a power plant is another way of reducing the cost. A cogeneration plant, often called a dual purpose plant, is one that supplies heat for a thermal desalination unit and produces electricity for distribution to the electrical grid. Most of the MSF distillation plants, especially in Arabian Gulf countries, are paired with power plants in a cogeneration configuration (Al-Mutaz and Al-Namlah, 2004). This type of combination is considered to be more thermodynamically efficient and economically feasible than single purpose power generation and water production plants (Hamed et al., 2006) and reduces the energy needed for thermal desalination by one third to one-half (Winter et al., 2002).

Coupling renewable energy sources such as solar, wind and geothermal energy with desalination systems can play an important role in cost effective and energy efficient way and, from the environmental point of view, can decrease greenhouse gas emissions. Dramatic increase in fuel prices and the environmental impact of burning such fuels has led to the exploitation of renewable energy sources (RES). While energy from wind source is often combined with membrane desalination (Energy, 2012), solar technologies typically suit thermal desalination due to the large amount of heat obtained from the sun. Although RES may be an attractive solution to minimize energy consumption and reduce green gas emissions, the total cost of water production using such alternative energy replacement appears

to be very high (Karagiannis and Soldatos, 2008). In some cases, the cost of solar powered MSF is almost ten times that as for fossil fuel powered MSF (Al-Hamahmy et al., 2016).The high cost resulting from using RES can be attributed to the use of expensive energy storage systems.

Operational cost, on other hand, is another area where the cost can be reduced through better operation and maintenance schemes. While raw material costs are competitive in the global economy, the only way to achieve the target is by reducing the cost of labour, utility and other maintenance cost.

Although the basic configuration of the MSF process has not changed over the last few decades, the improvement quality of the antiscalants and using newer material of constructions has led to a decrease in the investment cost of desalination (Reddy and Ghaffour, 2007). The use of hybrid systems such as MSF-RO, gradual increase of TBT from 90 $^{\circ}$C to 112 $^{\circ}$C, increase in the brine chamber load and the increase in the unit size from 19,000 to 90,000 m^3/day are considered to be the main improvements that have led to a significant reduction in MSF desalination cost (Ghaffour et al., 2013). Operating costs also experienced a decrease through optimization process by optimizing maintenance schedule, product water quality, operating temperature and flow rates. However, care should be taken when such parameters are optimized at the expense of the equipment costs. Increasing the top brine temperature for example requires large amount of steam which in turn may require larger reboilers. Also, increasing the flow rates of the seawater or the recycle brine require different size and power of pumps.

1.7 MSF Desalination Plant Parameters

Multi-stage flash distillation (MSF) system modelling involves a number of operating and design variables that have great influence on the performance of multistage flash MSF desalination plants. An estimation of all these variables requires both analytical solutions and experimental/field analysis. These variables can be classified as design variables and operating variables.

1.7.1 Design Parameters

1.7.1.1 Top Brine Temperature (TBT)

Top brine temperature (TBT) is the temperature of the recirculation brine after it is heated by the low pressure steam in the brine heater. It plays an important role in describing the performance of MSF process. It has direct effects on the distillate production and the levels in each flash chamber. It can be used to control the whole plant in addition to load control. This means for each plant production, there is a certain top brine temperature which depends on the seawater inlet temperature. This temperature should be maintained within a specified range because it gives many indications to the operators of the MSF desalination plant. For example, high TBT is mostly an indicator of high steam consumption (Abdul-Wahab et al., 2007). Most of the multistage flash desalination plants (MSF) operate at top brine temperatures (TBT) of 90 - 120 ^{o}C (Hamed et al., 2001, Mussati et al., 2004, Hawaidi and Mujtaba, 2010a, Hawaidi and Mujtaba, 2010b). Increasing the TBT can cause an increase in the production rate and the performance ratio. The former increases because of an increase in the flashing range, whereas the latter increases due to the decrease in the latent heat of vaporization of water at higher temperature (Abdul-Wahab et al., 2012). Moreover, the increase in the top TBT results in decrease in the specific heat transfer area. This is due to the increase in the flashing range and the temperature drop per stage, which in turn increase the driving force for heat transfer (El-Dessouky et al., 1998, Abdel-Jabbar et al., 2007).

The upper value of TBT depends on the type of chemicals used for feed treatment and on the brine concentration. According to Hawaidi (2013), for acid treatment the TBT is limited to 121 ^{o}C, for polyphosphate treatment the limit is 90 ^{o}C and about 110 ^{o}C for high temperature additives. Operating the plant at the higher temperature limits of 120 ^{o}C tends to increase the efficiency; however it also increases the potential for detrimental scale formation and accelerates corrosion of metal surfaces (Aly and El-Figi, 2003, Mussati et al., 2004). Also, operating the plant below the lower value, less than 90 ^{o}C, can cause the pressure difference in the vent condenser to become insufficient, which in turn causes an incomplete extraction of non-condensable gases (NCGs), followed by instability and possible

vapour side corrosion problems (Al-shayji et al., 2005). The top brine temperature TBT has very little influence on the specific cooling water flow rate (El-Dessouky et al., 1995). In addition, (Abdel-Jabbar et al., 2007) reported that the top brine temperature has little effect on the stage length. Also, increasing the TBT leads to small variation of the specific flow rate for cooling water and of specific flow of the brine recycle.

Since operating the plant at high TBT increase the efficiency of the plant, the main challenge facing the designer is the ability to operate at high TBT while avoiding scale formation. This can reduce the heat transfer area and in turn lowers capital costs and increase the performance ratio PR.

There are some attempts to operate the MSF plants at a TBT as high as 130 °C by removing portions of calcium and/or sulphate from seawater. Recently, Helal et al. (2012) suggested the idea of incorporating a nanofiltration (NF) unit to the MSF plant for the partial removal of bivalent scale forming ions from the makeup stream to enable operation at high TBT. However, installing NF unit for pre-treatment seems not to be economically feasible due of the high operation cost (Altaee and Sharif, 2015a).

1.7.1.2 Number of Stages

Typically, the number of stages in the MSF plant can vary between 4 and about 40 (Mussati et al., 2004). The maximum stage number is limited by the pressure difference required to move the flashing brine from one stage to another (Darwish, 1991).

In MSF-BR, the number of the stages in the rejected section HRJ is usually taken equal to three in a large plant. According El-Dessouky et al. (1998), the single-stage heat rejection cannot be applied because of the intersection temperature profiles of the feed seawater and condensing vapour. The two-stage heat rejection section is not practical because of the low terminal temperature difference found in the first flashing stage. This analysis leads to the conventional MSF system, which includes three stages or more in the heat rejection section. The HRJ section with three stages provides stable operation and practical values for the specific cooling water flow rate and heat transfer area.

Darwish et al. (1995) stated three factors that affect the choice of number of stages. These are as following:

  ➢ The maximum number of stages is limited by the available pressure difference between the stages (especially the bottom stages) to move the brine from one stage to another;

  ➢ The increase in temperature range allows a greater increase in the number of stages; and

  ➢ The pumping cost (especially for the cross tube type) and added cost of water boxes and tube sheets may limit the number of stages.

As the number of stages increases, the specific heat transfer area requirement decreases. Thus, increasing the number of stages reduces the capital cost of the unit to a certain limit until the cost of manufacturing additional stages is greater than the saving in the heat transfer area (Aly and El-Figi, 2003).

In their study, to lower the blow-down brine temperature, Fiorini and Sciubba (2005) demonstrated that blowdown stream is more sensitive to the number of stages than to the TBT. Increasing the number of stages decreases the temperature of the blow-down brine.

For once through, increasing the number of stages from 24 to 32 has a significant effect on the performance ratio PR for fixed top-brine temperature TBT. The performance ratio increases as the top-brine temperature increases (Baig et al., 2011). Hamed et al. (2000) reported that the Jeddah II distiller, working at a TBT of 115°C, yields the high performance ratio (PR) of around 11.5 due to the great number of stages.

Darwish et al. (1995) reported that the Sirte MSF plant in Libya used to have the largest number of stages (39) among other built plants at that time. That plant was the long tube design, once through operation, with TBT of 118°C, and a performance ratio PR of 10, with a 2.2 MGD capacity. It is to be mentioned that the Sirte MSF plant was removed in 2010 and new MED plant and power station (dual purpose) are planned to be installed in the near future.

1.7.1.3 Fouling Factor

Fouling is the accumulation of undesired solid materials at the phase interfaces. Build-up of fouling film leads to an increase in resistance and deteriorates the performance of process equipment such as membranes and heat exchangers (Al-Anezi and Hilal, 2007). Seawater always has the tendency for scale formation and fouling problems due to dissolved salts and finely suspended solids. In thermal desalination process such as MSF, the phenomenon of fouling as scale formation is mainly caused by crystallization of alkaline such as calcium carbonate ($CaCO_3$), and at higher temperature, Magnesium hydroxide $Mg(OH)_2$. Non-alkaline such as calcium Sulphate ($CaSO_4$) is also considered the most common scales found in MSF (Al-Sofi, 1999).

Fouling factor (FF) is a design parameter that has a great influence on the heat transfer area. The value of the FF is usually obtained from operating experience. Commonly recommended fouling factors for untreated seawater are 0.08 m^2.K/kW for temperatures below 50 °C and 0.17 m^2.K/kW for temperatures above 50 °C (Darwish et al., 1995). In recent MSF designs, realistic values of FF, between 0.07 and 0.11 (m^2.K/kW), are used to keep the cost of heat transfer area down. The choice of high FF, for example 0.2 (m^2.K/kW) in MSF design gives more heat transfer than that actually required (Darwish and Alsairafi, 2004). Increasing the fouling resistance from 0 to 0.001 m^2.K/W resulted in a 400% reduction in the overall heat transfer coefficient. Moreover, considering the fouling factor in the design process of the heat exchangers has a noticeable impact in increasing the required surface area (Baig et al., 2011).

1.7.2 Operating Parameters

1.7.2.1 Seawater Feed Temperature and Flowrate

Feed temperature is an important operational parameter that is imposed on the desalination plants by the seasonal climatic conditions. Change in seawater temperatures directly affects the yield of the MSF desalination plants (El-Dessouky et al., 1999, Tanvir and Mujtaba, 2007, ElMoudir et al., 2008), fouling formation inside the tubes of the brine heater (Hawaidi and Mujtaba, 2010b), the heat transfer in the reject section, the temperature of the makeup and thus of the

recirculating brine (Maniar and Deshpande, 1996) and consequently the plant overall performance.

The seawater temperature depends on the locality and the time of the year. It varies in Kuwait from 10 °C to 35 °C (Darwish et al., 1995). In summer, the highest temperature of the Mediterranean Sea is in the Gulf of Sidra (Libya), where the average temperature in August is about 31 °C (Boxer and Salah, 2010), whereas in winter this temperature could drop to as low as 12 °C (El-Mudir et al., 2004). This variation in the temperature of the feed seawater can lead to a difference by 10% of the plant productivity (Abduljawad and Ezzeghni, 2010).

Since the temperature of the cooling seawater can be as low as 12 °C, its mass flow rate is required to be decreased in order to achieve reasonable flashing brine temperature in the bottom stages. However, the decrease in the cooling seawater flow rate can result in a decrease in its velocity to that lower than the acceptable minimum (about 1.5 m/s). It can also decrease the temperature (and consequently the pressure) in the chamber stages and increase the specific volume to unacceptable limits resulting in unstable operation. For this reason, in the MSF-BR plant, a part of the rejected seawater can be recirculated and mixed with feed seawater to keep the cooling seawater inlet at a reasonable temperature and avoid the problems created by a low-temperature inlet (Darwish et al., 1995). The MSF plants require inlet seawater flow around 8 to 10 times the distillate flow rate for cooling and feed make-up (Morton et al., 1996).

In the once through process, analysis also indicated that both the temperature of the seawater leaving the flashing chamber in the final stage and the temperature of seawater entering the desalination plant have an influential effect on the performance ratio (Baig et al., 2011). For fixed steam temperature, an increase in the seawater temperature causes the TBT and bottom brine temperature (BBT) to be increased, although, the distillate product and the performance ratio decreased (Tanvir and Mujtaba, 2006a). This is true because the performance ratio and the distillate product are affected by the decrease of the amount of the heat removed. Also, decreasing seawater flow rate results in increasing the system temperature and subsequently the performance ratio PR (Bodalal et al., 2010).

1.7.2.2 Make-up Flowrate

Here the make-up flow is the portion of the cooling water leaving the rejection section HRJ and added to the recirculation brine by either direct mixing with the brine recirculation or introducing it into the bottom of the last stage. The make-up flow affects the temperature of the recirculation brine and thus affects the flashing process (Maniar and Deshpande, 1996). As the make-up flow increases, the brine level increases leading to reduction of the flashing efficiency and vice versa, whilst decreasing the make-up flow rate results in decrease in the brine level and consequently improve the flash efficiency (Alatiqi et al., 2004). Moreover, increasing the make-up flow leads to decrease in the salt concentration in the brine stream. This is very important since the make-up keeps the salt concentration constant inside cooling tubes and lower steam consumption and also decreases the blowdown salt concentration (Said, 2013). The make-up flow rate is 3-4 times that of the fresh water produced (Helal, 2005). As it was mentioned previously, treatment of the intake seawater is limited to make-up flow only which makes MSF-BR consumes less additives chemical than MSF-OT.

1.7.2.3 Steam Flowrate and Temperature

Most of the heat required to run the MSF desalination plants is thermal energy in the form of a low pressure heating steam (El-Dessouky et al., 1995). This steam normally has a pressure between 4 and 7 bars, and it is necessary to bring down its pressure to around 2 bars to ensure saturated steam flow. Consequently, the steam becomes superheated with a temperature closed to 160 ^oC. This temperature is then decreased to 110-120 ^oC resulting in change of its state from superheated to saturated steam. The saturated steam condenses around the external surface of the brine heater tubes, where the cooling brine is circulating, resulting in an increase in the cooling brine temperature from about 88 ^oC at the inlet to the TBT (95 - 110 ^oC) (Gambier et al., 2002).

Due to the fouling and scale formation, the TBT drops resulting in a decrease in the product rate. Thus, to maintain the TBT as well as the product rate at the desired values, it is essential to increase the steam temperature or its flow rate (Al-Shayji, 1998). Indeed, increasing the steam temperature cause an increase in the TBT which, in turn, increase the production rate. However, this leads to a

decrease in the brine level due to the vapour leaking across the stages (Alatiqi et al., 2004). Hamed et al. (2000) carried out a thermo-economic analysis of MSF plants in Saudi Arabia and found that increasing the steam temperature in the brine heater from 95 °C to 105 °C results in about 30% increase in thermodynamic losses. In general, the minimum steam temperature required to heat up the feed seawater in the brine heater should be 5 °C to 10 °C higher than the TBT (Alatiqi et al., 1999).

On the other hand, increasing the steam flow rate can cause an initial increase in the production rate and then it saturates as the heat transfer capacity in the heater unit with a given transfer area becomes almost constant. Therefore by increasing the steam flow rate the increase in production rate can no longer be attained (Bandyopadhyay et al., 2005).

1.7.2.4 Brine Recirculation Flow

Beside the TBT, the brine recycle flow is considered to have a strong effect on performance of the plant. Both parameters (the TBT and the brine recycle flow rate) can be manipulated to achieve maximum performance ratio PR and maximum distillate production rate without violating any plant constraints (Abdul-Wahab et al., 2012). Helal et al. (2012) reported that increasing the recycle flow rate from 0.725 to 0.85 of the maximum recycle pump capacity led to about 17.1% increase in plant capacity at a top brine temperature of 110 °C. In addition, increasing the brine recycle flow results in an increase in the brine level in each flash chamber and a decrease in the flashing efficiency due to the reduction in the residence time in the stages. Also, for fixed TBT, the brine recycle flow directly affects the steam consumption. The higher the brine recycle flow, the higher the amount of steam required (Maniar and Deshpande, 1996).

The recirculated brine is completely independent of the number of stages and depends only on the TBT, as the flashing range increases, the specific recirculated brine decreases and consequently the pumping cost decreases (Aly and El-Figi, 2003). On the other hand, increasing the recycle flow rate is convenient and increases distillate production, but moving too much from the design point would inevitably affect the overall MSF plant cost (Fiorini and Sciubba, 2005).

The maximum rate for the recycle flow is limited by the maximum allowable velocity in the cooling tubes, as higher velocities cause erosion of the tube material (Abdul-Wahab et al., 2012). The allowable velocity inside the tubes should be between 1.5 m/s and 2.3 m/s (Helal, 2003, Abduljawad and Ezzeghni, 2010).

1.7.2.5 Brine Level

The brine levels in the flash stages are quickly affected by the steam supply temperature or flow rate (Husain et al., 1994). Brine levels in all stages should be high enough to seal the interstage orifices and prevent blow-through. However, high brine level increases the thermodynamic non-equilibrium losses and should be low enough to ensure less equilibration losses. An adjustable level controller is required with high sensitivity over the permissible range of brine level. This controller is one of the most important control loops in the MSF plant since the level in all stages is controlled by adjusting the brine level in the last stage (Darwish et al., 1995).

1.7.2.6 Concentration Ratio

The concentration ratio is defined as the ratio of the saline concentration of the brine blowdown exiting from the multi-stage distiller to the saline concentration of the raw feed water. In most MSF plants, the concentration ratio value varies between 1.54 and 2 (Al-Mutaz et al., 2006).

Under certain temperatures and concentration, calcium sulphate in the hemi-hydrate form can form a deposit. To avoid operation under the region where sulphate scale can form, it is essential to check the brine concentration. The relationship between temperature and concentration for calcium sulphate deposits from normal seawater is shown in Figure 1.11. The area below the $CaSO_4$ line is the non-scale-forming area (Darwish et al., 1995). It is to be noted that a similar curve is usually drawn for the locality where the desalter is built.
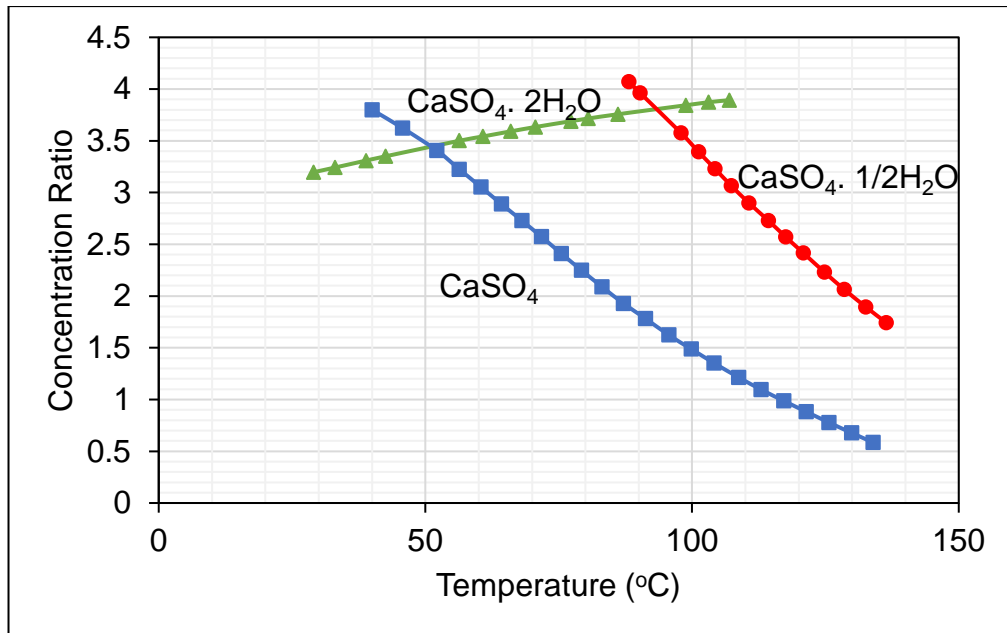
Figure 1.11: Solubility of calcium sulphate as a function of temperature and brine concentration (Hamed and Al-Otaibi, 2010).

1.7.2.7 Scale of Formation

Scale formation, which affects heat transfer and reduces flow velocities inside the condenser tubes of desalination plants, is of great concern for the performance of the thermal desalination process. The performance of MSF plants is mainly affected by the condition of heat transfer surfaces, therefore, scales on these surfaces by seawater containing dissolved salts can reduce the efficiency of the heat transfer process resulting in poor performance of the plant. The main scale-forming components as ions of seawater are calcium, magnesium, bicarbonate and sulphate (Hamed and Al-Otaibi, 2010). As mentioned previously, the factors which are responsible for scale formation in MSF plants are the salt concentration and the high TBT.

Control of scale formation on heat transfer surfaces can be achieved by using several commercial antiscalants available in the market mostly derived from condensed polyphosphates, polyelectrolytes and organophosphonates (Hamed and Al-Otaibi, 2010). However, the dosing rate of anti-scaling is very sensitive as under-dosing leads to scale formation while overdosing is believed to enhance sludge formation (Hamed et al., 1999). In general, the required dosage of

antiscalants is strongly dependant on the TBT and the seawater make-up flow rate.

Hamed and Al-Otaibi (2010) conducted a study on MSF pilot plant under harsh operating conditions using different type of antiscalants. The plant was also operated under the same conditions, but without antiscalants. Their results revealed that antiscalants were effective in suppressing scale formation under the selected operating conditions. However, many MSF plants are operating at high dosage antiscalants resulting in high costs. Thus, dosage rates optimization of antiscalants is essential for lowering the pre-treatment cost.

1.7.2.8 Performance ratio

The performance ratio PR is the indicator of the efficiency of the MSF plant. The performance ratio PR is defined by the amount of distillate obtained by condensing 1 kg of the heated steam in the brine heater. The PR can be used as indicators for the designers to estimate the number of stages. For most of the operating plants, the number of stages ranges between slightly higher than twice the PR to little lower than four times the PR (Darwish et al., 1995). The thermal performance ratio and the specific heat transfer area are two main process parameters that have strong impact on the unit product cost (El-Dessouky et al., 1995). According to Baig et al. (2011), the PR is mostly affected by the brine outlet and inlet temperatures, number of stages, top-brine temperature TBT, and the fouling resistance. Helal et al. (2012) and Abdul-Wahab et al. (2012) reported that the main variables that affect the performance of the plant were the TBT and the brine recycle flow rate. Increasing one of these variables leads to increase the performance ratio and distillate product. However, increasing them over limited value can give negative results; therefore, optimum value of these variables must be obtained to maximize the performance ratio and distillate product.

1.8 MSF Desalination Problem

Although, the MSF process is a reliable technology for producing potable water, it is not the first choice in some parts of the world for new developments due to high cost of fuel and high tendency of fouling. Although significant improvements

and progress has taken place over years in this aspect, it is believed that there is more room for cost reduction through operational and design improvement.

One way of cost reduction through operational improvement is by implementation of advance control strategies. Currently, typical MSF plants in the world operate under conventional proportional-integral-derivative (PID) type control. Although it could meet the minimum requirement of control (Ismail, 1998), its linearity can be an obstacle in controlling highly sophisticated systems such as complex MSF plant which contain nonlinear variables. Thus, implementation of advanced process control technique can be a cost effective approach to energy conservation and increased process profitability.

Understanding fouling phenomena is another way of cost reduction where the cost can be reduced through decreasing the condensing area of the tubes bundle and also avoiding frequent shutdowns of the plant for cleaning. Water with soluble salts increase the tendency to scale which can reduce the heat transfer rate and increase energy consumption. Thus, the heat transfer area of most thermal equipment are overdesigned to compensate for fouling. This increase in the heat transfer area could lead to an increase of about 30% of the total cost (Gill, 1999). Moreover, understanding the behaviour of fouling could extend the period of running the plant before the next shutdown for cleaning. This can heavily reduce the annual operating cost resulting from maintenance and cleaning process.

Apart from fouling, the release of NCGs such as air and carbon dioxide from the brine to the vapour space can work as insulated materials and reduce the heat transfer rate. Although this problem is solved by the venting system, increasing in the number of venting point results in more vapour escaping from the stages and thus resulting in a decrease in the performance ratio of the plant.

1.9 Scope of the Research

The use of mathematical models and optimization software is playing an important role for design and operation purpose to provide a very detailed analysis. Regarding MSF process, the majority of the optimization studies share a common goal: minimizing the operating cost and improving the productivity. According to the variation with time, there are two types of mathematical models:

steady state and dynamic models. The steady-state model does not vary with time and is used for design purposes as well as for parametric studies of existing plants for performance evaluation and operational optimization. Dynamic models, on the other hand, vary with time and are used for trouble shooting, fault detection, reliability, start-up and shutdown conditions, and to implement advanced control (Gambier and Badreddin, 2004).

There are several published literatures, as presented in chapter 2, which have been dealing with rigorous mathematical modelling and mathematical optimization of MSF desalination processes. However, due to numerous number of the desalination model equations, the whole picture of the mathematical model has not been achieved yet. Effect of NCGs and Kinetic model (fouling and scaling) have received little attention and there are a limited number of publications which have considered their effect on desalination performance (Said, 2013).

Most previous studies have paid little attention to the effect of NCGs on the overall heat transfer coefficient and plant performance. The presence of NCGs such as carbon dioxide, nitrogen, oxygen, and argon that is caused by air leakages to stages and the release of brine dissolved gases has, even in small amount, great effect on the heat transfer rate at the vapour side of the stage condensers. Due to the low conductivity of these gases, they work as insulation material and decrease the heat transfer rate and in turn, affect the plant performance. Recent studies by Alasfour and Abdulrahim (2009) and Said et al. (2010) included NCGs correlations in their models to study the effect of NCGs on the heat transfer rate. However, a fixed value for the amount of NCGs was considered for all the plant stages. In reality, an installation of venting system plays an important role on increasing the heat transfer rate by extracting the NCGs to the atmosphere or to the evacuating system. The evacuated system is installed in series for some stages and in parallel for other stages, making the amount of NCGs vary from stage to stage. Thus, in this work, the mass concentration of NCGs is included in the dynamic model of MSF. The release rate is studied using Henry's law and the NCGs concentration is varied from stage to stage to analyse the optimum design of venting system and study the effect of NCGs on the OHTC.

Fouling and scale of formation is another serious problem encountering in the MSF process. As highlighted by Mujtaba (Mujtaba, 2008, Mujtaba, 2010), at high temperature, water with soluble salts allows deposits to form scale which can reduce the heat transfer rate and can increase specific energy consumption and operating costs. This can cause frequent shutdowns of the plant for cleaning. Although a number of studies have been carried out on the experimental study of scaling and corrosion only a handful focused on the modelling (or attempts to modelling) of scale formation in MSF process (Al-Anezi and Hilal, 2007, Hawaidi and Mujtaba, 2010a, Mubarak, 1998, Wangnick, 1995). Most of these models except (Al-Rawajfeh et al., 2008, Al-Rawajfeh et al., 2014, Hawaidi and Mujtaba, 2010a, Said et al., 2012) have been developed and studied on their own but have not been a part of the MSF process models. Al-Rawajfeh (2008) and Al-Rawajfeh et al. (2014) correlated the deposition of calcium carbonate to the released rate of carbon dioxide in a steady state model based on coupling of mass transfer with chemical reaction. Hawaidi and Mujtaba (2010b) developed a linear dynamic model for brine heater fouling to study the impact of fouling with seasonal variation of seawater temperatures. Said (2013) extended Hawaidi and Mujtaba's study to include the effect of fouling in the stages by development of steady state model. However, during the fouling process, the MSF process experiences a continuous change in salinity and temperature of the recycle brine which has been neglected in all previous studies. Moreover, the fouling due the deposition of magnesium hydroxide, which is a common fouling type, has never been modelled in MSF. Therefore, in this work, a dynamic fouling model considering the precipitation of calcium carbonate and magnesium hydroxide will be developed to investigate the behaviour of fouling in the flashing stages with different velocities and with continuous change in salinity and temperature.

Recent studies (Hawaidi, 2013, Hawaidi and Mujtaba, 2010b, Hawaidi and Mujtaba, 2011b, Said et al., 2010, Said, 2013) on the effect of time varying fouling, seasonal variation of seawater temperature, daily and or seasonal variation of freshwater demand on the operation, design and cost of production required the change in the MSF process operating conditions to meet the optimum operation. These changes indicated the need for more investigations on the current control strategies.

Most of the MSF plants are currently operated under conventional Proportional Integral Derivative Controller (PID) due to its simplicity and well recognition by the industry (Al-Gobaisi et al., 1994). However, PID control is linear and cannot efficiently control highly sophisticated systems which contain nonlinear variables. The availability of advanced process control (APC) strategies nowadays can be utilized to be implemented into MSF process. APC such Generic Model Control (GMC) and Fuzzy control are well-known control techniques that have been used widely in the past to control nonlinear systems.

Therefore, GMC control and GMC-Fuzzy control will be developed and introduced to the MSF process to control and track the set points change of the most important variables in the MSF plant; namely the output temperature of the brine heater (TBT) and the Brine Level (BL) in the last stage.

1.10. Aim and Objectives of the Research

The main focus of this research is to cut operational cost of MSF plant by implementing advanced control strategies and studying the dynamics of fouling inside the condenser tubes of the flashing stages through development of more accurate dynamic models. To accomplish the above aim, the following objectives were carried out:

- ➢ To carry out extensive literature review on MSF desalination process and the steady state and dynamic modelling,
- ➢ To develop a very detailed dynamic model using gPROMS software based on mass and heat balances, heat transfer equations and equilibrium correlations for the heat recovery and heat rejection stages. Thermo-physical property correlation of brine solutions showing their dependence on temperature and salt concentration have been used,
- ➢ To validate the results obtained from the model using actual plant data that was collected from different resources,
- ➢ To study the effect of NCGs on the heat transfer coefficient for different stages based on the configuration of the venting system and find out the optimum configuration of the plant's venting system that to lead to optimum performance of the MSF process,

➢ To develop and implement two control strategies namely GMC control and GMC-Fuzzy control and compare them to the conventional PID controls, and

➢ To develop a dynamic fouling model that predicts the crystallization of calcium carbonate and magnesium hydroxide inside the condensing tubes of the MSF plant.

1.11 Thesis Structure

This research has been carried out in different stages and covered a number of tasks that are reported in different chapters. The thesis consists of seven chapters that are presented as following:

Chapter one: Introduction

In this chapter, a short description about the need of desalination and the efforts that made to improve the available techniques through a model-based technique are presented. The water shortage problems in the world and in North Africa in particular and the need for water desalination are described in details. The general description of multistage flash desalination plant process is presented. The chapter also includes discussion of the main design and operation parameters that affect the performance of the MSF desalination process. The scope of the thesis is introduced followed by description of the aims and objectives of the research. The objectives, further, are broken down into specific points.

Chapter two: Literature review

A literature review of previous work on simple and detailed steady state and dynamic modelling is presented. Detailed review about the previous work on NCGs, fouling and control strategies are also presented. Different types of simulators package that used in dynamic simulation and optimization for MSF process are presented.

Chapter three: Modelling and simulation of MSF process using gPROMS

A detailed dynamic mathematical model for MSF process is presented. The model comprises of mass and energy equations which are supported by physical and thermodynamic properties correlations. The model equations are introduced

into gPROMS software and simulation run is carried out to validate the model's steady state and dynamic state results against actual plant data.

Chapter four: The effect of venting system design for non-condensable gases

The released rate of NCGs and their effect on the overall heat transfer coefficient are described in this chapter. Also, the venting system design is studied by variation of the location of venting points to keep the concentration of NCGs under control.

Chapter five: Generic model control (GMC) and Hybrid Fuzzy-GMC control

In this chapter, designs of a GMC control and a hybrid Fuzzy-GMC control are presented and implemented in MSF process to control and track the set points change of the two most important variables in MSF plant; namely the output temperature of the brine heater (TBT) and the Brine Level (BL) in the last stage. To check the performance of all controller strategies in tracking the set points, an optimization problem was formulated to obtain four optimum values for the TBT and BL for four different seasons.

Chapter six: Dynamic fouling model

Fouling caused by deposition of calcium carbonate and magnesium hydroxide was modelling and simulated in gPROMS in this chapter. The model involves the deposit and removal rates of fouling with and without antiscalant. Also, the model takes into account the effect of ions strength of seawater species on the solubility concentration of calcium carbonate and magnesium hydroxide.

Chapter seven: Conclusions and future work

Final conclusions of this work are presented. Some problems and interesting points were raised during this study and these are presented in this chapter.

CHAPTER TWO

Literature Review

2.1 Introduction

The high cost of thermal desalination processes such as MSF leads the computational community for more investigations and development to reduce the cost by using mathematical models and process simulators. All desalination plants designers are interested in designing their units at minimum cost with high efficiency. For production of potable water that is to be produced by seawater desalination, the designers are faced with the problem of choosing the right configuration of the plant, as well as the other equipment needed to conduct the process at minimum cost. Thus, an interest in using computer technology to perform a process design in a systematic way has been applied in the areas of simulation and optimal design.

Desalination modelling refers to formulating a set of mass and energy balance equations that describe mathematically the process units of MSF plant, namely flash stages, brine heater, condensers, mixers and splitters. The model equations are to be supported by the physical and thermodynamic properties of brine, distillate, and water vapour as well as the heat transfer coefficients. In the simulation phase, the formulated model is solved by using a suitable solution procedure, as well as by entering the values of independent process variables. Due to the complexity of the process and the huge number of equations, the solution can be conducted with the aid of a computer, which is termed as computer-aided simulation (Husain et al., 1993). For design purposes, the model provides the engineers with reasonable results for each particular task within a reasonable time and at lower cost. The benefit of designing a piece of equipment on a computer is that it can be tested before it is bought or constructed. It is much safer for the designers to make mistakes on the computer than on the plant. For operational purposes, it tests the effect of different parameters, examines internal vapour and liquid loading, develops better insight into the working of the process and ultimately leading to the optimal operation and control of the process.

According to the time-dependence, there are two types of process models: steady state and dynamic models. The steady-state model does not depend on the time. It describes the process through a set of algebraic equations. Design models of continuous processes are always steady-state models. Dynamic models, on the other hand, are time-dependent and they contain differential equations and supporting algebraic equations. The difference between steady state and dynamic is the value of the accumulations. For example, the following is the general conservation equation for mass and energy balances.

$$Input \quad - \quad Output \quad + \ Generation \ - \ Consuption \ = Accumulation$$

$$\begin{Bmatrix} Enters \\ through\ the \\ system \\ boundaries \end{Bmatrix} - \begin{Bmatrix} Leaves \\ through\ the \\ system \\ boundaries \end{Bmatrix} + \begin{Bmatrix} Generated \\ by\ the \\ system \end{Bmatrix} - \begin{Bmatrix} Consumed \\ by\ the \\ system \end{Bmatrix} = \begin{Bmatrix} Buildup \\ within\ the \\ system \end{Bmatrix}$$

The above equation is applicable for dynamic model, however, setting the value of accumulation to zero, the equation become valid for steady state model.

In this chapter, comprehensive review on modelling of MSF literature studies including steady state analysis and dynamic analysis. The review provides a critical evaluation and summary for the main features of these studies including the objective of each study. In addition, NCGs effect on the MSF and fouling models will be reviewed in this chapter. Moreover, a detailed review on the control strategies of MSF plants is also presented in this chapter. The review also includes some available simulators used for simulating MSF process.

2.2 MSF Steady State Model

Different steady-state models are used for design purposes as well as for parametric studies of existing plants for performance evaluation and operational optimization. However, steady state model cannot be used for control purpose (Gambier and Badreddin, 2004).

A number of steady state models have been developed in the last three decades. There are two types of steady state models, simple and rigorous analytical models. Simple mathematical models of the MSF process are based on simplifying assumptions which are not sufficiently accurate since they generate a large discrepancy of the model's results when compared to actual data. However,

they are very useful to provide quick estimation of the main process variables, whereas rigorous models provide more accurate and useful information for system design and simulation (Hamed et al., 2004).

From the literature, the following assumptions are made in the development of simple models for the MSF system:

- ➢ Steady state operation.
- ➢ All the saline liquid droplets are removed by the demister and thus the distillate product is salt free.
- ➢ The subcooling of the condensate or superheating of the vapour is negligible.
- ➢ Constant heat transfer area in each section of the plant.
- ➢ Constant physical properties: this means assuming constant values (not as a function of temperature and salinity) for the specific heat at constant pressure for the flashing brine, the latent heat for evaporation.
- ➢ Constant overall heat transfer coefficient: this assumption is based on the first assumption. As long as the physical properties are constant, then the overall heat transfer coefficient is constant since the variation of the heat transfer coefficient depends on the physical properties.
- ➢ Constant thermodynamic losses: assuming the thermodynamics losses, such as boiling point elevation and non-equilibrium allowance, constant can make the calculations of the flashed off temperature and condensed vapour more easily.
- ➢ Constant latent heat of vaporization: this value is assumed constant and evaluated at the average temperature for the flashing brine.
- ➢ Negligible heat losses to the surroundings: this is a common assumption among all models since adiabatic system is assumed. Moreover, the calculations of the heat losses are very difficult and require knowledge of the external heat transfer area of the system.
- ➢ Negligible heat of mixing: this is true since the released heat of mixing one cubic meter of water is much smaller than the heat required for vaporizing the same amount of water.

➢ Negligible heat and vapour losses due to venting system: small part of the product water vapour is lost in addition to heat losses through the venting system. Neglecting these values simplifies the calculations of the model.

A simple model was presented by Mandil and Ghafour (1970). They assumed constant physical properties, heat transfer coefficients and temperature drop in all stages. The results of the model provide a closed form analytical solution that are used to calculate the specific heat area and the performance ratio. Coleman (1971) developed a simple, stage-to-stage calculations model to formulate a method for cost optimization. He assumed constant specific heat capacity for the water flowing through the condenser, linear boiling point temperature elevation (BPE) against salinity concentration, constant overall heat transfer coefficient in the condenser tubes and no fouling. Model equations were linearized and reformulated for ease of sequential or iterative solution. Moreover, he used high temperature operation (steam temperature 300 ᵒF) and seawater temperature of 70 ᵒF.

Soliman (1981) relaxed the assumptions further by providing different values for different parameters in the different sections of the plant. The model assumed a linear temperature profile and constant value for heat transfer coefficient in each section. The latent heat of vaporization of water is assumed constant and independent of temperature. He considered different operating parameters for each plant section and assumed constant value for BPE losses; however, the non-equilibrium allowance (NEA) effect was neglected. The model was very fast in convergence and suitable for optimization.

Darwish (1991) developed a simple model of MSF process in an attempt to arrive at a better quantitative evaluation of design and operating parameters on MSF process performance. The following assumptions were made to make the model simple: constant and average temperature drop of the flashing stream per stage, average latent heat of vapour and specific heat of distillate, constant and average values for the cooling water and brine streams. Fouling factor was included to be different from section to section; however, its effect on heat transfer coefficient was not mentioned. Another simple model was presented by El-Dessouky et al. (1998) to study the performance of the MSF process. The analysis is based on performance characteristics for a number of simplified configurations starting

from single stage flashing unit to multistage flash unit with brine recirculation. They concluded that the MSF with brine recirculation is the most sufficient configuration where the heat rejection section is not less than three stages.

Despite the fact that the simple models are useful to provide quick estimates of the main process characteristics, their main disadvantage is the deviation between the results of the model and the actual plant data due to the simple assumptions mentioned before. In addition, it is unable to provide the whole picture for the entire process. Therefore, more detailed models are required, where the physical properties are calculated as a function of temperature and salinity, to provide more accurate and useful information for system design and simulation. Rigorous or detailed models include correlations for temperature losses, pressure drop, stage temperature profiles and the heat transfer coefficients.

The above assumptions in the simple model are relaxed more in the development of detailed model of MSF process:

- ➢ Steady state operation.
- ➢ The distillate product is salt free.
- ➢ The heat losses to the surroundings are negligible.
- ➢ As for simple model, heat of mixing is negligible.
- ➢ The subcooling of the condensate or superheating of the vapour is negligible.
- ➢ Constant heat transfer area in each section of the plant.
- ➢ All the saline liquid droplets are retained in the demister.

Glueck and Bradshaw (1970) were among the earliest to present a model for MSF plants with higher degree of rigour and few assumptions taking into account the variation of heat transfer coefficient. However, no results were presented and the used properties correlations were not included in their work. It is to be mentioned that this model was used for dynamic behaviour as well. Beamer and Wilde (1971) developed a physical and economic model using stage-to-stage calculations to optimize MSF plant. Their calculations started from the cold end to the hot end of the plant with the brine heater the last stage. The available values of the stream variables on one side of a stage as well as the stage

parameters would allow the solution of the stage model to reach the stream variables on the opposite side of the stage.

Barba et al. (1973) have developed a simple and a rigorous models for control and simulation of existing MSF plants. They carried out stage-to-stage calculations starting from the hot end of the plant using online computer control system. The simple model solution was then used to provide the initial guesses for the rigorous model. The fouling factors were calculated as average values for each of the six stages in the recovery section. Rautenbach and Buchel (1979) developed a mathematical model with a modular structure to design and simulate different configurations of a desalination plants including MSF process. The material properties within the model's equations were known functions of temperature and concentration. Their modular approach showed some kind of robustness to handle design and simulation of MSF plants. The solution of the model was done by stage-to-stage calculation starting from the hot end of the plant. However, to compute the output stream variables, the solution of sequential modular approach required complete knowledge of the input streams and the equipment characteristics. Omar (1983) used his model, which was developed in his work in 1981, to simulate and model MSF using stage-to-stage calculations to solve the model equations. The mathematical model was translated into a Fortran IV computer with the aid of an IBM 370 machine. The program can be used to either design or simulate plants accurately in actual operation. Thermodynamic losses such as boiling point elevation and the non-equilibrium allowance were included.

Helal et al. (1986) developed a rigorous method to solve the detailed steady state model of the MSF plant. The method depends on decomposition of the large non-linear equations, which describe the behaviour of MSF desalination plant, into smaller subsets followed by iterative sequential solution of these subsets. The new feature of the method was the formulation of enthalpy balance and heat transfer equations, after linearizing them, into a tridiagonal matrix (TDM) form and then solved by the Thomas algorithm. The extensive testing of the computer program developed using this method showed that the method is numerically stable and convergence is rapidly approached over a wide range of initial conditions. The model included temperature losses across demister and

condenser tubes. Constant fouling and other thermodynamic properties are taken into account.

Similarly to Helal et al. (1986), Al-Mutaz and Soliman (1989) developed a model to simulate MSF plant. However, they used the orthogonal collection method to calculate the stream profiles across the stage by selecting very few stages to be solved instead of solving mass and energy balance for all stages. The authors claim that the method is twice as fast as the TDM model and requires less computational time compared to the TDM method. Steady state models were developed by (Husain et al., 1993, Husain et al., 1994) when an advance computational platform (SPEEDUP) was used to solve the model equations. Another model was developed by Thomas et al. (1998). All of these models are described later in dynamic models. Their steady state equations were obtained by setting the time derivative terms to zero.

Aly and Fathalah (1995) used the TDM technique to present a steady state mathematical model to simulate MSF system with additional correlations for heat transfer and thermo-physical properties. The model was used to study plant performance over extended ranges of TBT and cooling seawater temperature. Results showed that uprating is a promising technique for increasing the production rate through elevated values of TBT. However, fouling and scale formation were the main concern. El-Dessouky et al. (1995) described a detailed steady state mathematical model to analysis the MSF desalination process. Their model takes into account the effect of fouling factors and the presence of NCGs on the overall heat transfer coefficients in the condensing tubes. However, the effect of NCGs on the overall heat transfer was neglected assuming that all NCGs were extracted by the venting system. The model also considered the heat transfer losses from the stages and the brine heater to surrounding and through rejection of the NCGs. In 1996, (El-Dessouky and Bingulac) developed an algorithm for solving the equations simulating the steady state behaviour of MSF desalination process. The presented algorithm is a type of stage-to-stage calculations approach and starts from the hot end of the plant. The main advantages of the proposed algorithm were: (1) less sensitive to initial guess, (2) fewer iteration steps to obtain the required solution and (3) no derivative calculations were required. The developed algorithm was implemented using the

computer aided design (CAD) interactive package L-A-S (Linear Algebra and Systems).

Rosso et al. (1997) presented a model similar to that previously developed by Helal et al. (1986). It is based on detailed physicochemical representation of the process, including in particular the geometry of the stages, the mechanism of heat transfer and the role of fouling. The model was not only used for design purpose, but it was also used to support the development of a dynamic model as it will be mentioned later in dynamic model, where the time dependent behaviour of the plant can be studied.

Helal et al. (2003) developed a mathematical model to study the feasibility of hybridization of (RO) and MSF to improve the performance of the MSF and reduce the cost of desalted water. The design equations representing the process models as well as cost model were presented in their work. The calculations were carried out using SOLVER optimization tool of Microsoft Excel® software to maximize plant capacity. The model was based on the one developed by Soliman (1981), however, several additions and modifications were introduced to account for the different design variations. Aly and El-Figi (2003) described a steady state mathematical model to analysis both MSF and MED. For the MSF process, the model accounts for the geometry of the stages, the mechanism of the heat transfer and also the role of fouling and its effect. The main goal of the study was to produce desalted water at lower price by changing operating variables. The results obtained from the model were compared to actual data and good agreement was obtained. Abdel-Jabbar et al. (2007) developed a mathematical model for MSF process. This study was motivated by the need for an integrated model on design of large scale MSF units. Clean operation is assumed and consequently no fouling was taken into account. The model focused on evaluation of the weir loading, stage dimensions of the condenser tubes bundle, demister dimensions, as well as the flow rates and temperature profiles.

Tanvir and Mujtaba (2006a) presented steady state model for MSF process using gPROMS modelling tool. In their model, instead of using empirical correlations from literature, a Neural Network (NN) based correlation developed earlier (Tanvir and Mujtaba, 2006b) is used to determine the BPE. This correlation is embedded in the gPROMS based process model. It was found that the NN based

correlations can predict the experimental BPE very closely. They obtained a good agreement between the results reported by Rosso et al. (1997) and those predicted by their model. In 2008, the same authors developed a model based on Helal et al. (1986) incorporating neural network (NN) based correlation for physical properties estimation. Using MINLP technique within gPROMS model builder, the number of flash stages as integer variable and few significant operating parameters such as steam temperature, recycled brine flow and rejected seawater flow are optimized while minimizing the total annual cost of the process. The results revealed the possibility of designing stand-alone flash stages which would offer flexible scheduling in terms of connecting new units and efficient maintenance of the units throughout the year. The neural network (NN) technique had been used by Hawaidi and Mujtaba (2011b) to develop a correlation which is used to calculate dynamic freshwater demand/consumption profiles at different times of the day and season.

Alasfour and Abdulrahim (2009) formulated and implemented a rigorous steady state mathematical model using process simulation software IPSEpro®. For accurate simulation, the flashing stage was decomposed into three main compartments; flashing pool, distillate tray and tube bundle. The thermo-physical correlations are considered as a function of temperature and salinity. Moreover, to account for the effect of small changes in temperature, the energy balance of the model was carried out using stream enthalpy instead of the specific heat. The energy losses from the flashing stage and the brine heater were taken into consideration. The effect of NCGs on the overall heat transfer coefficient was considered in their model. However, assuming a constant amount of NCGs in all stages resulted in some disagreement in overall heat transfer coefficient and heat flux between actual results and simulation results.

Hawaidi and Mujtaba (2010b) developed a steady state mathematical model of MSF based on the basic laws of mass and energy balances along with the support of the physical properties correlations. Calculations of fouling factor were included in their model by developing a simple linear dynamic fouling factor profile that allows calculation of a fouling factor at different operation time (season). gPROMS model builder software is used for model development, simulation and optimization. The model is validated against the simulation results reported in the

literature. The model is then used to study the impact of a changing brine heater fouling factor under the variation of the seawater temperatures. Also, for fixed water demand and for a given steam and top brine temperature, the impact of fouling on the performance ratio also studied. Said et al. (2010) described a steady state model of MSF process including correlations which consider the effect of the presence of NCGs and fouling factors on the overall heat transfer coefficient. The simulation results showed decrease in overall heat transfer coefficient as NCGs concentration increase. Also, compared to the results obtained by Rosso et al. (1997) and Tanvir and Mujtaba (2006a) which were without NCGs, Said's results showed an increase in steam flow rate due to the presence of NCGs by 0.015 (wt%).

Abdul-Wahab et al. (2012) also developed a mathematical model for the MSF plant. The model was solved using the TDM method suggested by Helal et al. (1986) and was based on basic principles of physics and chemistry that describe the stage occurring in the desalination process. Most of the parameters that are known to affect the operation of the MSF plant were taken into account in building the model. No heat losses, fouling or NCGs were considered. The model was considered to be sufficient and accurate since its results were compared with vendor simulation results and the actual operating plant data for the MSF desalination plant, and matching was found to be very good.

A summary for the most of the previous studies on the steady state modelling of the MSF process is shown in Table 2.1.

Table 2.1: Previous work on steady state models for MSF desalination

Authors, Year	Description of the Model	Objective
Mandil & Ghafour, 1970	A simple model with constant thermo-physical properties.	Optimization of multistage flash desalination
Gluek & Bradshaw, 1970	A higher degree of rigorous model with few assumptions. Include heat transfer variation, fouling, boiling point elevation.	To provide an accurate representation of a typical MSF plant
Coleman, 1971	Simple stage-to-stage calculations model, constant specific heat for cooling brine, linear TE correlation, no fouling/scaling.	Cost Optimization
Soliman, 1981	Simple model with linear temperature profiles, constant heat transfer coefficient, constant boiling point elevation (TE).	Examining the effect of cooling water temperature and flow rate
Flower & Karanovic, 1982	A simple model with further relaxation assumptions. Vapour temperature for all stages is assumed.	Further relaxation of the assumptions.
Omer, 1983	Stage to stage simulation program. Thermodynamic losses and non-equilibrium were included.	Simulation and design of MSF
Helal et al, 1986	Rigorous stage to stage model. Physical properties are a function of temperature and nonlinear TE correlation. Fouling and other properties were included.	Developing new technique to solve the large system of nonlinear equations.
Al-Mutaz & Soliman, 1989	Steady state model based on Helal et al. New method called orthogonal collect was used to calculate the stream profile by selecting few stages.	Simulation of existing of MSF.
Darwish, 1991	Simple model. Constant average value for specific heat and latent heat. Fouling and NCGs were neglected.	Study the effect of some operating and design parameters.
Aly & Fathalah, 1995	Mathematical model using TDM technique. Additional correlations for heat transfer and physical properties.	Exploring MSF plant performance by extending TBT and cooling water temperature.
El.Dessouky et al, 1995	Mathematical model including: constant fouling factor, NCGs and heat losses to surroundings.	Analysis and predicting performance of existing MSF plants.

Table Cont'd

El.Dessouky & Bingulac, 1996	Model based on stage to stage approach. Less sensitive to initial guesses and few iteration steps.	Developing algorithm to solve huge number of equations.
Rosso et al, 1997	Model similar to Helal et al. Including geometry of the stage, mechanism of heat transfer and role of fouling.	Simulation for design purpose and dynamic model development.
El.Dessouky et al, 1998	Simple model with constant value for specific heat and overall heat transfer coefficient. Fouling and NCGs not included.	Study the performance of different simplified configurations of MSF.
Helal et al, 2003	Mathematical model based on Soliman. Linear temperature profiles, constant heat transfer coefficient and latent heat.	Study the feasibility of hybridization of (RO) and MSF.
Tanvir & Mujtaba, 2006a	Mathematical model including NN based correlation to determine the TE.	Developing new TE correlation instead of using from literature.
Abdel-Jabbar et al, 2007	Model focused on evaluation of the weir loading stage dimensions of the condenser tubes bundle and demister dimensions.	Modelling and simulation of the performance of large MSF units.
Tanvir & Mujtaba, 2008	Mathematical model including NN based correlation for physical properties.	Optimal performance at minimum cost.
Alasfour and Abdulrahim, 2009	Rigorous model includes energy losses, effect of NCGs and using stream enthalpy instead of specific heat.	Detailed Simulation of MSF process.
Hawaidi & Mujtaba, 2010b	Mathematical model including simple linear dynamic fouling factor profile.	Studying the changing brine heater fouling factor with varying seawater temperature.
Said et al., 2010	Steady state model considered the effect of the NCGs and fouling on heat transfer coefficient.	Study the effect of the NCGs on the performance of MSF.
Abdul-Wahab et al., 2012	Mathematical model based on Helal et al. heat losses, fouling and NCGs were not considered.	Study the performance of MSF under variation of some parameters.
This work	Mathematical mode considered the release of NCGs and their effect on the overall heat transfer coefficient.	Study the optimum location of the venting points.

2.3 MSF Dynamic Model

Dynamic models are used for unsteady-state simulations of the process and for control purposes. In both cases, the model of the process must be connected to the model of the control system to accomplish the simulation of the whole process (Husain et al., 1993). Dynamic models are useful in trouble shooting, fault detection, reliability, start-up and shutdown conditions and to implement advanced control (Gambier and Badreddin, 2004). It is also can be used to validate steady state models for $t \to \infty$.

Apart from the assumptions mentioned in detailed steady state model, the following additional assumptions are stated in the development of dynamic model:

➤ The model is developed using lumped parameter analysis, the mass considered to be perfectly mixed and spatial variation were not explicitly considered.

➤ Neglecting the presence of non-condensable gases and blow-through phenomenon.

➤ For each stage the liquid and vapour are in equilibrium.

➤ Mass cooling brine in condenser tubes remains constant and there is no accumulation of salt in the condenser tubes.

➤ The non-equilibrium parameter depends on water temperature and salt content.

It is believe that Glueck and Bradshaw (1970) were the first to develop a dynamic model to provide an accurate representation of a typical MSF plant. In their model, the flash stage is divided into four compartments, with streams and their capacities interacting materially and thermally among themselves. However, including a differential energy balance to the model combining with vapour space and distillate in the flash stage made the model over specified.

According to Reddy et al. (1995a) and other authors, a second effort of transient modelling was made by Delene and Ball (1971). They designed a digital code to simulate a large MSF desalinating plant dynamically. They considered the MSF process as consisting of two well mixed tanks to provide better representation of

the holdup of cooling brine flowing inside the tube. Empirical correlations were used to calculate evaporation rates and interstage flow, however, the NCGs in the vapour were not considered. Reddy et al. (1995a) also mentioned that Ulrich in 1977 carried out a simulation of MSF using Delene and Ball's model and found good agreement between measured and simulated results; however, significant deviations in the cooling water rate were noted.

Yokoyama et al. (1977) described a dynamic and physical model to predict start-up characteristics of MSF plant. The time dependence characteristics of MSF plant such as flashing brine, coolant temperature, brine level and heating steam flow rate to brine heater were calculated by HITAC 8450 Computer using Runge-Kutta-Gill Method. Two cases were considered for analysis of brine level behaviour. One was for no flashing phenomenon and the other was for flashing in the chamber. They mentioned that the difference between the actual and numerical results was due to the measurement error and estimated value of orifice coefficient.

Furuki et al. (1985) developed a dynamic model similar to the previous models by (Glueck and Bradshaw, Delene and Ball, and Yokoyama et al.) but used different brine flow equations to solve an automatic control system for the MSF process. For orifice flow equations, hydraulic formulas were applied. The model was used to study the start-up characteristic of the plant and to control the brine levels to avoid blow-through or liquid pile up on the stages. The dynamic stability of the plant was also studied by a real time dynamic simulator. Rimawi et al. (1989) solved a dynamic model for MSF once through plant. Nine stage variables are calculated by simultaneous solution of a set of energy and mass balances dynamic equations as well as thermodynamic relations and flow rate correlations. For duration of 15 seconds, they observed rapid and nonlinear variation in the heights of the brine and distillate pool.

Husain et al. (1993) developed a model with flashing and cooling brine dynamics. This model was improved later by the same authors (Husain et al., 1994) by considering distillate dynamics. The model was solved by two methods, one using SPEEDUP package, and the other using a specifically written program based on Tridiagonal matrix method (TDM) formulation. For period of 90 minutes, the steam flow rate to the brine heater was reduced by 26 percent, the simulation

results obtained showed good agreement with the actual data for the same reduction of the steam flow in the real plant. Moreover, their studies showed that the brine levels in the flash stages are quickly affected by the steam flow rate and temperature. Reddy et al. (1995a) made more improvements to the model and included brine recycling which gave more accuracy and faster convergence. Reddy et al. (1995b) have reported a holdup and interstage flow model for accurate estimation of liquid level upstream of the orifice.

A theoretical model which simulate the transient behaviour was reported by Aly and Marwan (1995). The model was based on coupling the dynamic equations of mass and energy balances for brine and product tray within flash stages. The model was solved by combination of Newton-Raphson and Runge-Kutta methods. A step increase in feed water temperature was investigated and responses of the system variables in different stages were illustrated. Maniar and Deshpande (1996) carried out a dynamic model applying empirical correlations for the evaporation rates. The degrees of freedom based on a dynamic model were used to determine the number of controlled and manipulated variables. The SPEEDUP package was used to simulate the MSF process.

A complete model for steady state as well as for dynamic simulation was proposed by Thomas et al. (1998). The models, steady state and dynamic, were based on the same set of equations and were of the same order. The flashing stage was divided into four compartments; flashing brine tray, product tray, vapour space and condenser tubes. The simulation code had been written in C and implemented in a UNIX-based system. However, the absence of a controller in the simulation resulted in a discrepancy between the actual and predicted responses.

Falcetta and Sciubba (1999) described a dynamic simulation of MSF plant using a modular simulator (CAMEL). Originally, the code was developed with the purpose of simulating thermal power plants only, but its structure was designed to simulate MSF plant. The authors validated their model against experimental data and the results showed good agreement between the two. However, the lack of details of the mathematical model makes it difficult to critically assess the model.

Mazzotti et al. (2000) developed a dynamic model of MSF taking into account stage geometry and including variations of the physical properties as a function of temperature and concentration as well as thermodynamic losses. The model equations are solved by LSODA routine. The results obtained by this model were not compared with previous results due to the lack of detailed information in the literature about the operating parameters adopted. However, some nonlinear dynamic features of the model make it useful in order to develop optimal control strategies.

In 2001, Tarifa and Scenna presented a dynamic simulator for MSF desalination plant. It takes into account the dynamics of heaters and stages, hydraulic, standard instrumentation and control systems. Using Delphi 5.0, a computer visual language, the simulator studied the effects of faults that may affect a MSF system, which might be caused by the failure of the pumps, heaters and controllers. Since this model was formed by a large algebraic equation system (AEs) combined with large ordinary differential equation system (ODEs), Tarifa et al. (2004) developed a new method called heuristic selection (HS) to increase the solution conversion and the robustness of the model presented by (Tarifa and Scenna, 2001). The HS method produces a set of decision variables, a set of subsystems, a set of variables for iteration, a set of equations for verification and all of the possible calculation sequences. The purpose of developing such method was to develop a dynamic simulator for MSF desalination process.

Shivayyanamath and Tewari (2003) developed a simulation program to predict dynamic behaviour of MSF plants. Using FORTRAN 95 and the Runge-Kutta technique, stage-to-stage calculations have been carried out to simulate and model the start-up characteristics of MSF plant. Variations of all the thermodynamic properties with temperature and salinity were considered. Apart from neglecting the distillate holdups, the inter stage brine flow rates are assumed to be constant. This reduced the model to simulation of the energy dynamics within the brine heater and flashing stages. Therefore, it was possible to determine the start-up time to reach steady state conditions.

Gambier et al. (2002) presented a hybrid dynamical model of the brine heater for the MSF plant with satisfactory simulation results. The nonlinear model was implemented in Matlab/Simulink, where algebraic equations were implemented

as S-function. The model could be used to study the system behaviour by simulation, supervisory control and fault handling. Due to the fact that most models are too large for control design as well as for fault detection, where models have to be computed in real time, reduce dynamic model was presented by Gambier and Badreddin (2004) for analysis and control design purpose. For control purpose, the model was simpler than the models derived from the physics of the underlying process. A block oriented library for Matlab/Simulink was presented so that different plant configurations can be implemented as block diagram to simulate the system and to test control algorithms. The main obstacle was the lack of real time data.

Sowgath (2007) presented a detailed dynamic MSF process model describing the physical behaviour of the plant and the operating procedure. The model considered non-equilibrium effects, demister pressure drop and the brine and distillate hold up equations. The model was validated at steady state against literature results and good agreement was obtained between the model's results and those from literature. David et al. (2007) used gPROMS to develop a comprehensive dynamic model of the MSF. The model presented several new features including details of temperature losses, blow through mechanism and correlations for the heat transfer coefficients, transport properties, and thermodynamic properties. An attempt was made to simulate the '*the blow-through*' phenomenon inside brine orifices and the presence of NCGs, which always neglected in the previous works. However, the model was applied for an experimental unit and was not validated against real plant operating data. Later, Al-Fulaij et al. (2010) extended the work of David et al. (2007) to simulate dynamic and steady state performance of MSF-OT using gPROMS. The model results showed good agreement against field data of industrial scale MSF-OT units.

Bodalal et al. (2010) presented a dynamic model to predict the performance of MSF plant using a dynamic analysis. The model developed was based on coupling the dynamic equations of mass, energy and momentum. The model was solved using the fifth order Runge-Kutta method and was able to investigate the effects of some key parameters such as sea water concentration and other thermal parameters that may affect the general performance of the MSF plant during transient as well as steady state operation condition.

Hawaidi and Mujtaba (2011b) developed a dynamic model for storage tank linked to freshwater line of the MSF process which helps avoiding dynamic changes in operating conditions of the process. The model was solved using gPROMS tool. For a given design configuration, the operation parameters were optimized at discrete time intervals (based on the storage tank level which is monitored dynamically and maintained within a feasible level, while the total daily cost is minimized. Al-Fulaij et al. (2011) developed a mathematical model for MSF-BR plant that includes the demister losses, distillate flashing and NCGs. The model was coded and solved using gPROMS. Before using the model to predict the stability regimes of the plant and study the plant behaviour under some operating conditions, it was validated for steady state and dynamic operation. However, the model neglect the heat losses to the surroundings and also the NCGs are considered as mass of vapour and their effect on the overall heat transfer coefficient was not studied. Recently, Sowgath and Mujtaba (2015) developed an operational schedule for a particular spring day by carrying out a dynamic optimization formula using MSF dynamic model. For fixed fresh water demand and maximum performance ratio, the steam temperature profile of MSF process is optimized with subject to the variation of the intake seawater temperature.

A summary for the most of the previous work studies on the process dynamics of the MSF process is shown in Table 2.2.

Table 2.2: Previous work on dynamic Models for MSF since 1970

Authors, Year	Type/Description of Model	Limitations
Gluck and Bradshaw, 1970	The flash stage was divided into four compartments, streams were interacting materially and thermally among themselves.	Over specified.
Delene and Ball, 1971	Designed a digital code to simulate MSF by considering the MSF process as consisting of two well mixed tanks, holdup of cooling brine is included.	Simple and no fouling or NCGs.
Yokoyama et al., 1977	Model using Runge-Kutta-Gill Method to predict start-up characteristics such as flashing brine and coolant temperature.	Estimated value of orifice coefficient was not accurate.
Hussain et al., 1993	Dynamic model with flashing and cooling brine using SPEEDUP package and Tridiagonal matrix method (TDM) formulation.	No venting system for NCGs and no fouling.
Reddy et al., 1995	Improvement of Hussain's model by including brine recycle, a holdup and interstage flow were.	No venting system for NCGs and no fouling.
Aly and Marwan, 1995	Dynamic model solved by combination of Newton-Raphson and Runge-Kutta methods.	No venting system for NCGs and no fouling.
Maniar and Deshpande, 1996	Using SPEEDUP package for dynamic model, empirical corrections for the evaporation rates, some of controlled variables were investigated.	No venting system for NCGs and no fouling.
Thomas et al., 1998	Using simulation code written in C and implemented in a UNIX-system. The flashing stage was divided into four compartments.	A difference between the actual and model results due to non-inclusion of the controller.
Mazzoti et al., 2000	Dynamic model including: stage geometry, variation of the physical properties as a function of temperature and concentration.	Not compared with the previous results due to the lack of detailed information in the literature.
Shivayyanamath and Tewari, 2003	Using FORTRAN 95 and Runge-Kutta method, stage-to-stage calculations, variation of the physical properties with temperature and salinity.	No venting system for NCGs, no fouling and neglecting the distillate holdups.

Table Cont'd

Gambier and Badreddin, 2004	Dynamic model for analysis and control design purpose. Using Matlab/Simulink.	Lack of real time data.
Sowgath, 2007	A model considered non-equilibrium effects, demister pressure drop and the brine and distillate hold up equations.	No venting system for NCGs and no fouling.
Hawaidi and Mujtaba, 2011	Dynamic model for storage tank linked to fresh water line. gPROMS used to solve for temperature variation.	The dynamic model for the storage tank not for MSF process.
Al- Fulaij et al., 2011	Dynamic model that included the demister losses, distillate flashing and NCGs. The model was solved used gPROMS.	The effect of NCGs was neglected.
Said et al., 2012	Dynamic model for storage tank linked to fresh water line. gPROMS used to solve for the temperature variation and water demand.	The dynamic model for the storage tank not for MSF process.
Sowgath and Mujtaba, 2015	Dynamic model for optimization purpose. Operational schedule was developed to optimize the steam temperature.	A simple model that neglected the NCGs and variation of fouling
This work	A detailed dynamic model included GMC and hybrid Fuzzy-GMC control and dynamic fouling.	A dynamic venting system was not included in this model

2.4 Fouling Model

As mentioned in the previous chapter, fouling on heat transfer surfaces, due to scale formation caused by high temperature, is the most critical factor in thermal desalination industry. With time, these materials continuously build up a fouling film causing an increase in the thermal resistance and reducing the performance of process equipment (Al-Anezi and Hilal, 2007). The performance of MSF plants is mainly affected by the condition of heat transfer surfaces, therefore, scales on these surfaces by seawater containing salts can impede the rate of heat transfer and reduce the efficiency of the heat transfer process resulting in poor performance of the plant. Moreover, increasing the layer thickness of the scales results in narrowing the tubes pass and consequently increase the energy

consumption (of pumps) to maintain a constant flow rate. Seawater always has the tendency for scale formation and fouling problems due to dissolved salts and finely suspended solids. As highlighted in Mujtaba (Mujtaba, 2008, Mujtaba, 2010), at high temperature, water with soluble salts allows deposits to form scale which can reduce the heat transfer rate and can increase specific energy consumption and operating costs. This can cause frequent shutdowns of the plant for cleaning. Due to the fouling tendency, the MSF pumps and the heat transfer equipment are overdesigned with allowable 20 to 25% excess in heat transfer surface area thus increased capital cost. This results in an increase of about 30% of the total cost (Gill, 1999).

The fouling process cannot be avoided under any circumstances and thus scheduled cleaning is required. However, understanding and accurate simulation of the fouling process can help the designers to reduce the overestimated design fouling factor and thus, reduce the cost of extra surface area.

Although a number of experimental studies have been carried out on the effect of scaling and corrosion, scale formation at the heat transfer surface is still not understood properly and it is main drawback link in the design of heat transfer equipment. Moreover, the complexity and nonlinearity of MSF process due to a continuous change in temperature and salinity makes the prediction of fouling behaviour difficult. One of the early attempts to model fouling behaviour was conducted by Kern and Seaton (1959) when they confirmed that the fluid velocity plays an important role in limiting the increase of the fouling thickness by considering a constant rate of deposition and increasing removal rate, so that the process of fouling reaches steady state when the removal rate becomes equal to the deposition rate (Cooper et al., 1983). Although it is a simple model and ignored several parameters that may be responsible for the scale formation, it is considered to be the basic model on which further models have been developed. Hasson et al. (1968) developed a diffusion model to control only $CaCO_3$ scale deposition in heat transfer surface. Experimental data from double pipe heat exchanger was used to validate their model and found out that the scale growth of $CaCO_3$ varies with Reynold's number and is only slightly dependent on surface temperature. Later, Gazit and Hasson (1975) developed a kinetic model to study the parameters that affect the $CaCO_3$ scale formation in film flow desalination

process. Using a heated aluminium tube, the main parameter to be examined was the effect of evaporation temperature on the kinetics of scale formation.

Taborek et al. (1972) developed a fouling model to study $CaCO_3$ scaling in a cooling tower. It was assumed that the rate of deposition depends on the flow velocity. However, the model was criticized on having many unknown variables and no experimental data were presented to estimate these variables. Hasson et al. (1978) developed an ionic diffusion model to predict the fouling rates of $CaCO_3$. Later, in 1981, Hasson modified his model to predict the crystallization rate of $CaSO_4$ (Sheikholeslami, 2000). Cooper et al. (1983) adopted the Kern and Seaton model to study the behaviour of fouling in MSF under different operating conditions. Cooper and his co-workers concluded that the behaviour of fouling in MSF plants cannot be explained by linear relationship between fouling and time and such relationship was shown to be invalid. Müller-Steinhagen and Branch (1988) modified Hasson's ionic diffusion model to calculate the scaling rate of $CaCO_3$ in double pipe heat exchanger. However, the drawback of these models is that they do not account for removal rate since they relied on the Hasson's assumption that the equation is valid for flow velocity less than 0.8 m/s.

Mubarak (1998) developed a kinetic model for scale formation based on experimental data to study the reaction mechanism leading to $CaCO_3$ deposition and calculate the deposition rate with and without the presence of antiscalant at fixed TBT (90 ^{o}C). Brahim et al. (2003) developed a model to calculate the $CaSO_4$ scale formation using computational fluid dynamics (CFD) code FLUENT. The results showed a good agreement with experimental data. Bohnet (2005), describes a fouling model which involves rate of deposition correlation of second order reaction of $CaSO_4$ and combines diffusion rate and reaction rate to eliminate the unknown concentration of the calcium and carbonates ions at the solid-liquid surface. The model describes the transport, deposition and removal of the scale. Mwaba et al. (2006) developed a semi-empirical correlation to predict the nucleation phase of the fouling scale in heat exchanger by introducing roughness enhancement factor. It was assumed that for the case of $CaSO_4$, the deposit rate was controlled by the surface reaction and neglected the diffusion rate assuming that the concentrations of the ions in the bulk and at the solid-liquid surface are the same. The model was validated against experimental data and

good agreement was obtained between the model prediction and the experimental data.

Al-Rawajfeh (2008) developed a model combining mass transfer and chemical reaction to calculate the release of CO_2 and its relation to the deposition of $CaCO_3$ in once through and brine recirculation MSF process. Segev et al. (2012) developed a kinetic diffusion model that allows the study of multicomponent transport of all ionic species involved in carbonic fouling system. The effect of pH level on the deposition rate was studied using simplified and rigorous models. Based on Brahim's work (Brahim et al., 2003), Zhang et al. (2015) developed a generic CFD model to predict the fouling behaviour of $CaSO_4$. The model avoided the simplification step adopted by Brahim et al. (2003) by coupling solution domain with fouling layer domain through bi-directional transfer.

Despite the large aforementioned publications on the fouling process, most of these models have been developed and studied on their own but have not been a part of the MSF process models. Moreover, most of the studies were conducted on heat exchanger, which can be found in many industries as stand-alone units. However, in MSF plants, the flashing stages can be considered as a series of connected heat exchangers where the fouling behaviour becomes more complex and hard to predict due to the continuous change of the temperature and salinity

While the majority of the developers of the MSF models use a constant fouling factor in their studies, which may lead to excessive or unnecessary overdesign, only a handful of studies focused on the modelling (or attempts to modelling) of scale formation in MSF process. Moreover, most of the experiments used a velocity less than 1 m/s where in the MSF process however, the velocity is between 1.5 m/s and 2.3 m/s (Helal, 2003).

During their comprehensive study to compare different types of antiscalant at fixed TBT and concentration factor, Hamed and Al-Otaibi (2010) estimated the fouling factor as the difference between the overall heat transfer coefficient at scaled condition and at clean condition. A regression analyses was used to obtain a linear correlation that describe the fouling factor. Hawaidi and Mujtaba (2010b) developed a linear dynamic model for brine heater fouling to study the impact of fouling with seasonal variation of seawater temperatures. Said et al. (2012) extended Hawaidi and Mujtaba's study to include the effect of fouling in the

stages using a steady state MSF model. These regression models do not consider a number of variables that may have critical effects on the fouling behaviour and consequently inaccurate results would be expected (Malayeri and Müller-Steinhagen, 2007). Al-Rawajfeh et al. (2014) extended the Al-Rawajfeh's work (Al-Rawajfeh, 2008) to develop a fouling model for MSF process. The model was implemented on brine recirculation and once through MSF process with and without antiscalant. The results were compared to experimental data and simulation results from literature. However, the model only accounted for the deposit rate and neglected the removal rate.

Although the above few publications are well established, all of them have neglected the dynamic variation of seawater salinity and temperature. In the brine recirculation MSF process in particular, the temperature and salinity of the recycled brine change with the change in fouling rate. A summary for the most of the previous work studies on the fouling models in MSF process is shown in Table 2.3.

Table 2.3: Previous work on fouling Models in MSF

Authors, Year	Type/Description of Model	Limitations
Mubarak, 1998	A kinetic fouling model to estimate the crystallization of $CaCO_3$.	Constant temperature and neglect of salinity effect.
Al-Rawajfeh, 2008	Steady state fouling model to estimate the deposition of $CaCO_3$ by calculating the CO_2 release.	Constant salinity. Neglect of the removal rate and velocity effect.
Hamed and Al-Otaibi, 2010	A linear correlation to predict dynamic fouling factor.	Simple model at constant temperature and salinity
Hawaidi and Mujtaba, 2010b	A linear dynamic fouling model for brine heater with variation of seawater temperature.	Simple model and neglected the effect of salinity.
Said et al., 2012	Steady state fouling model for MSF stages.	The effect of salinity was neglected.
Al-Rawajfeh et al., 2014	Steady state fouling model to estimate the deposition of $CaCO_3$ and $CaSO_4$.	Constant salinity. Neglect of the removal rate and velocity effect
This work	Dynamic fouling model considered deposit and removal rate to predict the crystallization of $CaCO_3$ and $Mg(OH)_2$.	The model focused only on the fouling inside the condensing tubes.

2.5 Non-Condensable Gases (NCGs)

The non-condensable gases (NCGs), as the name implies, are not able to condense inside a condenser, unlike steam. These gases have boiling points so low that, for any operating temperature in the MSF process, they will remain in the gas phase. The presence of these gases (NCGs) in process water can have a serious impact on thermal desalination of seawater, which can reduce the performance and decrease the efficiency of the whole desalination plant, and consequently a cost increase in most thermal desalination units. The trap of these gases (NCGs) inside the condensation zone can cause the following:

➢ The surface area taken up by the NCGs will not be available for the steam to be condensate (Low heat transfer area), and

➢ The NCGs will reduce the overall heat transfer coefficient of the vapour inside the tube (Low heat transfer coefficient).

According to the heat transfer equation $Q = U \times A \times \Delta T$, any decrease in the heat transfer area or overall heat transfer coefficient will result in decrease in the amount of the transferred heat between the steam and the cooling seawater. In order to get the same amount of transferred heat, the temperature difference has to be increased. Consequently large amount of heating steam is required, which will reduce the performance ration PR of the plant (El-Dessouky and Ettouney, 2002).

Even low concentrations of NCGs gases can cause a severe reduction of the overall heat transfer coefficient and hence the performance of desalination process (Al-Anezi and Hilal, 2007). The most common NCGs in the MSF desalination plants are air (N_2 and O_2), argon and CO_2 and they are present in the plants due to the following causes:

➢ Small amount of all atmospheric gases are dissolved in the seawater feed.

➢ The leakage of ambient air through flanges, man-holes and instrumentation nozzles into the flash chambers due to the vacuum conditions present.

➢ Release of carbon dioxide from decomposition of the bicarbonates at high
or from the breakdown of the bicarbonates by acidified seawater with
mineral acids.

When the brine enters the flash chambers in MSF plants, the NCGs are released,
due to their low boiling points and the decreases of CO_2 solubility at lower
pressure, and carried with the steam into the plant (Glade et al., 2005). Steam
releases its latent energy to the process and condenses in the heat transfer area,
but the NCGs do not condense.

Carbon dioxide dissolves in the condensate and lowers its pH value causing, in
presence of O_2, serious corrosion problems in the vapour side of the flashing
zone and consequently leading to tube leakages and plant outages and reduces
the lifetime of the plant. Furthermore, accumulation of NCGs in multistage flash
(MSF) plant can lead to pressure losses for interstage brine transfer causing high
brine levels (Glade and Al-Rawajfeh, 2008). In addition, the release of CO_2 from
the evaporating brine increases the pH to higher values and considerably
influences the concentrations of HCO_3^-, CO_3^{-2}, H^+, and OH^- ions in the brine and
plays an important role in alkaline scale formation (Glade and Ulrich, 2003, Al-
Rawajfeh et al., 2005, Al-Anezi and Hilal, 2007).

Due to the low thermal conductivity of the NCGs, these gases create an insulating
resistance and hence affect the efficiency of the heat transfer for condensation,
increase the energy consumption and consequently reduce the lifetime of
desalination plants. Thus, removing them is essential to the efficient operation of
all desalination plants.

For NCGs to be removed from the feed seawater, the MSF-BR plants are usually
equipped with a deaerator, where molecularly dissolved gases namely nitrogen,
oxygen and argon can be removed almost completely from the make-up flow.
However, only part of the CO_2 can be removed by simple deaeration. For the CO_2
to be removed, the addition of a strong acid to the feed water and a decarbonator
are required. The acid lowers the pH value of the feed water and causes the
conversion of the bicarbonate and carbonate ions to dissolved molecular CO_2
which is then released almost completely in the decarbonator (Al-Anezi and Hilal,
2007, Glade and Al-Rawajfeh, 2008).

It is to be mentioned that for MSF-OT, which is not equipped with a deaerator, the O_2, N_2, and Ar content entering the plant with the feed seawater can be removed almost completely in the first three stages. This can be done by an adequate venting system which is installed in the MSF plants. Also, in MSF-BR, the liberated CO_2 and the remaining O_2, N_2 and Ar inside the flash chambers can be removed.

The main purpose of the venting system is to remove the NCGs in order to reduce their concentration. However, another usage of the venting system in MSF plants is to reduce the pressure inside the flash chambers, particularly during start-up, and hence more steam is produced at low temperature.

2.6 Control Strategies

Desalination plants are large and complicated. They are also energy-and cost intensive and above all, crucial to life support in several regions of the world. Consequently, these plants must meet high standards of performance, including optimality, cost effectiveness, reliability, and safety. The MSF plants are currently facing an enormous challenge in reducing the cost and increasing profitability. As a result, the MSF technology has experienced a gradual decline in investment in the last few years compared to other techniques for desalting water. Hence, a significant improvement in MSF technology is required in order to remain attractive for capital investors. Improved process control is a cost effective approach to energy conservation and increased process profitability.

Most industrial plants are non-linear in nature; the complexity of their non-linearity varies according to the physical function of each process. MSF desalination is a highly complex nonlinear process (Ismail, 1998, Ali et al., 1999, Lior et al., 2012); however, its non-linearity is represented in some operation conditions such as limitation on the brine temperature at the brine-heater outlet. Furthermore, the need for continuous monitoring of liquid levels in the flashing chambers is necessary to avoid loss of efficiency due to blow-through or loss of boiling due to flooding in the flash chambers. Therefore, an efficient and accurate control system in the plant to maintain the operation at optimum conditions is required.

Most of the MSF plants are currently operated under conventional PID controller due to its simplicity and well recognition by the industry (Algobaisi et al., 1991). However, PID controller is linear and cannot efficiently control highly sophisticated systems which contain nonlinear variables. Moreover, the tuning of the PID parameters is considered to be the main concern by engineers due to the time consuming and inefficiency. Although a lot of effort has been made to improve the tuning of PID parameters, there is no adequate single method to obtain optimum values for these parameters. Nevertheless, due to the change of the operating conditions of the MSF, the fixed tuning of PID controller for one condition would not be optimal due to change in sea water temperature seasonally and variable water demand and thus, new optimum values of PID parameters are required which can be consider as time consuming (Al-Gobaisi et al., 1994). The availability of powerful computer tools opened the way to implement the advanced process control (APC) strategies.

A number of studies have been conducted in the past few decades to implement APC strategies in the MSF desalination processes. Maniar and Deshpande (1996) applied Constrained Model Predictive Control (CMPC) for the MSF process. The manipulated variables for the controllers were calculated by solving an optimization problem with respect to the operating constraints. Though the authors obtained reasonable results, the nonlinearity of MSF process cannot be controlled well using linear CMPC. Later, Ali et al. (1999) utilized a reduced model to implement a robust control of MSF the process using Nonlinear Model Predicted Control (NLMPC) which was able to drive the plant to its steady state with a reduced computational time. Li et al. (2012) proposed a Cascaded Quadratic Dynamic Matrix Control (QDMC) as one of the MPC strategies for a Reverse Osmosis (RO) desalination process. Compared to PID control, the results revealed that the QDMC outperform the traditional PID control. Although it was developed four decades ago, Fuzzy Logic Controllers (FLC) are popular due to their ability to control very complicated systems (Alatiqi et al., 1999). Jamshidi et al. (1996) designed and implemented fuzzy controllers for MSF process to control the TBT. A genetic algorithm was applied to fuzzy control of a brine heater unit in MSF plant. The simulation results of the controlled TBT showed a significant improvement in convergence to the desired set point and

reducing oscillations and overshoot. Ismail and AbuKhousa (1996) combined a set of fuzzy rules to introduce a controller that resembles Proportional-Integral-Derivative (PID-like FLC). The controller was then introduced into the MSF process to control TBT. Ismail (1998) studied the capability of Fuzzy Model Reference Learning Control (FMRLC) for the TBT. In comparison with the conventional PID and direct fuzzy logic, the results showed that the FMRLC outperformed the other two types. For the same purpose of controlling TBT, Olafsson et al. (1999) designed and applied simple fuzzy control to brine heater in MSF process. In most of their study cases, the results showed that FLC can perform better or equally well as the conventional PID controller.

Neural Network System (NNs) is another technique used as APC to handle complex and nonlinear process. Ali et al. (2015) provided an excellent review on the application of NN based control (state observers) in many engineering systems. After successful implementation of NN techniques as optimization control strategy for seawater-desalination solar-powered membrane distillation unit by Porrazzo et al. (2013), Tayyebi and Alishiri (2014) proposed a nonlinear inverse model control strategy based on neural network for a MSF desalination plant. Using three-layer feed forward neural network, three loops were designed for controlling the TBT, the brine level in the last stage and salinity. A summary for the most of the previous studies on the control strategies implemented in MSF process is shown in Table 2.4.

Table 2.4: Previous work on advanced control strategies implemented in MSF

Authors, Year	Type/Description of Model	Objectives
Maniar and Deshpande, 1996	Constrained Model Predictive Control (CMPC) was designed to control the TBT, brine level and distillate flowrate.	Optimize plant performance and minimize the energy consumption.
Jamshidi et al., 1996	Genetic algorithms was applied to Fuzzy Logic Controller (FLC) to control the TBT.	To improve the convergence of the controller and reduce the oscillations.
Ali et al., 1999	Nonlinear Model Predictive Control (NLMPC) was designed to control the TBT and distillate flowrate.	To validate the performance of MSF reduced model against large size model.
Ismail AbuKhousa, 1996	PID integrated with FLC to develop Hybrid PID-Like-FLC to control the TBT.	To improve the performance of the control system in MSF plants.
Ismail, 1998	Fuzzy Model Reference Learning Control (FMRLC) to regulate TBT	To improve the performance of the control system in MSF plants.
Olafsson et al., 1999	Fuzzy logic Controller was developed to control the brine heater process.	To improve the operating performance of MSF plants.
Tayyebi and Alishiri, 2014	Designed neural network inverse model control to control the TBT, brine level and salinity.	To improve the control system in MSF plants.
This work	Generic Model control (GMC) and hybrid Fuzzy-GMC controller are designed to control the TBT and brine level.	To reduce the operating cost by improving the control system in MSF plants.

2.7 Dynamic Simulation and Optimization

Dynamic simulation of the MSF process can provide better understanding in system fault analysis, which could be caused by improper operating conditions. The data collected from simulation program are essential to propose, design and evaluate advanced control system for MSF process (Alatiqi et al., 2004). Due to the use of advanced software, the MSF process went through several dramatic modifications and improvements that have led to massive increase in the unit

capacity from 500 m^3/day in 1960s to 75,000 m^3/day in 1990s (Borsani and Rebagliati, 2005). It is clear that the development of desalination technologies over the recent years has been achieved due to the development process simulators. In fact, these are inexpensive tools that can be used for process performance analysis and design purposes (Al-Fulaij et al., 2011).

Optimization, on the other hand, is the use of the simulators to increase the efficiency and the performance ratio of the MSF plant at lower cost. The MSF plant operators can optimize their multi-stage flash distillation plants to operate at peak efficiency. Applications for simulation include:

- Optimizing the MSF plant to maximize the performance ratio ;
- Designing optimum operating conditions based on salt concentration and seasonal variation of the seawater temperature;
- Testing plant dynamic performance at different plant loads;
- Understanding impact of fouling on the plant performance and improve the efficiency of the anti-scale additives;
- Enhancing control strategies for cost reduction and improve product quality; and
- Diagnosing the adverse effects of NCGs on heat transfer rate.

Dynamic simulations can be carried out either off-line or on-line. In the former, there is no connection to the real plant and the input data are taken from a file. However, in the latter case, the input data are directly received from the actual operating data. In addition, it is necessary to support the simulators with proper correlations of various properties such as brine densities, concentrations, specific heat, liquid and vapour enthalpies, heat transfer coefficients and thermodynamic losses (Husain et al., 1993).

The use of general simulators for dynamic simulation is still limited. With increase in the complexity of the mathematical models of wide range of process units, advanced simulators are required to be more flexible, having robust solving procedures, comprehensive user interface and the capability to interface with external programs. However, several simulation tools used to model the MSF process are available in the literature. Husain et al. (1993) used SPEEDUP simulator, which possesses the capability for both steady state and dynamic

simulation, to simulate MSF plant. The top brine temperature (TBT) was set at 90 ^{o}C; the steam flow rate was reduced by 26% to study its effect. The actual plant data were available for similar change and compared to the simulation results. Good agreement between both sets of data was obtained. According to the authors, more simulations were carried out by introducing step changes in the steam and seawater inlet temperature; however, these results were not presented.

SPEEDUP was also used by Maniar and Deshpande (1996) to investigate the MSF control problem and find suitable control strategy to improve plant operations. The constrained model predictive control (CMPC) was used to provide set points to the existing PID controllers (Proportional-Integral-Derivative). In maximizing production, the results obtained showed an increase of the distillate flow rate from 18.89 tons/min to a maximum value of 21.67 tons/min. In term of energy minimization, the steam consumption was reduced from 2.581 tons/min to 2.520 tons/min while maintained the distillate flow rate at 18.89 tons/min. consequently, the performance ratio, which is a ratio of the distillate product produced over the steam consumed, increased by 2.45%.

Aly and Marwan (1995) used a computer program to simulate the dynamic configuration of the plant. The program was run on an IBM/XT 8088 compatible machine; however, the name of the program was not mentioned. Thomas et al. (1998) used simulation code written in C and implemented in a UNIX-based system. The simulation studied the effect of step changes in steam flow rate to the brine heater. After steady state reached, the steam flow rate was decreased by 5%, and then the model was allowed to run for 5000 seconds and after that the steam flow rate was increased by 5%. The responses of the plant model was also compared with that of the real plant and the results obtained were comparable.

Falcetta and Sciubba (1999) used modular simulator called 'CAMEL'. The MSF desalination process; a complete, 20-stage desalination plant was simulated under steady state and unsteady state operating conditions. Due to the lack of real data, the only attempt to validate the simulator in dynamic simulation was a step change of 12 degrees in the TBT set point from steady state winter conditions to derive the plant to a set point equivalent to summer condition, when

the TBT is low. In 2000, (Mazzotti et al.) used LSODA routine to dynamically simulate the MSF plant. In their simulation, four cases were studied; increase and decrease of the seawater temperature, decrease of seawater flow rate and finally increasing the steam temperature. The main parameter used to evaluate the process performance was the performance ratio between the product flow rate and the steam flow rate. However, no quantitative comparison with real plant responses was made.

Tarifa and Scenna (2001) studied the impact of faults that may affect the MSF desalination plant using Delphi 5.0, a computer visual language simulator. In addition to the operating parameters, the simulator allows the modification of MSF topology and design parameters such as number of stages, valve size, pump characteristics, stage and heater dimensions. The simulator was tested with data from real plants and it has shown a good performance. In 2002, (Gambier et al.) used MATLAB-SIMULINK to develop a hybrid model for a brine heater in a MSF desalination plant. The simulation software was used to analyse the behaviour of top brine temperature (TBT) when steam flow rate and the brine flow rate changed. In 2004, Gambier & Badreddin used a block-oriented library for MATLAB-SIMLINK to simulate different plant configurations as block diagram and to test control algorithms. Bodalal et al. (2010) used a computer package based on MATLAB with menu driven user interface to study the effect of the seawater flow rate, the steam temperature, and the seawater temperature on the performance of MSF plant. Good agreement was obtained when the simulator results were compared with some of the previous results and the actual data for more than one plant.

Sowgath (2007) used gPROMS software within a dynamic optimization framework to optimize steam temperature profile of the MSF process. For simulation purposes, incremental increase in steam temperature from 97 ^{o}C to 116.5 ^{o}C resulted in an increase in the plant production. For optimization purposes, on the other hand, several steps in changing seawater temperature were made to maximize the performance ratio (PR) of the MSF plant. David et al. (2007) simulated a dynamic behaviour of MSF plant using gPROMS. An attempt was made to simulate start-up operations and good agreement between their results and with those from literature was obtained. Their results showed that the

system responds with an increase in the temperature of all the stages due to an increase in the inlet brine temperature. Al-Fulaij (2011) used the gPROMS software to study the dynamic behaviour of MSF process by the analysis of the MSF dynamic response upon making step changes in the system operating parameters. In particular, the effect of steam temperature to the brine heater was studied and found out that the increase of steam temperature was limited to 2% of the design value. That is because the brine level in the flashing stages was less than the gate height, which in turn enables the vapour to escape which would stop the flashing process and the simulation. Also, according to the author, it was not possible to reduce the steam temperature by more than 3% because the brine level will increase until it fills the entire vapour space below the demister, which is not feasible during operation.

Said (2013) used the gPROMS software to simulate an intermediate storage tank linked between the MSF process and the customer to add more flexibility in meeting the customer demand. For design purposes, some operating parameters were optimized at discrete time interval while minimizing the total operating cost. The optimization results showed that an increase in the total operating cost occurs with decrease in the number of stages. In addition, the simulation studied the freshwater demand during weekend days and working days. During low consumption of freshwater, there was increase in the tank level and plant production, consequently the plant operates at maximum value of seawater rejected flow rate and at minimum value of brine cycle flow rate and vice versa.

A summary for the most popular simulators used for the process dynamics of the MSF process is shown in Table 2.5

Table 2.5: Simulators used for dynamic MSF process

Authors, Year	Software	Objective
Hussain et al. ,1993, 1994	SPEEDUP	Simulation
Aly & Marwan, 1995	-	Simulation
Maniar &Deshpande, 1996	SPEEDUP	Control and optimization
Thomas et al, 1998	SPEEDUP	Simulation
Falcetta & Sciubba, 1999	CAMEL	Simulation
Mazzotti et al, 2000	LSODA	Simulation
Tarifa & Scenna, 2001	Delphi 5.0	Simulation
Gambier & Badreddin 2002, 2004	MATLAB-SIMULINK	Simulation and control
Sowgath, 2007	gPROMS	Simulation and optimization
David et al, 2007	gPROMS	Simulation
Al-Fulaij, 2011	gPROMS	Simulation
This work	gPROMS	Simulation, modelling and control

2.8 Conclusions

In this chapter, a very detailed review has been presented on steady state and dynamic state models for MSF process. Also, the chapter has included some studies on optimization and simulation of MSF plants. In addition, the literature review covered detailed review on the fouling and NCGs, which are considered to be the main concern and have great impact on the performance of the MSF process.   Different control strategies that are implemented in MSF plants are also presented in this chapter. Based on the literature review, a dynamic model of the MSF process will be discussed in the next chapter.

CHAPTER THREE

Dynamic Modelling and Simulation of MSF Process

3.1 Introduction

Mathematical models of MSF process are well known in the literature and have been used successfully to simulate and optimize MSF process. Over the last three decades, mathematical models have been improved from simple to very detailed models and as a result, the MSF plants have gained a dramatic improvement in thermal performance and capacity. The basic approach of modelling is to utilize mathematical relationships among process variables. These relationships should include an accurate description of (i) mass/material balance, (ii) energy balance, (iii) thermal efficiency, (iv) physical properties (such as heat capacity, density, Boiling Point Temperature Elevation due to salinity, heat of vaporization), (v) Heat Transfer Coefficients (reflecting effect of fouling and NCGs), (vi) pressure and temperature drop, (vii) geometry of brine heater, demister, condenser, stages, vents (viii) inter-stage flow (orifice) (ix) thermodynamic losses including the non-equilibrium allowance and demister losses and (x) kinetic model for salt deposition and corrosion (Mujtaba, 2010).

In the last three decades, there has been interest in using computer modelling for choosing the most successful configurations. Therefore, many computing methods have been developed as tools to aid the designer in finding the optimum arrangement. Using a computer program, complicated calculations, which would take up to a month to complete by hand calculation, could be solved rapidly and accurately in few seconds. gPROMS is one of the available software packages and has been used successfully for modelling, simulation and optimization of the MSF process. It has many features such as the possibility of building the model at different levels. Apart from the availability, the gPROMS model builder was chosen for several reasons as cited from (Tanvir and Mujtaba, 2008):

- ➢ The model development time is reduced because the solution algorithm needs not to be written rather needs to be specified.
- ➢ The same model can be used for different simulation and optimization activity.
- ➢ The model does not have to be re-written with changing set of input specifications.
- ➢ The gPROMS model can be readily integrated with automation software, MS Office or any of the other standard tools (PROII, ASPEN PLUS, MATLAB, MATLAB Simulink, etc.) of the modern process manufacturing organization.
- ➢ gPROMS has an intelligent editor for easy construction and maintenance.

In this chapter, a comprehensive dynamic model of MSF is developed based on the basic laws of mass balance, energy balance and heat transfer equations. The model is supported by physical and thermodynamic properties of brine, distillate and water vapour. Temperature losses due to boiling elevation, non-equilibrium allowance and temperature losses through demister are also included. Most of these correlations are nonlinear and independent on salinity and temperature. The gPROMS model builder 4.1 is used to solve the equations. Finally, the model is validated against actual plant data reported by Al-Shayji (1998) and Alasfour and Abdulrahim (2009).

3.2 Model Equations

The model equations and supported physical properties correlations are reported by (Helal et al., 1986, Husain et al., 1993, Rosso et al., 1997, Thomas et al., 1998, El-Dessouky and Ettouney, 2002, Tanvir and Mujtaba, 2006a, Al-Fulaij et al., 2010, Said et al., 2010, Hawaidi and Mujtaba, 2011b, Reddy et al., 1995a). It is to be noted while most of the authors share the same correlations to predict the physical properties, some of them, like (Tanvir and Mujtaba, 2006a), used their own developed correlations to predict temperature elevations. Also, it is to be mentioned that most of the basic equations of mass and energy balance were citied from (Reddy et al., 1995a). To carry out the mathematical modelling of the MSF plant, the following assumptions are made to give credibility to the model:

> ➢ The distillate product leaving any stage is salt free.
> ➢ The model is developed using lumped parameter analysis, the mass considered to be perfectly mixed and spatial variation were not explicitly considered.
> ➢ Subcooling of the vapour condensate is taken into consideration.
> ➢ The distillate is assumed to be withdrawn from each stage separately and not connected to the next stage's tray.
> ➢ Heat of mixing is negligible.
> ➢ Mass cooling brine in condenser tubes remains constant and there is no accumulation of salt in the condenser tubes.
> ➢ The non-equilibrium parameter depends on water temperature and salt content.

When inputting mathematical equations into simulation software, it is inevitable that some difficulties would arise when simulating the process. Therefore, in order to avoid these difficulties, the complex MSF process can be split into different levels for simulation and then is built up using gPROMS feature of hierarchical structure. The purpose of this procedure is to identify any early mistakes and correct them before building the full-configured model. From the modelling point of view, it is easier to model a single flash stage at low hierarchy scale and then use the flow streams and physical properties correlations to connect all the stages. A high hierarchical level is then used to model the entire MSF process.

3.2.1 Single Stage Model

Figure 3.1 shows the schematic diagram for single stage. The following equations can be written for single stage (j) at dynamic state

3.2.1.1 Flash Chamber

Mass balance:

$$\rho_B \times A_P \times \frac{dL_B}{dt} = B_{in} - B_{out} - V_B - NCGs \tag{3.1}$$

where B_{in} is the brine flow rate entering the stage, B_{out} is the brine flow rate leaving the stage, V_B is the released vapour from the brine in mass flow rate, $NCGs$ is

the released NCGs in mass flow rate, ρ_B is the brine density, A_P is the brine pool area and L_B is the height of the brine inside the stage.
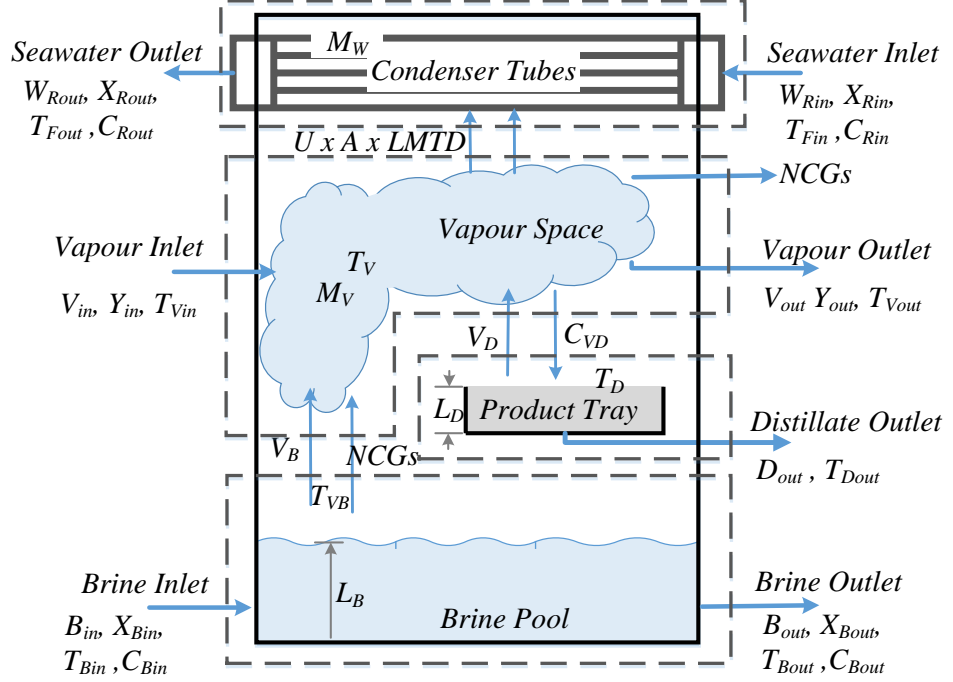
Figure 3.1: A typical stage in MSF plant

Salt balance:

$$\rho_B \times A_P \times L_B \times \frac{dX_{Bout}}{dt} = B_{in} \times X_{Bin} - X_{Bout}(B_{in} - V_B - NCGs) \tag{3.2}$$

where X_{Bin} and X_{Bout} are the salt concentrations of the brine entering and leaving the stage respectively.

Non-condensable gases balance in brine:

$$\rho_B \times A_P \times L_B \frac{dC_{Bout}}{dt} = B_{in} \times C_{Bin} - C_{Bout}(B_{in} - V_B) - NCGs(1 - C_{Bout}) \tag{3.3}$$

where C_{Bin} and C_{Bout} are the mass fraction of NCGs in the brine entering and leaving the stage respectively.

Non-condensable gases stripping rate

The NCGs stripping rate is given by the following equation (Al-Fulaij et al., 2010)

$$NCGs = B_{out}(C_{Bout} - C_{Be})\gamma \tag{3.4}$$

Where C_{Be} is the equilibrium mass fraction of NCGs in the brine and γ is the efficiency of degassing process.

Enthalpy balance:

$$\rho_B \times A_P \times L_B \frac{dH_{Bout}}{dt} = B_{in}(H_{Bin}\text{-}H_{Bout}) \text{ -}V_B(H_{VB}\text{-}H_{Bout}) \text{ - } NCGs(H_{NCGs}\text{-}H_{Bout}) \quad (3.5)$$

$$H = Cp \times (\Delta T), \quad\quad\quad (3.6)$$

$$Cp = f(X_B, T) \quad\quad\quad (3.7)$$

Where *H* is specific enthalpy, C_p is specific heat at constant pressure and it is function of temperature and salinity of the stream, and *ΔT* is the temperature difference between stream temperature and the reference temperature.

Temperature drop correlations:

The flashed vapour from the brine has a temperature value less than the brine temperature by the boiling point elevation (*BPE*) and non-equilibrium allowance (*NEA*).

$$T_B = T_{VB} + BPE + NEA \quad\quad\quad (3.8)$$

3.2.1.2 Vapour Space

Mass balance:

$$\frac{dM_V}{dt} = V_B + V_{in} + V_D + NCGs - C_{VD} - V_{out} \quad\quad\quad (3.9)$$

Non-condensable gases balance in vapour phase:

$$M_V \frac{dY_{out}}{dt} = V_{in} \times Y_{in} + NCGs(1 - Y_{out}) - Y_{out}(V_{in} + V_B + V_D - C_{VD}) \quad\quad (3.10)$$

Here, *V_in* and *V_out* are the vapour mass flow rates that enter and leave a single stage. *Y_in* and *Y_out* are the mass fraction of NCGs that enter and leave the stage. In some stages, the vented NCGS are purge as outlet gases instead of venting to the next stage according to the installed venting system.

Enthalpy balance:

$$\frac{dM_V H_{Vout}}{dt} = (V_B \times H_{VB}) + (NCGs \times H_{NCGs}) + (V_{in} \times (1 - Y_{in}) \times H_{Vin})$$
$$+ (V_{in} \times Y_{in} \times H_{NCGsin}) + (V_D \times H_{Vout}) - (C_{VD} \times H_{VD}) -$$
$$(V_{out} \times Y_{out} \times H_{NCGsout}) - (V_{out} \times (1 - Y_{out}) \times H_{Vout} - Q \quad\quad (3.11)$$

Q in equation (3.11) is the heat transfer rate from the vapour space to the condenser tubes to heat the brine in the condenser tubes. Q will be defined later

in tubes bundle section. Additional to the vapour space equations, the following equations are used in the model to define the total hold up of the vapour in the vapour phase.

Vapour hold up:

$$M_V = \rho_V \times V_v \tag{3.12}$$

Vapour volume space:

$$V_v = A_P \times (h_s - L_b) - A_D \times L_D - V_{tubes} \tag{3.13}$$

Where ρ_V is the density of the vapour, V_v the volume of the vapour space and h_s the height of the stage.

Temperature of the Vapour space:

Similar to equation (3.8), further drop of the flashed vapour temperature occurs due to the demister and thus the vapour temperature is less than flashed vapour temperature by demister drop.

$$T_V = T_{VB} - \Delta T_{DEM} \tag{3.14}$$

3.2.1.3 Product Tray

Mass balance:

Here, unlike all the previous published work, it is assumed that the distillate product from previous tray is withdrawn outside the stage and does not enter the next stage.

Thus, the material balance around the distillate tray is written as:

$$\rho_D \times A_D \times \frac{dL_D}{dt} = C_{VD} - V_D - D_{out} \tag{3.15}$$

where D_{out} is the distillate flow rate leaving the stage, C_{VD} the condensate rate of the vapour around tube bundle and V_D the amount of vapour leaving the distillate tray. L_D is the height of the distillate in the product tray, A_D the area of the product tray and ρ_D the density of the distillate (fresh water).

Enthalpy balance in distillate tray:

$$\rho_D \times A_D \times L_D \times \frac{dH_{Dout}}{dt} = C_{VD}(H_{VD} - H_{Dout}) - V_D(H_{Vout} - H_{Dout}) \tag{3.16}$$

Temperature of the distillate:

Here, unlike in other studies, the subcooling of the condensate vapour is assumed and thus, the temperature of the distillate is different from the vapour temperature. However, there is no available equation at the present to calculate the drop in the temperature as in equations (3.8 and 3.14). Therefore, the following equation is developed to calculate the distillate temperature.

$$V_D \times H_{Vout} = C_{VD} \times (H_{VD} - H_{Dout})$$ (3.17)

In the above equation, if T_V is equal to T_D, then there is no vapour release (V_D) from distillate tray.

3.2.1.4 Tubes Bundle

Mass balance:

$$\frac{dM_W}{dt} = W_{Rin} - W_{Rout}$$ (3.18)

For heat rejection section stages, W_{Rin} is replaced by W_{Fin}.

Salt balance:

It is assumed that there is no accumulation of salt in the tube bundle and thus:

$$X_{Rin} = X_{Rout}$$ (3.19)

Similarly, for heat rejection section stages, X_{Rin} is replaced by X_{Fin}.

Enthalpy balance:

Overall energy balance on stage

$$M_W \times \frac{dH_{Wout}}{dt} = W_{Rin}(H_{Win} - H_{Wout}) + Q$$ (3.20)

Here, Q is the same as that one in the equation (3.11) and it can be defined as:

$$Q = U \times A_S \times LMTD$$ (3.21)

Where the *U* is the overall heat transfer coefficient and *LMTD* is the logarithmic mean temperature difference.

$$LMTD = \frac{(T_{Fout} - T_{Fin})}{\ln\left[\frac{(T_D - T_{Fin})}{(T_D - T_{Fout})}\right]}$$ (3.22)

It is to be mentioned T_D presents the condensate vapour around the tubes and T_V presents the vapour temperature around the tubes and they have the same value.

A_s is the heat transfer surface area of the tubes which is defined as:

$$A_S = N_t \times \pi \times d_o \times L_t \tag{3.23}$$

Where N_t is the number of tubes per bundle, d_o is the outer diameter of the tube and L_t is the tube length.

Mass hold up:

The mass hold up (M_W) in equation (3.20) is calculated as:

$$M_W = \rho_B \times V_{tubes} \tag{3.24}$$

And the volume of the tubes is defined as:

$$V_{tubes} = \frac{\pi d_i^2}{4} \times N_t \times L_t \tag{3.25}$$

3.2.2 Last Stage Model

In MSF-BR process, the material and energy balance calculations of the last stage is different from other stages in term of brine flow rate. As shown in Figure 3.2, the recycle brine is withdrawn from the last stage and the stage is fed with seawater makeup from the seawater leaving the heat rejection section. The distillate and vapour balances are similar to the other stages.

3.2.2.1 Flash Chamber

Mass balance:

$$\rho_B \times A_P \times \frac{dL_B}{dt} = B_{in} + F_{last} - B_{out} - Rec - V_B - NCGs \tag{3.26}$$

$$F_{last} = W_{Fin} - W_{CW} \tag{3.27}$$

$$Rec = W_{Rin} \tag{3.28}$$

where F_{last} is the sea water makeup that enters the stage, Rec is the recycle brine flow rate leaving the last stage of heat rejection section and entering the last stage of the heat recovery section as W_{Rin}. W_{Fin} and W_{cw} are intake feed seawater and the rejected seawater flows to the sea respectively.

Salt balance:

$$\rho_B \times A_P \times L_B \times \frac{dX_{Bout}}{dt} = B_{in} \times X_{Bin} - F_{last}(X_{Bout} - X_{Fout}) + Rec(X_{Bout} - X_{Rec})$$

$$-X_{Bout}(B_{in} - V_B - NCGs) \tag{3.29}$$

Here X_{Rec} is the seawater concentration of the recycle brine that enters the last stage of heat recovery section and X_{Fout} is equal to X_{Fin} and it represents the seawater salt concentration.
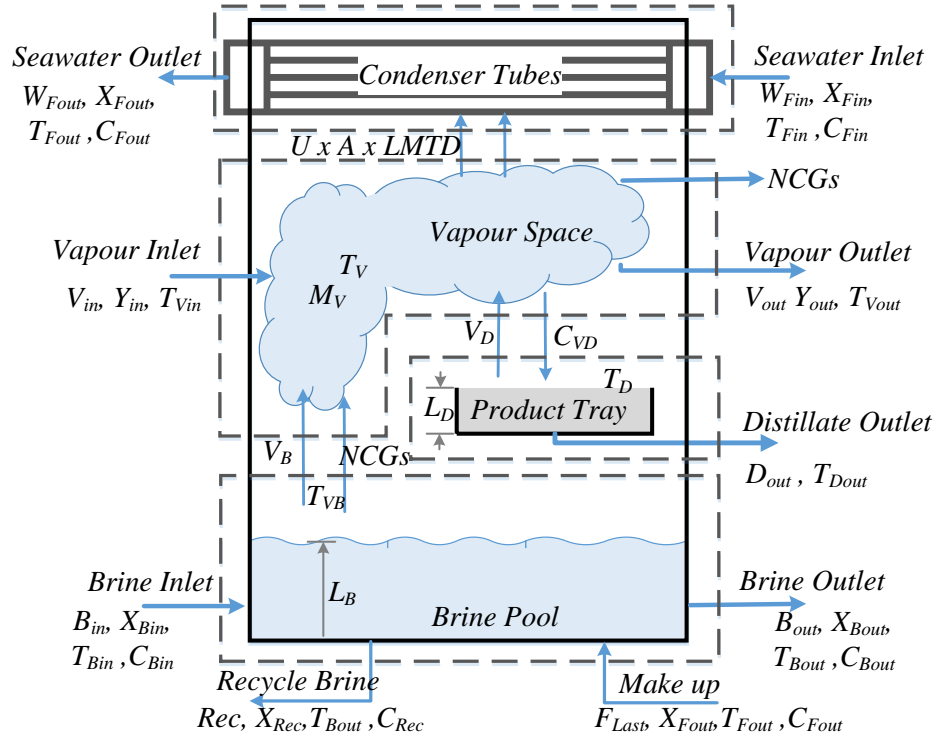
Figure 3.2: Schematic of last stage in MSF plant

Non-condensable gases balance in brine:

$$\rho_B \times A_P \times L_B \frac{dC_{Bout}}{dt} = B_{in} \times C_{Bin} + F_{last}(C_{Fout} - C_{Bout}) - Rec(C_{Rec} - C_{Bout})$$

$$-NCGs(1 - C_{Bout}) - C_{Bout}(B_{in} - V_B) \tag{3.30}$$

where C_{Fout} and C_{Rec} are the mass fraction of non-condensable gases in seawater and recycle brine respectively.

Enthalpy balance:

$$\rho_B \times A_P \times L_B \frac{dH_{Bout}}{dt} = B_{in}(H_{Bin} - H_{Bout}) - F_{Last}(H_{Bout} - H_{Flast})$$

$$-V_B(H_{VB} - H_{Bout}) - NCGs(H_{NCGs} - H_{Bout}) \tag{3.31}$$

Here, there is no need to carry out an energy balance to calculate the recycle brine temperature because the recycle brine leaves the stage at the same temperature of blow down stream. However, this is not the case for salt and gases concentration which will be calculated in section (3.2.4) in equations (3.42 and 3.43).

3.2.3 Brine Heater Model

In the brine heat, there is no mass transfer and it is similar to the balance of tubes bundle in the single stage and thus the only available balance is the energy balance. Schematic diagram of the brine heater is shown in Figure 3.3 and the following equations describe the performance of the brine heater.
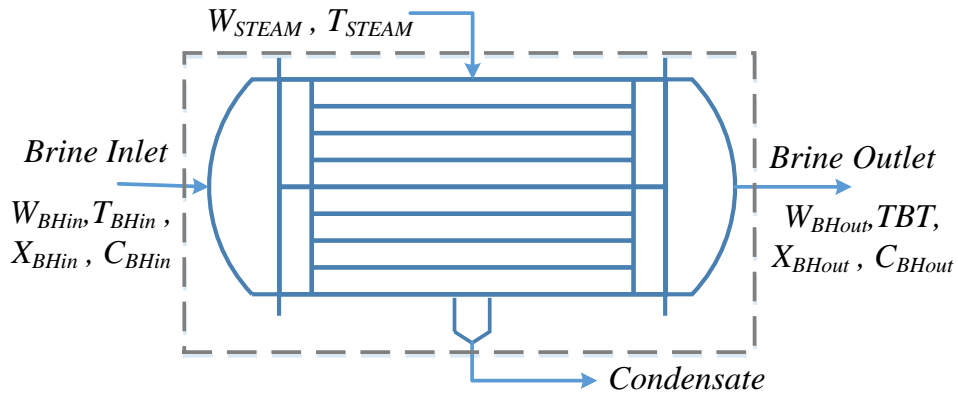
Figure 3.3: Schematic of brine heater in MSF plant

Mass and salt balances:

$$\frac{dM_{BH}}{dt} = W_{BHin} - W_{BHout} \tag{3.32}$$

$$X_{BHin} = X_{BHout} \tag{3.33}$$

Where W_{BHin} and X_{BHin} are the recirculation brine flow rate and its salt concentration respectively leaving the tube bundle at first stage and entering the brine heater, while W_{BHout} and X_{BHout} are the brine flow rate and its salt concentration respectively leaving the brine heater and entering the first stage of the flash chamber of the heat recovery section.

Enthalpy balance:

Overall energy balance around the brine heater

$$M_{BH} \times \frac{dH_{BHout}}{dt} = W_{BHin}(H_{BHin} - H_{BHout}) + U_{BH} \times A_{BH} \times LMTD_{BH} \tag{3.34}$$

Where U_{BH} is the overall heat transfer coefficient, A_{BH} the brine heater surface area and $LMTD_{BH}$ the logarithmic mean temperature difference. The heat transfer term in equation (3.34) ($U_{BH} \times A_{BH} \times LMTD_{BH}$) can be calculated as:

$$W_{STEAM} \times \lambda_{STEAM} = U_{BH} \times A_{BH} \times LMTD_{BH} \tag{3.35}$$

Where W_{steam} is the mass flow rate of the steam, λ_{steam} the latent heat of the steam. The logarithmic mean temperature difference ($LMTD_{BH}$) is calculated similarly to equation (3.22).

$$LMTD_h = \frac{(TBT - T_{BHin})}{\ln\left[\frac{(T_{steam} - T_{BHin})}{(T_{steam} - TBT)}\right]} \tag{3.36}$$

where *TBT* is the outlet temperature of the brine heater and T_{steam} is the temperature of the steam.

3.2.4 Multistage Model (*Higher Level*)

A higher level model is used to connect any two subsequent flashing stages or the brine heater with the first stage in the heat recovery section by relating the streams and physical properties to obtain the rest of variables. If (*j*) presents a stage, then (*j+1*) is the next stage and (*j-1*) is the previous stage.

Brine stream:

$$B_{in\ j} = B_{out\ j-1}, \qquad B_{out\ j} = B_{in\ j+1}, \qquad T_{Bin\ j} = T_{Bout\ j-1}, \qquad T_{Bout\ j} = T_{Bin\ j+1}$$

$$X_{Bin\ j} = X_{Bout\ j-1}, \qquad X_{Bout\ j} = X_{Bin\ j+1}, \quad C_{Bin\ j} = C_{Bout\ j-1}, \quad C_{Bout\ j} = C_{Bin\ j+1}$$

Vapour streams:

$$V_{in\ j} = V_{out\ j-1}, \qquad V_{out\ j} = V_{in\ j+1}, \qquad Y_{in\ j} = Y_{out\ j-1}, \qquad Y_{out\ j} = Y_{in\ j+1}$$

Tube bundle streams:

$$W_{Rin\ j} = W_{Rout\ j+1}, \quad W_{Rout\ j} = W_{Rin\ j-1}, \quad T_{Fin\ j} = T_{Fout\ j+1}, \quad T_{Fout\ j} = T_{Fin\ j-1}$$

$$X_{Rin\ j} = X_{Rout\ j+1}, \qquad X_{Rout\ j} = X_{Rin\ j-1}, \qquad C_{Rin\ j} = C_{Rout\ j+1}, \qquad C_{Rout\ j} = C_{Rin\ j+1}$$

As mentioned before, the aforementioned equations are applied only to connect subsequent stages, and thus attention should be paid when relating the last stage of the heat recovery section to the first stage of the heat rejection section.

Moreover, W_R is used in recovery section stages and W_F is used in rejection section stages.

Brine outlet flow rate:

To calculate the brine outlet flow rate, the following equation, which is given by El-Dessouky and Bingulac (1996), is used.

$$B_{out} = C_d \times W_{st} \times H_g \times \sqrt{(2\rho_b \Delta P)} \tag{3.37}$$

Where C_d is the orifice discharge coefficient, W_{st} the width of the stage in m, H_g the height of the gate in m, and ΔP the pressure drop between the stages which is obtained by using the following equation:

$$\Delta P = \left(P_j - P_{j+1}\right) + g\rho_B(L_{B,j} - L_{B,j+1}) \tag{3.38}$$

Where P is the pressure in Pa and L_B is the brine height. The subscripts j and $j+1$ refer to the stage under study and the next stage, respectively.

Distillate outlet flow rate:

The distillate tray is a concaved plate that has a slope to divert all collected water to a channel which connects all distillate trays. The channel, which is located between the trays and the demister is in parallel with the direction of the brine flow and is fed to the storage tank. Though the distillate flow outlet from single stage is assumed to be withdrawn separately and not connected to the next stage, the distillate trays are connected by a channel and thus the pressure drop between stages is used to calculate the distillate flow rate. Similar equation to the brine flow rate can be used.

$$D_{out} = C_C \times A_{pipe} \times \sqrt{(2\rho_D \Delta P)} \tag{3.39}$$

Where C_C is the distillate discharge coefficient, A_{pipe} the cross section area of the pipe m and ρ_D the density of the distillate. The pressure drop between the stages can be obtained by using the following equation:

$$\Delta P = \left(P_j - P_{j+1}\right) + g\rho_D(L_{D,j} - L_{D,j+1}) \tag{3.40}$$

Vented vapour and NCGs flow rate:

The vented vapour and NCGs whether to the next stage or to the surroundings can be estimated by the flowing equation:

$$V_{out} = k_V \times \sqrt{\rho_V (P_j - P_{j+1})} \tag{3.41}$$

Where k_V is a venting orifice discharge coefficient.

Recycle brine concentration:

As it can be seen from equations (3.29) and (3.30), the salinity and the concentration of NCGs of the recycle brine are different than those of the blowdown stream. Thus, to estimate the recycle brine salinity and NCGs concentrations, the following equations are used for the last stage (El-Dessouky and Ettouney, 2002):

$$Rec \times X_{Rec} + X_{Bout}(F_{last} - D_{Total}) = F_{Last} \times X_{Fout} + X_{Bout}(Rec - D_{Total}) \tag{3.42}$$

$$Rec \times C_{Rec} + C_{Bout}(F_{last} - D_{Total}) = F_{Last} \times C_{Fout} + C_{Bout}(Rec - D_{Total}) \tag{3.43}$$

The plant performance ratio can be calculated as following:

$$Performance\ ratio\ (PR) = \frac{D_{total}}{W_{steam}} \tag{3.44}$$

where D_{total} is the total distillate product and it is defined as:

$$D_{Total} = \sum_{j=1}^{N} D_j \tag{3.45}$$

Physical properties correlations that are used to relate stages variables and to solve the MSF model are presented in Appendix A. The degree of freedom analysis is presented in Appendix C.

3.3 Model Validation

The main concern for the researchers is usually the validity of the model and whether they build the right model. This can be achieved by comparing the simulation results to the actual plant data. Unfortunately, some institutions responsible for desalination plants are reluctant to give accurate and comprehensive data related to operation and maintenance of plants. This does not help in evaluating the situation and could delay more development in this field. However, in this work, the available actual data for the Azzour desalination plant was collected from different resources. Due to the similarity of the data collected from Al-Shayji (1998) and Alasfour and Abdulrahim (2009) for the same plant, it is assumed to be accurate actual data. It is to be mentioned that some data

missing from Al-Shayji (1998) are found in Alasfour & Abdulrahim (2009) and vice versa.

In this work, the dynamic model is built without any type of control and solved using gPROMS model builder software 4.1. The simulation results of this model are validated against real data of Azzour desalination plant, which is located in Kuwait and has 24 stages with capacity of 48 MGD. Table 3.1 presents the design and operating conditions of the plant. More detailed design data for stages and brine heater is available in Appendix B.

Table 3.1: Actual operational data for Azzour desalination plant

Variable	Unit	Value
Distillate	Kg/s	313
Steam flow rate to the brine heater	Kg/s	39
Recycle brine flow rate	Kg/s	3968
Intake sea water flow rate	Kg/s	2675
Brine blowdown flow rate	Kg/s	499
Makeup flow rate	Kg/s	813
Top brine temperature	^{o}C	91
Sea water inlet temperature	^{o}C	32
Steam temperature	^{o}C	100
Brine blowdown temperature	^{o}C	41
Makeup temperature	^{o}C	40
Distillate temperature	^{o}C	39

(Source: Al-Shayji (1998) and Alasfour & Abdulrahim (2009))

3.3.1 Steady State Validation

For steady state validation, the model is run for approximately 24 hours to reach steady state and then the obtained results were validated against actual data. As shown in Figure 3.4, a good agreement is obtained between simulation results and the plant data for the brine flow rate and distillate flow rate. As the brine flow rate decreases due to evaporation of pure water, the distillate flow rate in turn increases due to condensation of the released vapour from the brine. Figure 3.5 shows the brine temperature and pressure profile from stage to stage. As the temperature of the brine decreases due the flashing process, the pressure also

decreases to reduce the boiling point and keeps the continuality of the flashing process.
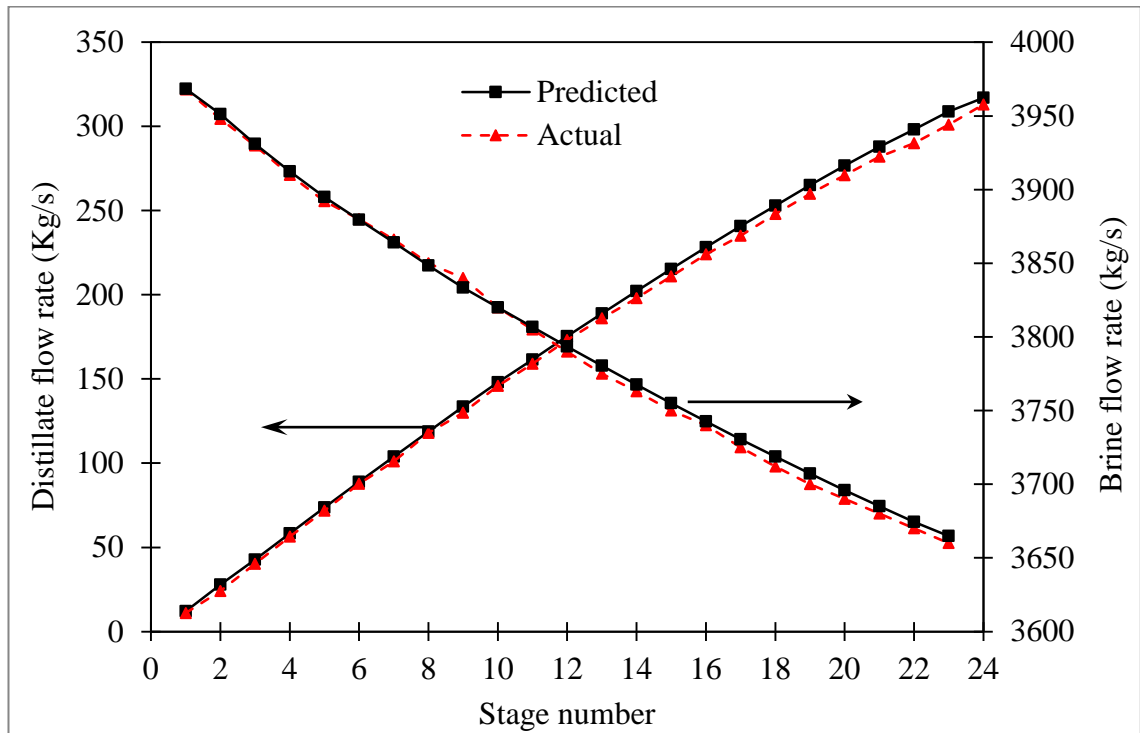
Figure 3.4: Distillate and brine flow rate at each stage.
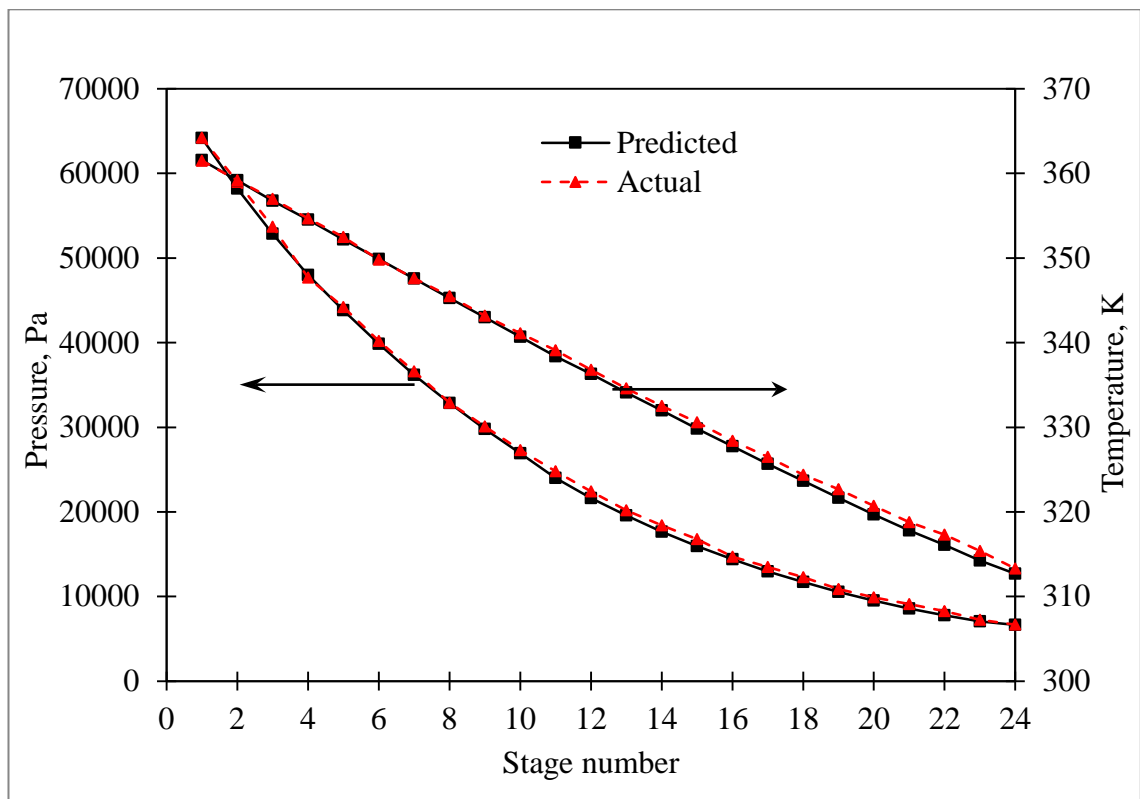
Figure 3.5: Pressure and temperature profile.
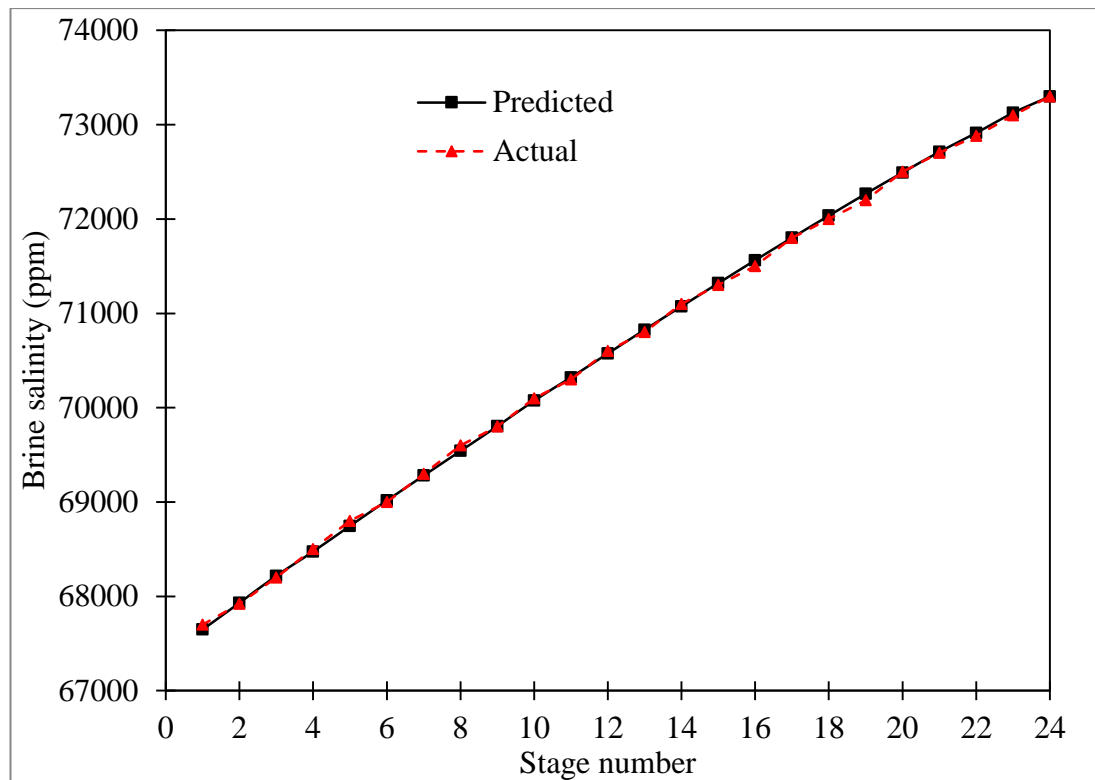
Figure 3.6: Brine salinity profile per stage

Furthermore, Figure 3.6 shows the brine salinity profile as the salinity increases due to the flashing process. In addition, regarding physical properties correlations, the difference between the brine temperature and distillate temperature is due to the temperature losses through demister, boiling point elevation (BPE) and non-equilibrium allowance (NEA). Figure 3.7 shows a comparison between simulation data and real data for BPE and NEA temperature losses. The BPE simulation result showed close agreement with the actual data. While the PBE is function of temperature and salinity, the NEA correlation is function of the brine height and temperature, and due to the lack of real data of the gate height, the simulation result is slightly different from the actual data. If accurate measurements of the gate height were available, the model may be able to predict data with much more accuracy.
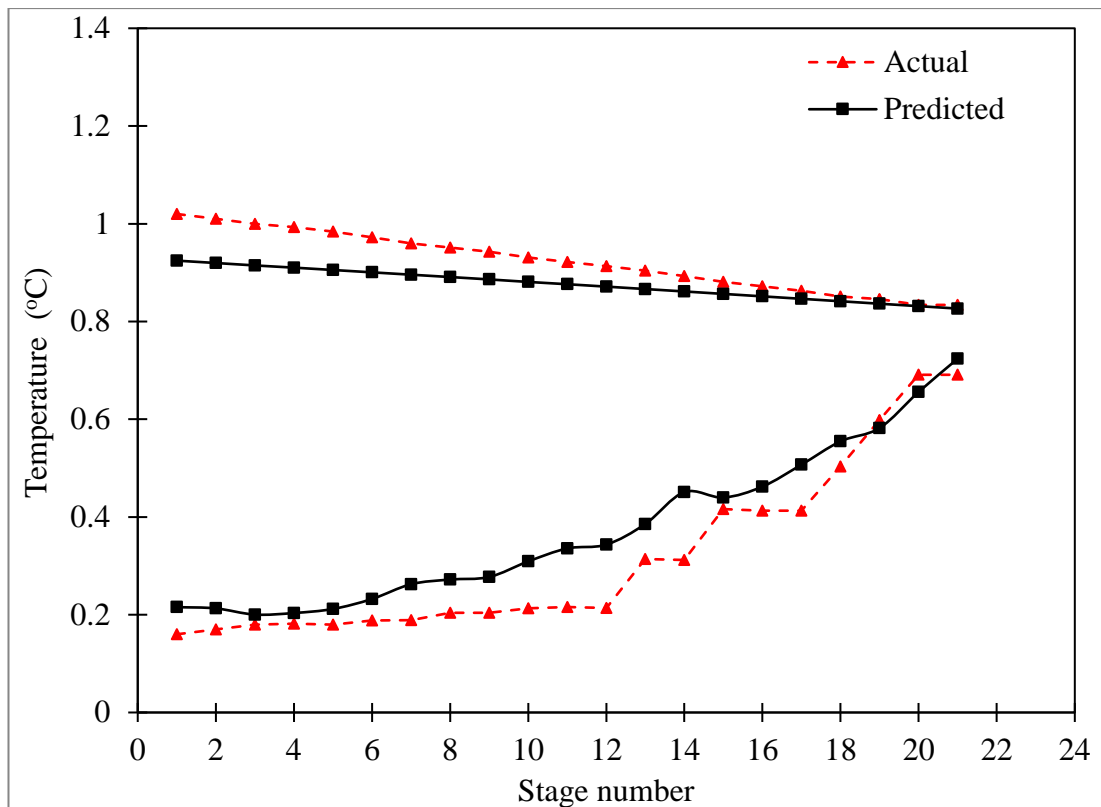
Figure 3.7: A BPE and NEA temperature losses profiles.

3.3.2 Dynamic Validation

Since real dynamic data is not available at present, thus for the sake of dynamic validation, two selected variables are perturbed and its effect on the plant is reported. There are many important variables that affect the MSF performance, recycle brine flow rate and intake seawater temperature are among them.

3.3.2.1 Variation of the Recycle Brine Flowrate

After reaching steady state, the recycle brine flow rate is increased by 5% for 4 hours, then decreased by 10% for another 4 hours, and then restored back to its initial value. The dynamic response of the brine level in certain stages and TBT temperature are monitored. Figures 3.8, 3.9 and 3.10 show the dynamic response of the brine levels, performance ratio and product and TBT respectively to the variation of the recycle brine flow rate. Due to the non-implementation of the level control system in the last stage, any change in the recycle brine should be small to avoid the dryness of the last stage. As it can be seen from Figure 3.8, the brine level in the first stage increases significantly compared to the fifth stage which its

level increases slightly. The increase in the brine level becomes less towards the cold end of the plant. In the middle stage, the level of the brine decreases resulting in decrease in the NEA and thus an increase in the condensate rate. In the last stage, where the brine recycle is withdrawn, the level of the brine drops down and then increases back to a level that is less than the previous level. In the second disturbance, the level in the first and fifth stages is dropped as low as the height of orifice while the level of the last stage increased slightly. It is important to monitor the level of the brine at all times because large increase or decrease in the brine level could affect the flashing process and the performance of the plant.
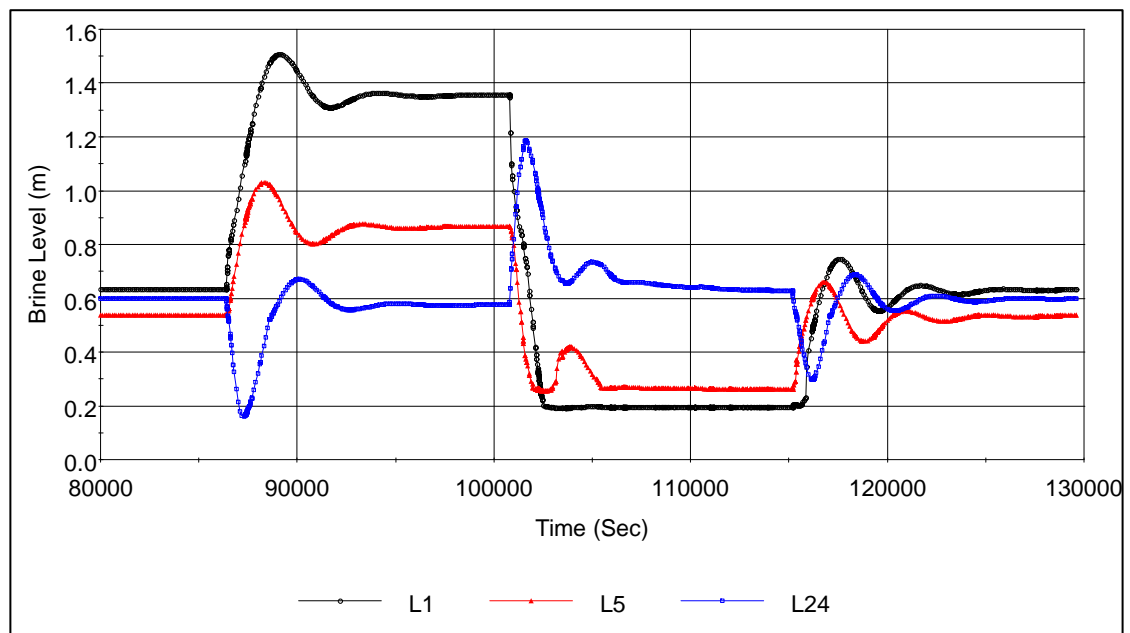
Figure 3.8: Dynamic response of brine level to the variation of the recycle brine flow rate.

Figure 3.9 shows the effect of the recycle brine variation on the total product rate and the performance ratio of the plant. As mentioned before, increasing the recycle brine flow rate leads to reduction in the brine level in the middle stages and thus increase the condensate rate. Therefore, the total production rate increases. However, though the production rate increases, the performance ratio of the plant decrease. This is due to the increase in the steam flow rate. As the recycle brine flow rate increases, it requires more steam and thus the performance ratio decreases.
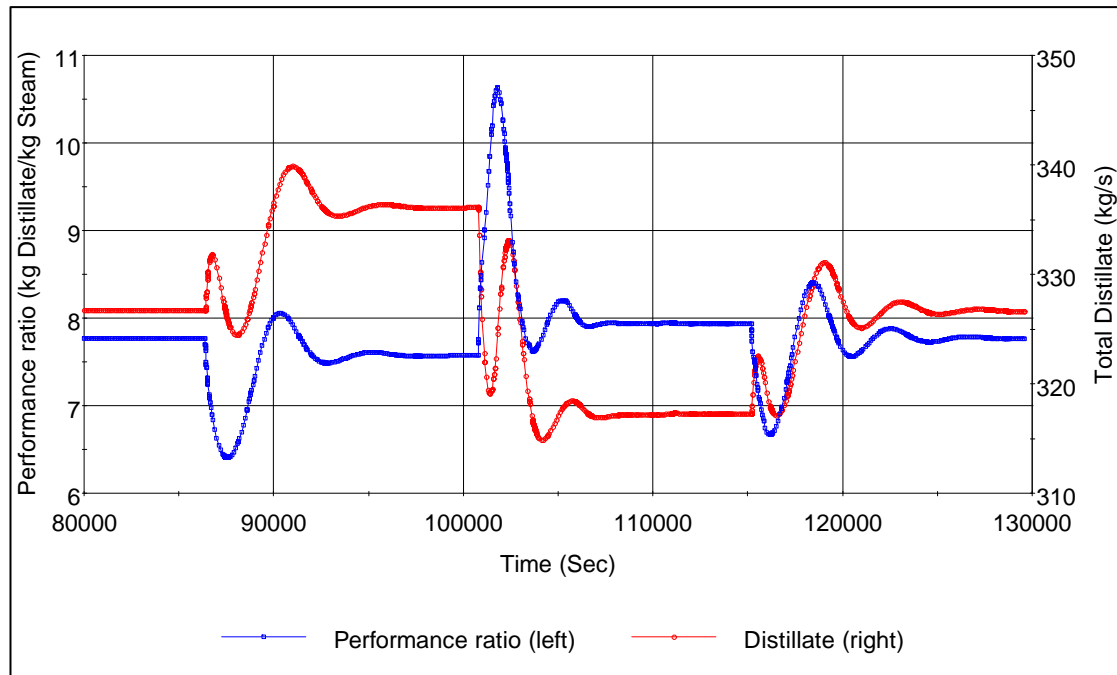
Figure 3.9: Dynamic response of performance ratio and distillate flow rate to the variation of the recycle brine flow rate.

However, this variation in the brine level and the performance ratio of the plant is not due the recycle brine flow rate only but other parameters are affected and consequently affect the brine level and the performance. Due to the missing of the top brine temperature (TBT) control loop, the TBT is also affected by the recycle flow rate and hence it affects the performance ration and the product rate. Figure 3.10 shows the inlet and outlet (TBT) temperature of the brine heater. As the recycle flow rate increases, the amount of heat gained from the flashing stage is not enough to keep its outlet temperature from the first stage at constant value and thus its temperature drops slightly leading to decrease in the outlet temperature of the brine heater (TBT). The drop of the TBT is another cause of the increase in the brine level in the first stage as it shown in Figure 3.8. If the TBT is controlled to be constant at its optimum value, the increase of the brine level in the first stage due to the increase in the recycle brine flow rate would be less than it is in figure 3.8. Moreover, the temperature difference between the outlet and inlet of the brine heat temperature is nearly constant for all interval and thus, the change in the performance ratio in figure 3.9 is due to the recycle brine flow rate only and the TBT has no effect. For constant temperature difference, the demand of the steam flow rate is due to the heat required for the recycle brine.
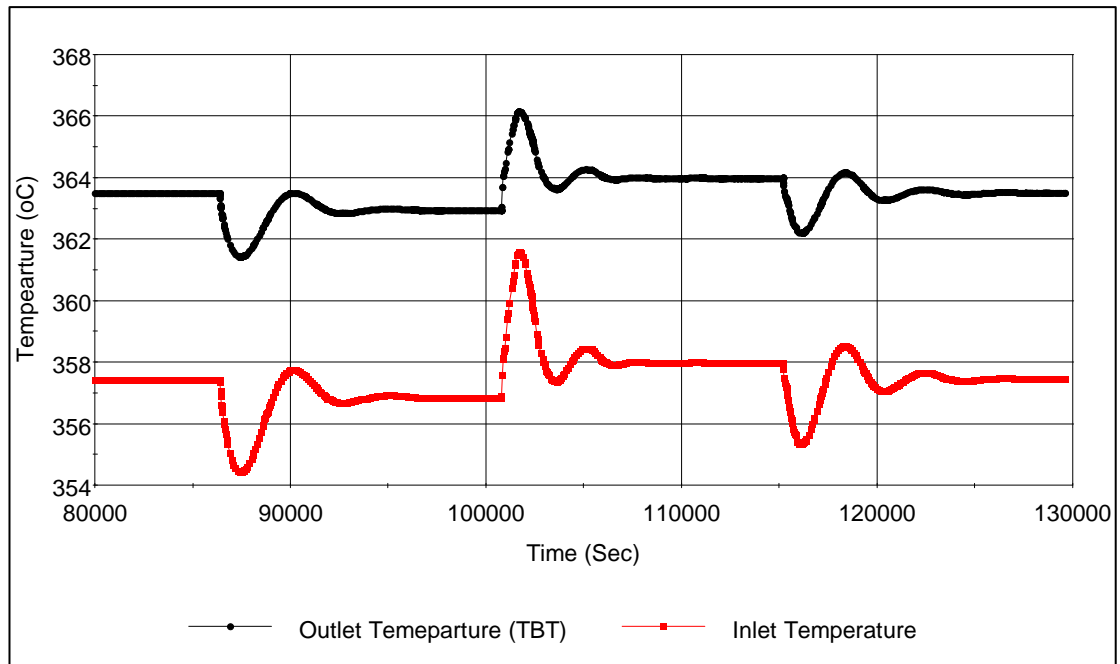
Figure 3.10: Dynamic response of the inlet and outlet temperature of the brine heater to the variation of the recycle brine flow rate.

3.3.2.2 Variation of the Seawater Temperature

The wide difference in seawater temperature during the day (also between summer and winter seasons) has a great impact on the product rate and plant performance (Hawaidi and Mujtaba, 2011). Most MSF plants operate in summer and winter mode, when the set point of the intake seawater temperature varies between 25 °C in the winter mode and 32 °C in the summer mode (Alatiqi et al., 1999). Thus, it is good choice to select the seawater intake temperature to test the dynamic validation of this model. It is important to mention that all the previous results were generated at summer mode (seawater temperature = 32 °C). Hence, the seawater temperature decreased to 25 °C for 8 hours before it is restored back to its initial value. Similar to the variation of the recycle brine flow rate, the same parameters are monitored in variation of the seawater intake temperature. Figures 3.11, 3.12 and 3.13 show the dynamic response of the brine levels, performance ratio and product and TBT respectively with the variation of the recycle brine flow rate.
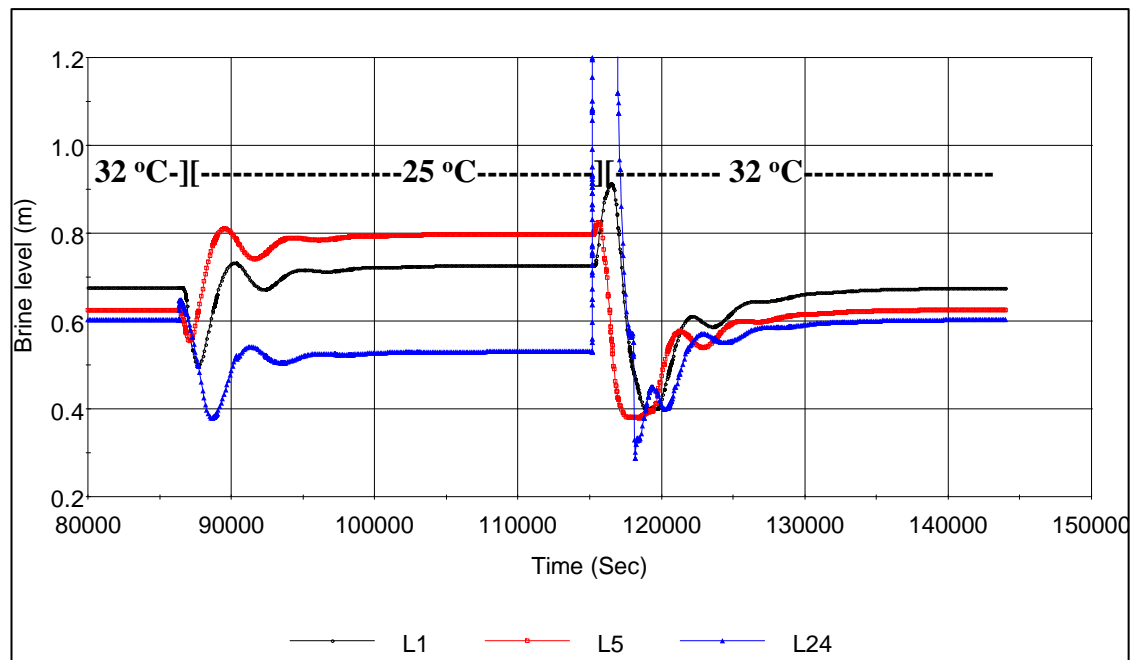
Figure 3.11: Dynamic response of brine level to the variation of the seawater temperature.

The decrease in the seawater temperature leads to reduction in the brine heater and flashing stages brine temperature and thus result in increase in the brine level in most of the stages. As it can be seen, the brine level in stage 1 and 5 increases. However, the increase of the brine level decreases toward the cold end of the plant where the last stage is located. In fact, the brine level in the last few stage is dropped as it can be seen for the last stage in figure 3.11. The drop in the brine level of the last few stages can be attributed to the missing control loop in the last stage.

It is well known that the production rate of MSF plants increases in winter due to the increases in the logarithmic mean temperature difference (LMTD) (Tanvir and Mujtaba, 2006c). Thus, the MSF plants are designed based on summer conditions when the minimum production rate is achieved. However, though the production rate increases, the performance ratio of the plant is decreased due the demand of the steam flow rate to heat the cold seawater. Figure 3.12 shows that decreasing the seawater temperature results in increase in the production rate and decrease in the performance ratio of the plant.
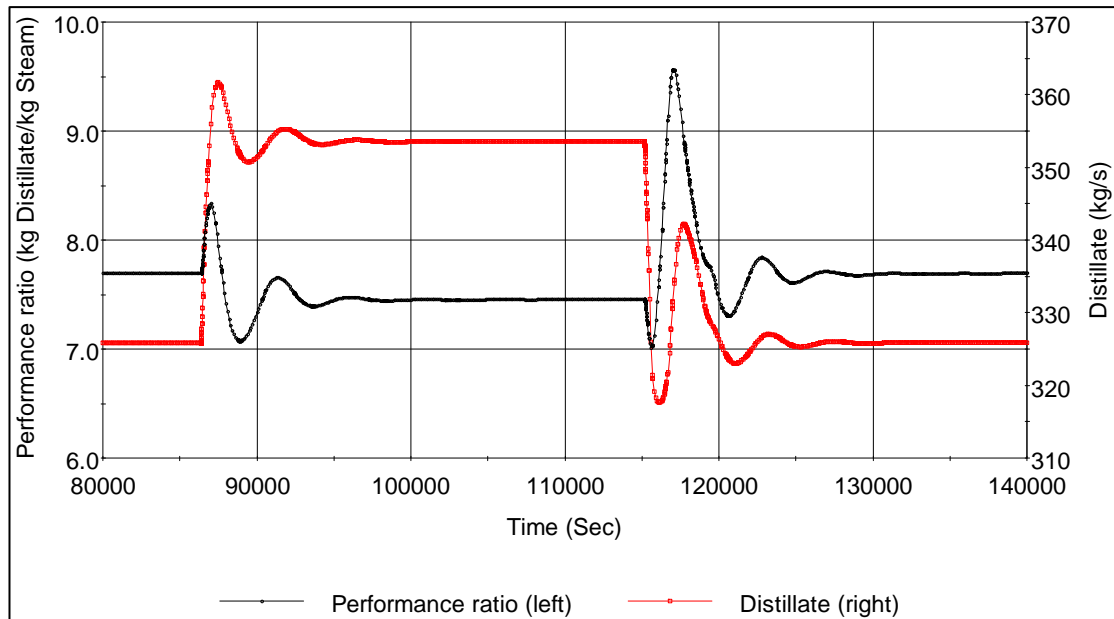
Figure 3.12: Dynamic response of performance ratio and distillate flow rate to the variation of the seawater temperature.
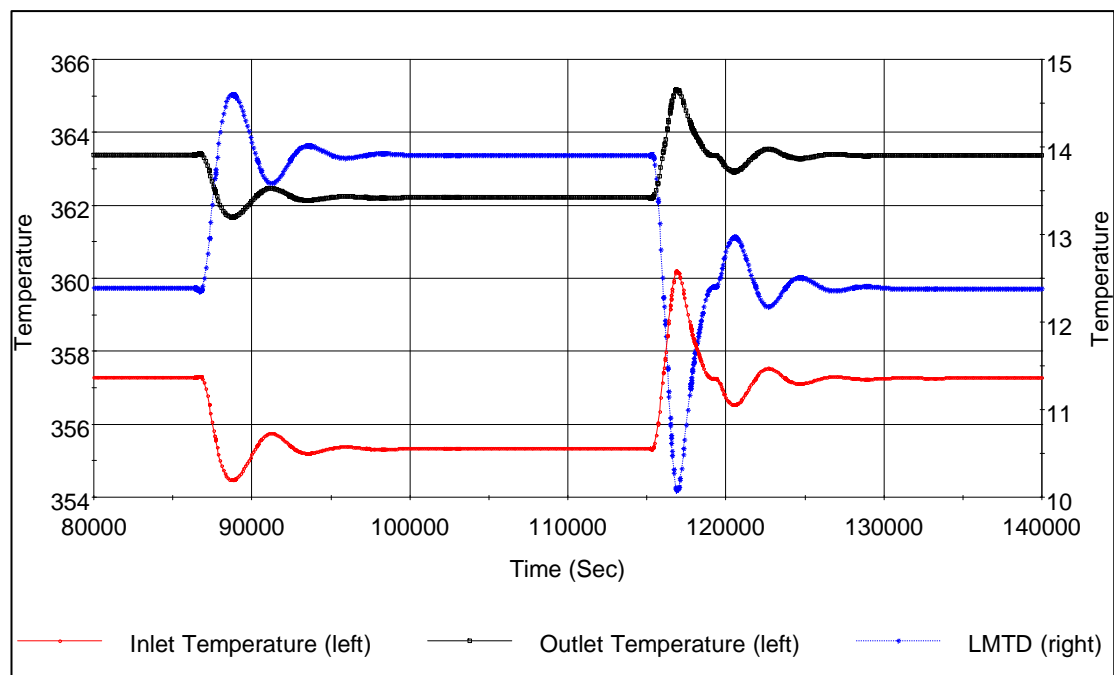
Figure 3.13: Dynamic response of the inlet and outlet temperature of the brine heater to the variation of the seawater temperature.

Finally, the inlet and outlet temperature of the brine heater are monitored to investigate the effect of the reduction in the seawater temperature of on the TBT temperature. As it can be seen in figure 3.13, both the inlet and outlet temperatures of the brine heater decrease with the decrease in the seawater

temperature. However, at constant steam temperature, the LMTD of the brine heater increases resulting in increase in the steam flow rate and consequently the performance ratio of the plant decreases.

3.4 Conclusions

In this chapter, a detailed dynamic state model has been presented for MSF process. The MSF stage was modelled as a single vessel and then all stages were modelled as chain of vessels. The developed model is based on a set of algebraic and differential equations that describe the mass and energy balances of the process and supported with physical properties correlations for all streams of brine, distillate and vapour. All the correlations are functions of temperature and salinity of the streams. Moreover, the temperature losses due to demister, boiling point elevation and non-equilibrium allowance were taken into account.

Note, in the model, the vapour and the distillate are not assumed to be in equilibrium state and thus their temperatures are different. In addition, the distillate from each stage is assumed to be withdrawn separately through channel and not involved in the next stage's material and energy balance (in line with industrial practice).

The developed dynamic model was implemented to analyse the MSF desalination process using gPROMS software. The available actual data for Azzour desalination, which was reported by Al-Shayji (1998) and Alasfour and Abdulrahim, (2009), was available and thus it was possible to validate the simulation results against these data. The model simulation results were validated against actual data and good agreement was obtained. Also, dynamic response of the model was validated against similar results reported in the literature. The developed model in this chapter will be used later for further investigations.

CHAPTER FOUR

The Effect of Venting System Design for Non-condensable Gases

4.1 Introduction

Fouling and the release of NCGs are of great concern for the performance of the thermal desalination process. In thermal desalination process such as multistage flash desalination (MSF), the performance of plant is mainly affected by the condition of the heat transfer surfaces. Therefore, accumulation of fouling and NCGs can reduce the efficiency of the heat transfer process resulting in poor plant performance. Unlike steam, the NCGs do not have the ability to condense inside a condenser and thus they remain in the gas phase resulting in a serious impact on the performance of thermal desalination of seawater (Al-Rawajfeh et al., 2003). Even low concentrations of NCGs gases can cause a severe reduction of the overall heat transfer coefficient and hence the performance of the desalination process (Al-Anezi and Hilal, 2007). According to Semiat and Galperin (2001), a half-percent of air in steam can reduce the heat transfer by 50%. The most common NCGs in the MSF desalination plants are air (N_2 and O_2), argon and CO_2 and they are present in the plants due to the leakage of ambient air through flanges, release of carbon dioxide from decomposition of the bicarbonates, and dissolved gases in the seawater feed (Said et al., 2010). Removing these gases through a venting system is vital to the efficient operation of all desalination plants.

There are several studies concerning the release of NCGs in thermal desalination processes. Seifert and Genthner (1991) and Genthner and Seifert (1991) developed analytical model to estimate the amount of NCGs in the MSF chambers and their variation from stage to stage depending on venting points. The authors studied the effect of NCGs on the vapour side heat transfer coefficient (h_o) by variation of different values of NCGs concentration in the first stage of the MSF plant. Genthner et al. (1993) studied the effect of NCGs on the

vapour side heat transfer coefficient as a function of radial tube bundle location by varying the NCGs concentration in the first stage. However, despite the importance of these studies, they were developed and studied on their own and have not been a part of the whole MSF process performance evaluation.

As mentioned in chapter two, although the mathematical models of MSF process are well known in the literature, a very limited number of publications considered the effect of NCGs in their model. Only Reddy et al. (1995a) and Al-Fulaij et al. (2010) included the amount of NCGs in the mass balance equations. Recent studies by Alasfour and Abdulrahim (2009) and Said et al. (2010) included NCGs correlations in their models to study the effect of NCGs on the heat transfer rate however. While Alasfour and Abdulrahim (2009) used a fixed value for the NCGs concentration, Said et al. (2010) used different values of NCGs but were constant for all stages. In reality, an installation of the venting system at different points makes the amount of NCGs vary from stage to stage.

In this chapter, the model developed in chapter three is used to analyse the design of venting system and the effect of NCGs on the OHTC. The model includes the mass flow rate of NCGs in the material balance equations. The release rate is studied using Henry's law and the NCGs concentration is varied from stage to stage based on the location of venting points.

4.2 Process Description

When the brine enters the flash chambers in MSF plants, the NCGs are released due to the sudden reduction of the partial pressure and low boiling points of these gases, and thus they evaporated with the steam into the vapour space (Glade et al., 2005, Al-Rawajfeh, 2008). Steam will release the latent energy to the process and condense on the heat transfer area, but the NCGs do not condense and reduce the available heat transfer area. At high temperature as in the case of MSF, the NCGs (mainly CO_2) become less soluble (Al-Anezi et al., 2008) and as a result most of these gases are evaporated in first MSF stage, rest in the following stages (Genthner et al., 1993). As the temperature drops through stages, the increase in the salinity of the brine plays another factor of reducing the solubility of CO_2 (Al-Anezi et al., 2008).

Due to condensation process around the tubes bundle, vapour moves toward the heat transfer surface and condenses. NCGs move with the steam up to the wall where they accumulate. The NCGs can migrate back into the centre of the tubes bundle, against the massive flow of the condensable gas resulting in an increase in the concentration of NCGs (Semiat and Galperin, 2001) and thus a venting system is required to vent the concentrated NCGs to the vent system.

In MSF plants, the NCGs vented from the condenser tube bundle can be connected in series where the gases cascade from stage to another and finally vented to the evacuated system, or in parallel where the gases from each stage are vented directly to the evacuated system (Darwish et al., 1995). Most of the MSF plants use a combination of parallel and series system due to the drawbacks of using single type. Figure 4.1 shows a schematic diagram of the venting system of MSF plant where the first few stages are connected in parallel due to high concentration of NCGs while the rest of stages are connected in series.
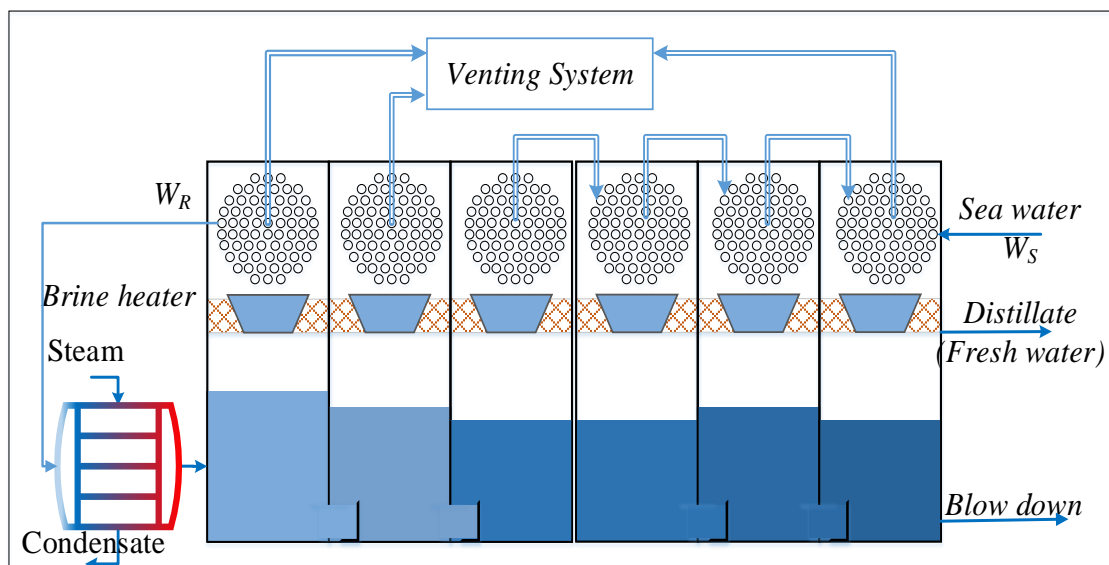
Figure 4.1: Typical venting arrangement in MSF plants.

4.3 Model with Effect of NCGs

While the air is almost evaporated (more than 95%) in the first stage, the CO_2 is continuously liberated in small amount in each stage due to the low degassing rates and high solubility of CO_2 compared to other gases (Genthner et al., 1993). Therefore, for the previous reason, the NCGs dissolved in seawater are assumed to be only CO_2. Henry's law constant reported by (Carroll et al., 1991) to calculate

the equilibrium concentration of the CO_2 in brine is used. Due to the limitation of Henry's law the sea water is assumed to be dilute solution. Also the NCGs released from chemical reaction is neglected and only physical phenomenon of NCGs release is considered.

Henry's Law

$$C_{MOLEQ} \times He = Y_{MOL} \times P \qquad (4.1)$$

Henry's constant for CO_2:

$$Ln(\frac{He}{MPa}) = -6.8346 + 1.2817 \times \frac{10^4}{T_B} - 3.7668 \times \frac{10^6}{T_B{}^2} + 2.997 \times 10^8/T_B{}^3 \qquad (4.2)$$

Where *He* is Henry's constant as a function of temperature, C_{MOLEQ} mole equilibrium concentration of CO_2 in water, Y_{MOL} the mole fraction of CO_2 in vapour, *P* the total pressure in Pa and T_B the brine temperature in K. The correlation is valid for

$$273 < T_B < 433 \; K$$

The NCGs stripping rate is given by the following equation (Al-Fulaij et al., 2010) as mentioned in chapter three (3.4).

$$NCGs = B_{in}(C_B - C_{Be})\gamma \qquad (3.4)$$

Where C_B and C_{Be} are mass fraction and the equilibrium mass fraction of NCGs in brine respectively and γ is the efficiency of degassing process.

4.4 Results and Discussions

As mentioned previously, the overall heat transfer coefficient (OHTC) is affected by fouling resistance and accumulation of NCGs around tubes bundle. Previous studies by Alasfour and Abdulrahim (2009) and Said et al. (2010) assumed constant value for the amount of NCGS in all the stages. In a real plant, the released gases from the brine increase the amount of the NCGs in the first stage resulting in decrease in the overall heat transfer coefficient. However, as the venting system start to vent the NCGs and decrease the amount of NCGs, the OHTC increases in the next few stages. For the validation purpose, the OHTC of this model is plotted against actual plant data and Alasfour and Abdulrahim (2009) results (Figure 4.2). As can be seen, there is a close match between the

model's prediction and the actual plant data in term of the variation of the concentration of NCGs and their effect on OHTC. The error is due to mismatch of the location of venting points and the concentration of NCGs in the seawater between this model and the actual plant data. Moreover, the model predicted effectively the effect of NCGs on the OHTC in the first stage. As can be seen, the OHTC in the first stage in the actual data and this model is very low due to high concentration of NCGs. Though Alasfour and Abdulrahim (2009) results are in good agreement to the actual plant data between stages 9 and 21, there is large discrepancy for stages 1 to 8. This disagreement against actual data was due to their assumption of a constant value of NCGs in all stages. Moreover, their OHTC seems to be linear and the effect of the venting system is not accounted for in their results.
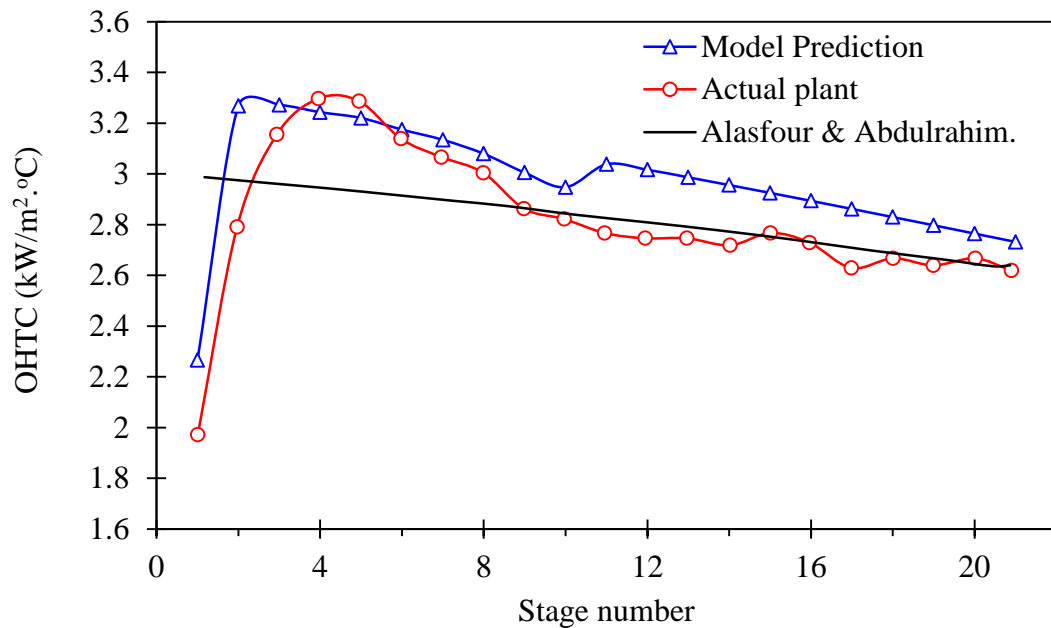
Figure 4.2: Overall heat transfer coefficient profile.

It is worth mentioning that the fouling factors are assumed to be 0.12 and 0.176 m^2 $^oC/W$ in the heat recovery and heat rejection sections, respectively. Also, a value of 100 ppm of CO_2 is assumed in the entering sea water. Figure 4.3 shows the amount of NCGs released per stage. As it can be seen, most of the CO_2 liberated in the first few stages due to the low solubility of CO_2 at high temperature.
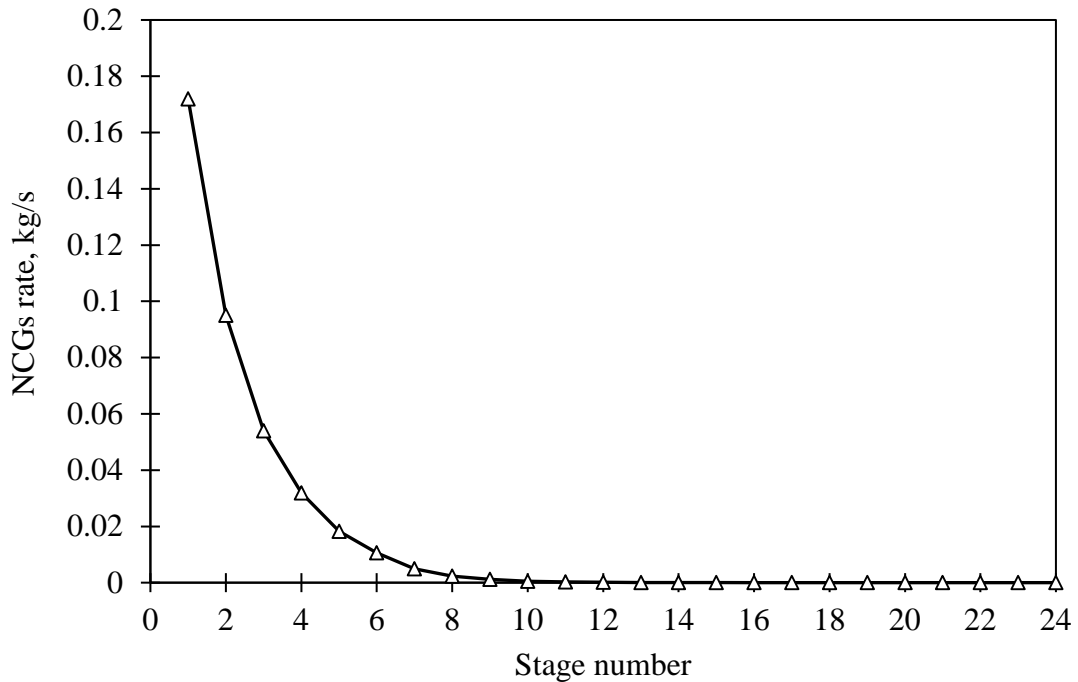
Figure 4.3: NCGs release per stage

4.4.1 Variation of Venting Points Location

Said et al. (2010) reported that the NCGs have no significant effect on OHTC until the concentration of NCGs exceeds 0.05 (wt. %). Also, they reported that from 0.05 up to 0.06 (wt. %), a significant decreased in OHTC occurred. Therefore, in this model, the venting points were assumed to be installed in different stages to avoid the increase of NCGs over 0.05. In most MSF plants, venting points in the first stage and last stage are essential. The former due to high release of NCGs in the first stage and the latter is required to vent the accumulated gases from the rest of stages. Overestimate of the number of venting points result in unnecessary vapour losses with the vent and a higher energy consumption of the venting system. For a constant fouling factor and fixed value for dissolved gases in the entering seawater, then:

CASE 1: If venting point is installed in the 2nd stage as shown in Figures 4.4 and 4.5, then two more venting points, wherever they are installed, are required to keep the NCGs at less than 0.05 wt%. This gives five venting points in total. In Figure 4.4, the third and fourth venting points are installed in the 3rd and 11th stages. In Figure 4.5, on the other hand, the third and fourth venting points are installed in the 6th and 21st stages. However, the difference between the two

figures is the performance ratio (PR) which is 7.74 kg product per kg steam in the former and 7.86 kg product per hg steam in the latter.

CASE 2: If venting point is installed in 3rd stage instead of the 2nd stage, then only one extra venting point is required to keep NCGs under control as shown in Figure 4.6. Having less number of installed venting points, the PR is slightly improved to 7.9 due to the less vapour escaped through venting system.
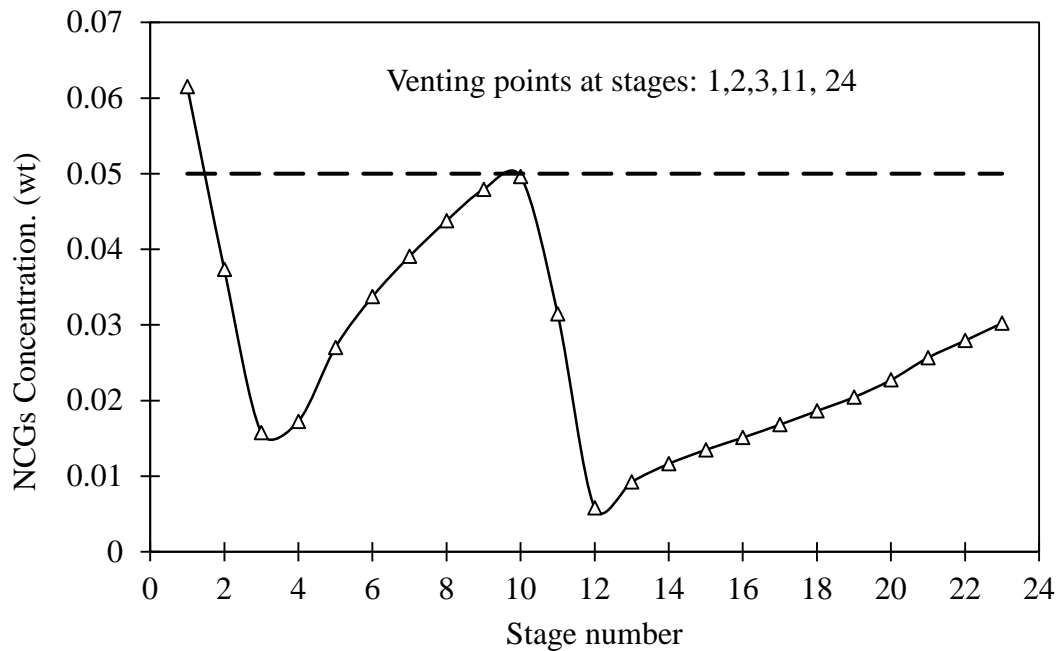
Figure 4.4: Venting in the first three stages and other two stages
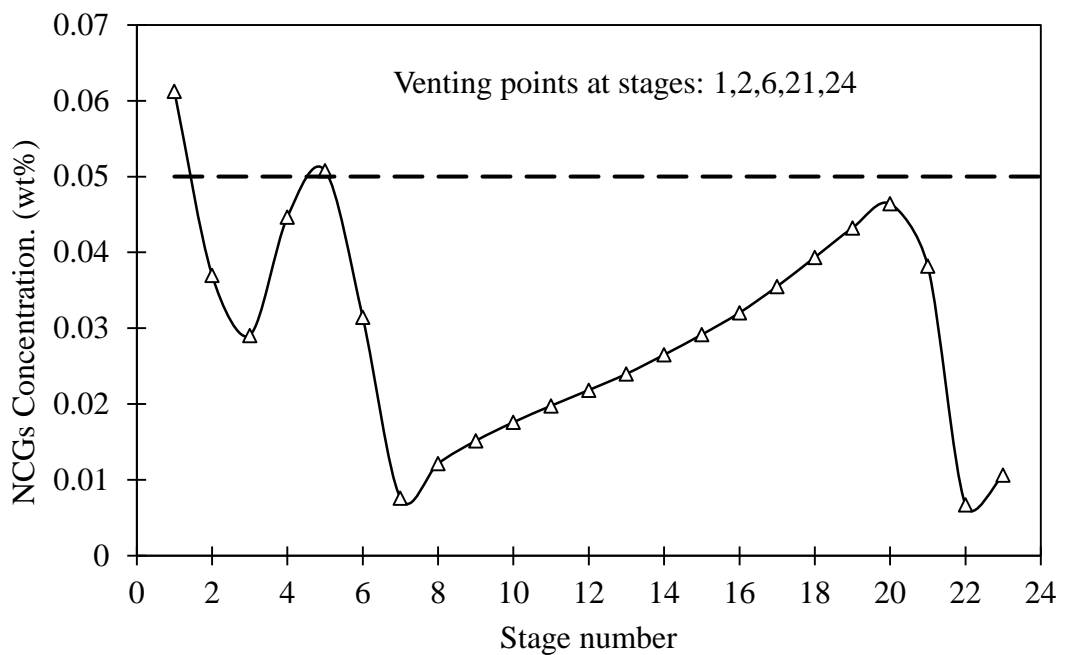
Figure 4.5: Venting in different stages (Five points)
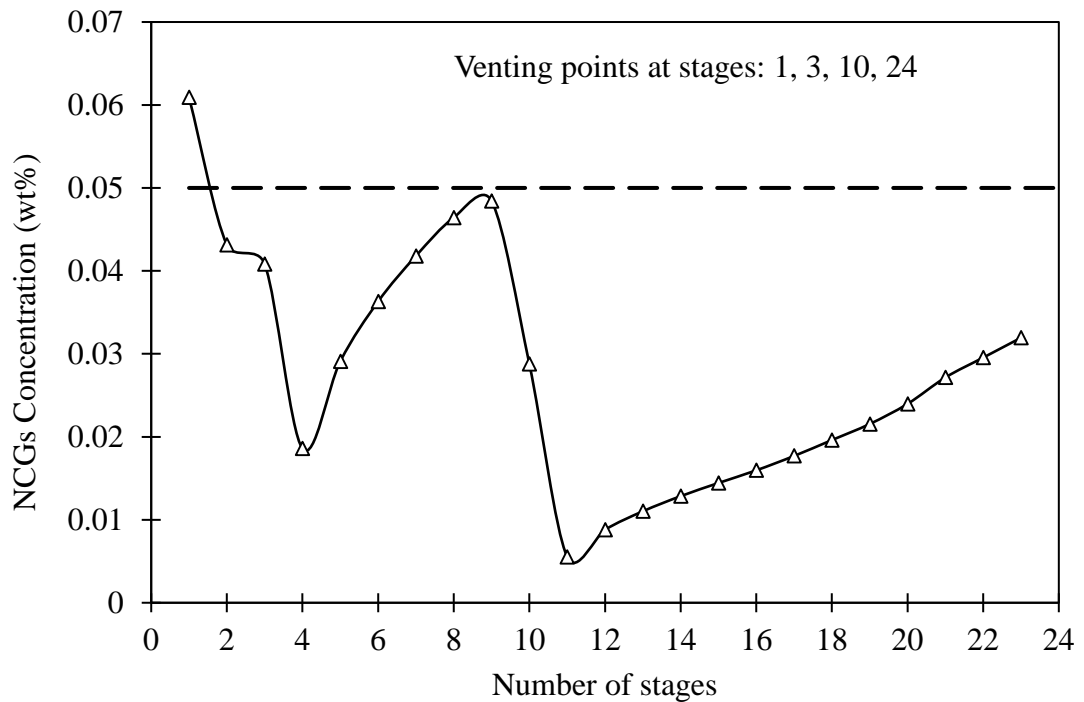
Figure 4.6: Venting in only four stages

4.4.2 Effect of NCGs on the OHTC.

Alasfour and Abdulrahim (2009) and Said et al. (2010) obtained similar pattern of OHTC due to their fixed value of NCGs concentration in every stage. Alasfour and Abdulrahim (2009) assumed 0.04 (wt. %) NCGs concentration in every stage and Said et al. (2010) used different value up to 0.06 (wt. %) but constant in every stage. The OHTC correlation they used which was reported by (El-Dessouky and Ettouney, 2002) shows that the OHTC is affected only if the NCGs concentration exceeds 0.05 (wt. %) as shown in Figure 4.7. Here, the venting points' locations are more relaxed to allow the concentration of NCGs to reach 0.055 (wt. %) to show clearly the effect of these gases on the OHTC. Different cases are studied and the results are plotted in Figure 4.7.
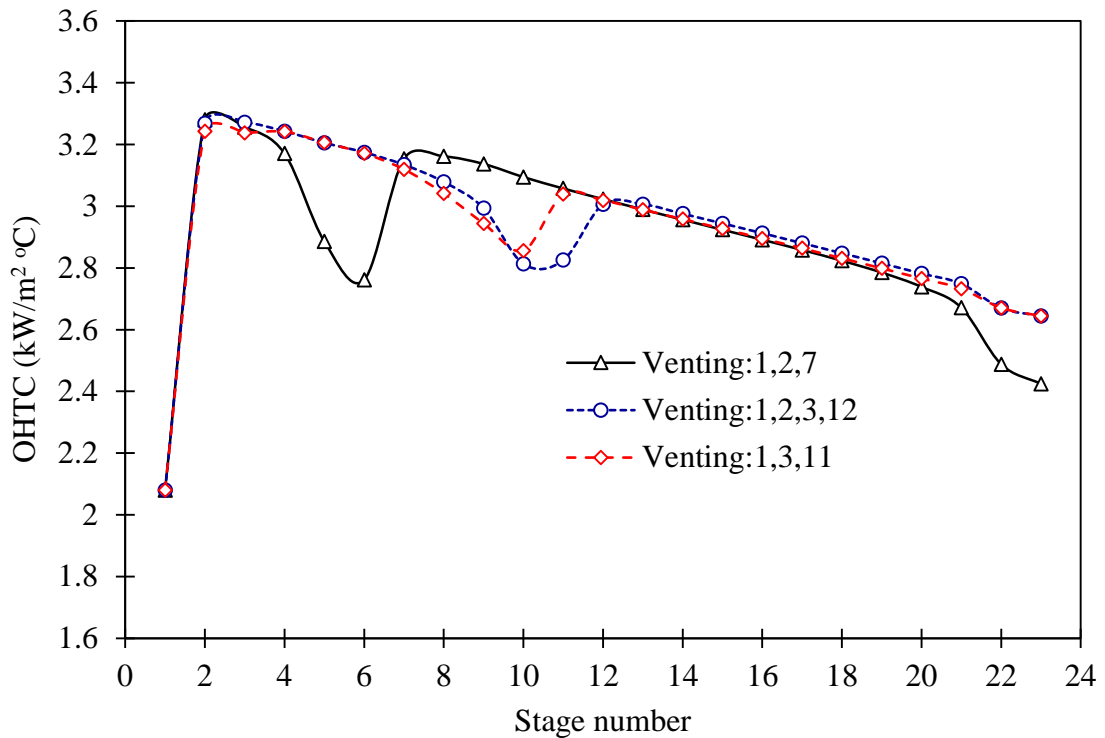
Figure 4.7: Overall heat transfer coefficient profile for different venting points location

CASE 1: When venting points are installed in 1st, 2nd, 7th and in the last stage, the OHTC drops in the 5th and 6th stages to 2.88 kW/m² °C and 2.76 kW/m² °C respectively due to the increase of the NCGs concentration to 0.055 (wt. %) and 0.056 (wt. %) respectively. Thus, venting point is required to vent NCGS and as result the OHTC increased to the normal value. Also, OHTC is affected in the first stage and second stage in the rejection section due to the increase of NCGs concentration in these stages.

CASE 2: When venting points are installed in 1st, 2nd, 3rd, 12th and in the last stage or 1st, 3rd, 11th and in the last stage, the OHTC will only decrease to 2.81 kW/m² °C in stage 10 where the concentration of NCGs reaches 0.053 (wt. %).

It is important to mention that in all cases the concentration of the NCGs in the first stage is around 0.06 (wt. %) due to high release of the NCGs. At this concentration, the OHTC is found to be as low as 2.08 kW/m² °C compared to 3.26 kW/m² °C in the second stage.

4.5. Conclusions

In this chapter, the dynamic model, which was developed in chapter three, was used to study the effect of the venting points on the performance of MSF plants and also it is used to study the effect of NCGs on the OHTC. The gases dissolved in the seawater are mostly liberated with the vapour produced in the first stage due to the high temperature and low solubility and thus venting in the first stage is essential. In order to avoid high NCGs concentration in the downstream stages, vents are installed in second or third stages. Additional venting points are provided at intermediate stages and at the final stage. The location of venting points is very important and plays an essential role in designing MSF plants. Based on the simulation results, it was found out that venting point installed in the third stage rather than in the second is very important and more efficient in term of reducing energy losses and increase performance ratio.

Similar to Said et al. (2010), the effect of NCGs on the OHTC was clearly noted especially if the concentration of the NCGs exceeds 0.05 (wt. %). It was found out that at 0.055 (wt. %), the OHTC is reduced by 12% in the first stage and up to 37.5% if the concentration of NCGs reaches 0.06. Thus, for better performance it is required to keep the NCGs concentration less than 0.05 (wt. %). NCGs less than 0.05 affect heavily the vapour side heat transfer coefficient but due to the fouling resistance, this effect is nearly negligible when it comes to the OHTC. However, the aforementioned results may become slightly different if the release of NCGs due to chemical reaction is considered.

CHAPTER FIVE

Generic Model Control (GMC) and Hybrid Fuzzy-GMC Control in Multistage Flash (MSF) Desalination

5.1 Introduction

Generic Model Control (GMC) is a well-known advanced control technique that has been used widely in the past and was developed by Lee and Sullivan (1988) as a result of the intense desire to develop a model that could handle nonlinear processes like those encountered in the chemical industry. Cott and Macchietto (1989) applied GMC strategy as controller to track the reactor temperature set point. Vega et al. (1995) applied GMC controller experimentally and by simulation a batch cooling unseeded crystallization process to control crystallizer temperature. Aziz et al. (2000) used GMC to design a controller for a batch reactor to track the optimal temperature profiles. Ghasem et al. (2003) implemented GMC controller to the two-phase model of a non-isothermal fluidized bed catalytic reactor to control the temperature inside the reactor by tracking new set point and handling the disturbance. In tracking the optimal temperature set point profile of batch reactor, Arpornwichanop et al. (2005) applied GMC algorithm to drive the temperature of the batch reactor to follow the desired profile. Mujtaba et al. (2006) coupled GMC with NNs as a controller to estimate the heat release in a exothermic reaction. Karacan et al. (2007) proposed multivariable generic model control (MGMC) to control the top and bottom product temperatures of a packed distillation column. Ekpo and Mujtaba (2008) used GMC controller in batch polymerization of methyl methacrylate to track the set point optimal temperature profile with neural networks as an online heat release estimator for the system. Kamesh et al. (2014) used GMC to track the set point of a reactor temperature of an industrial multiproduct semi-batch polymerization reactor.

The aforementioned publications used GMC algorithm to control the temperature in their systems. GMC is also used widely to control other type of variables such as pH, concentration and purity. For instant, Sousa et al. (2004) proposed GMC-fuzzy algorithm for the pH control of the enzymatic hydrolysis of cheese whey proteins. Kathel and Jana (2010) implemented GMC algorithm in two different forms, namely real and ideal GMC, to control a high-purity reactive batch distillation column. DU et al. (2013) applied GMC algorithm in sewage processing to control the concentration of dissolved oxygen based on the hybrid model. Fu and Liu (2015) implemented GMC controller in a heat integrated air separation column to control the purity of the Nitrogen and Oxygen products.

From the foregoing review, the GMC has been proved to be simple, robust and strategic in controlling various types of process parameters. Hence, the decision to use it to control the TBT and BL in MSF plant.

There is no known use of GMC as a controller strategy in MSF plants. In this chapter therefore, the GMC control strategy is designed and introduced to the MSF process to control and track the set points of the two most important variables in the MSF plant; namely the output temperature of the brine heater (TBT) and the Brine Level (BL) in the last stage. In addition, a GMC control hybrid with Fuzzy logic controller to develop hybrid (GMC-Fuzzy controller) is used for the same purpose. The objectives of this study are: firstly, to obtain optimum TBT and BL profiles for four different seasons throughout the year by minimizing the Total Seasonal Operating Cost (TSOC); secondly, to track the optimum TBT and BL profiles using PID and GMC controllers with and without the presence of constraints; thirdly, to examine how both types of controllers handle the disturbances which occur in the plant. Note, all previous studies on the control of MSF process were restricted to one particular season (for a single seawater temperature). Also, they were restricted to track a set point change without simultaneously disturbing any of the systems' other parameters. Here both have been relaxed in this study.

5.2. Optimization Problem

The wide difference in seawater temperature during the day (also between summer and winter seasons) has a great impact on TBT and BL, consequently,

product rate and plant performance are affected. The seawater temperature depends on the locality and the time of the year and it can be varies between 15 ^{o}C and 35 ^{o}C (Hawaidi and Mujtaba, 2010b). (Darwish et al., 1995) reported that it can be as low as 10 ^{o}C in Kuwait. At low temperature, its mass flow rate has to be reduced to achieve reasonable flashing brine temperature in the bottom stages. However, the decrease in the cooling seawater flow rate can result in a decrease in its velocity to lower than the acceptable minimum (about 1.5 m/s) (Darwish et al., 1995). For this reason, most MSF plants operate in summer and winter mode, when the set point of the intake seawater temperature varies between 25 ^{o}C in the winter mode and 32 ^{o}C in the summer mode (Alatiqi et al., 1999).

For fixed operating conditions, the MSF plants produce more fresh water in winter (low seawater temperature) than in summer (Tanvir and Mujtaba, 2006c). However, this production pattern goes counter to the demand of fresh water (Hawaidi and Mujtaba, 2011a). Tanvir and Mujtaba (2008) minimized the operating cost by optimizing the number of stages based on seasonal variation of the seawater temperature. For fixed fresh water production and TBT, Hawaidi and Mujtaba (2010b) studied the effect of seawater temperature on the operating cost of the MSF process. Hawaidi and Mujtaba (2011b) conducted an optimization study to demonstrate the optimum design and operation of MSF process to meet the variable demand of fresh water through the day and the year at fixed TBT.

For control purpose, an optimization study is conducted to obtained different optimum values for TBT and BL based on four different seasons. Based on seawater temperature profile presented by Hawaidi and Mujtaba (2010b), four different values of the seawater temperature are considered; 20 ^{o}C, 28 ^{o}C, 32 ^{o}C, and 24 ^{o}C for winter, spring, summer and autumn respectively (Figure 5.1). To obtain different values of the TBT, a fixed number of stages and fixed fresh water product are considered. Moreover, to obtain different values of BL, more constrains are introduced to maintain the brine level in all stages at reasonable level and thus optimal values for BL are obtained for each season.

Figure 5.1: Variations of seawater temperature and set point profiles for four seasons (Hawaidi and Mujtaba, 2010b)

For the following design parameters; fixed number of stages, fixed fresh water demand and fixed steam temperature, four values of the intake sea water temperature are investigated to determine the optimum *TBT*, *BL*, *Rec* and *W$_S$* by minimizing the Total Seasonal Operating Cost (TSOC).

The Optimization Problem (OP) is described as follows;

OP   Min   TSOC
            TBT, BL, Rec, Ws

Subject to:

    Equality constraints

        Process model $f(x, u, v)$ $= 0$

$$D_{end} = D^*_{end}$$

    Inequality constraints

$$(85\,°C) \leq TBT \geq (98\,°C)$$

$$(0.3\,m) \leq BL \leq (0.8\,m)$$

$$\left(11500\frac{ton}{hr}\right) \leq Rec \leq \left(17200\frac{ton}{hr}\right)$$

$$\left(7600\frac{ton}{hr}\right) \leq W_S \leq \left(13600\frac{ton}{hr}\right)$$

where D_{end} is the total capacity of the plant and D^*_{end} is the fixed water demand (=1296 ton/hr). The boundary values of Rec and W_S are chosen based on the minimum and maximum allowable values of the water velocity in the condenser tubes between 1.5 and 2.3 m/s (Helal, 2003).

The objective function equation (TSOC) is obtained from Hawaidi and Mujtaba (2011) and the Total Annual Cost (TAC) is defined as

$$\text{TAC (\$/year)} = \text{CPC} + \text{STC} + \text{TOC} \tag{5.1}$$

where CPC is the Annualized Capital Cost, STC is the Storage Tank Cost and TOC is the Total Operating Cost. Since the CPC and STC are function of the plant configuration and constant for all seasons, then the only variable cost here is the TOC. Hawaidi and Mujtaba (2011b) defined the TOC as following:

$$TOC\ (Total\ Annual\ Operating\ Cost, \$/year) = C_1 + C_2 + C_3 + C_4 + C_5 \tag{5.2}$$

Where

$$C_1\ (Steam\ cost, \$/year) = 8000 \times W_{steam} \times [(T_{steam} - 40)/85] \times 0.00415 \tag{5.3}$$

$$C_2\ (Chemical\ cost, \$/year) = 8000 \times [D_{end}/1000] \times 0.025 \tag{5.4}$$

$$C_3\ (Power\ cost, \$/year) = 8000 \times [D_{end}/1000] \times 0.109 \tag{5.5}$$

$$C_4\ (Maintenance\ cost, \$/year) = 8000 \times [D_{end}/1000] \times 0.082 \tag{5.6}$$

$$C_5\ (Labour\ cost, \$/year) = 8000 \times [D_{end}/1000] \times 0.1 \tag{5.7}$$

Although the TSOC value varies from season to season, for simplicity purposes, the TOC can be assumed equally distributed and thus the TSOC can be defined as following:

$$TSOC = TOC/4 \tag{5.8}$$

The value of 8000 in equations 5.3 to 5.7 is the assumed to be the operating hours per year. The last value in equations 5.3 to 5.7 is the cost in $/ton unit. The unit of D_{end} in equations 5.4 to 5.7 is in kg/hr. More details on the calculations of TOC can be found in Hawaidi and Mujtaba (2010b, 2011b).

5.3. Control Strategy

For safety purpose, most MSF plants have many control loops to maintain steady state and overcome the instability caused by the start-up of the plant or failure in one of the plant components. Maniar and Deshpande (1996) and Ismail (1998) mentioned nine controlled variables with nine corresponding manipulated variables as the main process variables to be controlled. Al-Gobaisi et al. (1994) mentioned that most existing MSF plants could be controlled by 4 to 6 primary loops. However, in these studies two main control loops were TBT control loop and BL control loop as without these two loops the plant cannot be controlled at all. In this study, a GMC control was implemented in these two control loops.

1. Top brine temperature (TBT). This is the temperature of the recirculation brine after it is heated by the low pressure steam in the brine heater. It plays an important role in describing the performance of MSF and has direct effects on the distillate production and the levels in each flash chamber. It can be used to control the whole plant in addition to load control and for each plant, there is a certain top brine temperature which depends on the seawater inlet temperature

2. Last stage brine level (BL): The brine levels in the flash stages are quickly affected by the steam supply temperature or flow rate (Husain et al., 1994). Brine levels in all stages should be high enough to seal the interstage orifices and prevent blow-through. However, the high BL increases the thermodynamic non-equilibrium losses and should be low enough to ensure less equilibration losses. An adjustable level controller is required with high sensitivity over the permissible range of BL. This controller is one of the most important control loops in the MSF plant since the level in all stages is controlled by adjusting the BL in the last stage (Darwish et al., 1995).

5.3.1 Proportional Integral Derivative (PID) Control

The PID controller is widely used and recommended for a variety of control problems and can be used for many industrial systems. The controller parameters can be tuned by using trial and error methods, or any of the classical tuning

techniques such as Zeigler Nicholas. For many process control problems, good results can be achieved by tuning PI, or PID using conventional methods, which rely on the knowledge and skill of the control engineer However, due to the change in conditions of the MSF plant during its operation, tuning PID parameters are always considered as time consuming and challenging.

The simplest form of PID controller can be represented by:

$$C(t) = k_c \left(e(t) + \frac{1}{\tau_i} \int_0^t e(t)dt + \tau_D \frac{de(t)}{dt} \right) \qquad (5.9)$$

Where k_c is the proportional gain, τ_i the integral time, τ_D the derivative time constant, e the error (controller input), and C the controller command (controller output).

5.3.1.1 Tuning of the PID Controller

As mentioned in the previous section, different methods can be used to tune the PID controller parameters. The most common method is the integral performance criterion. In this work, an optimization based method is used to minimize the Integral Absolute Error (IAE), the Integral Time Absolute Error (ITAE) and Integral Square Error (ISE) and the PID parameters (k_c, τ_i, τ_D) are optimized to give minimum error. Since initial values of PID parameters are required to conduct the optimization problem, Ziegler-Nichol's method is used to obtain the initial values for PID parameters.

The optimization problem (OP) is described as following

OP   Min   IAE, ITAE and ISE

k_c, τ_i, τ_D

Subject to:

    Equality constraints

        Process model $f(x, u, v) = 0$

    Inequality constraints

$$-100 \leq k_c \leq 100$$

$$0.0 \leq \tau_i \leq 100$$

$$0.0 \leq \tau_D \leq 100$$

The results of the optimization problem for TBT and BL loops are presented in Table 5.2. Figures 5.2 and 5.3 show the performance of both controllers, TBT and BL respectively, using the three types of optimization criterion (ISE, IAE and ITAE). The optimum values from best method are used later in the control comparison. It has to be mentioned that two optimization functions are used here. One is to optimize the parameters of the TBT controller loop and another is to optimize the parameters of the BL controller loop.

5.3.2 Generic Model Control (GMC) Strategy

Since its development by Lee and Sullivan (1988), there has been growing interest in the use of GMC, which has been demonstrated to have certain robustness for a wide range of process nonlinearity against model mismatches. GMC is relatively easy to implement and does not require linearizing the nonlinear process (Aziz et al., 2000).

The GMC control algorithm can be written as following;

$$\frac{dy}{dt} = k_1\left(y_{sp} - y\right) - k_2 \int \left(y_{sp} - y\right)dt \tag{5.10}$$

where y is the measured variable and y_{sp} is the desired value of the control variable. As in the case of the PI controller, the first expression of the above equation $k_1\,(y_{sp}\text{-}y)$ is required to bring the process from a large distance towards steady state, but some offset would exist. The second expression $k_2 \int(y_{sp}\text{-}y)dt$ however, is required to eliminate the offset of the controller. The values of the tuning parameters used to obtain the desired response. More details of the model can be found in Lee and Sullivan (1988).

In the brine heater of MSF process, the dynamic model equation relating the TBT as controller variable to the steam flow rate (*Ms*) as a manipulated variable can be written as;:

$$\frac{d(T_{B0})}{dt} = \frac{(M_s \times \lambda) - W_R \times Cp \times (T_{B0} - Tc_{in})}{M_{bh} \times Cp} \tag{5.11}$$

Here, T_{B0} is the TBT, W_R the brine flow rate, *Cp* the heat capacity of the brine, Tc_{in} the temperature of the brine entering the brine heater, λ the latent heat released by the condensate steam and M_{bh} the brine mass hold up inside the

brine heater tubes. To solve for the control, the actual output rate is set equal to the desired output rate. In other words, setting Equation (5.10) equal to Equation (5.11) and substituting T_{B0} for y and T_{B0_sp} for y_{sp}.

$$\frac{(M_S \times \lambda) - W_R \times Cp \times (T_{B0} - Tc_{in})}{M_{bh} \times Cp} = k_1\left(T_{B0\_sp} - T_{B0}\right) + k_2 \int \left(T_{B0_{sp}} - T_{B0}\right) dt \qquad (5.12)$$

Solving for the manipulated variable, Ms, the following equation can be obtained.

$$M_S = \frac{1}{\lambda} \times \left(\begin{array}{c} M_{bh} \times Cp \times \left[k_1\left(T_{B0\_sp} - T_{B0}\right) + k_2 \int\left(T_{B0\_sp} - T_{B0}\right)dt\right] \\ + \left[W_R \times Cp \times (T_B - Tc_{in})\right] \end{array} \right) \qquad (5.13)$$

Ms gives the amount of steam flow rate required to control the outlet temperature of the brine heater.

Similarly, the above procedure can be followed to implement the GMC method to control the brine level in the last stage. Firstly, the process model equation relating the brine level, L_B, as controller variable to the brine flow rate leaving the last stage (B_{out}) as manipulated variable must be defined. Equation (5.14) is the material balance equation in the last stage, and can be used here to calculate the change of the brine level, L_B, in the last stage.

$$\frac{dL_B}{dt} = \frac{(B_{in} + F - B_{out} - V_B - Rec)}{A_S \times \rho_B} \qquad (5.14)$$

where B_{in} is the brine flow rate leaving the previous stage, F the makeup flowrate fed to the last stage, B_{out} the blow down flow rate leaving the last stage, V_B the vapour leaving the brine pool, and Rec the recycle brine flow rate. To solve for the control, Equation (5.14) must be equalized to Equation (5.10) and substituting L_B for y and L_{B_sp} for y_{sp}.

$$\frac{(B_{in} + F - B_{out} - V_B - Rec)}{A_S \times \rho_B} = k_1\left(L_{B\_sp} - L_B\right) + k_2 \int\left(L_{B\_sp} - L_B\right)dt \qquad (5.15)$$

Solving for the manipulated variable, B_{out}, Equation (5.16) can be obtained.

$$B_{out} = B_{in} + F - V_B - Rec - \left[A_S \times \rho_B \times \left(k_1\left(L_{B\_sp} - L_B\right) + k_2 \int\left(L_{B\_sp} - L_B\right)dt\right)\right]$$
$$(5.16)$$

Bout gives the amount of blow down flow rate required to maintain the BL in the last stage at the desired level.

5.3.2.1 Tuning of the Generic Model Controller

Lee and Sullivan (1988) provided a figure that outlines the relation between two variables, ξ and τ. Tuning GMC can be obtained by choosing a better combination of ξ and τ. The choices should be reasonable and require understanding of the system's natural dynamic response. By choosing reasonable values of ξ and τ, the two tuning parameters k_1 and k_2 are obtained using Equations (5.17 and 5.18).

$$k_1 = \frac{2\xi}{\tau} \tag{5.17}$$

$$k_2 = \frac{1}{\tau^2} \tag{5.18}$$

It is important to mention that different values of k_1 and k_2 are obtained for different control loops. More details of the procedure in choosing ξ and τ can be found in Lee and Sullivan (1988).

5.4. Results and Discussion

Simulations with optimization of the MSF process for four different seasons and optimization of PID controller parameters, TBT and BL controls were carried out using gPROMS builder model. First, the MSF process was optimized at fixed plant capacity and four different values of seawater temperature by minimizing the TSOC. For the sake of stability, other variables such as recycle brine (Rec) and the intake seawater flow rate (W_S) were relaxed to fluctuate for limited values. Since the steam is coming from a different source, its temperature is fixed and only the steam flow rate is varied to achieve the optimum TBT. The results of the optimization are shown in Table 5.1. The table also includes the optimum brine recycle and intake seawater flow rate at fixed capacity for four different seasons. Therefore, the operator has to change these values to their next values after every season. It should be mentioned that the optimum values for TBT and BL for four seasons are developed for control purpose and cannot be relied on to make accurate performance. More parameters must be considered to draw final design evaluation.

Table 5.1: Optimum values for TBT & BL in four seasons.

Season	Seawater Temp set point (°C)	TBT (°C)	BL (m)	Rec (ton/hr)	Ws (ton/hr)
Winter	20	88	0.36	13889	10208
Spring	28	92	0.43	14607	12705
Summer	32	94	0.47	15026	12896
Autumn	24	90	0.43	14257	12533

The main objective of this study is to evaluate the performance of GMC controller comparing to conventional PID controller by tracking the set points change of TBT and BL respectively. The PID controllers are introduced to the model and their parameters are tuned (Table 5.2).

Table 5.2: Optimum PID parameters for TBT and BL control loops.

Interval	Criterion	Parameters of PID Controller		
		k_c	T_i	t_D
TBT	ISE	1.2873	0.0052	0.1481
	IAE	2.01	0.014	1.04
	ITAE	1.6776	0.062	0.976
BL	ISE	5.44	0.193	15.308
	IAE	30.41	1.182	1.16
	ITAE	39.89	0.06	1.435
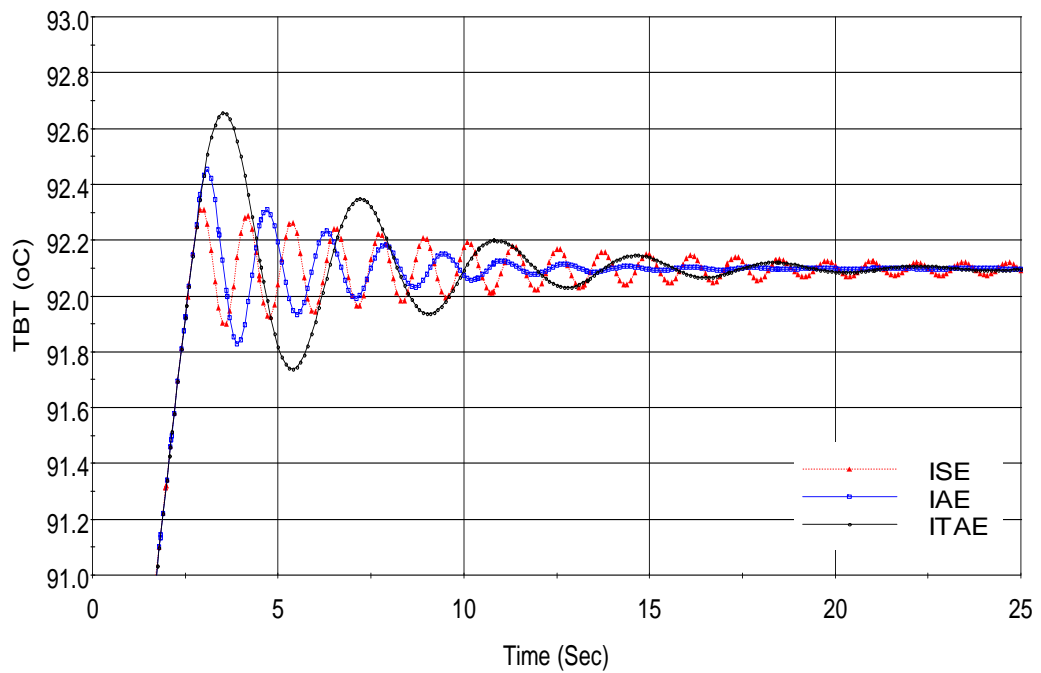
Figure 5.2: Step response of the optimally tuned PID parameters TBT loop.
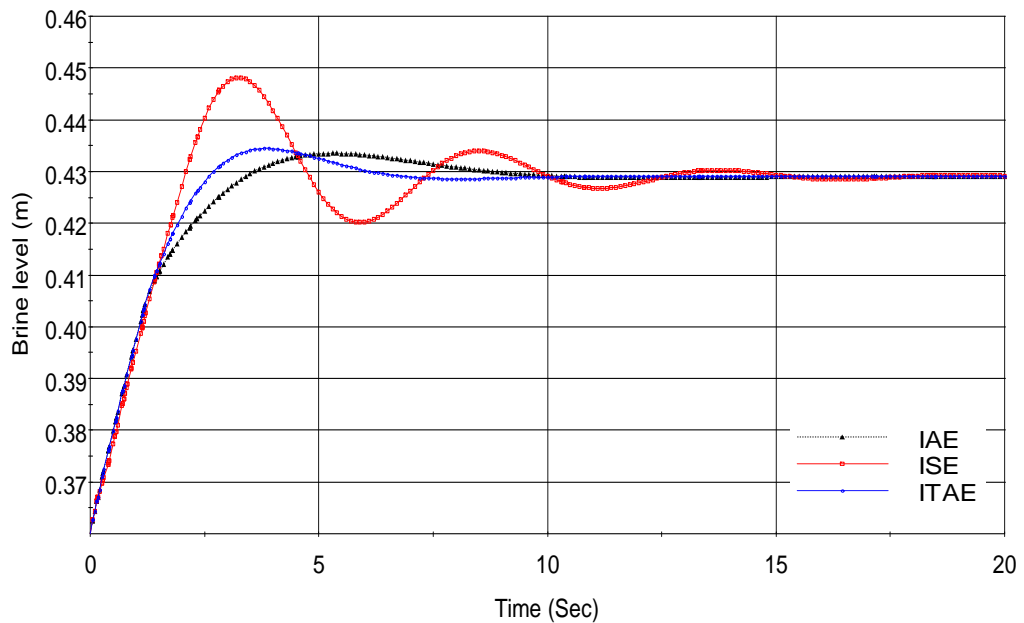
Figure 5.3: Step response of the optimally tuned PID parameters BL loop.

To select the best technique that used to minimize the error and thus giving optimum values of PID parameters, the results presented in Table 5.2 are plotted in Figures 5.2 and 5.3 respectively (Only for Spring operation conditions). It is to be mentioned here that the optimum values obtained by optimization techniques were very aggressive in some cases. As it can be seen from Figure 5.2, the values obtained for TBT loop using ISE and IAE criteria are very aggressive and

take a long time to settle down while those from ITAE, although have overshooting, seem to be close to optimum and less aggressive. For, BL loop, however, the values obtained using ITAE seem to be less aggressive and giving very smooth curve. Thus, the optimum values of PID parameters obtained by ITAE criteria are considered to be our choice for both loops. This choice applies for all seasons.

For tuning GMC parameters for TBT loop, Cott and Macchietto (1989) recommended a value of 10 for ξ to eliminate the overshoot. However, Lee and Sullivan (1988) mentioned that the selection of GMC parameters depends on the system's natural dynamic response. In this work, the value of 10 for the ξ that gives less overshoots is selected. τ is calculated using the graphical method proposed by Lee and Sullivan (1988) which gives 16 sec for TBT loop and 8 sec for the BL loop.

For each controller loop, three case studies were performed to examine the performance of each type of controller in the set points tracking, disturbance and constraint handling.

5.4.1 Top Brine Temperature Loop (TBT)

5.4.1.1 Set Point Tracking

Figure 5.4 shows the control performance of the PID and GMC controller for tracking the set point change of TBT based on different seasons. For each season's data, the model is run for 40 seconds to reach steady state before changing the new set of data for the next season. For reader interpretation convenience, the results of process variables and manipulated variables were plotted together in one figure (Figure 5.4). In all cases, GMC controller was performing smoothly and reach the set point in less time. The PID controller, on the other hand, expressed oscillatory response more than GMC before returning to the set point while the GMC controller did not reveal any sluggish response, move smooth towards the new set point, and provide better performance over PID in tracking the set point. Similar behaviour can be observed for the manipulated variables (steam flow rate). For PID, the steam flowrate looks unstable in attempt to bring the process variable (TBT) back to the set points for

all seasons. However, the steam flow rate behaviour for the GMC controller was smooth and stable while controlling the process variable.
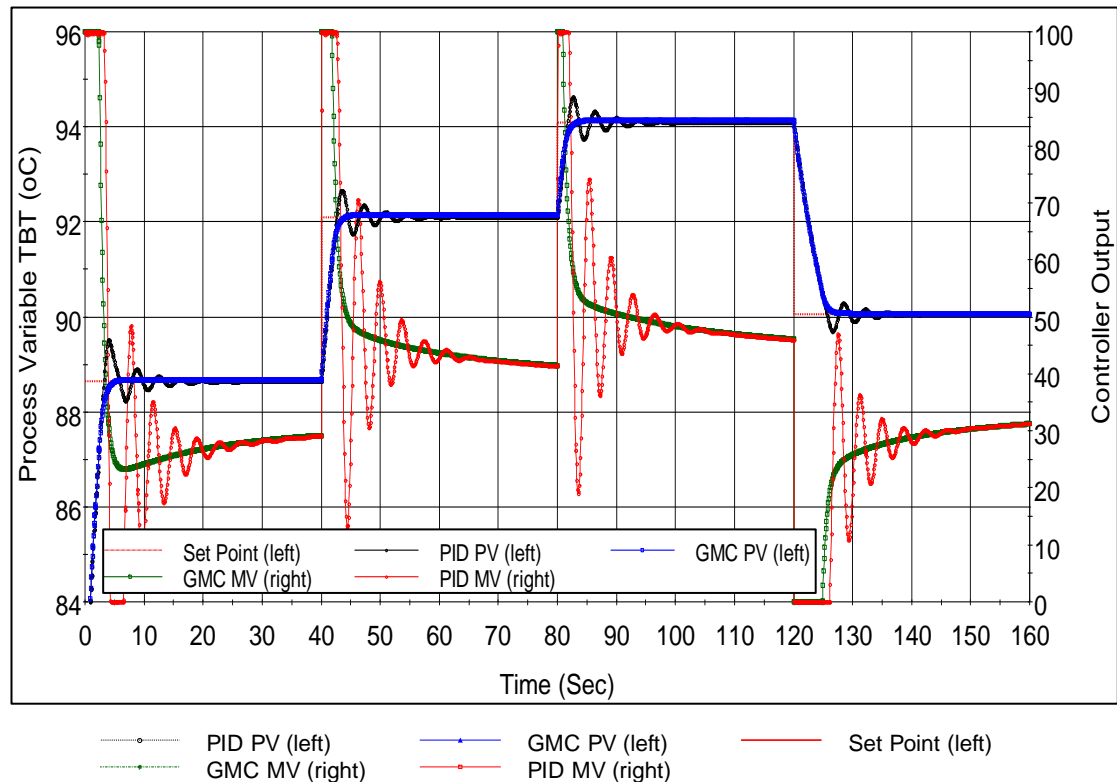
Figure 5.4: Tracking the TBT set points for four different seasons using GMC & PID controllers

5.4.1.2 Disturbance

Disturbance normally occurs in MSF plants due to failure of pumps or valves. In order to examine the capability of the controller in handling the disturbance, a change in the brine recycle flow rate was introduced in this case at a regular interval of 50 sec by increasing its value by 6%, decreasing by 14% and then increasing by 8%. The process was assumed that it runs in the autumn season when the disturbance occurred. The recycle flow rate was chosen as the disturbance because it affects the TBT and BL at the same time. Figure 5.5 shows the performance of both controllers in handling the disturbance. As it can be seen, the GMC controller acts vary fast and provides better performance in returning the temperature to steady state. Also as expected, a perfect GMC (with no modelling error) should not have significant change in the PV when disturbances enter the system. However, the PID controller exhibits some oscillatory response and could not reach the set point fast and takes a long time

to reach steady state. The manipulated variables reacted simultaneously as their process variables. When increasing the recycle brine flow rate by 6%, the steam flow rates increased to provide enough heat to keep the TBT constant. Similarly when the recycle flowrates decreased by 14%, the steam flow rates dropped to maintain constant TBT. For PID controller, the behaviour of the steam flow rate follows the same behaviour of the process variable with some oscillatory response while the steam flow rate using GMC controller behaves smoothly and fast to keep in the TBT constant.
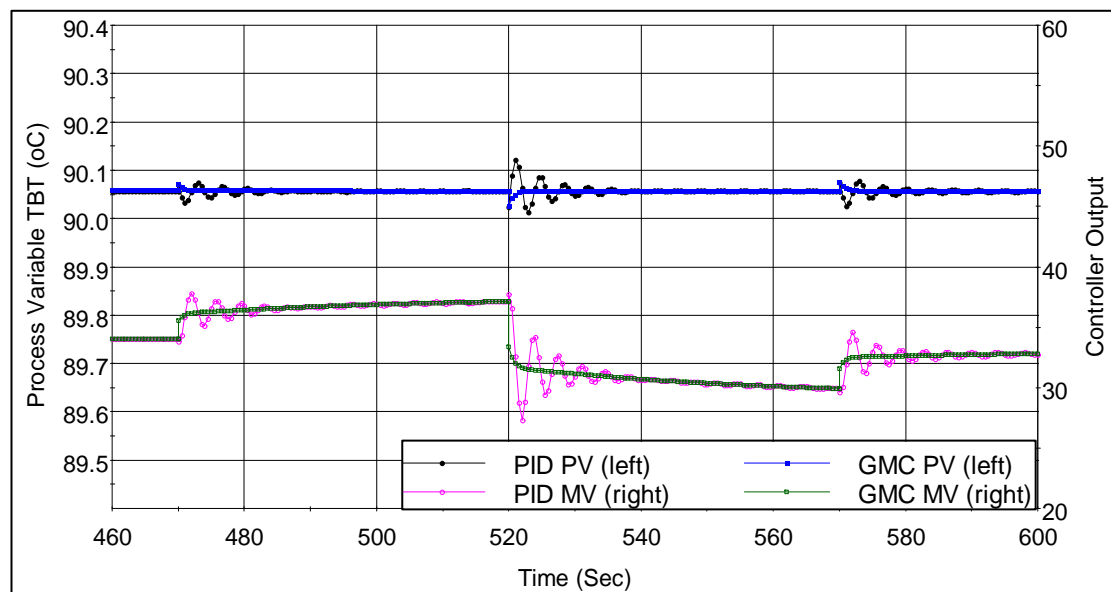
Figure 5.5: Handling the disturbance to control the TBT using GMC and PID controllers

5.4.1.3 Constraint Handling

The availability of steam depends on external source and thus it could be limited to a certain amount. Here, similar to the first case, the set points of the TBT was altered based on the four different seasons. However, the steam flow rate was assumed to be limited and hit the lower and higher limits to bring the controlled variable to its set point. As it can be seen in Figure 5.5, the set point was raised in spring season and thus more steam than required was needed to raise the TBT to its new set point. Thus, the steam hit the constraint of 100% for short time resulting in delay of the PID controller to reach the set point compared to the first case. The same results can be seen when the set point was further raised to 94 ^{o}C in summer. This is due to the reason that when the set point was increased,

the controller sent signal to the steam valve to fully open. However, due to the lack of available steam, the PID controller struggle to bring the process back to its steady state. In autumn, when the set point was changed to 90.06 ^oC, the steam flow rate was constrained by 0% and thus again the controller took a long time to bring the TBT to its new set point. In comparison with the GMC controller, it seemed that GMC controller performs similarly in handling the constraints because the availability of the steam that control the process and thus both controllers behave similarly and slowly. Figure 5.6 shows that the steam hit the constraint of 100% and 0% for the same time as it was shown for PID. However, when the available steam is adequate for the appropriate temperature, the GMC controller performs faster and smoothly and exhibit less oscillatory or sluggish response compared to PID controller when experienced large overshooting in particular when the set point was further increased in summer period.
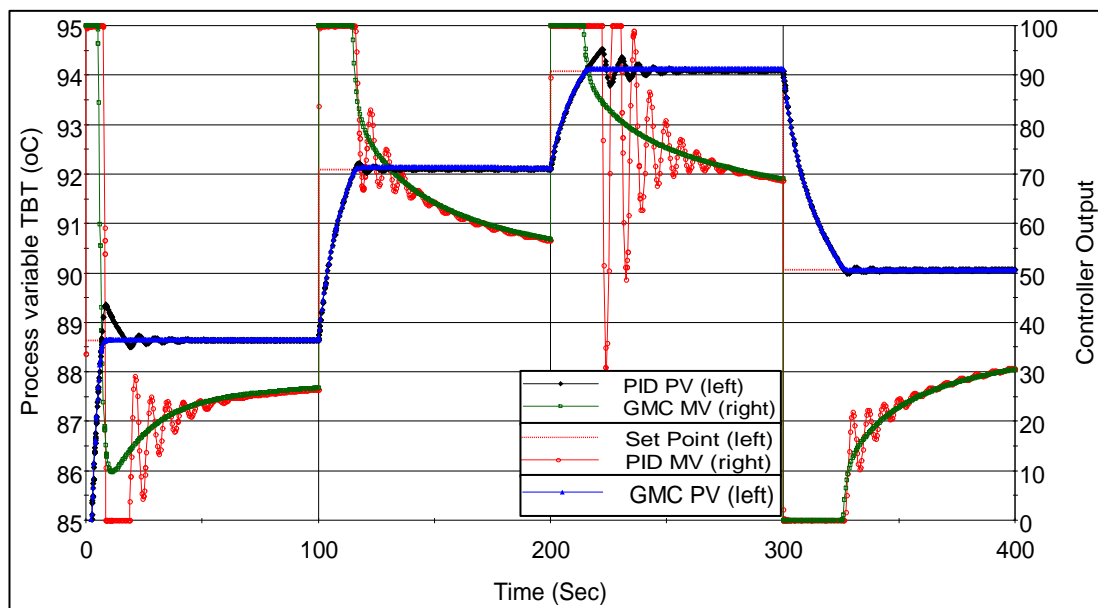
Figure 5.6: Tracking the TBT set points using GMC and PID controllers with constraints.

5.4.2 Last Stage Brine Level Loop (BL)

5.4.2.1 Set Point Tracking

Although, there was no large difference in the BL set points for different seasons, the difference was quite reasonable when examining the controller's performance. Figure 5.7 shows the responses when the set points were changed

based on four seasons. The PID and GMC controllers were implemented to track the new set points. In all intervals (Season interval), the GMC controller over performed the PID controller and reached the set point faster. The PID showed slight sluggish response and took some time to reach the set point. When the set points were increased from winter to spring and again from spring to summer, the GMC controller reached the set point at the same time with PID, however, while PID showed a slight overshoot, the GMC remains constant and kept the BL stable. The reason of the both controller crossed the set point at the same time is that the tuning of GMC parameters were tuning based on the time that PID cross the set point as it was mentioned before. The behaviour of the manipulated variables (Blow down) were identical to the performance of the process variables (brine level). The manipulated variable of GMC was smooth while the manipulated variable of the PID experienced slight overshooting to bring the level of the stage back to its set point.
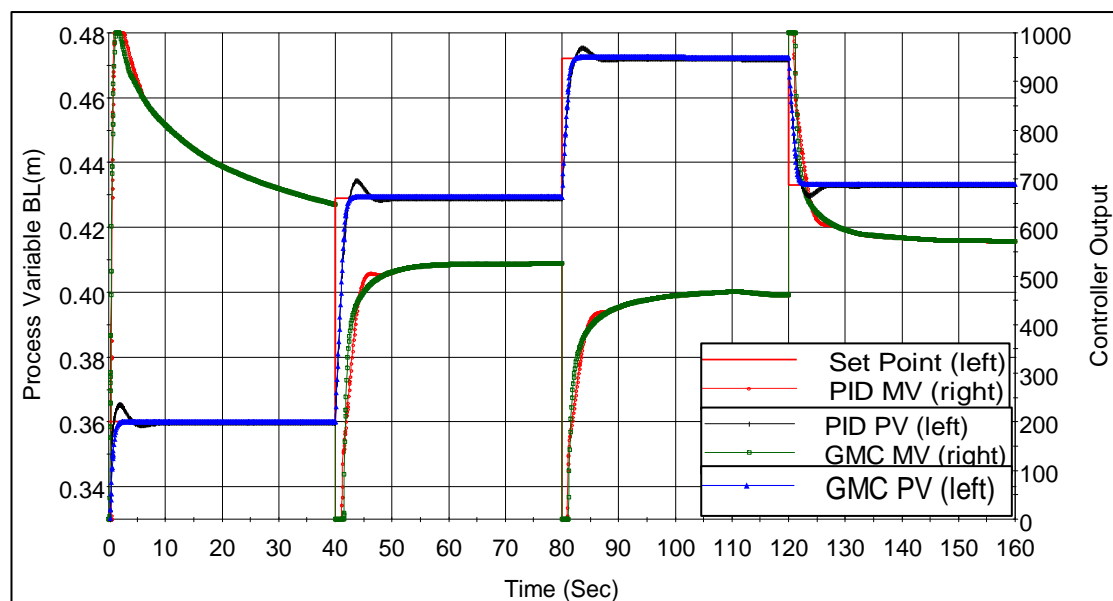
Figure 5.7: Tracking the BL set points for four different seasons using GMC & PID controllers

5.4.2.2 Disturbance

Similar to the case 2 in TBT loop, the same disturbance of the brine recycle was introduced to the process and the behaviour of both controllers were observed. Both loops (TBT and BL) work simultaneously and any set points change or disturbance affects both loops at the same time. Thus, the same step change in

the brine recycle was introduced to BL loop. As it can be seen in Figure 5.8, the GMC controller over performed the PID controller in bringing the process back to its steady state very fast, while the PID controller showed some overshoot before reaching the set point. The GMC work perfectly in handling the disturbance and no change occurred to the process.
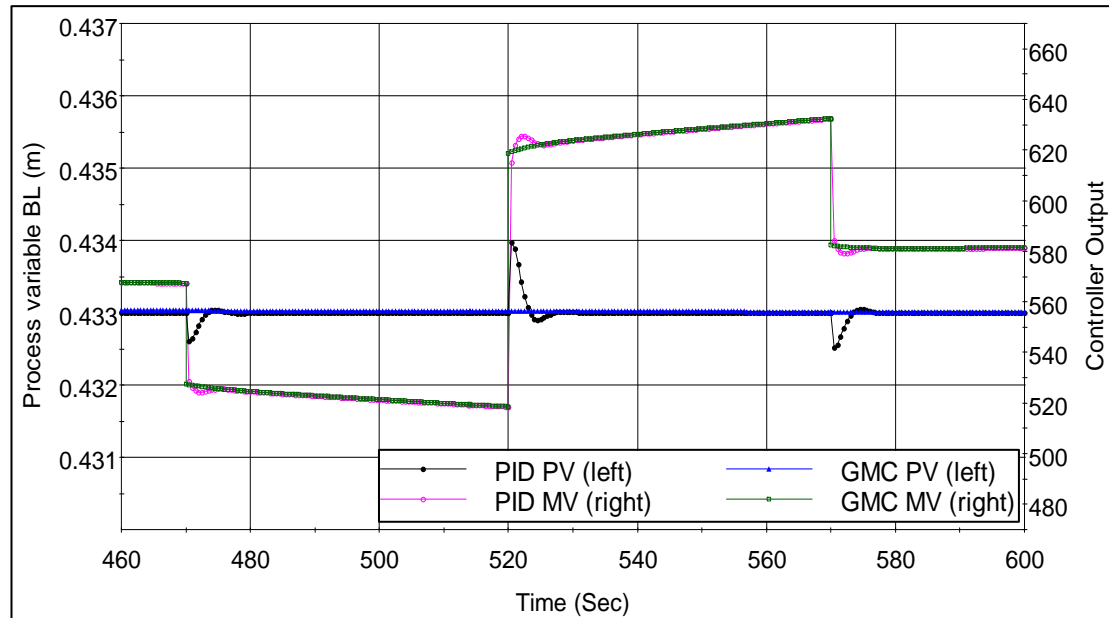
Figure 5.8: Handling the disturbance to control the TBT using GMC & PID controllers

5.4.2.3 Constraint Handling

The valve controlling the blowdown flow is assumed to be open at fixed positions to study the performance of the controllers under the constraints. Thus, the set points of the BL was changed based on the four different seasons and the valve position was assumed to be limited and reached the lower and higher limits to bring the controlled variable to its set point. As it can be seen from Figure 5.9, though both controllers worked well in controlling the process, GMC outperformed PID in bringing the process to steady state fast at the start-up of the plant. Both valves were hitting 0% and 100% (lower and upper limit) to bring the process to steady state, however, the valve controlled by GMC started to be stable first to maintain the BL constant. When the set point of BL was increased from 0.36 m in winter to 0.429 m in spring and raised again in summer up to 0.742 m, the valve of the blowdown were closed completely. Due to the constraints, the valve position reached its lower limit in attempt to increase the BL to its set points. Here,

both controllers PID and GMC behave similarly in controlling the process well. Again, in the final season (autumn) when the set point was changed from 0.472m to 0.433 m, the valve position reached the higher limit for few seconds to bring down the BL to its new set point. The GMC controller worked better here in autumn (last interval) in reaching the set point quickly. Regarding the manipulated variable behaviour, the manipulated variables for both controllers behave similarly as it was in Figure 5.6, however, PID manipulated variable react few seconds behind GMC manipulated variable. Despite their close performance in controlling the BL, the GMC has more stability over PID controller and could easily accommodate all the process changes.
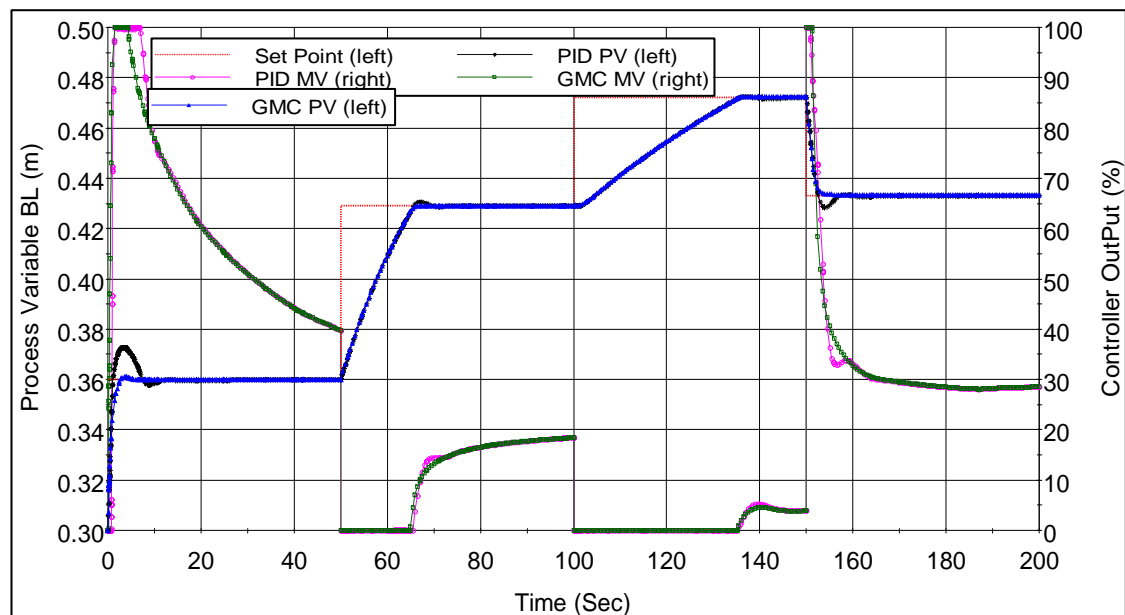
Figure 5.9: Tracking the BL set points using GMC and PID controllers with constraints.

5.5. Hybrid Fuzzy-GMC Control

In the previous part, a Generic Model Controller (GMC) was used successfully to control MSF desalination plant over four distinct seasons (winter to autumn). Two single loops of controller are working simultaneously in gPROMS to control the TBT and the brine level (BL) of the last stage. The MSF plant control system is operated at optimal conditions based on the seawater intake temperature. However, in order to improve the control performance, several attempts have been made to implement hybrid type of Advanced Process Control (APC)

strategies in MSF process. Although it was developed nearly five decades ago, Fuzzy Logic Control (FLC) has greater advantage over conventional PID control in addressing real time complex nonlinear systems. However, despite being robust, efficient and easy to implement, FLC is less efficient at handling complex control problem when it is used on its own (Jamshidi et al., 1996). Applying genetic algorithm (GA) to the FLC to control TBT in MSF process was used successfully to improve the convergence to the final desired set point and reduce the oscillations (Jamshidi et al., 1996, Akbarzadeh et al., 1997). Hybrid PD-like FLC approach was obtained by Ismail and AbuKhousa (1996) and applied to first order plus dead time to control TBT in a 18 stage MSF plant. To enhance the performance, an integration effect was added to the output of the PD-like FLC to produce PID-like FLC. Ismail (1998) presented a Fuzzy Model Reference Learning Control (FMRLC) to regulate the TBT of large MSF plant. The FMRLC was found to outperform the PID and direct fuzzy controllers. Olafsson et al. (1999) applied PI to Takagi-Sugeno type FLC to design PI-Like-TSFLC controller. Their results showed the stability of FLC in their most simulation cases.

Most of the above studies concluded that further exploration of an integrated FLC and more applications to other MSF control loops are needed. In this section, hybrid FLC-GMC controller is designed and implemented in MSF process to control the two most important variables namely TBT and BL. Without involving model reduction or approximations, a simulation of detailed dynamic mathematical model for the MSF process was carried out using gPROMS model builder. Similar optimal values for TBT and BL that were obtained in the previous chapter are used here.

5.6 Control Strategy

The hybrid control system of FLC and GMC has been presented in this section. The FLC as main controller and GMC as control trajectory have been combined to present a hybrid fuzzy-GMC control. The objectives of this control system are to control the TBT and the BL of the last stage. Figure 5.10, shows the control system block diagram that is used in this study. The control framework use a FLC structure which compromises of four interface; Fuzzification, Fuzzy Rules, Inference System, and Defuzzification.
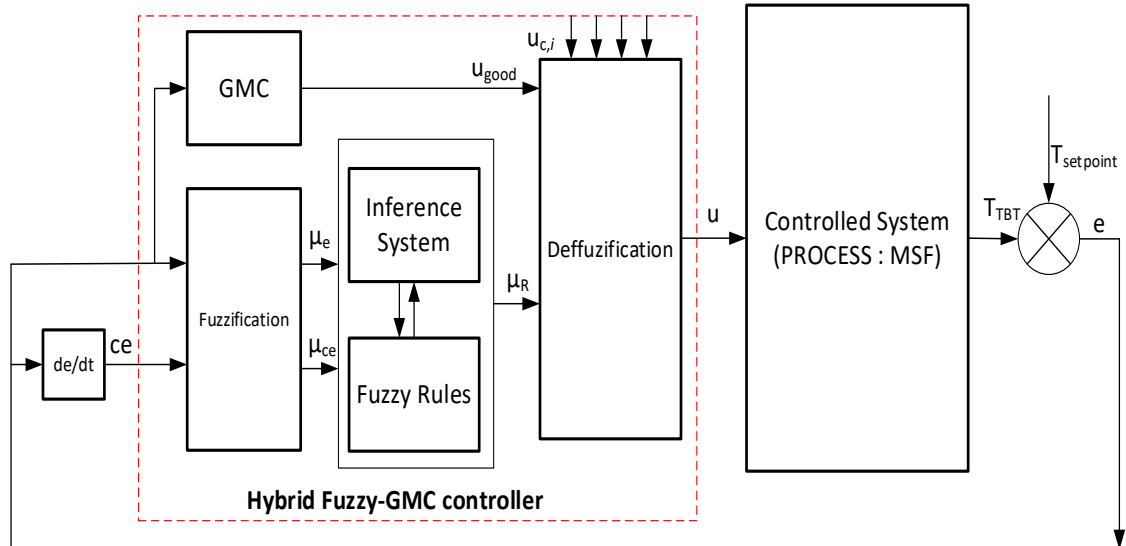
Figure 5.10: Controller structure of Hybrid Fuzzy-GMC in TBT control loop

While, GMC is used to guarantee the control trajectory in fuzzy system satisfied the reference value in control loop. The GMC controller equation has been integrated as one of the function in output membership function in the Defuzzification element. As the outcome, fuzzy inference will compute an appropriate control action, which is based on plant characteristic (from GMC) and expert knowledge (from fuzzy system). The hybrid Fuzzy-GMC computation will be discussed in the next section.

5.6.1 Hybrid Fuzzy-GMC Controller Design

In this section, the configuration of the FLC for TBT control is discussed. The controller uses two inputs and one output; the error (e) and the change of error (ce) as the input while the controller output (u) is the amount of steam flowrate require to control the outlet of the brine heater in MSF plant in the TBT loops or the brine blowdown flow rate in the case of BL loop. The input fuzzy set is characterised into five Gaussian membership functions (for e) and three triangular membership functions (for ce) with every inputs being normalised between the range (universe of discourse) of - 8 to 8 ℃ and -0.1 to 0.1 respectively. As shown in Figure 5.11, the input, (x) is fuzzified into a systematic fuzzy set where the input value (crisp value) is mapped into a corresponding linguistic input. The fuzzified inputs in the fuzzy set are bounded within range of 0 and 1.
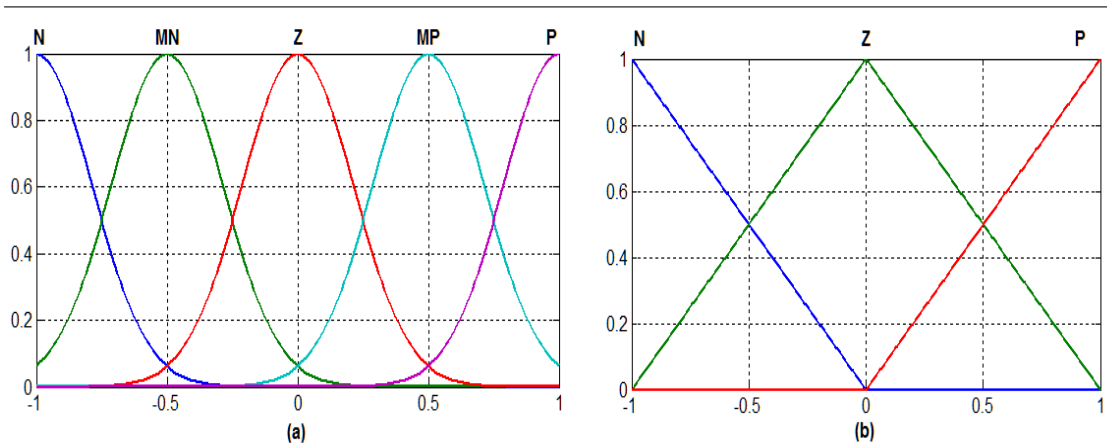
Figure 5.11: Inputs membership function for (a) error and (b) change of error

The membership function for error ($\mu_{e,i}$) and change of error ($\mu_{ce,i}$) can be defined as in Eq. 5.19 and Eq. 5.20 respectively.

$$\mu_{e,i}(x_1) = \exp\left\{\frac{-(x_1-a_i)^2}{2b_i^2}\right\} where \ i = 1,2..5 \tag{5.19}$$

$$\mu_{ce,i}(x_2) = \begin{cases} 0, & x_2 \leq a_i \\ \frac{x_2-a_i}{b_i-a_i}, & a_i \leq x_2 \leq b_i \\ \frac{c_i-x_2}{c_i-b_i}, & b_i \leq x_2 \leq c_i \\ 0, & c_i \leq x_2 \end{cases} \quad where \ i = 1,2,3. \tag{5.20}$$

In FLC, dynamic behaviour of controller is characterised by the linguistic definition of rule, based on expert knowledge of plant heuristic. The rule in the form of **IF** (condition is fulfilled) **THEN** (consequence of action can be inferred). For instance, **IF** the *error* is *negative* **AND** *change of error* is *positive*, **THEN** the valve is closed. The fuzzy rule for TBT control loop is shown in a concise form in Table 5.3.

Table 5.3: Fuzzy Rule of TBT control loop system

IF e → / **AND** ce↓	Positive	Mid Positive	Zero	Mid Negative	Negative
Positive	Mid Open	Good	Mid Close	Mid Close	Close
Zero	Mid Open	Mid Open	Good	Mid Close	Mid Close
Negative	Open	Mid Open	Mid Open	Good	Mid Close

The rule is to stimulate the human reasoning toward logic concept and in artificial fuzzy reasoning, the implication between inputs membership and the inference of fuzzy rules are important and it will be used to compute the final FLC output (conclusion). The "AND" operator is used for inputs implication between the error and change of error and it can be written as Equation 5.21. The minimum value of input membership will be used in fuzzy inference to obtain a degree of association in fuzzy rules.

$$\mu_{R,i} = MIN\left(\mu_{e,i}(x_1),\ \mu_{ce,i}(x_2)\right) \tag{5.21}$$

A Takagi-Sugeno type function has been selected for the inference system and the output of the membership inference ($\mu_{R,i}$) is processed with the pre-defined output membership function ($u_{c,i}$). The fuzzy output is divided into five membership functions comprised of control action from GMC equation (Equation 5.22) and several constants ($u_{c,i}$). Details of control action for GMC can be referred to Lee and Sullivan (1988).

$$G_x f(x, u, d, t) = k_1(y^* - y) + k_2 \int (y^* - y) dt \tag{5.22}$$

At one instance, the final control action can be obtained from the distribution of several possible membership output which is based on the output value and degree of association. The formulation can be realized for discrete system as in Equation 5.23 (Centre of Area method). This mechanism is known as defuzzification which convert the range of value of relevant fuzzy output into non-fuzzy control action (crisp value).

$$u = \frac{\sum_{i=1}^{n}\left(\mu_{R,i} \cdot u_{c,i}\right)}{\sum_{i=1}^{n}\left(\mu_{R,i}\right)} \tag{5.23}$$

A similar method is carried out in designing the FLC controller for brine level control in MSF plant.

5.7 Results and Discussion

The previous results of optimization of the MSF process for four different seasons are used here (See section 5.2). The main objective of this study is to evaluate the performance of hybrid Fuzzy-GMC controller comparing to GMC control by

tracking the optimum condition of TBT and BL based on different seasons and handle the disturbance that may occur to the system.

5.7.1 Set Point Tracking

Figure 5.12 and Figure 5.13 show the set points change during four seasons for TBT and BL respectively. Figure 5.12 represents the response gained by the proposed fuzzy-GMC compared to that of the GMC controller in tracking the TBT set point. For 50 seconds interval, the proposed controller shows significant improvements in overshoot, rise time and steady state settling time compared to GMC controller for all four intervals. In tracking the BL set point, similar improvements were obtained using the proposed controller (Figure 5.13).

5.7.2 Disturbance

In this case, a sudden variation of the recycle flow rate was imposed by 10% increase and decrease in its flow rate to observe the performance of both controllers in handling the disturbance. The reason for choosing recycle flow rate as disturbance is that it is the only parameter that can affect the TBT and BL at the same time. Figure 5.14 shows the fuzzy-GMC controller outperformed GMC in bringing the TBT back to its set point. However, in BL loop, although the fuzzy-GMC response was smooth, pure GMC looks slightly more robust over the proposed controller (Figure 5.15).
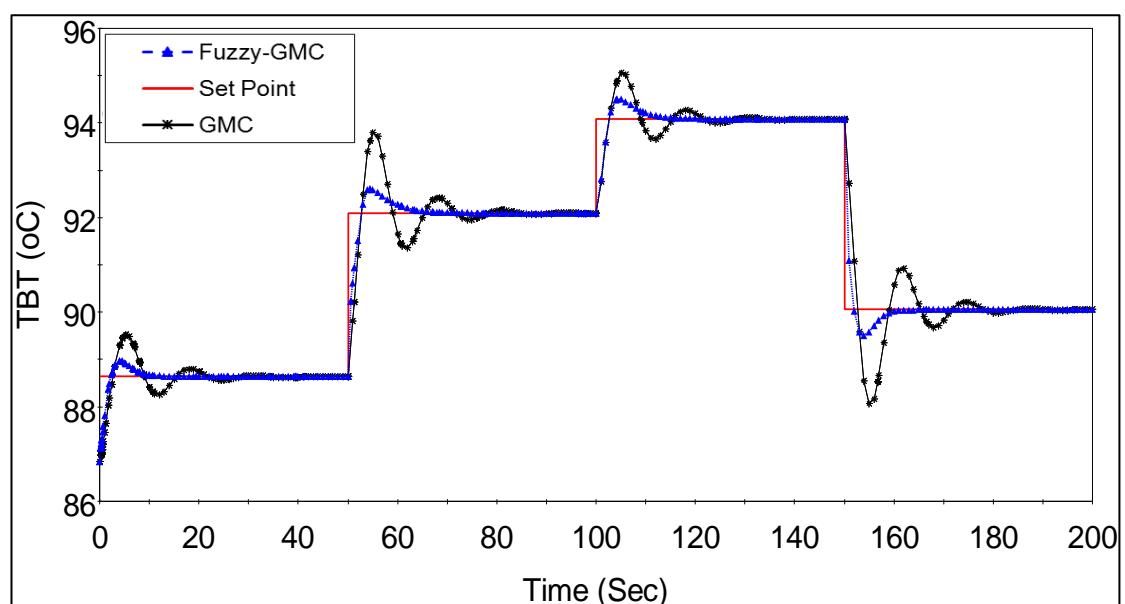
Figure 5.12: Tracking the TBT set points using Hybrid Fuzzy-GMC and GMC
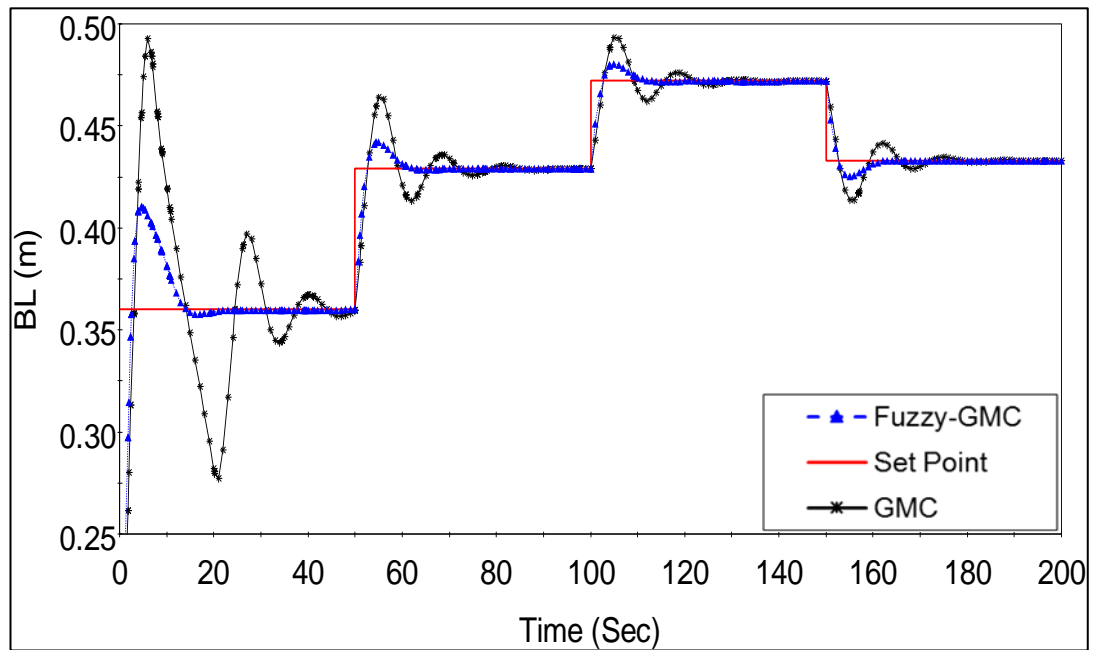
Figure 5.13: Tracking the BL set points using Hybrid Fuzzy-GMC and pure GMC
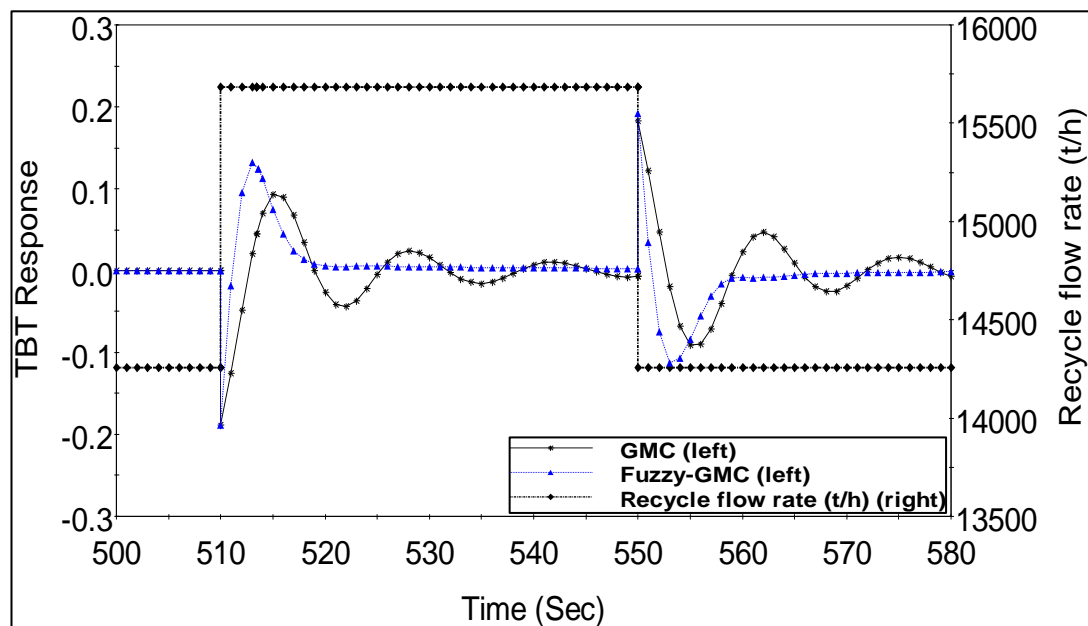
Figure 5.14: Handling the disturbance to control the TBT using Fuzzy-GMC & pure GMC controllers
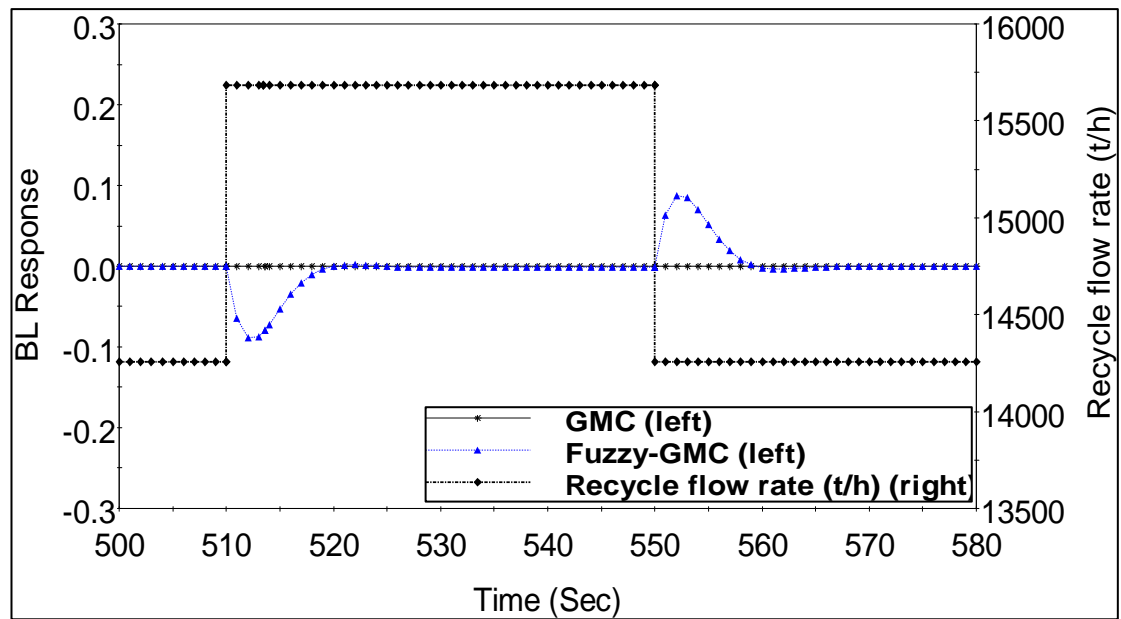
Figure 5.15: Handling the disturbance to control the BL using Fuzzy-GMC & pure GMC controllers

5.7.3 Effect of Control Strategy on the Performance Ratio

The performance ratio obtained from tracking the set point using both controllers as described in section (5.7.1) is plotted to observe its behaviour due to the change in the temperature (TBT) (Figure 5.16). As it can be seen, similar patterns to Figure 5.12 can be obtained for the performance ratio. Under Fuzzy-GMC control, the performance ratio behaves smoothly without any oscillations while under pure GMC control, the performance ratio shows some overshoot as response to the fluctuation of the TBT before reaching steady state. Although the TBT reaches steady state in 50 seconds as seen in Figure 5.12, the performance ratio takes a longer time to reach steady state (Figure 5.15). In addition, the performance ratio decreases as the temperature (TBT) increases (Spring and Summer) and increases as the required TBT decreases (Winter and Autumn). Since the production rate of MSF plants increases in winter due to the increase in the logarithmic mean temperature difference (LMTD) (Tanvir and Mujtaba, 2006c), for a fixed fresh water production rate, as in this case, the amount of energy required decreases. In spring and summer, however, the MSF process requires more energy to maintain the fresh water product at the same demand level and hence the performance ratio drops.
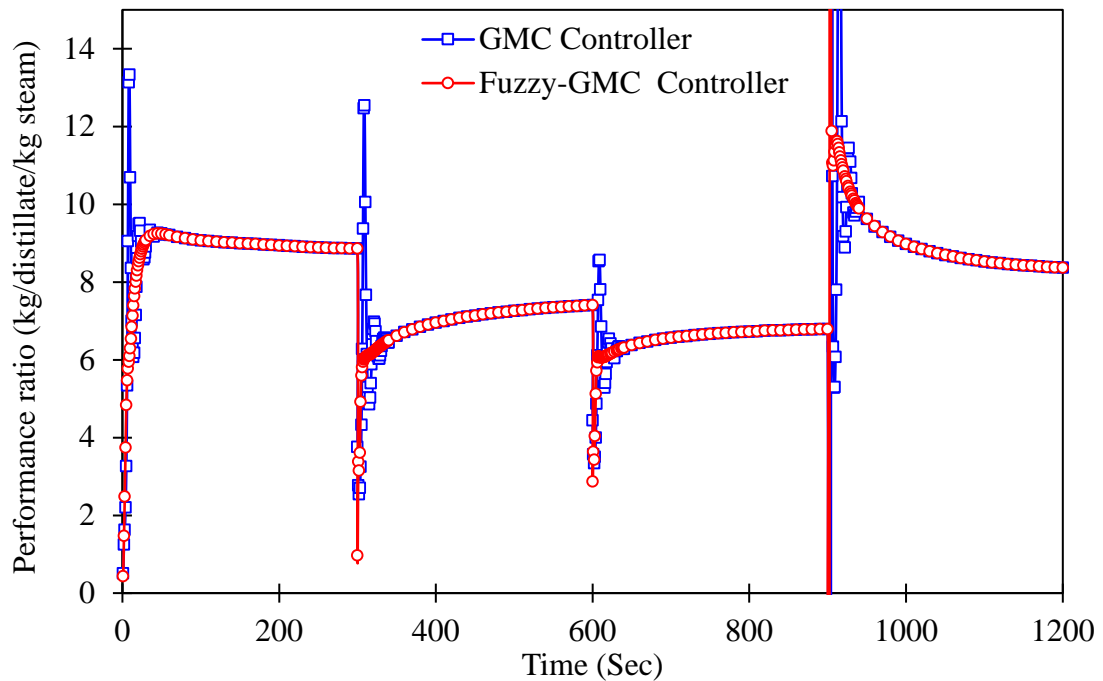
Figure 5.16: The performance ratio profile in tracking the TBT set points.

5.8 Conclusions

The work presented in this chapter focused on the implementation of GMC control and hybrid fuzzy-GMC control in MSF desalination plants. Since most MSF plants are operated under conventional PID control, the proposed GMC control can improve the control process in MSF plants. To carry out the control process, detailed dynamic model of MSF process was developed and implemented using gPROMS model builder. Two controller loops, namely TBT and BL, were designed to investigate the performance of the GMC controller. For each loop, three cases were carried out; tracking the set points without constraints, tracking the set points with constraints and handling the disturbance. Different values for TBT and BL set points were selected for four seasons in the year based on optimization process. The disadvantage of PID controller is its linearity and time consumption in tuning its parameters. However, GMC is easy to use and can handle nonlinear systems. Also, the tuning of the GMC parameters is very simple.

In comparison to the PID controller, the results indicate that the GMC is a powerful and robust strategy in controlling MSF plants and outperformed the PID in all cases. In handling the disturbance for example, the GMC control the process easily without showing any oscillatory or overshoot. In TBT loop, although both

controllers reached the set points at nearly the same time, the GMC reached the set points with less overshoot and more smoothly. However, in the BL loop, GMC controller appeared to be fast and more robust in controlling the level with and without the presence of the constraints and outperformed the PID controller.

In the BL loop, it is important to mention that both controllers were not just used to track the set point but to overcome the change of other variables such as the recycle flow rate, intake seawater temperature and intake seawater flow rate. Here, the GMC controller looks even better in tracking the set points. While the PID controller exhibits some oscillatory behaviour, the GMC controller reaches the set point quickly and remains constant for the whole period. This behaviour was monitored for all four seasons.

Most importantly, it is the simplicity of the tuning procedure of the two controllers. While PID parameters took a long time to be tuned and thus it is time consuming, the GMC parameters were tuned quickly based on known plant speed and graphical method.

Although most of the applications of the GMC algorithm were in controlling the temperature, here, the GMC was used successfully to control the level of the brine in MSF as well as the temperature of the brine heater and has revealed its controllability to handle nonlinear system under different set points change with and without constraints.

Hybrid fuzzy-GMC controller was also developed for MSF desalination process in this work by introducing the "If-then" fuzzy rule into GMC controller to improve the process performance by recompensing the mismatches that occur in pure GMC controller. Although the proposed controller outperformed pure GMC in tracking the temperature and brine level and handle the temperature disturbance, more work is required to improve fuzzy-GMC to handle level disturbance.

CHAPTER SIX

Dynamic Modelling of Heat Exchanger Fouling in Multistage Flash (MSF) Desalination

6.1 Introduction

In thermal desalination process such as MSF, scale formation is mainly caused by precipitation of calcium carbonate ($CaCO_3$), and at higher temperature, magnesium hydroxide $Mg(OH)_2$. Both of them are commonly referred to as alkaline scales. The HCO_3^- normally break down to form CO_3^{2-} at temperature above 45 ^oC causing the precipitation of $CaCO_3$ once its solubility limit is exceeded. El Din and Mohammed (1989) conducted experimental study and found that the $CaCO_3$ starts to form above 65 ^oC and reaches its maximum value at 80 ^oC while $Mg(OH)_2$ starts precipitating around 75 ^oC and increases steadily with temperature. Non-alkaline scale such as calcium sulphate ($CaSO_4$), on the other hand, is also considered to be the most common type found in MSF processes (Al-Sofi, 1999). In fact, El-Dessouky and Khalifa (1985) checked preheater tubes of once through MSF plant after 10 years of operation and found out that the most common scale was calcium sulphate. Wildebrand et al. (2007) reported some calcium sulphate growth at around 75 ^oC with increase in the salinity. Unlike alkaline scales, which results from the decomposition of bicarbonates, $CaSO_4$ scale result from the reaction of components that already exist in the seawater (Shams El Din et al., 2005).

Calcium carbonate can crystallize into three different forms; vaterite, calcite and aragonite, where the latter is more expected to form in high salinity water (Zhong and Mucci, 1989). Also calcium sulphate occurs in three different forms namely; anhydrite ($CaSO_4$), hemihydrate ($CaSO_4.1/2H_2O$) or dehydrate (gypsum) ($CaSO_4.2H_2O$). Nevertheless, Anhydrite sulphate scale ($CaSO_4$) would be expected to form at temperature above 40 ^oC due to its low solubility (Figure 6.1)

(Al-Ahmad and Aleem, 1994), most of the calcium sulphate scale in thermal units is hemihydrate (Najibi et al., 1997, Al-Rawajfeh et al., 2014). However, Zhao and Chen (2013) reported that gypsum is more likely to form as scale on the surface at temperature range of 40-98°C, while anhydrite and hemihydrate are precipitated above 98 °C. Moreover, during their experimental study at around 60 °C, Bansal et al. (2001) found out that only gypsum was formed as deposit. In fact, there is a long history of controversy about the correct value of the saturation solubility of the anhydrite. Marshall and Slusher (1968) experimentally determined the solubility product *(K$_{sp}$)* of anhydrite between 100 °C and 200 °C and produced a correlation to calculate the solubility at lower temperature. Though there is no solubility measurements at 100 °C, the solubility line was obtained by extrapolating the solubility product from lower and higher temperature. Thus, solubility product above 100 °C is more accurate than for the same line at lower temperature. With regards to the temperature in this investigation, which is below 109 °C, there is an agreement that no formation of anhydrite occurs below 109 °C (Freyer and Voigt, 2003).

For gypsum, which also has solubility concentration lower than hemihydrate (Figure 6.1), Partridge and White (1929) reported that gypsum is converted into hemihydrate in less than one day when in contact with water at 100 °C. Freyer and Voigt (2003) also confirmed that if the gypsum is heated above the transition temperature, it will be converted into hemihydrate by dehydration solid state reaction.
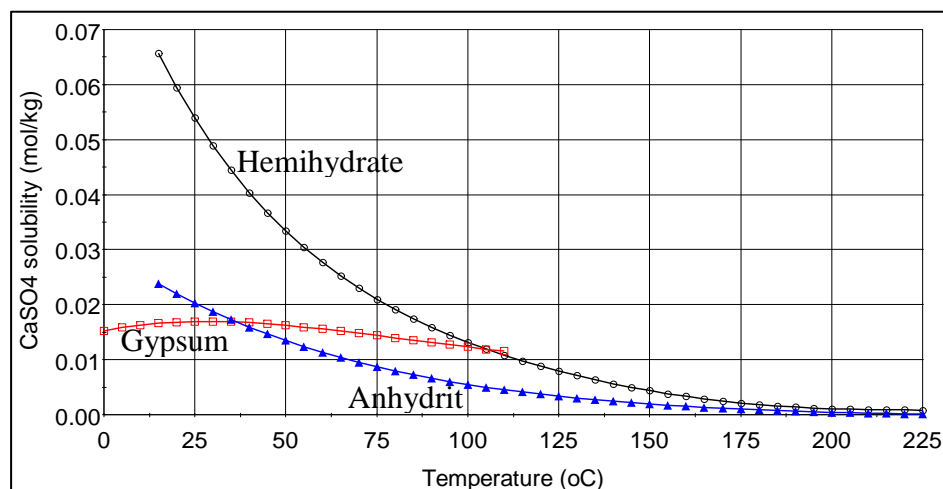
Figure 6.1: The solubility of CaSO₄ in its three different forms (Freyer and Voigt, 2003)

In brine recycle MSF, which has recovery and rejection sections, the concentration of Ca^{2+}, Mg^{2+} and CO_3^{2-} ions are higher in the recovery section than in the rejection section due to the mixing of the recycle brine with water make up while HCO_3^- is higher in the rejection section (Shams El Din and Mohammed, 1994). Shams El Din et al. (2005) conducted physicochemical analysis of MSF flash chambers that operates at TBT (112 °C) and found out that the first three stages were fouled completely by $Mg(OH)_2$ while stages 4 was mixed with $Mg(OH)_2$ and $CaSO_4$ and the scale in stage 5 was entirely $CaSO_4$. Again the $Mg(OH)_2$ appeared in the following stages (from stage 6 onward) up to stage 9 with increasing amount of $CaCO_3$. Besides the TBT, the scale rate also depends on the concentration of bicarbonate and the partial pressure of CO_2 (Mubarak, 1998). Al-Sofi (1999) believed that the scale formation would be expected to form at low temperature without the need for CO_2 release.

Fouling is an extremely complex process that may be explained by mass and heat transfer and chemical reaction equations with respect to the properties of the scale material and the water. At heated surfaces, the fouling process undergoes five stages as follows (Kazi, 2012):

- Initiation: slow nucleation of the fouling species at the surface to prepare the heated surface for more unsteady state growth of scale formation.

- Transport: it is the transport of the fouling species to the surface by diffusion process due to concentration difference between the bulk phase and the liquid-solid surface. Particle size and the velocity of the bulk play an important role in accelerating or decelerating the transport process.

- Attachment: it is the accumulation of the fouling species on the surface. Density, elasticity and roughness of the surface material play an important role in sticking these species on the surface and thus, not all the transported species have to be deposited.

- Removal: the disengagement of the fouling species from the surface into the bulk phase due to higher velocity, shear force and the roughness of the surface, and,

- Aging: after a period of time, the strength of the deposited scale can vary with time resulting in break off of the scale into parts.

In the MSF process, fouling due to crystallization, precipitation and chemical reaction are the most common. In some cases, corrosion fouling can be found as a result of chemical treatment of the scale formation. These types of fouling are affected strongly by number of factors such as time, surface temperature, velocity of the bulk, diffusion rate of the ions, bulk composition, solubility of the scale species and the pH of the seawater. For carbonate systems, the amount of carbonate species is related to the pH as shown in Figure 6.2 (Glade and Al-Rawajfeh, 2008). The increase in the seawater pH causes the condition of calcium carbonate to be super-saturation that in turn results in scale deposit. Therefore, controlling the pH value is required to prevent excessive carbonate scale formation. Calcium sulphate, however, is pH independent and tends to deposit in different forms once its solubility limitation exceeds (Helalizadeh et al., 2000). Höfling et al. (2003) reported that the saturation index for $CaSO_4$ is almost constant between pH 4 and pH 10.
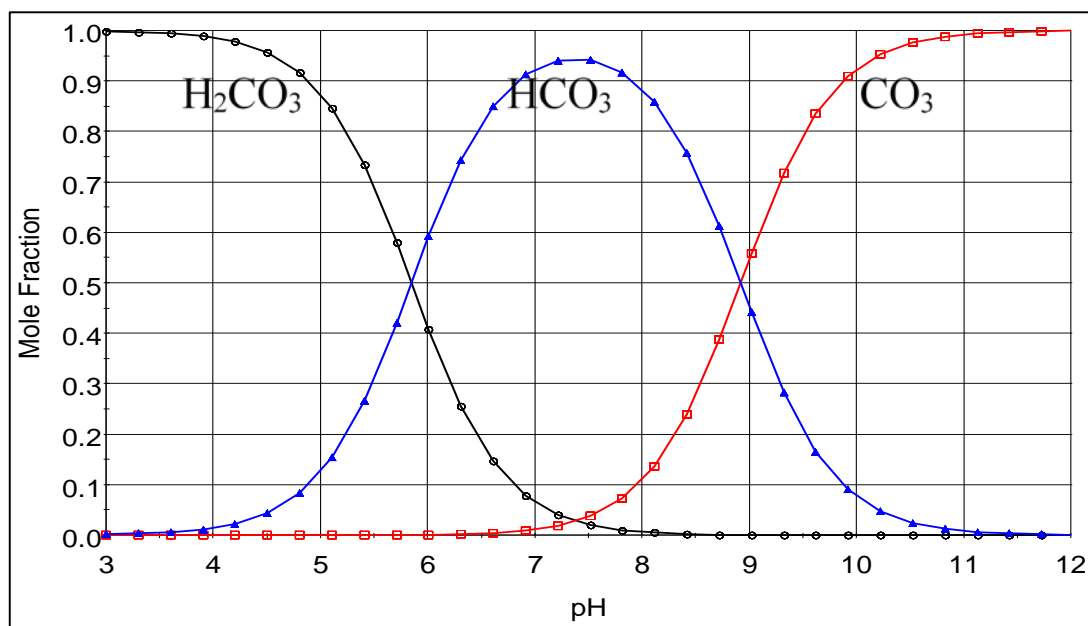
Figure 6.2: Mole fraction of CO_2, HCO_3 and CO_3 as a function of pH in carbonate system at (T = 25 °C and salinity = 35 g/l) (Glade and Al-Rawajfeh, 2008).

Complete prevention of scale formation is impossible. However, a mitigation or control of fouling on heat transfer surfaces is possible and can be done chemically or mechanically. By chemical means, acid such as H_2SO_4 can be added to cause reduction of the bicarbonate or the use of one of the commercial scale inhibiters

which are derived from condensed polyphosphates, polyelectrolytes and organophosphonates (Hamed and Al-Otaibi, 2010). However, improper control of the dosing rate of anti-scaling can lead to undesirable results. Salt can grow and build up around antiscalant molecular chain resulting in the additive being less effective (Al-Sofi, 1999). Mechanical cleaning is another way of scale removal. There are two ways of mechanical cleaning used in desalination plants; offline cleaning (by brushes) while the plant is off and online cleaning (by balls) while the plant is under operation (Al-Ahmad and Aleem, 1994).

Based on the above information and the literature review in chapter two, a dynamic fouling model is developed and incorporated into the MSF dynamic process model to predict fouling in the MSF condensing tubes at different temperature and velocity. The proposed dynamic model considers the attachment and removal mechanisms in the fouling phenomena with more relaxation of the assumptions such as the density of the fouling layer and salinity of the recycle brine. While calcium sulphate might precipitate at very high temperature, only the crystallization of calcium carbonate and magnesium hydroxide are considered in this work.

6.2 Scale Formation Mechanism

Calcium carbonate and magnesium hydroxide are known in practice as the alkaline scales. With the increase of the seawater temperature entering the MSF plant, a number of reactions take place as reported by several researchers:

$$2\ HCO_3^- \leftrightarrow CO_2\uparrow + CO_3^{2-} + H_2O \tag{6.1}$$

El Din et al. (2002) and Mubarak (1998) mentioned that the previous reaction can occur in two sequence steps namely:

$$HCO_3^- \rightarrow CO_2\uparrow + OH^- \tag{6.2}$$

Followed by fast acid neutralization step

$$OH^- + HCO_3^- \rightarrow CO_3^{2-} + H_2O \tag{6.3}$$

Segev et al. (2012) and Olderøy et al. (2009) reported that the aforementioned reactions (6.2 and 6.3) can be followed by other reactions like:

$$HCO_3^- \leftrightarrow CO_3^{2-} + H^+\uparrow \tag{6.4}$$

$$H^+ + HCO_3^- \leftrightarrow CO_2\uparrow + H_2O \tag{6.5}$$

However, reaction (6.5) was reported by Patel and Finan (1999) and El Din et al. (2002) as acidification reaction of seawater to mitigate the decomposition of HCO_3.

In the presence of calcium ions, carbonate ions react with calcium ions to cause the deposit of $CaCO_3$ once its solubility exceeds the limit.

$$CO_3^{2-} + Ca^{2+} \rightarrow CaCO_3\downarrow \tag{6.6}$$

The summation of equations (6.2, 6.3 and 6.6) or equations (6.4, 6.5 and 6.6) can lead to the same reaction equation that present the precipitation of $CaCO_3$.

$$2HCO_3^- + Ca^{2+} \rightarrow CaCO_3\downarrow + CO_2\uparrow + H_2O \tag{6.7}$$

At higher temperature, reaction (6.3) becomes reversible and so the carbonate ions would hydrolyse to form bicarbonate according to the following reaction:

$$CO_3^{2-} + H_2O \rightarrow HCO_3^- + OH^+ \tag{6.8}$$
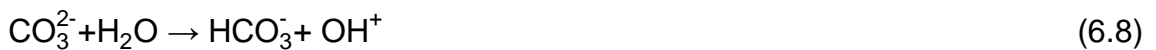
In the presence of magnesium, the resulting hydroxyl ions from reaction (6.8) can react with magnesium to cause the deposition of $Mg(OH)_2$ once its solubility reach saturation point.

$$2\,OH^- + Mg^{2+} \rightarrow Mg(OH)_2\downarrow \tag{6.9}$$

Comparing reaction (6.9) to reaction (6.3), Mubarak (1998) reported that reaction (6.3) is faster than reaction (6.9) though the precipitation of $Mg(OH)_2$ is thermodynamically more favourable. Regarding the deposition of calcium sulphate, calcium and sulphate ions react to form calcium sulphate according to the following reaction:

$$SO_4^{2-} + Ca^{2+} \rightarrow CaSO_4\downarrow \tag{6.10}$$

The reacting species such as (Mg^{2+}, Ca^{2+}, CO_3^{2-}, SO_4^{2-}, HCO_3^-, OH^-) are transferred towards the heat exchanger surface due to the diffusional phenomenon and react at the surface resulting in deposition of fouling. When the deposit layer reaches a certain thickness, not only the reactant products would deposit but also other species would start to stick due to the increase in the roughness of the surface. This explains the changeable structure of the fouling

layer (Slesarenko et al., 2003). The released gases such as CO_2, on the other hand are kept in solution and later are transferred away from the heat transfer surface and evaporated inside the flash chamber resulting in NCGs around outside tubes bundle surface. More details of such gases can be found in chapter four. It is important to mention that the formation of CO_2 inside the tubes leads to a decrease in the pH (Al-Rawajfeh et al., 2014) and consequently lowers the tendency of deposit to certain limit. However, as the brine enters the flash chambers, the CO_2 released into the vapour space results in an increase in the pH and thus more deposit is expected in the flash chambers.

Calcium carbonate is known to be a major scalant in MSF plants since it starts to form at low temperature. Magnesium hydroxide, on the other hand, normally precipitates at temperature higher than 95 ^{o}C (Al-Anezi et al., 2008). However, despite the above discussion of the possibility of $CaSO_4$-$2H_2O$ (Gypsum) scale at low temperature, the situation may be different in MSF plants. In fact, there is large agreement that $CaSO_4$, in any forms, precipitates in MSF plants at temperature above 120 ^{o}C (Al-Sofi, 1999). Although, in this work, the TBT is fixed at a maximum value (119 ^{o}C), the highest temperature in the tubes is less than 112 ^{o}C (the outlet temperature of the first stage). Thus the precipitation of $CaSO_4$ is neglected in this work and only the precipitation of $CaCO_3$ and $Mg(OH)_2$ are considered in this work. However, the formation of $CaSO_4$ is expected in the brine heater tubes.

6.3 Process Description

The seawater (W_s) and the recycle brine water (Rec) flow through a bundle of large number of pipes, which are connected by water boxes, in counter current direction of the brine flow leaving the brine heater (Figure 6.3). The temperature of the seawater and recycle brine water increases gradually as it pass through the tubes bundle due to the condensation process inside the flashing chambers.
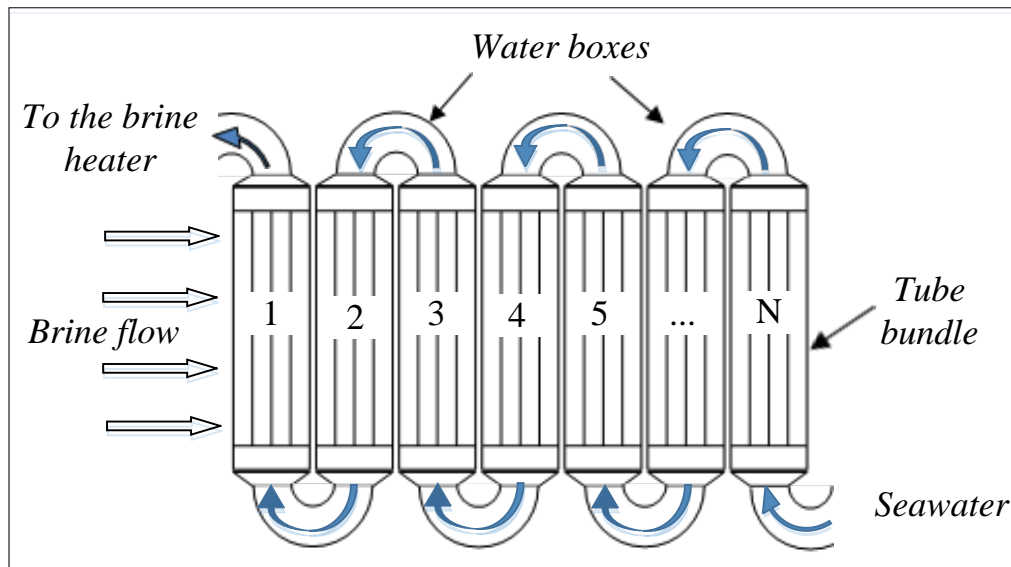
Figure 6.3: Schematic of tubes bundles and water boxes of MSF process

The deposited scale, mainly $CaCO_3$ and $Mg(OH)_2$, starts to accumulate in different amount according to their concentration and temperature of the inner side of the tube surface. Stage number 1, for example, is expected to have the highest amount of scale due the high temperature and low solubility concentration. Although the fresh seawater intake has higher Ca^{2+} concentration, no large deposit is expected to form in the rejection section stages due to the low temperature. In the summer period, fresh intake water enters the last stage (stage 24) at $T_s = 32$ °C and leaves the rejection section from stage 22 at $T_1=40$ °C.

In MSF-BR, the recycle brine is almost a closed loop flow as can be seen in red dashed line in Figure 6.4. Thus, any change in the conditions of the recycle brine inside the tubes bundle can affect the conditions of the flash chambers and consequently affect the whole process. In continuous precipitation of fouling, the situation becomes more complex as there is a continuous change in heat flux, temperature and salinity. The continuous deposition of foulants on the inner surface of the tubes leads to reduction in heat flux to the brine inside the tubes and thus results in a temperature drop. Moreover, this reduction in heat flux leads to less vapour condensation around the tubes and consequently increase the vapour volume and the pressure inside the chamber.
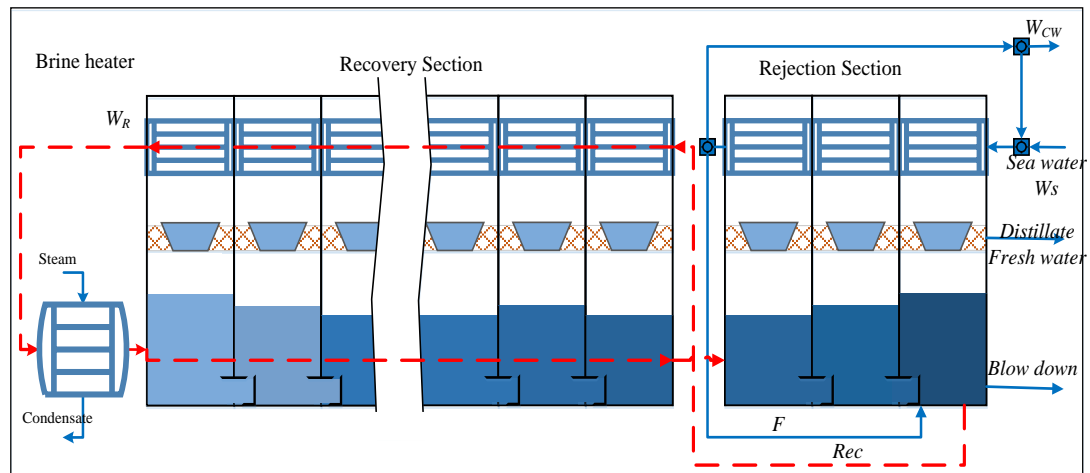
Figure 6.4: Schematic of MSF-BR process showing the recycle loop

Since the main concept of MSF process is the evaporation of water under vacuum, this increase in the pressure inside the chamber may lead to less vapour to flash and as result, the temperature of the brine and the vapour increase. Since the brine inside the tubes is recirculated from the last stage, its temperature increases with time causing an increase in the temperature inside the tubes. To make the situation more complex, the reduction of the amount of evaporation from the brine leads to decrease in the brine salinity which in turn affect the solubility of the calcium carbonate in seawater.

6.4 Fouling Model

During the fouling model building process, the following important assumptions are considered in this work:

- Lumped distribution of fouling deposit along the tubes is considered.

- Pressure drop due the fouling between inlet and outlet of the tubes is neglected.

- Volumetric flow through the tubes as assumed constant and therefore, the velocity change due to change in cross sectional area is considered.

- The heat flux though the tubes bundle is not constant.

- The salinity variation due to the change in the amount of condensate is considered.

Depending on the process variables and fouling mechanism, the combination of the previous five stages mentioned earlier (Section 6.1) can lead to the four observed fouling behaviour to describe the rate of fouling as shown in Figure 6.5 (Taborek et al., 1972).

- Linear rate: a straight line indicates a constant growth rate of deposit with time and with negligible removal rate;

- Falling rate: a curved line indicates increase in the growth rate of deposit with increase in the removal rate after some time;

- Asymptotic rate: a curved line indicates increase in the growth rate of deposit as well as gradual removal to reach a steady state with time when both rates equal each other; and,

- Saw-tooth shape rate: deposition rate exhibits a general increase trend punctuated with periodic decrease due to the shedding of fouling deposits. The deposit then builds up and detached continuously.
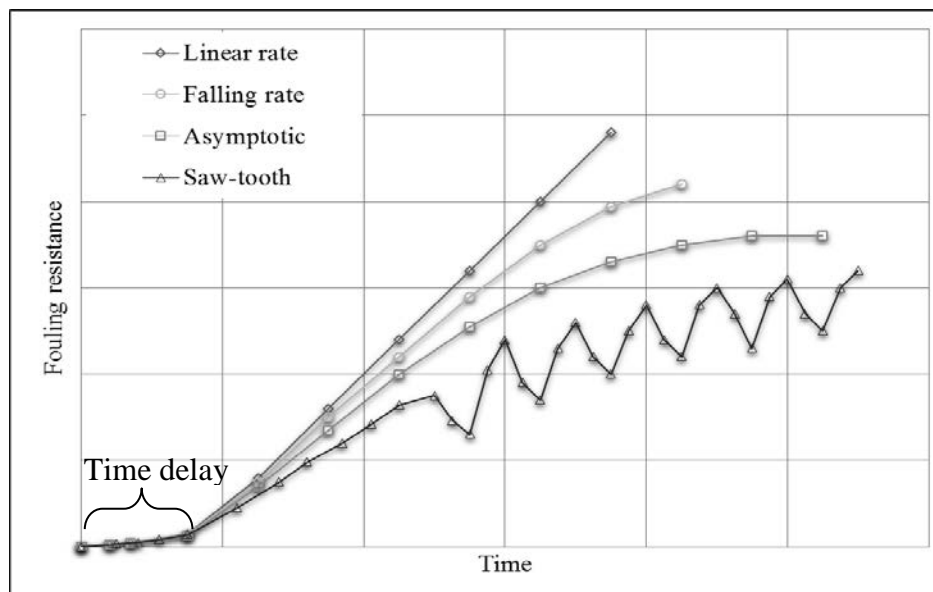
Figure 6.5: Possible fouling resistance versus time curves (Al-Ahmad and Aleem, 1994).

6.4.1 Deposition Rate

Based on the above descriptions of fouling behaviour rate, a good model that can be close to real behaviour is the model that consider the growth and removal rate

of the scale. The net rate of deposition can be calculated as the difference between the total deposition rate and the removal rate:

$$\frac{dm_f}{dt} = m_d - m_r \tag{6.11}$$

Where m_f, m_d and m_r are the net deposit mass rate, the total deposit mass rate and the removal mass rate per unit area respectively. The total mass deposit rate can be described using ions diffusion transport rate and/or surface reaction rate as shown in Figure 6.6.

The first step of scale formation is the transportation of species toward the heated surface as a result of concentration difference between the bulk phase (C_b) and the solid-liquid surface (C_i). The ions diffusion transport rate can be written as follows:

$$\frac{dm_d}{dt} = k_D(C_b - C_i) \tag{6.12}$$

Where k_D is the mass transfer coefficient, C_b the concentration of the ions in the fluid (bulk phase) and C_i the concentration of the ions at the solid-liquid surface.
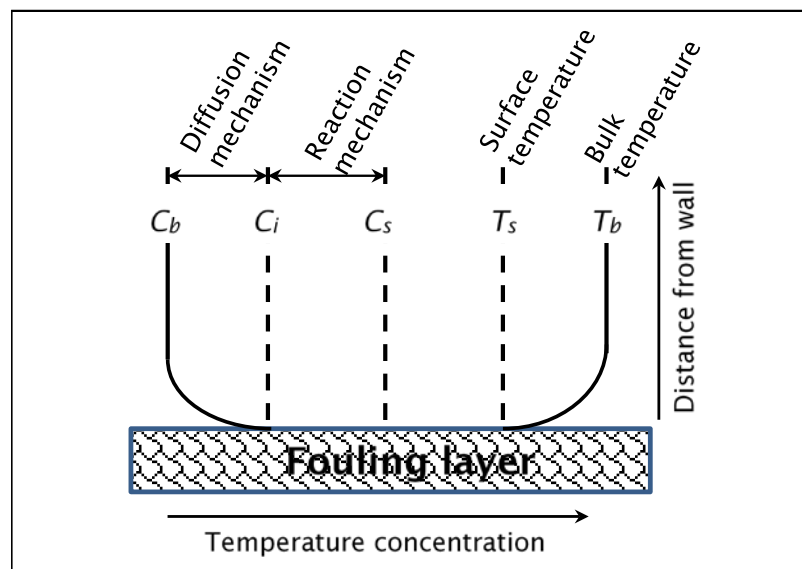
Figure 6.6: Concentration and temperature profiles at the heat transfer surface
(Hasson et al., 1968)

The second step is the accumulation of these transported species on the crystal layer at the heated surface as a result of concentration difference between the solid-liquid surface (C_i) and the saturation concentration (C_s). The rate of deposition from the reaction process can be calculated as follows:

$$\frac{dm_d}{dt} = k_r (C_i - C_s)^n \tag{6.13}$$

Where k_r is the reaction rate constant, C_s the saturation concentration and n reaction order. For the deposition of $CaCO_3$, the reaction order is assumed to be of second order as it correspond to the number of ions (Ca^{2+} and CO_3^{2-}) (Brahim et al., 2003). Due to the difficulty of estimating the concentration of the ions at the solid-liquid surface (C_i), most of the work in the literature assumes that all the species are transported to the surface and thus the surface reaction mechanism is considered to be the main controller of the rate of deposition. Helalizadeh et al. (2000) and Fahiminia et al. (2007) reported that at low velocity, fouling is controlled by the diffusion rate while at high velocity, the controller mechanism changes to be reaction rate mechanism. Moreover, Najibi et al. (1997) assumed that the fouling process is controlled by diffusion mechanism when the velocity falls below 0.9 m/s. Also, Andritsos (1996) reported strong indication of diffusion controlled process when they tested two velocities below 0.9 m/s on the activation energy. Augustin and Bohnet (1995) and Pääkkönen et al. (2012) reported that the crystallization of $CaCO_3$ is reaction controlled. If the reaction mechanism is assumed to be the controlled mechanism, then equation (6.13) can be used to describe the rate of deposition on heated surface areas at appropriate surface temperature and species concentration. The concentration driving force in equation (6.13) has been described by Hasson et al. (1978) as the difference between solubility product K_{sp} and the concentrations of calcium and carbonate ions. The reaction order of the formation of calcium carbonate was assumed as first order reaction ($n = 1$) as reported by Hasson et al. (1968).

$$\frac{dm_d}{dt} = k_r ([Ca].[CO_3] - K_{sp}) \tag{6.14}$$

where the solubility product of calcium carbonate can be defined as

$$K_{sp} = [Ca^{2+}].[CO_3^{2-}]$$

Similar form of the concentration driving force in Equation (6.13) can be found in the literature to describe the crystallization rate of calcium carbonate or concentration reduction of calcium ions. Smith and Sweett (1971) presented six forms to describe the concentration driving force gradient term (C_b-C_s) with reaction order ranges from 1.8 to 2.14 in the temperature range 30 °C and 90 °C.

In order to include the diffusion rate, Bohnet (1987) combined equations (6.12 and 6.13) by reformulation and summation to eliminate the unknown interfacial concentration C_i to develop an equation (Equation 6.15) for precipitation of calcium sulphate where the deposition rate depends on both diffusion and reaction rates. Helalizadeh et al. (2005) and Pääkkönen et al. (2015) used Bohnet's equation to calculate the crystallization fouling of calcium carbonate on the heat exchange surface. Thus, in this work, the deposition of calcium carbonate will be assumed to depend on both diffusion and reaction mechanism according to the following equation:

$$\frac{dm_d}{dt} = \beta \left[\frac{1}{2}\left(\frac{\beta}{k_r}\right) + (C_b - C_s) - \sqrt{\frac{1}{4}\left(\frac{\beta}{k_r}\right)^2 + \left(\frac{\beta}{k_r}\right)(C_b - C_s)} \right] \qquad (6.15)$$

The mass transfer coefficient β can be calculated as a function of the Sherwood number (Sh) and the diffusion coefficient (D).

$$\beta = \frac{Sh \times D}{D_h} \qquad (6.16)$$

The Sherwood number can be calculated as following.

$$Sh = 0.034 \times Re^{0.875} \times Sc^{1/3} \qquad (6.17)$$

Where Re is the Reynolds number, Sc the Schmidt number and D_h the hydraulic diameter. The diffusion coefficients for calcium and carbonate system species can be found in (Segev et al., 2012).

The Reynolds and Schmidt numbers can be calculated from the following equations.

$$Re = \frac{\rho_w \times v \times D_h}{\mu_w} \qquad (6.18)$$

$$Sc = \frac{\mu_w}{\rho_w \times D} \qquad (6.19)$$

Pääkkönen et al. (2015) suggested to include the effect of flow velocity by introducing time scaling factor to equation (6.13) to become:

$$\frac{dm_d}{dt} = k_r'(C_i - C_s)^n \times \frac{\mu_w}{\rho_w V^2} \qquad (6.20)$$

Where V is the friction velocity and it can be calculated as following:

$$V = \sqrt{\frac{\tau_f}{\rho_w}} \qquad (6.21)$$

The τ_f is the surface shear stress of the bulk flow and ρ_w the density of the fluid. The surface shear stress can be calculated using friction factor according to the follow equation:

$$\tau_f = f\rho_w \frac{v^2}{2} \qquad (6.22)$$

Thus, the combination of diffusion and reaction mechanism model (equation 6.15) becomes:

$$\frac{dm_d}{dt} = \beta \left[\frac{1}{2} \left(\frac{\beta \rho_w V^2}{k_r \mu_w} \right) + (C_b - C_s) - \sqrt{\frac{1}{4} \left(\frac{\beta \rho_w V^2}{k_r' \mu_w} \right)^2 + \left(\frac{\beta \rho_w V^2}{k_r' \mu_w} \right) (C_b - C_s)} \right] \qquad (6.23)$$

The reaction rate constant (k_r) depends on the surface temperature (T_s) according to the Arrhenius equation.

$$k_r' = k_{r0}' \times e^{(-Ea/RT_s)} \qquad (6.24)$$

Where k_{r0}, Ea, and R stand for pre-exponential constant, reaction activation energy, gas constant and the fouling surface temperature respectively. It is to be noted here that prior to the fouling, T_s is equal to the temperature of the tubes wall. However, as the thickness of the fouling layer increases, the temperature of the wall, the temperature of the fouling surface and the salinity of the recycle brine are due to a change as described in section 6.3.

Although calcite has slightly lower saturation concentration, the aragonite is more likely to deposit. X-ray analysis in the Helalizadeh et al. (2000) study revealed that 99% of the calcium carbonate scale was aragonite. Thus, it is assumed that the calcium carbonate scale in MSF tubes is aragonite. To calculate the solubility product of aragonite, Plummer and Busenberg (1982) developed an equation to calculate the solubility product as a function of the temperature. However, in MSF process, the salinity of the brine water changes continuously due to the variation of the temperature and heat flux through the walls of the tubes. The solubility product, K_{sp} increases with pressure and salinity and decreases with temperature (Al-Anezi and Hilal, 2007).Thus, it is important to consider the effect of activity coefficient of the seawater species. The solubility product of calcium carbonate is given by

$$K_{sp} = K_{sp}^0/(\gamma_{Ca}.\gamma_{CO3}) \tag{6.25}$$

where $K^o{}_{sp}$ of aragonite can be calculated using Plummer and Busenberg's equation:

$$Log(K_{sp}^0) = \left[-171.9773 - 0.077993 \times T_s + {2903.293}/{T_s} + 71.595 \times Log(T_s)\right] \tag{6.26}$$

where γ is the activity coefficient of a component, k_{sp} in molar units and T_s in Kelvin.

The activity coefficient can be calculated using extended WATEQ-Debye-Huckel's equation as cited by Al-Anezi and Hilal (2007).

$$Log(\gamma_i) = -A_{DH}z_i^2 \frac{\sqrt{I}}{1+Ba_i\sqrt{I}} + b_i I \tag{6.27}$$

Where A_{DH} is the Debye-Huckel parameter, z the charge of the ion, B the temperature dependent parameter, a_i and b_i the ion specific parameters of component i and I the ionic strength which is defined by:

$$I = {1}/{2} \sum z_i^2 m_i \tag{6.28}$$

The crystal growth of magnesium hydroxide is associated with the consumption of magnesium ions and thus it can be calculated by estimating the decrease in the magnesium concentration using the following equation (Sung-Tsuen and Nancollas, 1973).

$$-\frac{dMg^{2+}}{dt} = k_r' \left[\left([Mg^{2+}].[OH^-]^2\right)^{\frac{1}{3}} - [K_{sp}]^{1/3}\right] \tag{6.29}$$

Thus,

$$\frac{dm_{Mg(OH)2}}{dt} = -\frac{dMg^{2+}}{dt} \tag{6.30}$$

Unlike calcium carbonate, the rate of deposition of magnesium hydroxide is assumed to be first order. The calculation of the solubility product K_{sp} for magnesium hydroxide is similar to that for calcium carbonate. (The reader should be aware of the mass and molar units when applying equations 6.29 and 6.30).

For Mg(OH)$_2$, the solubility product can be calculated from the following correlation (Myasnikov et al., 2013):

$$Log(K_{sp}^0) = 14.723 - \frac{3472.3}{T_s} - 0.04642 \times T_s \tag{6.31}$$

Since this model is applied in the MSF plant that contains several stages working as heat exchangers, the bulk concentration, C_b, is decreased throughout the stages due to the precipitation process and thus the calcium ions of the rest of the plant stages are calculated based on the following equations:

$$Ca_{(j+1)} = Ca_{(j)} - CaCO_{3(j)} \tag{6.32a}$$

$$Mg_{(j+1)} = Mg_{(j)} - Mg(OH)_{2(j)} \tag{6.32b}$$

where *j* presents the stage number and the ions are in mole units.

The total rate of deposition of $CaCO_3$ and $Mg(OH)_2$ can be evaluated as the sum of both substances.

$$\frac{dm}{dt} = \frac{dm_{CaCO3}}{dt} + \frac{dm_{Mg(OH)2}}{dt} \tag{6.33}$$

To calculate the other seawater species such as (HCO_3, CO_3, CO_2, OH, H) at different temperatures and salinities, the carbonate system equations which has been described in (Al-Rawajfeh et al., 2014) can be used. For a given initial total alkalinity (TA) and initial total carbon dioxide (TC), the value of seawater pH can be obtained by solving the following equation

$$[H^+]^3 + (TA + K_1)[H^+]^2 + (TA.K_1 + K_1.K_2 + K_w - TC.K_1)[H^+]$$

$$-K_1.K_2.\frac{K_w}{[H^+]} + (TA.K_1.K_2 - K_1.K_w - 2.TC.K_1.K_2) = 0 \tag{6.34}$$

The pH is the negative logarithm of H^+. K_1 and K_2 are the first and the second dissociation constants for carbonic acid respectively. K_w is the dissociation constant for water at a specific ions strength and temperature. These constants can be calculated based on the following equations (Eid Al-Rawajfeh, 2007):

$$Ln(K_1) = 2.18867 - 2275.035/T_s - 1.468591 \times Ln(T_s) + (-0.138681 - $$
$$9.33291/T_s) \times S^{0.5} + 0.072648 \times S - 0.00574938 \times S^{1.5} \tag{6.35}$$

$$Ln(K_2) = -0.84226 - 3741.1288/T_s - 1.437139 \times Ln(T_s) + (-0.128417 - $$
$$24.41239/T_s) \times S^{0.5} + 0.1195308 \times S - 0.0091284 \times S^{1.5} \tag{6.36}$$

$$Ln(K_w) = 148.9802 - 13847.26/T_s - 23.6521 \times Ln(T_s) + (-5.977 - $$
$$118.67/T_s + 1.0495 \times Ln(T_s)) \times S^{0.5} - 0.01615 \times S \tag{6.37}$$

Where *S* is a salt concentration in g/l. After knowing the hydrogen ion concentration (H^+) from equation (6.34), the unknown concentrations of the carbonic system species (OH^-, HCO_3^-, CO_3^- and CO_2) can be calculated according to the following equations (Hasson et al., 1978, Müller-Steinhagen and Branch, 1988):

$$[OH^-] = K_w/[H^+] \tag{6.38}$$

$$[HCO3^-] = \frac{TA+[H^+]-[OH^-]}{(1+2\times K_2/[H^+])} \tag{6.39}$$

$$[CO3^{2-}] = \frac{TA+[H^+]-[OH^-]}{2\times(1+[H^+]/2K_2)} \tag{6.40}$$

$$[CO2] = \frac{[H^+]}{K_1} \times \frac{TA+[H^+]-[OH^-]}{(1+2\times K_2/[H^+])} \tag{6.41}$$

The TA in equivalents per litre is equal to:

$$TA = [HCO_3^-] + 2[CO_3^{2-}] + [OH^-] - [H^+] \tag{6.42}$$

and TC is equal to:

$$TC = [HCO_3^-] + [CO_3^{2-}] + [CO_2] \tag{6.43}$$

In this work the goal is to estimate the fouling in the MSF tubes and no evaporation of water or escape of CO_2 occurs here. Both TA and TC are consumed when $CaCO_3$ precipitates (Al-Rawajfeh et al., 2014). Thus, the values of TA and TC in the following stages can be calculated from the following equations:

$$TA_{(j+1)} = TA_{(j)} - CaCO_{3(j)} - \frac{1}{2} Mg(OH)_{2(j)} \tag{6.44}$$

$$TC_{(j+1)} = TC_{(j)} - CaCO_{3(j)} \tag{6.45}$$

6.4.2 Removal Rate

Increased fouling thickness reduces the tube cross-sectional area and gradually increase the pressure drop and in some cases can cause a complete block of the tubes. With time, due to the increase of the shear force, the accumulated scale becomes weak and more fragile and parts of the rate of deposition starts to breakdown. This mechanism is called removal rate and it was assumed to be

proportional to the wall shear stress of the flow and inversely proportional to the layer's shear strength (Bohnet, 1987). The removal rate can be calculated using the following equation:

$$\frac{dm_r}{dt} = k_{rem} \frac{\tau_f}{\sigma_f} \rho_f \left(\frac{\mu_w g}{\rho_w}\right)^{1/3} \tag{6.46}$$

where k_{rem} is a constant related to the removal rate, σ_f the shear strength of the fouling layer, ρ_f the density of the deposit and g the gravitational acceleration.

Shear strength can be calculated using the following equation (Bohnet, 1987):

$$\sigma_f = K.\frac{P_f}{N_f.x_f(1+\delta\Delta T).d_p} \tag{6.47}$$

Where P_f is the intercrystalline adhesion force, K a constant, N_f the number of defects in fouling layer, ΔT the temperature difference within the fouling layer, δ the linear expansion coefficient, x_f the layer thickness and d_p the crystal size.

Substituting Equations (6.47) into Equation (6.46) results in the following equation:

$$\frac{dm_r}{dt} = \frac{k_{rem}.N.x_f(1+\delta\Delta T).dp.\tau_f}{k.P_f} . \rho_f . \left(\frac{\mu_w g}{\rho_w}\right)^{1/3} \tag{6.48}$$

The term ($k.P_f/k_{rem}.N$) is calculated based on Krause's suggestion according to the following equation (Brahim et al., 2003)

$$\frac{k.P}{k_{rem}.N} = 83.2 \times v^{0.54} \tag{6.49}$$

And it follows

$$\frac{dm_r}{dt} = \frac{x_f(1+\delta\Delta T).dp.\tau_f}{83.2\times v^{0.54}} . \rho_f . \left(\frac{\mu_w g}{\rho_w}\right)^{1/3} \tag{6.50}$$

5.3 Fouling Resistance

The net mass deposit (dm_f/dt) in Equation (6.11) can be determined as a function of the mean thickness (x_f) and the density (ρ_f) of the crystal layer.

$$\frac{dm_f}{dt} = \rho_f \times \frac{dx_f}{dt} \tag{6.51}$$

Also, at any location of the heat transfer area, the fouling thermal resistance (R_f) can be calculated as a function of the mean thickness (x_f) and conductivity (λ_f) of the crystal layer.

$$\frac{dR_f}{dt} = \frac{1}{\lambda_f} \times \frac{dx_f}{dt} \qquad (6.52)$$

Thus, combining Equations (6.11), (6.51) and (6.52), the fouling thermal resistance rate can be calculated as a function of the deposit and removal rate.

$$\frac{dR_f}{dt} = \frac{1}{\lambda_f \times \rho_f} \times \left[\frac{d_{md}}{dt} - \frac{d_{mr}}{dt} \right] \qquad (6.53)$$

Equation (6.53) has been implemented in similar or different form by many researchers to predict the fouling behaviour in heated surfaces. However, over or under estimation of the parameters can lead to different shape of the fouling factor curve. Mwaba et al. (2006) reported that some of the studies presented fouling curve to be of an 'S' shape, depending on the roughness of the surface and concentration of the ions. The 'S' shape can be obtained if the nucleation period is considered in the development of fouling. The period of nucleation may vary from seconds to hours depending on the temperature, concentration and the velocity (Najibi et al., 1997). However, Figure 6.7 presented by Hamed and Al-Otaibi (2010) shows the fouling behaviour in MSF brine heater and the shape of the curve does not look like 'S' shape. This can be attributed to the fact that the nucleation period is very short and thus it can hardly be seen. Although Figure 7 was obtained at MSF brine velocity higher than 1.5 m/s, Brahim et al. (2003) and Zhang et al. (2015) results were consistent with Hamed and Al-Otaibi's results though their flow velocity was as low as 0.2 m/s. Moreover, although the removal rate was included in their model, their fouling curve looked linear and no major effect of the removal rate on the shape of the fouling curve was observed. This can be attributed to low fluid velocity or insufficient experimental time.
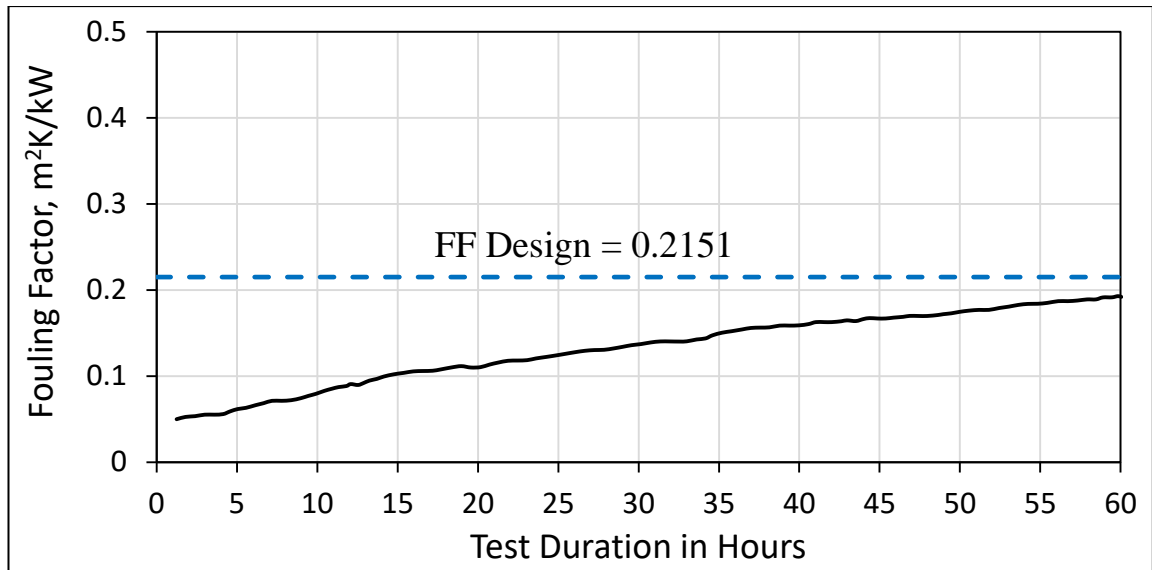
Figure 6.7: Brine heater fouling factor at TBT 119 ᵒC without antiscalant
(Hamed and Al-Otaibi, 2010).

While the flow velocity is well known as an important factor in removal rate, it also affects the rate of deposition. The fouling rate increase in low-velocity regions, especially where the velocity drops suddenly (Awad, 2011). Pääkkönen et al. (2015) mentioned that the rate of deposition increases as the residence time of the fluid increases (Low velocity). In MSF evaporation stages and heat exchangers in general, the evaporation tubes are connected to each other by water boxes where the velocity drops suddenly and thus more fouling is expected at the outlet tubes and on the shell side of the water boxes. In fact, ElMoudir et al. (2008) found that the scale was concentrated in hot outlet location of the stages and more than 50% of the outlet tubes were blocked (Figure 6.8). They assumed that 50% of the rate of deposition was accumulated at the water boxes and does not affect the overall heat transfer surface. This amount of the deposit at the outlet of the tubes could be as result of the removed particles from the tubes that stick again at the outlet of the tubes and in the water boxes due to the sudden decrease in the velocity.

To calculate the density of the fouling layer, Zhang et al. (2015) approach is adopted in this work. Zhang and his co-workers assumed that the fouling layer is a porous material with a porosity of ω. The fouling layer density correlation can be written as follows:

$$\rho_f = \omega \times \rho_{air} + (1 - \omega) \times \rho_{solid} \tag{6.54}$$

where ρ_{solid} is the density of the compact solid.

Since the assumed porous material is immersed in the bulk, the conductivity of the fouling layer is estimated based on Brahim et al. (2003)'s correlation. Here, it is assumed to be the arithmetic average value of thermal conductivity of deposit/water system.

$$\lambda_f = \frac{\lambda_{f,I} + \lambda_{f,II}}{2} \tag{6.55}$$

where

$$\lambda_{f,I} = \omega.\lambda_{water} + (1 - \omega).\lambda_{solid} \tag{6.56}$$

$$\frac{1}{\lambda_{f,II}} = \frac{\omega}{\lambda_{water}} + (1 - \omega)/\lambda_{solid} \tag{6.57}$$

where λ_{water} is the conductivity of pore medium (water) and λ_{solid} the thermal conductivity of compact solid.
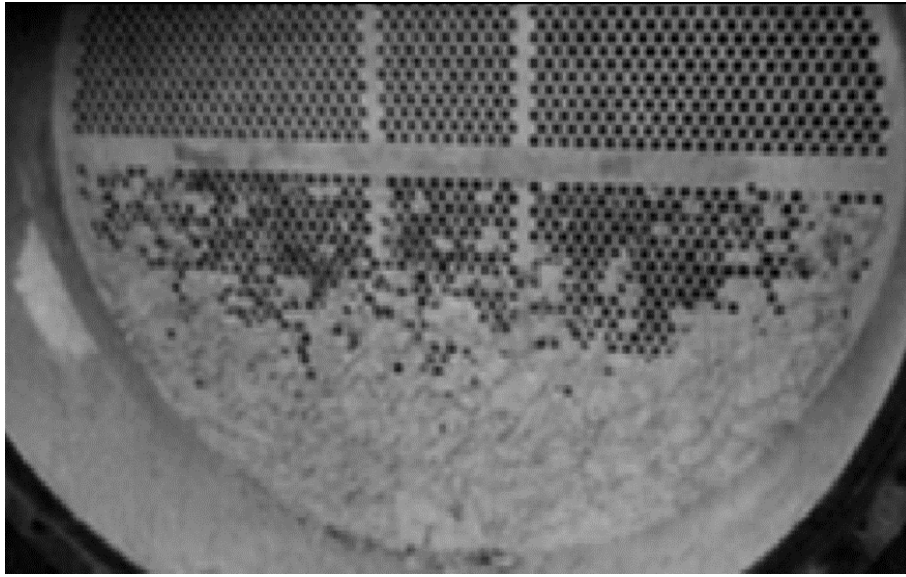
Elmoudir et al (2008). Process modelling in desalination plant operations. Photo 1. Page 435. *Desalination,* vol. 222, pp. 431-440.

Figure 6.8: Fouling in brine heater after operation for a period at TBT = 115 ºC (ElMoudir et al., 2008).

Finally, the fouling resistance can be introduced into the overall heat transfer coefficient equation as follows.

$$\frac{1}{U_o} = \left(\frac{d_o}{h_i d_i}\right) + \left(R_{f,i}\frac{d_o}{d_i}\right) + \left(\frac{d_o}{2k_t}\right) Ln\left(\frac{d_o}{d_i}\right) + R_{f,o} + \left(\frac{1}{h_o}\right) \tag{6.58}$$

Where d is the tube diameter in m, k_t the tube material thermal conductivity in kW/m.K, h the heat transfer coefficient in kW/m^2.K, and the subscripts o and i refer to the outer and inner tube surface respectively. While $R_{f,i}$ is the fouling resistance inside the tubes in m^2.K/kW, the outer fouling resistance, $R_{f,o}$, is kept constant in this work.

6.5 Results and Discussions

The dynamic model of fouling has been implemented using the gPROMS model builder and then it is incorporated into the whole MSF dynamic model that already has been presented in chapter three. The MSF process simulation is run for an adequate time with and without antiscalant to check the rate of deposition and the fouling rate. The chemical analysis of seawater that has been used in this work is presented in Table 6.1.

The pre-exponential constant, k_{r0}, and the activation energy, Ea, are calculated experimentally from the rate of deposition and saturation index using the Arrhenius equation (Augustin and Bohnet, 1995). There are no specific values for these parameters to be adopted for carbonate or magnesium systems. Pääkkönen et al. (2009) mentioned that these parameters vary largely depending on the velocity, and thus they conclude that more factors should be considered to calculate these parameters. However, for a diffusion controlled process, Andritsos (1996) reported a weak effect of the fluid velocity on the activation energy of carbonate system. Pääkkönen et al. (2015) found that the effect of activation energy is much stronger than the effect of pre-exponential constant. In the present work, and due to the lack of experimental data for fouling in MSF processes, values for k'_{r0} and Ea for calcium carbonate were assumed to be *1.8x10^{10} m^4/kg.s^2 and 68.21 kJ/mole* respectively. Studying precipitation of magnesium hydroxide has less attention than calcium carbonate and the number of studies of the precipitation of magnesium hydroxide are considerably less than that for calcium carbonate. However, Shams El Din and Mohammed (1994) reported that the amount of calcium carbonate in the water boxes of the first stages was approximately 7 times more than magnesium hydroxide. Thus, to match the ratio of calcium carbonate precipitation to magnesium hydroxide

precipitation, the values of k'_{r0} and Ea for hydroxide magnesium precipitation have been estimated to be *6.4×10^{18} kg/m^2.s and 120 kJ/mole* respectively.

Table 6.1: Chemical analysis of the seawater entering the heat rejection section

Parameters	Unit	Brine recycle to HRS
pH		8.2
Total alkalinity	mg/L as CaCO$_3$	106
Sulphate	mg/L	6081
Calcium	mg/L	894
Magnesium	mg/L	2886

(Source: Hamed and Al-Otaibi (2010))

6.5.1 Running the MSF Simulation without Antiscalant

Running the MSF simulation model with the predicted fouling factor and without antiscalant for long time may lead to infeasible solution. This happened due to the fact that overall heat transfer coefficient and flow velocity could reach unacceptable values which can make the MSF profess infeasible to operate. Thus, the simulation was run for a certain time to avoid unrealistic fouling.

As mentioned before (Section 6.3, Figure 6.3), the recycle brine is pumped from the last stage in HRJ (Stage 24) into the last stage of the HRS (Stage 21) at around 40 °C where it is heated gradually to around 112 °C at the outlet from stage 1 before the water enters the brine heater for further heating. Due to the increase in surface temperature and decrease of the saturation concentration from stage to stage, the deposit of both CaCO$_3$ and Mg(OH)$_2$ increased. The deposit rates of calcium carbonate and magnesium hydroxide per unit area are shown in Figures 6.9 and 6.10 respectively. As it can be seen, predicted that the calcium carbonate starts to precipitate at low temperature while magnesium hydroxide starts to precipitate at higher temperature. At low stage temperatures, the OH ions are too low to cause any precipitation of magnesium hydroxide. However, as the recycle brine flows through the stages and its temperature increases, the magnesium hydroxide's solubility limit is reached resulting in deposition of magnesium hydroxide. At saturated brine of calcium carbonate and magnesium hydroxide, the priority of crystallization depends on the Ca/Mg or

CO_3/OH ratio. Dooly and Glater (1972) reported that the precipitation of calcium carbonate will be favoured by an increase in the ratio of Ca/Mg or CO_3/OH. In this work, the participation of calcium carbonate from stage 21 to around stage 5 leads to reduction of the Ca/Mg ratio and thus precipitation of magnesium hydroxide becomes more favoured from stage 5 to the first stage.

Actual fouling data is hard to obtain from real plants due to the difficulties of having deposit sample from MSF tubes. However, Shams El Din and Mohammed (1994) conducted very rigorous analysis of the collected samples from flash chambers pools and water boxes from two different MSF plants. In their analysis, they reported that the mass of calcium carbonate deposition in the first three water boxes was approximately 7 times more than magnesium hydroxide. The $Mg(OH)_2$ starts to precipitate in stage 9 where the surface temperature is around 82 °C, which is consistent with the observations of Wildebrand et al. (2007) where they spotted a thin layer of $Mg(OH)_2$ crystal at 80 °C.

Figure 6.9 also shows that while there is a decrease of the precipitation of calcium carbonate in the first few stages, there is a slight increase in the middle stages. This can be explained by the increase in the vapour and brine temperatures in the middle flash chambers. As it can be seen in Figure 6.11, the surface temperature of the first few stages decreases with time due to fouling whereas the temperature in the middle stages increases. While there is a reduction in the surface temperature due to fouling, the vapour temperature inside the flash chambers increases leading to increase in the heat transfer flux and as a result, more deposition is expected in the middle stages. This increase in the $CaCO_3$ deposition in the middle stages may cause reduction in the Ca concentration and thus the deposition of calcium carbonate in the first few stages decrease and the deposition of magnesium hydroxide becomes more favourable over calcium carbonate. However, in the long run, the deposition of calcium carbonate and magnesium hydroxide decrease due to the decrease in the surface temperature. Moreover, the release rate of CO_2 can be good indicator of the rate of deposition of calcium carbonate. As shown in Figure 6.12, the concentration of CO_2 increases as calcium carbonate is produced according to the reaction in equation (6.7) and then starts to decrease with the decrease in the deposition of calcium carbonate.
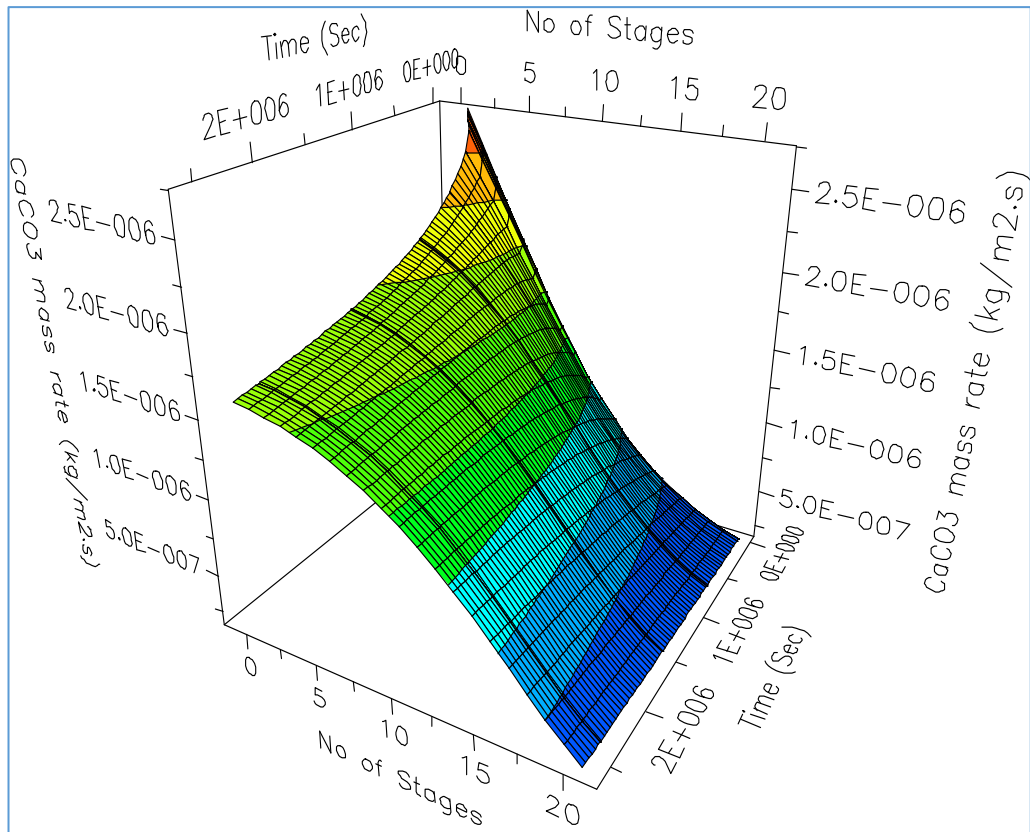
Figure 6.9: Calcium carbonate mass rate profile per unit area
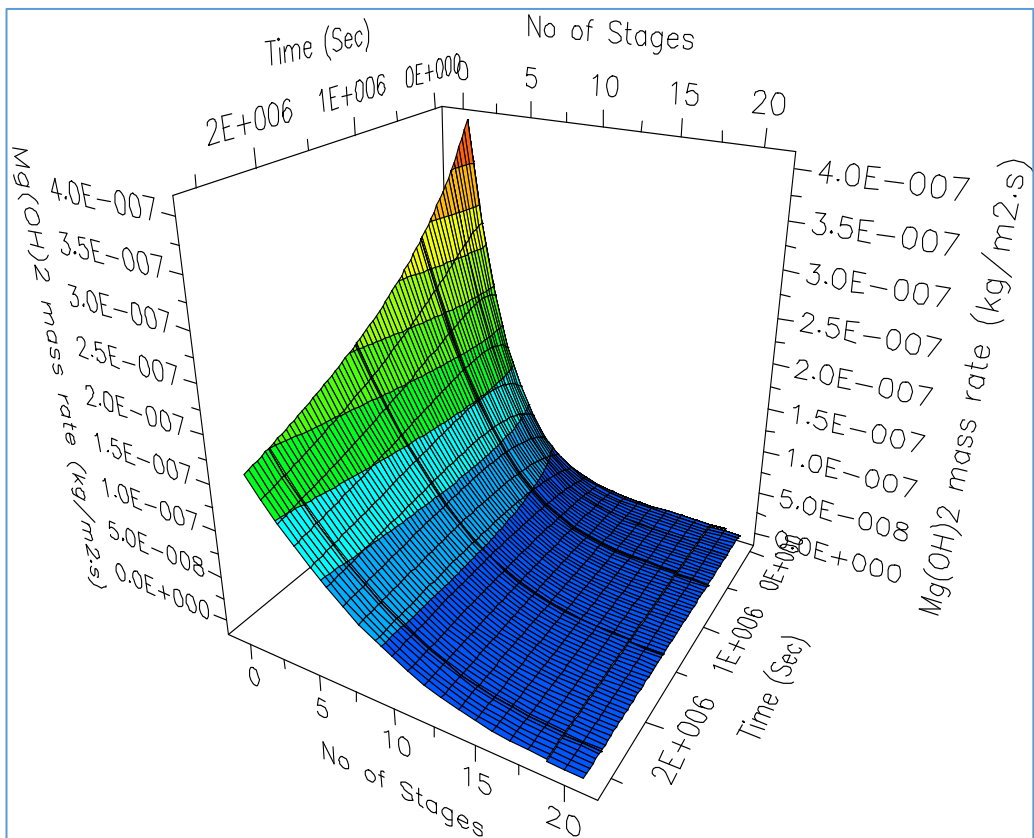
Figure 6.10: Magnesium hydroxide mass rate profile per unit area.
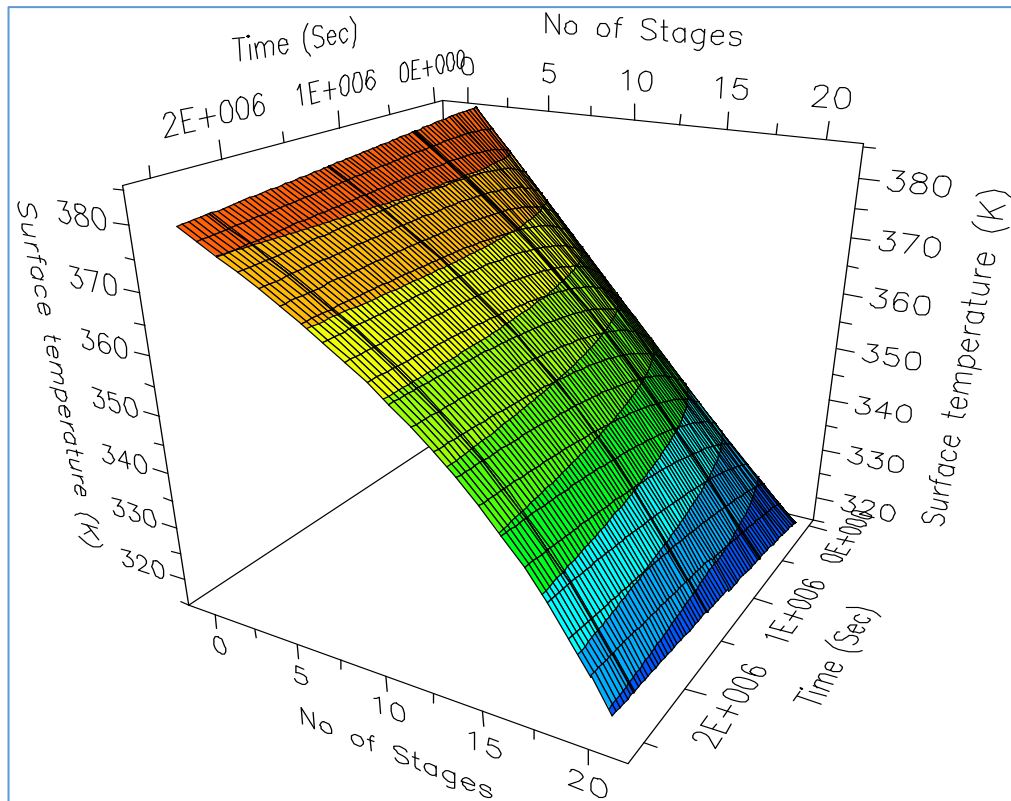
Figure 6.11: Surface temperature profile
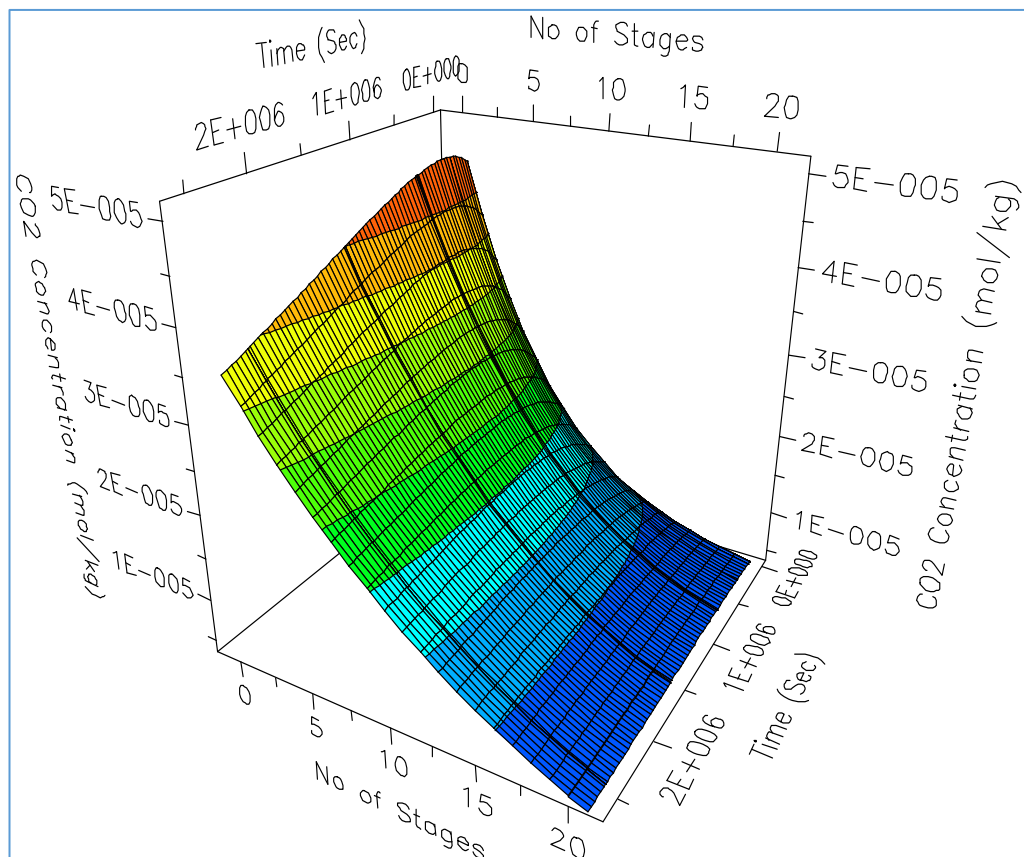
Figure 6.12: CO₂ concentration profile

Due to the lack of information of fouling without antiscalant, the fouling in the first stage, as it has the highest temperature (around 112 °C), is compared to the brine heater fouling without antiscalant presented by Hamed and Al-Otaibi (2010) in Figure 6.7. The results presented in Figure 6.13 show slight difference between this model's results and the extrapolated results presented by Hamed and Al-Otaibi (2010). This can be explained by the temperature difference between the brine heater and the first stage. Hamed and Al-Otaibi results were obtained in brine heater (119 °C) while this results was for the first stage (112 °C) in the MSF plant. Figure 6.14 shows the fouling profile per stages. Although Figures 6.9 and 6.10 show a decrease in the rates of deposition of calcium carbonate and magnesium hydroxide in the first few stages and an increase of that deposition in the middle stages, Figure 6.14 shows that the total accumulation of foulant is highest in the first stage and decreases in the subsequent stages as the temperature decreases.
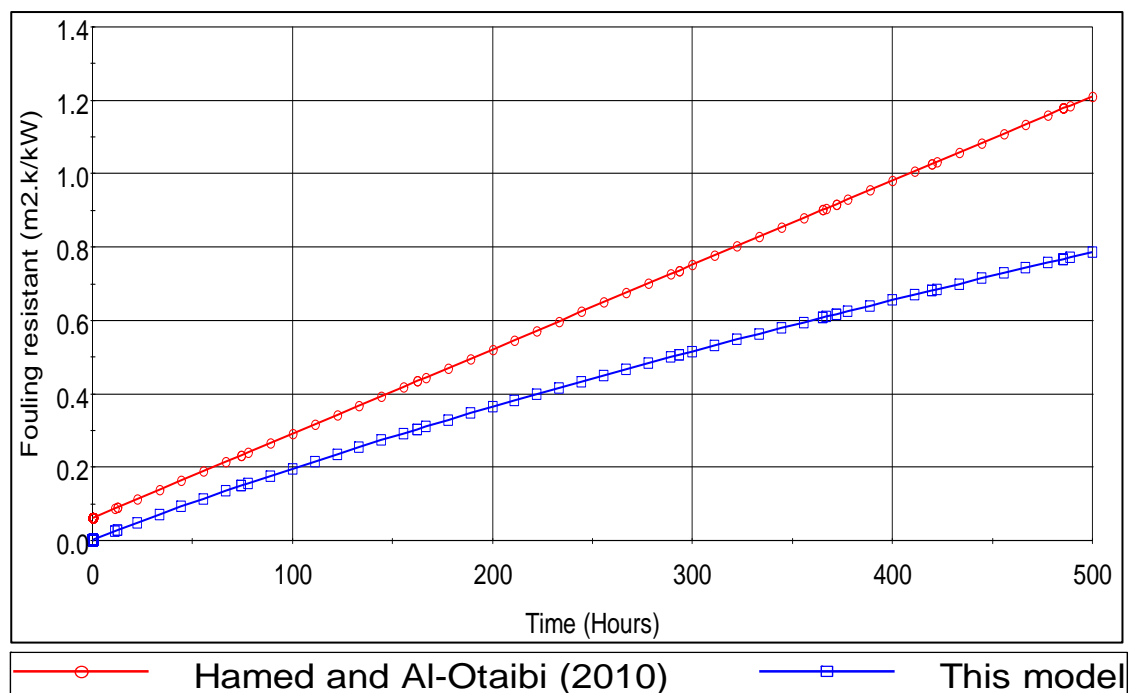
Figure 6.13: Predicted fouling resistance as a function of time.
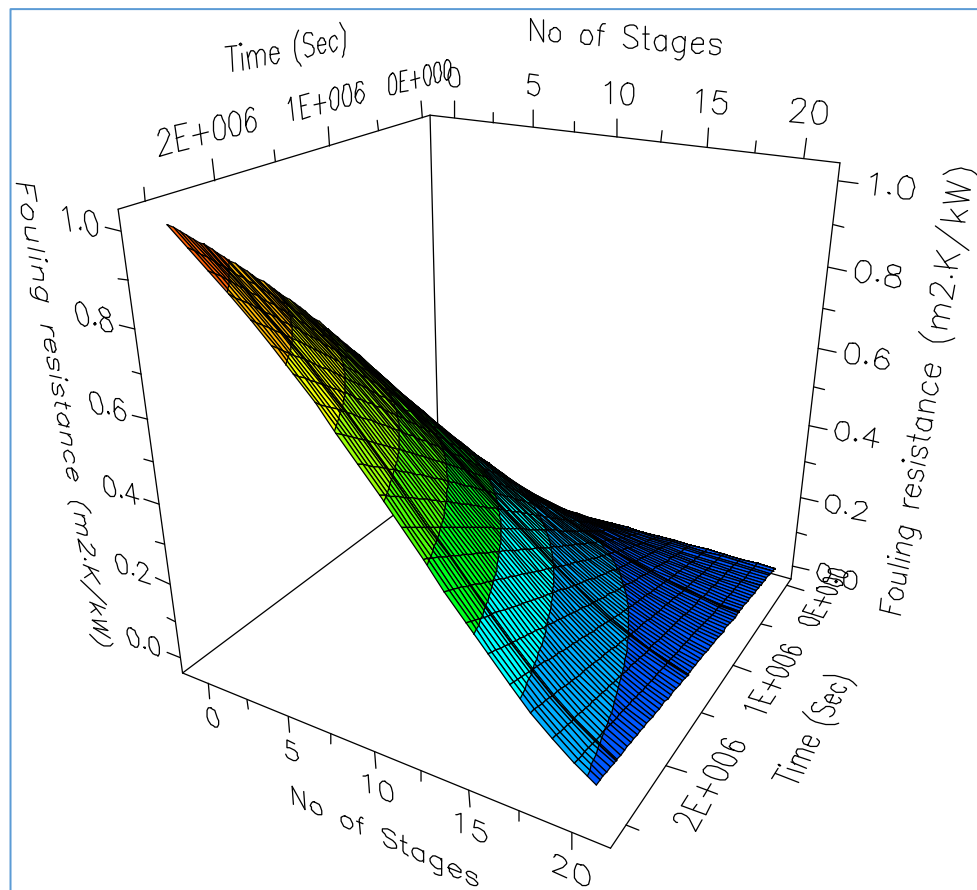
Figure 6.14: Fouling resistance profile as function of the number of stages and time

Considering the first stage as it has the highest temperature, Figure 6.15 shows the total rate of deposition per unit time together with the net rate of deposition and the removal rate. The total rate of deposition decreases with time due to the decrease in the surface temperature of the fouling layer. Alongside this decrease in the deposition rate, the removal rate increases due to the growth of the fouling layer and consequently the velocity of the brine increases causing more particles to be removed. With the increase of the removal rate, the net rate of deposition becomes less than the total rate of deposition by the difference of the total rate of deposition and the removal rate. The rapid or slow decrease in the net rate of deposition depends on the removal rate which is strongly dependant on the fouling layer thickness and brine velocity inside the tubes. Figure 6.15 also shows that the rate of deposition is nonlinear and it appears to approach steady state with time as there is enhancement in the heat transfer. Brahim et al. (2003) reported that the supersaturation at the interface is reduced due to the increase in the velocity and thus the heat transfer is improved. Moreover, the reduction in

the recycle brine salinity can also considered to be another parameter to slow the decrease of the rate of deposition. According to equation (6.26), the solubility product of calcium carbonate increases with the decrease in the temperature resulting in decrease in the rate of deposition. However, Mucci (1983) reported that the solubility product decreases with the decrease in the salinity resulting in increase in the rate of deposition. Thus, considering only the temperature effect is not sufficient to predict the rate of deposition. Due to the decrease in the recycle brine salinity, the solubility concentration of calcium carbonate does not increase the rate of deposition but rather it slows down the decrease caused by the drop in the temperature.
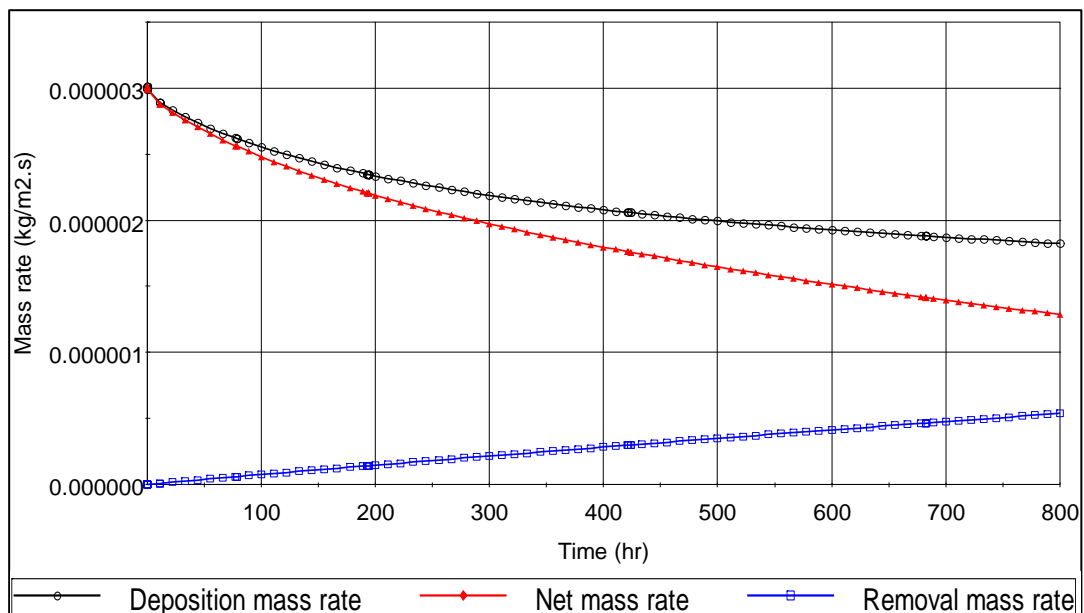
Figure 6.15: Rate of deposition together with removal rate and net rate.

6.5.1.1 Effect of Flow Velocity

In many studies, the effect of the flow velocity on fouling seems to vary depending on the controlling mechanism of the fouling. Although Helalizadeh et al. (2005) reported a decrease in the mass deposit rate with increase in the velocity during convection heat transfer and sub-cooled flow boiling experiment, Najibi et al. (1997), Helalizadeh et al. (2000) and Peyghambarzadeh et al. (2012) reported that the fouling resistance increases with increase in flow velocity. They explained that the diffusion mechanism has some control on the fouling resistance at certain velocities and then when the velocity increased further, the fouling became completely reaction control mechanism and the rate of deposition is flow velocity

independent. It is important to mention that the previous three studies were conducted to predict the fouling rate under subcooled flow boiling. Moreover, Andritsos (1996), who adopted the diffusion mechanism controlled process, reported increase in the rate of deposition with increase in the fluid velocity. They concluded that this trend was an indication of diffusion controlled mechanism. Pääkkönen et al. (2015), however, showed a decrease in the mass deposition rate of calcium carbonate with an increase in the flow velocity.

In the presence of fouling, at constant volumetric flow rate, the flow velocity inside the MSF tubes varies with time due the variation in the cross sectional area. However, different values of flow velocity can be set to observe its effect clearly. Hence, different values of flow velocity at the start of every run can be obtained by adjusting the recycle volumetric flow rate. In the present work, four different values of the recycle flow rate (3.25, 3.5, 3.75 and 4.0 m^3/s) were selected to obtain four different velocity values. Increasing the velocity by increasing the volumetric flow rate by 0.25 m^3/s results in a very slight increase in the rate of deposition of calcium carbonate as shown in Figure 6.16. However, further increase in the velocity results in decrease in the rate of deposition of calcium carbonate. Though Brahim et al. (2003) reported that the heat transfer can be improved due to the increase in the velocity, Pääkkönen et al. (2015) pointed out that reducing residence time of the fluid at the surface may decrease the probability of the foulant adhering to the surface. As can be seen in Figure 6.17, the predicted heat transfer was slightly improved with the increase in the velocity. Further increase in the volumetric flow rate to its maximum value (4.0 m^3/s) leads to more reduction in the rate of deposition of calcium carbonate though the heat transfer is improved. However, the variation in the salinity of seawater can play an important role in the fouling behaviour in MSF process. Increasing the recycle brine velocity can improve the heat transfer which further increases the salinity of the recycle brine. This can lead to decrease in the activity coefficients of the seawater ions and consequently increase the solubility product of calcium carbonate and magnesium hydroxide. Thus, the decrease in the concentration driving force results in a decrease in the rate of deposition.

Hence, different results can be obtained if the salinity is assumed to be constant. Here, Figure 6.18 shows the rate of deposition of calcium carbonate with different

velocities and at constant salinity. As it can be seen, the rate of deposition of calcium carbonate increases with the increase in the velocity. However, this increase in the rate of deposition is limited to certain velocities and with further increase in the velocity, it becomes temperature dependent and the velocity has no effect.
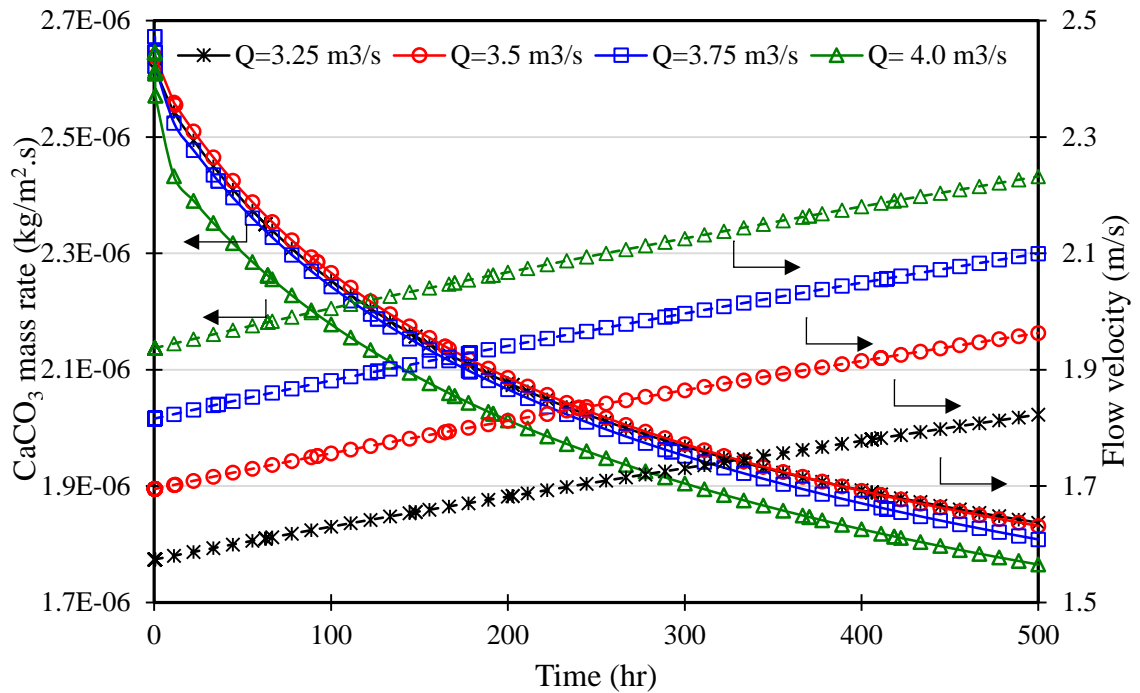
Figure 6.16: Effect of the flow velocity on the deposition rate of CaCO₃ (First Stage)
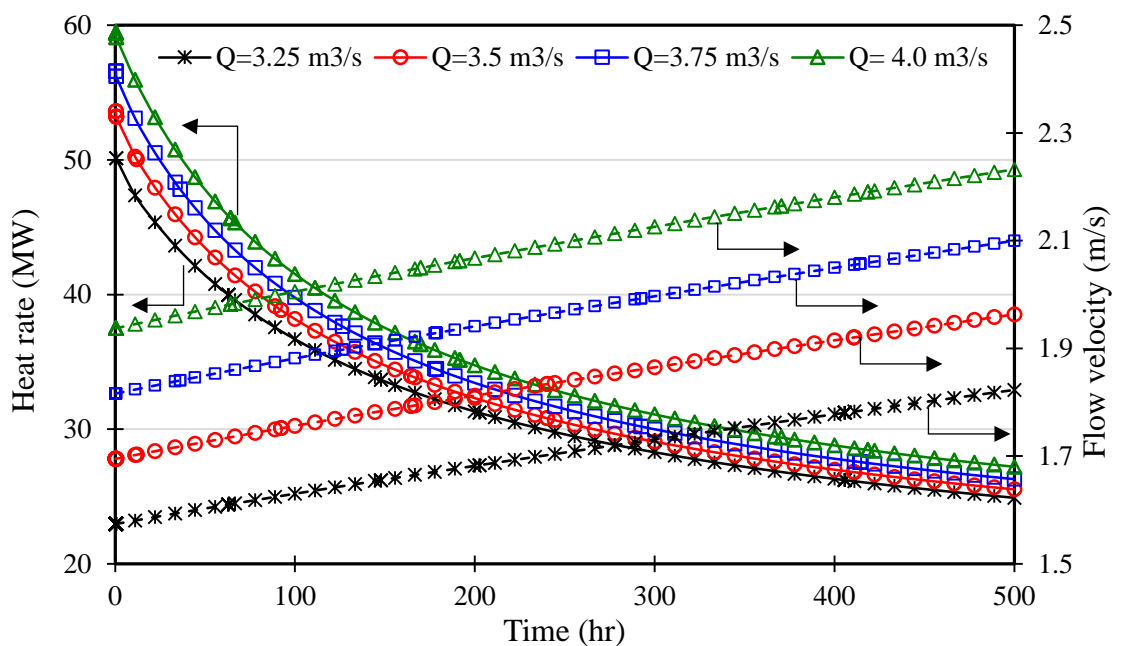
Figure 6.17: Effect of the flow velocity on the heat transfer rate (First Stage)
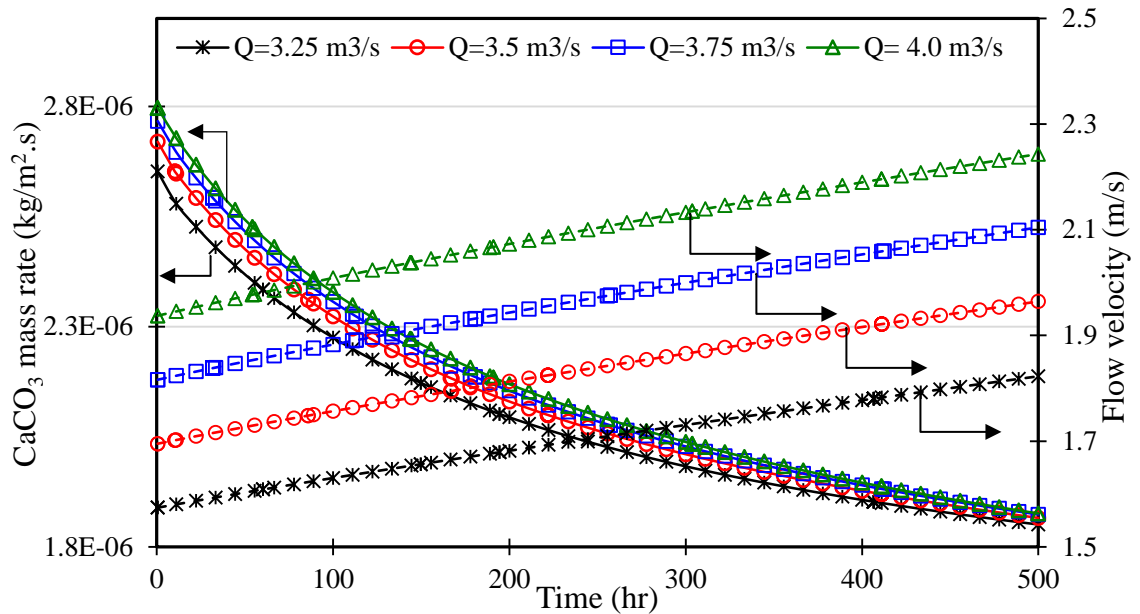
Figure 6.18: Effect of the flow velocity on the deposition rate of CaCO$_3$ at constant salinity (First Stage)

In the case of magnesium hydroxide, however, the rate of deposition increase with the increase in flow velocity. Due to the low solubility product of magnesium hydroxide, the activity coefficients of magnesium and hydroxide ions have little effect on magnesium hydroxide precipitation. Figure 6.19 shows that the increase in the magnesium hydroxide follows the same pattern as the heat transfer rate and thus it is believed that the precipitation of magnesium hydroxide is temperature dependent and the velocity has little or no effect.

However, despite the increase in heat transfer rate and the rate of deposition of magnesium hydroxide with increase in flow velocity and also slight increase and then decrease of deposition of calcium carbonate, at constant volumetric flow rate, the deposition of calcium carbonate and magnesium hydroxide and the heat transfer rate decrease with the increase in the velocity. This can be explained by the increase in the fouling layer thickness which affects the heat transfer rate and consequently affects the deposition rate of calcium carbonate and magnesium hydroxide.
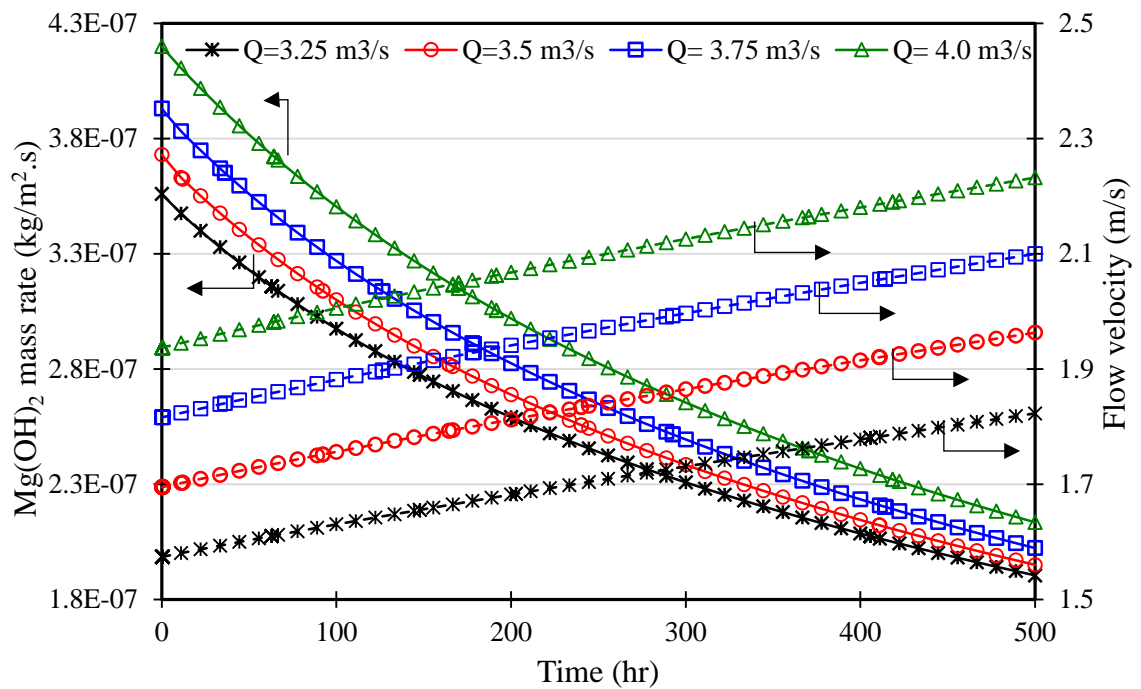
Figure 6.19: Effect of the flow velocity on the deposition rate of Mg(OH)₂ (First Stage)

Whilst the rate of deposition increases fouling, the removal rate, on the other hand, opposes the fouling mechanism. The removal rate depends on the thickness of the fouling layer and strongly on the flow velocity of the brine. Figure 6.20 shows the effect of the velocity on the fouling resistance and removal rate in the first stage of the MSF plant. Due to the increase in the thickness of the fouling layer and the velocity of the brine, the effect of the removal rate increases. As it can be seen from Figure 6.20, the effect of the removal rate on the fouling can be observed clearly after long time of simulation. Thus, high velocity can help to decrease the fouling rate by increasing the removal rate.
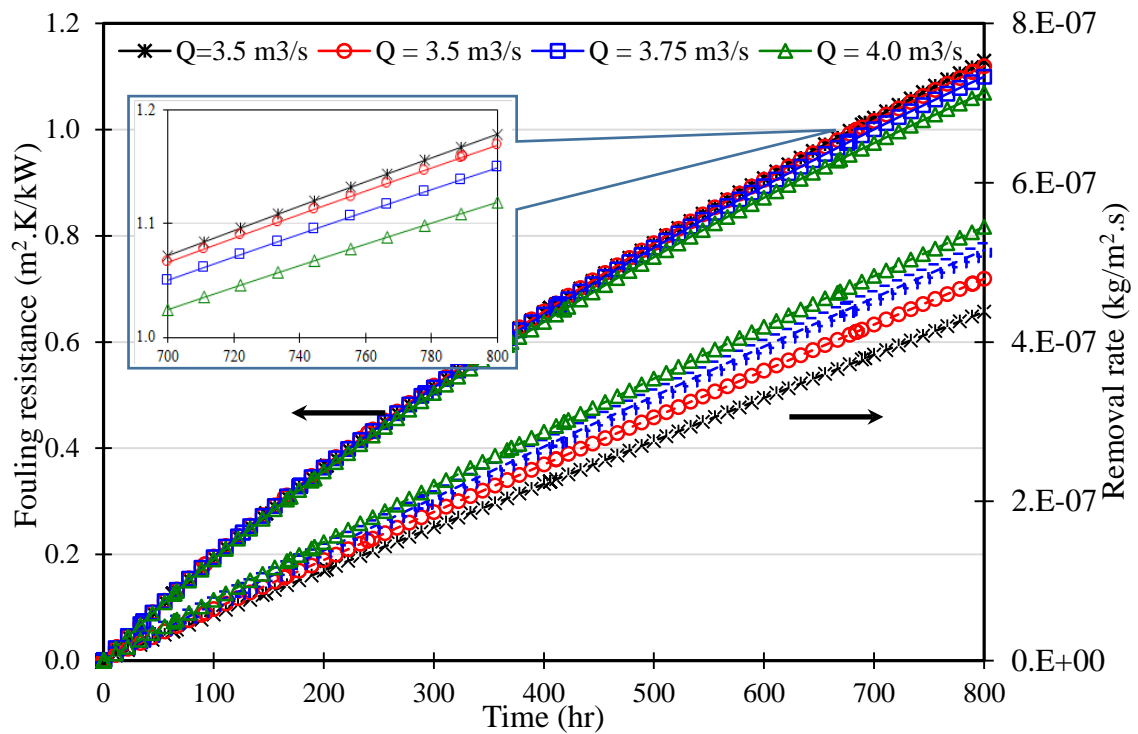
Figure 6.20: Effect of the flow velocity on the fouling resistance and removal rate (First Stage)

Though increasing the flow velocity results in decrease in the fouling with time, in MSF process, increasing the velocity could affect the efficiency of the plant. The efficiency of MSF process is estimated by the performance ratio (PR) which can be defined as the amount of produced distillate per 1 kg of heated steam in the brine heater.

Helal et al. (2012) and Abdul-Wahab et al. (2012) reported that the main variables that affect the performance of the plant were the TBT and the brine recycle flow rate. Increasing one of these variables leads to increase in the performance ratio and distillate product. Increasing the brine recycle flow rate may increase the distillate, however, increasing it over the design point would inevitably affect the overall MSF plant cost (Fiorini and Sciubba, 2005). Figure 6.21 shows the performance ratio at different velocities. As it is expected, the performance ratio decreases with increasing the velocity though increasing the velocity decreases the fouling rate and enhance the heat transfer rate. This reduction in the performance ratio can be explained by the increase in the amount of steam that is required to heat the recycle brine (Maniar and Deshpande, 1996). Thus,

optimum value of the brine recycle flow rate can be obtained to maximize the performance ratio and distillate product.
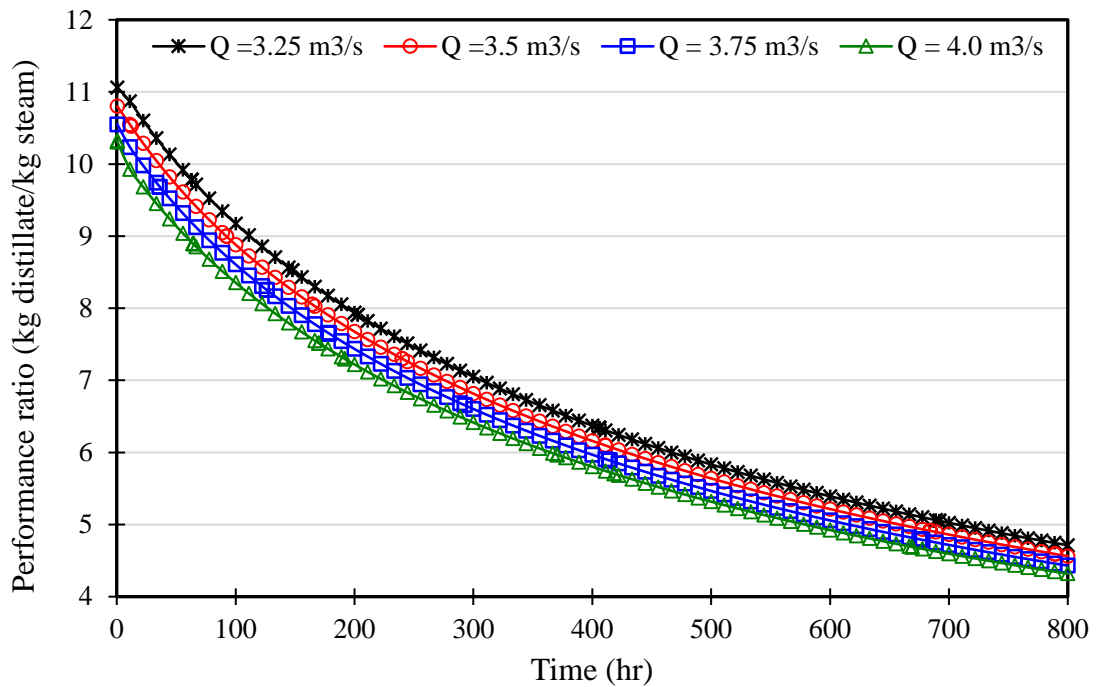
Figure 6.21: Effect of the flow velocity on the plant performance ratio in the presence of fouling.

6.5.1.2 Effect of Surface Temperature

Since the MSF stages operate at different temperatures, its highest value is in the first stage and decreases gradually from stage to stage due to the gradual pressure drop. The effect of the surface temperature can be seen in Figure 6.14 where fouling resistance is plotted against the number of stages. Due to the decrease in the inner surface temperature from the first stage towards the last stage, the fouling resistance rate decreases. However, different MSF plants operates at different TBT based on the different parameters such as seawater salinity, seawater temperature and specific design of the MSF plant. Hence, in order to observe the effect of TBT on the fouling behaviour, the Top Brine Temperature (TBT) is varied between 90 °C and 119 °C for four intervals (90, 100, 110 and 119 °C). This variation leads to the inner surface temperature in the first stage to be varied between 84 °C and 112 °C. Figure 6.22 and Figure 6.23 present the mass rate of deposition of calcium carbonate and magnesium hydroxide respectively at 4 different TBT values for a period of 800 hours. Indeed,

the mass deposit rate of both components increases with increasing the TBT. However, with the increase in temperature the rate of calcium carbonate deposition in the first stage decreases compared to the increase in the rate of deposition of magnesium hydroxide. This can be explained by the reduction of calcium and carbonate ions in the first stages due to the increase in the calcium carbonate in the middle stages. As mentioned earlier (Section 6.5.1), increasing the temperature causes an increase in the temperature of the flash chambers in the middle stages and hence it results in more deposition in the middle stages and reduction in the calcium and carbonates ion in the first stages. Figure 6.24 shows the rate of deposition of calcium carbonate per stage for 4 different TBT values after a period of 300 hours. Increasing the temperature shows an increase in the rate of deposition of calcium carbonate in the middle stages. This increase in the rate of deposition in the middle stage affects the concentration of calcium and carbonate in the first few stages.

The reduction in calcium and carbonate ions leads to decrease in the Ca/Mg and CO_3/OH ratio as reported earlier and thus, the deposition of magnesium hydroxide become more favourable. This can be seen clearly in comparison between Figure 6.22 and Figure 6.23 as the rate of deposition of calcium carbonate slows down (Figure 6.22), the rate of deposition of magnesium hydroxide increases rapidly with the increase in the temperature (Figure 6.23).
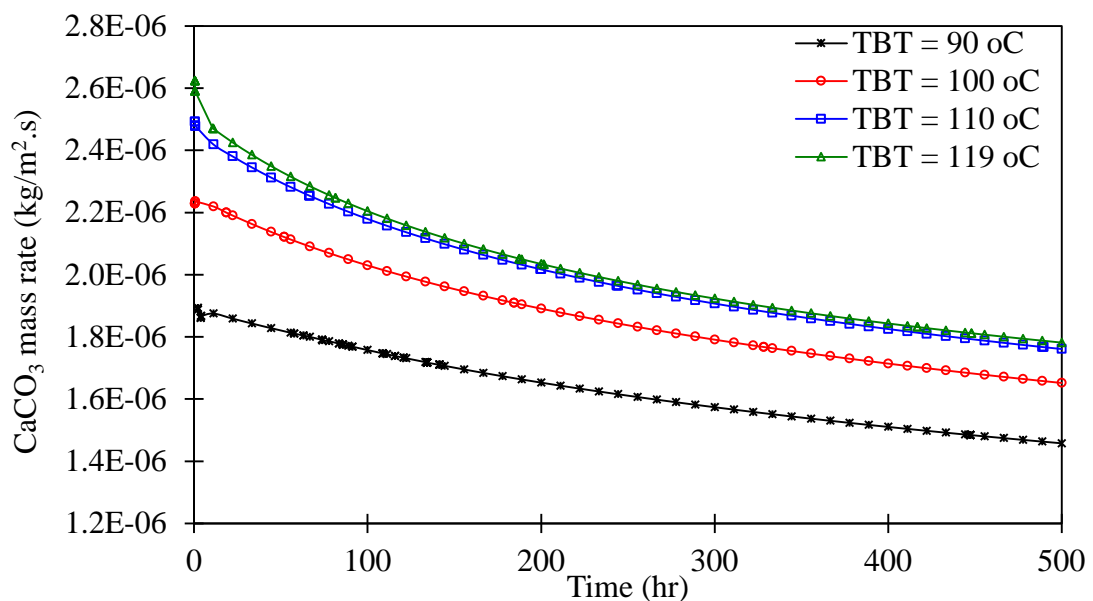
Figure 6.22: Effect of the surface temperature on the deposition rate of calcium carbonate (First Stage).
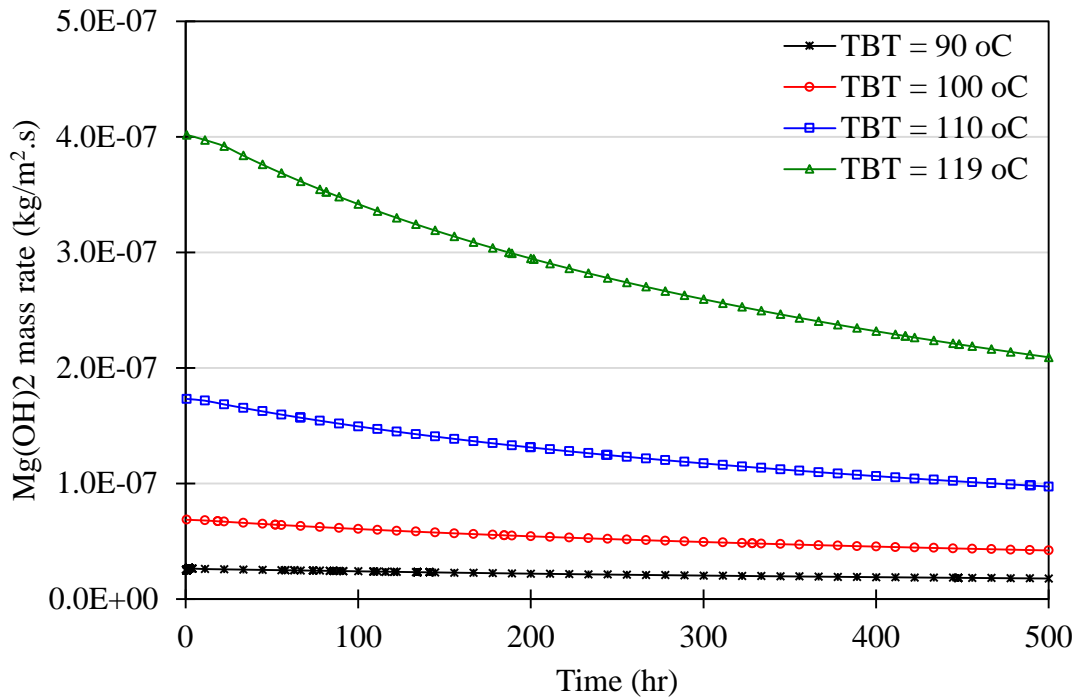
Figure 6.23: Effect of the surface temperature on the deposition rate of magnesium hydroxide (First Stage).
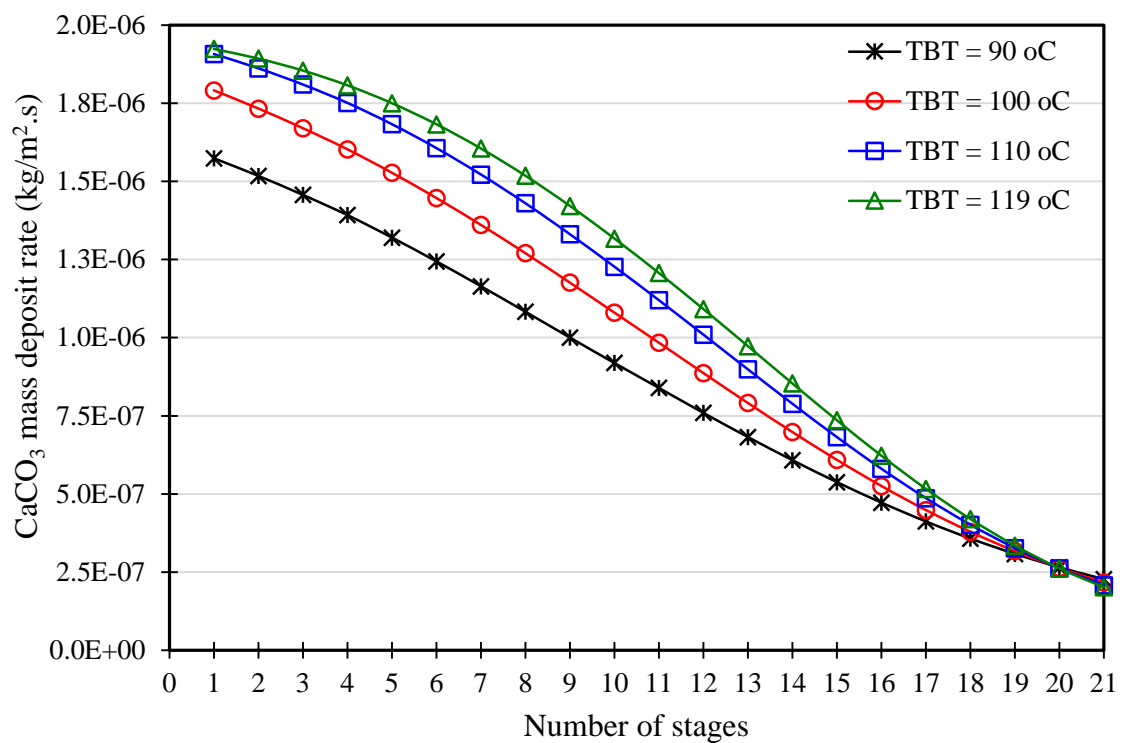
Figure 6.24: Rate of deposition of calcium carbonate per stages after 300 hours of operation for 4 different TBT values.

6.5.2 Running the MSF Simulation with Antiscalant

As mentioned earlier, MSF plants require scale prevention measures to reduce the concentration of bicarbonate by using one of the commercial antiscalants along with sponge ball cleaning to reduce the foulant thickness. The dosages rate of the antiscalants and the frequency of ball cleaning depends on the hardness of the seawater and the design of the MSF plants. Based on linear behaviour of the fouling, Hamed et al. (1999) estimated a period of around 375 and 483 days for use of polycarboxylic and polymaleic acids antiscalants, respectively before fouling reaches the design value. However, this period can vary between one plant to another depending on many parameters such as the type of the antiscalants, the dosing rate, tubes material and the operation conditions of the plant. For the removal processes using antiscalant, Andritsos (1996) reported experimentally that use of acidified water can dissolve 95% of the deposit in three hours.

In this work, the reduction of the deposit process can be done mathematically by decreasing the deposition growth i.e. increasing the removal rate once the thickness of the fouling layer reaches the design value. This can be done using task feature in gPROMS model builder. First, the software is allowed to run for period until the thickness of the fouling layer reaches the design factor, and then new value of one parameter that has great impact on removal rate is altered as there is external force (example; sponge balls) increases the removal rate. The process of cleaning will continue until the thickness is reduced to an acceptable thickness, and then the software runs again in normal fouling mode and so on. It is assumed that during the cleaning process, the total rate of deposition is negligible. By doing this, the process will run over long time without allowing the fouling factor to reach the design value. Hamed et al. (1999) mentioned that the fouling factor of the HRS remained almost constant during the whole period of the test. Moreover, Shams El Din and Mohammed (1994) reported the water boxes of one unit of the Umm Al-Nar desalination plant (Abu Dhabi, UAE) were never opened. Water boxes in another unit were opened only for inspection and repair. This long period without plant shutdown is a good indicator of the effectiveness of ball cleaning and the use of antiscalants in controlling scale formation.

The result of fouling in the first stage is compared to the heat recovery section (HRS) fouling with the use of polyphosphonate antiscalant that was presented by Hamed et al. (1999). Figure 6.25 shows the fouling resistance for the first stage together with Hamed et al. (1999) results for the period of 2500 hours. As it can be seen, the fouling factor is under control to be less than the design value (0.12 m^2.K/kW) for HRS.
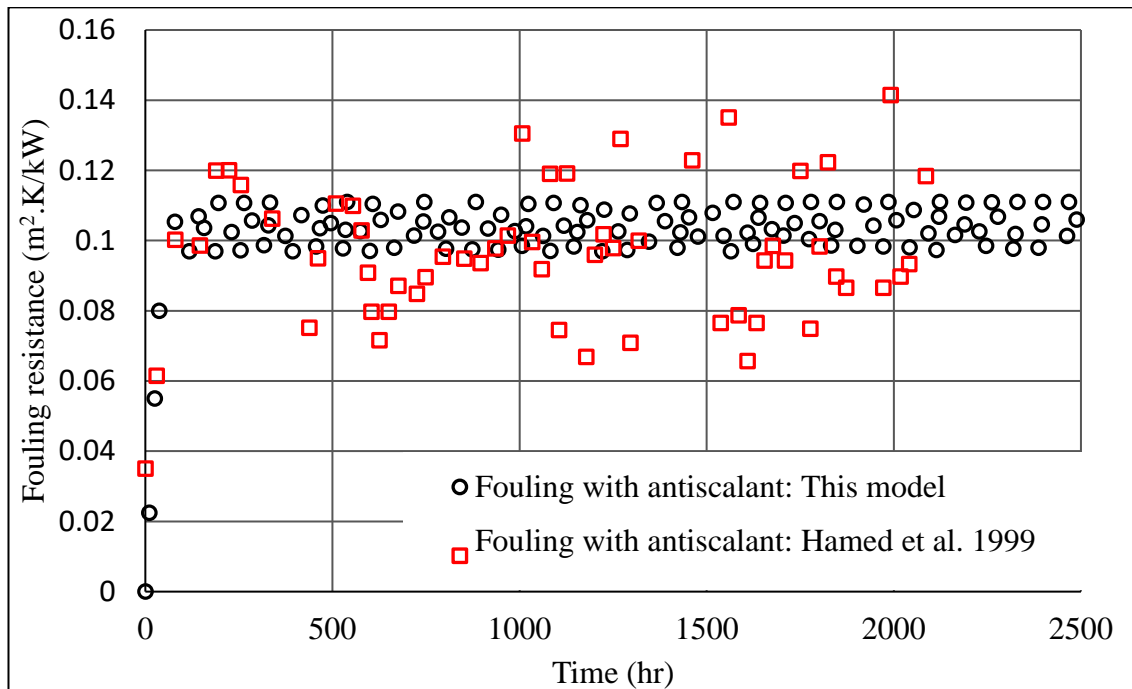
Figure 6.25: Estimated fouling resistance for the first stage in the presence of antiscalant

6.5.3 Performance Ratio and Plant Capacity

Theoretically, by simulation, the plant performance ratio and its capacity are constant for the whole operation period. This is true since the operation parameters, like fouling design factor and the sea intake temperature, are fixed to be constant. However, in reality the story is completely different due to the variation of some parameters. In the present work, the model starts with clean tubes resulting in higher performance ratio and higher plant capacity. With time, the deposits accumulate inside the tubes and the fouling layer starts to build up leading to decrease in the overall heat transfer coefficient and consequently causing massive reduction in the performance ratio as presented earlier in Figure 6.21. However, with the use of chemical antiscalants and ball sponge cleaning,

the deterioration of thermal performance of MSF process can be avoided and the degree of fouling can be controlled. Figure 6.26 shows the performance ratio of a typical MSF plant at fixed fouling factor and varied fouling factor with antiscalant for a period of 4000 hours. As it can be seen, at constant fouling factor, the performance ratio is constant for the whole period. However, with the presence of fouling, the performance ratio is higher at the beginning when the tubes are clean and then starts to decrease with time because of increase in the fouling resistance. As soon as the cleaning process starts, the performance ratio decreases slowly and then remains at constant values above the design value.
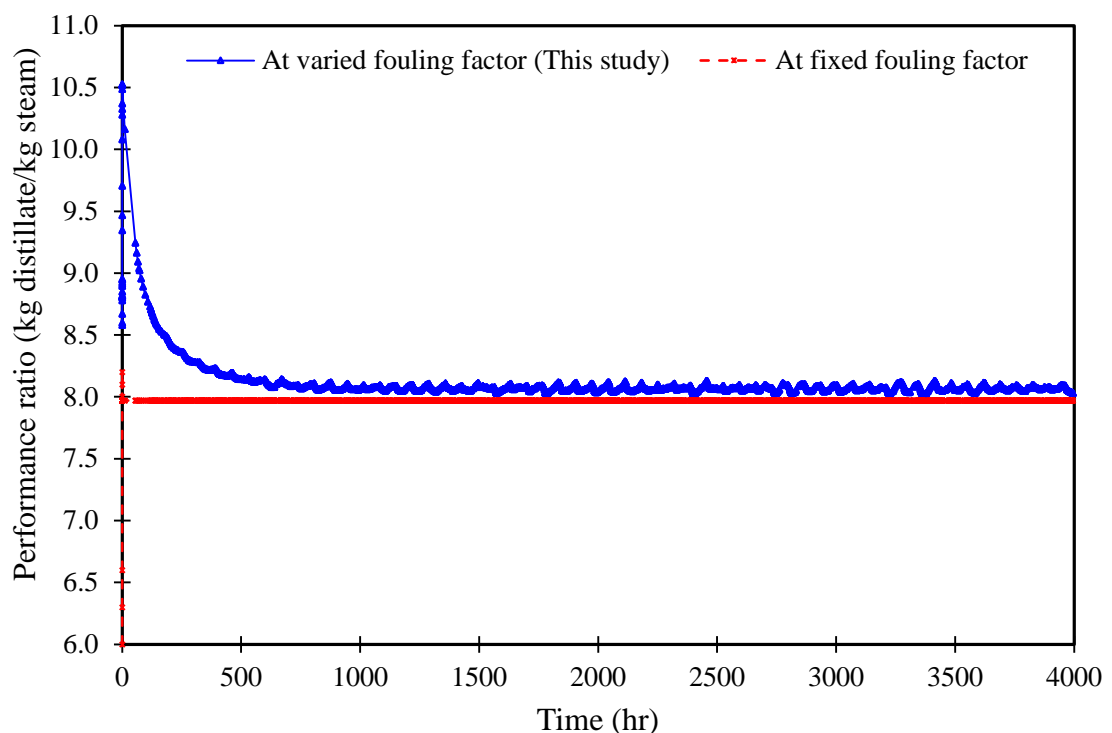
Figure 6.26: Performance ratio at fixed and calculated fouling factor

This effect can be seen in the plant capacity as well. The plant capacity, as can be seen from Figure 6.27, follows the same behaviour as the performance ratio. When the fouling factor is assumed constant, the capacity value continues to be constant for the whole period. However, in the presence of fouling, the plant capacity is at its highest value at the start of the process and then declines with time as the fouling resistance increase. The change in the plant capacity is not as much as the change in the performance ratio due to the fact that fouling resistance has great effect on the performance ratio and the total operation cost.
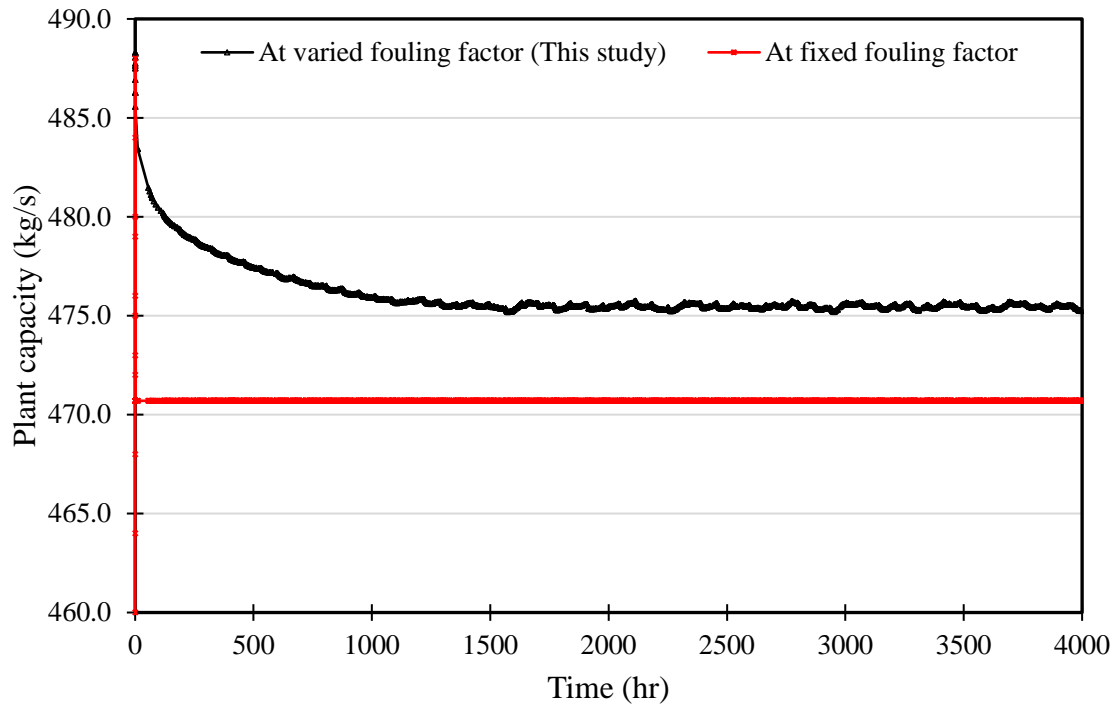
Figure 6.27: Plant capacity at fixed and calculated fouling factor with antiscalant.

6.5.4 Partial Removal of Divalent Ions.

In most MSF plants, the operating temperature (TBT) is limited in the range between 90 °C and 120 °C. This limitation of the TBT is to avoid the likelihood of high scale crystallization at higher temperatures. Increasing the TBT and consequently the flashing range temperature has great impact on the plant performance and the water production cost. Thus, partial removal or reduction of the divalent ions such as Ca^{2+} and Mg^{2+} from the intake seawater results in low or even zero fouling and thus allow for MSF plants to operate at higher TBT. There are several suggestions in the literature to pre-treat the intake seawater by different technologies such as nanofiltration (NF) and RO. Hamed et al. (2009) studied trihybrid of NF/RO/MSF to reduce the sulphate and calcium ions in the seawater. The treated outlet from RO was used as makeup flow to the last stage of the MSF process. In their study, this integration allows the MSF process to operate safely up to TBT of 130 °C. Al-Rawajfeh et al. (2012) carried out a study to predict the potential of calcium sulphate scale after using salts precipitators (SP) and NF unit as pre-treatment for MSF process. The results showed that for

50% pre-treated feed the TBT reached 145 ^oC and for 100% pre-treated feed, the MSF process could be operated at TBT of 175 ^oC.

In this section the intake seawater into the MSF process is assumed to be partially and fully treated with one of the available technology such as NF or RO. It is to note that no model or actual data is available to estimate the removal rate of the divalent ions from the seawater. However, it is assumed that the divalent ions are removed from the seawater in the range 0% to 100% in increments of 20%. Figure 6.28 shows the increase in the performance ratio with partial removal of the divalent ions (mainly Ca^{2+} and Mg^{2+}). This increase seems to be nonlinear with small improvement in the performance ration at 20% removal of the divalent ions and starts to improve slowly with more reduction in the divalent ions. In addition, the results indicate that even small amount of foulants could have a large effect on the performance ratio. As it can be seen, partial removal of the foulants up to 80% does not improve the performance ratio significantly. However, removal over 80% and up to 100% of the foulants can improve the performance ratio dramatically.

It is important to point out that these results have been carried out at constant TBT of 119 ^oC. The performance is thus expected to be improved further if the TBT is increased. The reason of not investigating the effect of TBT in this case is due to the dynamic behaviour of this model. Increasing the TBT leads to generation of more vapour and results in decrease in the brine level in the first few stages. Thus, to simulate the MSF process at higher TBT, the design configuration of the MSF plant such as the height of the gate has to be modified to control the brine level in the first few stages.
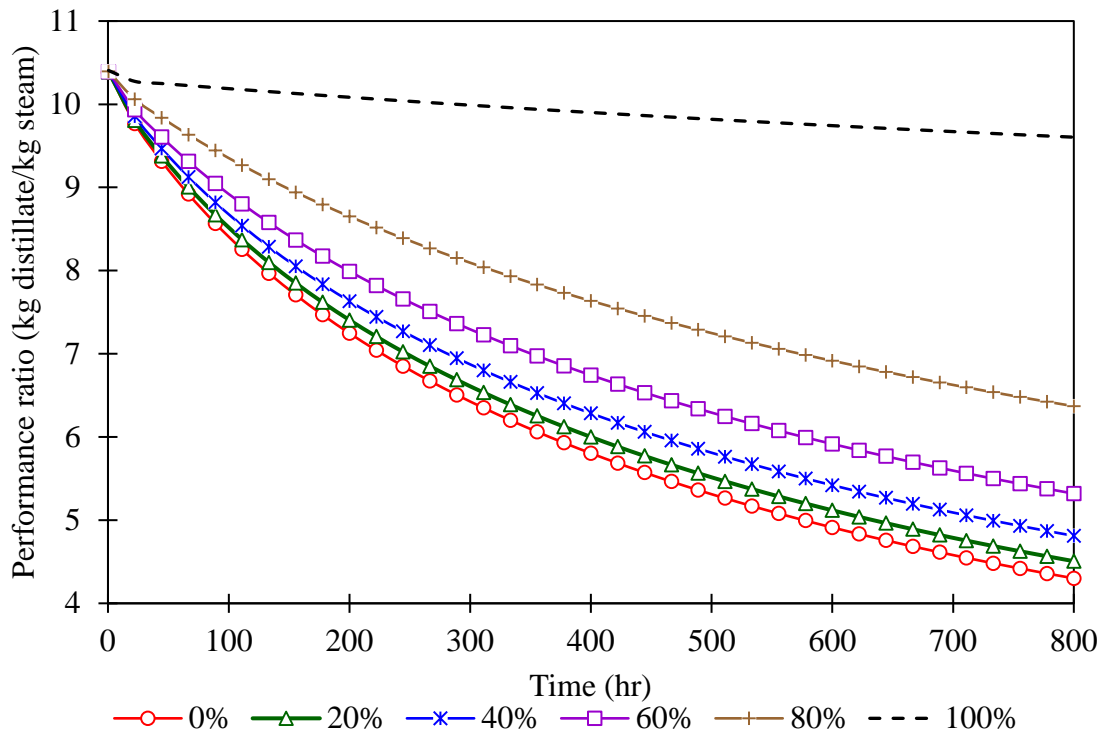
Figure 6.28: Effect of partial and full removal of divalent ions on the performance ratio

6.6 Conclusions

In this chapter, deposition of calcium carbonate and magnesium hydroxide scale on heated surface tubes of MSF process was studied through the use of a dynamic fouling model integrated into the MSF dynamic model. Brief description of the fouling phenomena was carried out to understand the fouling process in MSF plants. Very detailed review of the fouling models was conducted to obtain a suitable model that can be implemented in MSF plants. The fouling model of calcium carbonate was based on both diffusion and reaction mechanism. However, the deposition of magnesium hydroxide was modelled based on reaction mechanism only due to the lack of diffusion data. The results of the proposed model were in good agreement with most of the recent studies.

The MSF simulation model was carried out under very harsh conditions of TBT around 119 °C. However, to investigate the effect of temperature and velocity, different simulations were carried out at different TBT values and different volumetric flow. The results reveal that the potential of fouling increases with the increase in the stage temperature. Thus, it is important to operate MSF plants

between 90 ºC and 100 ºC to avoid rapid increase in fouling. Also, the results showed that the magnesium hydroxide deposition increased with the increase in the flow velocity due to the improvement of the heat transfer coefficient. However, calcium carbonate deposition decreased with the increase in the velocity. This was explained by the effect of the water salinity since another simulation carried out at constant salinity showed that the deposition of calcium carbonate increased with the increase in the velocity. However, the MSF plants should operate at a certain velocity to assure constant flow of the heat transfer to the brine inside the tubes.

Moreover, the results showed that the performance ratio of the plants deteriorated greatly due to the accumulation of foulants. The fouling process cannot be avoided and scheduled cleaning is required. The results showed that, with the use of mechanical and chemical cleaning, the performance ratio can be kept at a desired value. The results also showed that possible improvement of the plant performance and thus cost reduction can be achieved by partial removal of the foulants from the intake seawater using NF and RO or other similar technology

The simulation results from the proposed model show good agreement to the behaviour of the fouling in real plants and this can make remarkable contribution to the efforts to reduce the fouling and decrease the overestimated design fouling factor and hence, reduce the cost of extra surface area. Due to the difficulties of conducting experiments on real plants, most of the experimental studies have been carried by other researchers using small experiments or pilot devices. However, the complexity and nonlinearity of the MSF process due to the continuous change in the temperature and salinity makes such experiments ineffective in predicting the actual behaviour of the fouling. The only inexpensive available solution that can cope with the change of the temperature and salinity is by the means of simulation. The proposed model is capable of handling any range of data and process variables and can accurately predict the precipitation of calcium carbonate and magnesium hydroxide in heat exchanger surfaces.

CHAPTER SEVEN

Conclusions and Future Work

7.1 Conclusions

The rapid increase in the world's population and the scarcity of natural water resources have raised a major global challenge to overcome water crisis. In response to this increase, many countries are focusing on additional sources of water supply and increasing efforts to avoid water deficits in the near future. Although, it is considered as an expensive and last possible solution to providing fresh water, desalination technology has become the most important source of potable and industrial water for use in some world regions, especially the Middle East and North Africa. Among different types of desalinations techniques, the MSF desalting method is by far the most robust and reliable technology for the production of desalted water at large capacity despite its higher cost compared to other thermal desalination technologies. However, nowadays, the MSF process is facing challenges to cut the high cost of production and to improve the market shares (profitability). Therefore, better understand of the design and operation of MSF process through utilization of simulation and optimization tools can lead to reduction of the production cost and performance improvement.

In this work, the objectives were to (1) study the venting system design of MSF plant and the effect of the NCGs on the MSF performance and simulate the behaviour of these gases inside the flashing chambers, (2) design and implement advance control strategies that can handle a nonlinear system such as MSF and improve the efficiency of the plants, and (3) develop a dynamic fouling model that predict the crystallization of calcium carbonate and magnesium hydroxide inside the condenser tubes of the flashing stages. This work is motivated by the lack of studies on venting systems and fouling inside the tubes. The studies carried out in this project are new to the literature and increase the understanding of the behaviour of MSF process. Very detailed MSF mathematical model, fouling model and implementation of advance control can be further utilised to increase

the efficiency of the MSF process and cut production costs. However, to accomplish the above objectives, a detailed study has been carried out.

To begin with, a brief description of the water crisis and the need for desalination was presented to justify our choice of thermal desalination in general and MSF in particular. Moreover, the design and operation parameters of MSF process were also presented in detail to help understand their significance and impact on the overall performance.

In chapter two, a review of the literature studies on the detailed steady state and dynamic models was presented. The literature showed that these models have been improved over the years by relaxing more assumptions and increasing the accuracy of these models and making them more suitable for studying the behaviour of the MSF desalination plant. The chapter also included previous studies related to the NCGs and their effects on the MSF process. Moreover, previous studies on the implementation of control strategies on MSF plants and fouling models were also presented. Also, a list of useful tools that were used to help the operators to test the process on the computer before any attempt to be made on real plant were added.

In chapter three, a detailed dynamic model of MSF was developed based on the basic laws of mass balance, energy balance and heat transfer. The single stage was divided into four compartments (Brine pool, vapour space, distillate tray and condensing tubes) with interacting material and thermal streams. Unlike most of the previous studies, the main feature of this model was that the distillate tray was modelled differently where the distillate of the previous stage does not enter the next stage. Though involving the distillate stream from previous stage to the next stage has no effect on the material balance, it does have great effect on the energy balance. Thus, as in line with industrial practice, the distillate stream from each stage was withdrawn separately. Moreover, for the first time, the distillate and the saturated vapour were assumed not to be in equilibrium and thus their temperatures are different. Though, their temperatures are the same in the steady state, the difference can be observed when any disturbance is introduced to the process.

The model was supported by physical and thermodynamic properties of brine, distillate and water vapour. Temperature losses due to boiling elevation, non-

equilibrium allowance and temperature losses through demister were also included. Most of these correlations were nonlinear and independent on salinity and temperature. The gPROMS model builder 4.2 was used to solve the equations. The model simulation results were validated against actual plant data published in the literature and good agreement with these data was obtained. To test the applicability of the model to work at different conditions, the recycle brine flow rate and the intake seawater temperature were varied while the brine level and the performance ratio were monitored. The dynamic response of the model showed the model was stable and could work at different conditions.

In chapter four, the model developed in chapter three was used to study the design of venting system in MSF plant and the effect of NCGs on the OHTC. Mass flow rate of NCGs was introduced in the material balance equations of the model. Henry's law was used to estimate the equilibrium concentration of NCGs. The venting points were assumed to be installed in different stages to avoid the increase of NCGs. Due to high release of the NCGs in the first stage, the results revealed that it is essential to install venting point in the first stage. However, it was found that venting point installed in the third stage rather than in the second is very important and more efficient in terms of reducing energy losses and increasing performance ratio. In addition, a careful selection of the location of the venting point could minimise their number and thus increase the efficiency of the plant. Moreover, the results revealed that high concentration of NCGs heavily affect the OHTC. Thus, for better performance, it is essential to keep the NCGs concentration less than 0.05 (wt. %).

In chapter five, a generic model control system (GMC) was designed and implemented to the MSF process to control and track the set points of the two most important variables in the MSF plant; namely the output temperature of the brine heater (TBT) and the Brine Level (BL) in the last stage. To obtain different values for the TBT and BL set points, an optimization problem was developed and solved to obtain optimum TBT and BL values for four different seasons (winter, spring, summer and autumn). The GMC control was compared against the conventional PID controller. The results revealed that GMC controller performed better than the PID controller. Such results were expected due to the fact that GMC controller was built to control nonlinear systems while PID

controller can only handle linear systems. The good results of controlling MSF process using GMC control encouraged the development of another type of advanced control. The well-known Fuzzy control was used in conjunction with GMC control to develop a hybrid Fuzzy-GMC controller. By characterising the input fuzzy set into five Gaussian membership functions (for error) and three triangular membership functions (for change of error), the final control action can be obtained from the distribution of several possible membership output. The good membership output is, then, replaced by The GMC equation. In the case of tracking the set points, the results were superior against pure GMC control whether in the TBT loop or in the BL loop. In handling the disturbance of the TBT loop, the hybrid fuzzy-GMC was better than pure GMC controller. However, the pure GMC performed better than hybrid Fuzzy-GMC controller in handling the disturbance of the BL.

In chapter six, another important part of the thesis was presented. A fouling dynamic model was developed and presented to predict the crystallization of calcium carbonate and magnesium hydroxide inside the condensing tubes. The presented model was developed based on both diffusion and reaction mechanism of the seawater species. The model considered the deposit and removal rate of the fouling taking into account the effect of temperature, velocity and salinity of the seawater. Though there is large agreement among the researchers that the fouling increases with increase in the surface temperature of the tubes, there is little dispute about the effect of the velocity on the growth of fouling. The generated results, however, revealed that the effect of the velocity can be influenced by the level of the seawater salinity. Moreover, the results showed that though the crystallization of calcium carbonate and magnesium hydroxide increased with the increase in the velocity, the fouling in general decreased with the increase in the velocity. This was due to the effect of the removal rate at higher velocities. Also, the removal rate is directly proportional to the foulant layer and thus its effect on the fouling rate could be seen clearly with increase in the thickness of the fouling layer.

Though the cleaning process was not mathematically modelled here, the study highlighted the essential role that antiscalant can play in the cleaning of the condensing tubes surfaces of the MSF plants. The results showed that with the

use of antiscalant or other cleaning strategy, the performance of MSF plants can be maintained at the desirable rate over longer periods of operation.

7.2 Future Work

During the period of this project, several new ideas came up that need more exploration. Some are related to the improvement of MSF dynamic model whilst others require further investigation to reduce the cost of operating MSF plants. The following can be considered as good areas for future investigative work.

1. In all MSF models, changing the pressure of the venting system affect the mass flowrate of the outlet vapour and NCGs to the venting system but does not affect the pressure inside the stages. This is because the saturated pressure inside the stage is calculated based on the saturated vapour temperature in the vapour space. In industrial practice, decreasing the pressure of the venting system can create vacuum inside the stages and thus control the value of the stage pressure. From there, the mass flow rate of the vaporized water from the brine pool is calculated. This kind of modelling can be useful in (1) developing start-up and shutdown dynamic model of MSF, and (2) develop dynamic model for NCGs venting system.

   The former can help to determine and optimize the start-up and shutdown period of MSF plants. The latter can provide real picture to the mechanism of the venting system of NCGs and then more work can be done to improve this area in MSF process.

2. Fouling and scale is another serious problem that requires further investigations. Though the crystallization of magnesium hydroxide is a well known type of fouling in MSF plants, little attention has been paid to model its precipitation. Moreover, Shams El Din and Mohammed (1994) reported that part of fouling in MSF is made of silica and clay and not just chemical species. Thus, a model that consider mostly everything that may be expected to accumulate inside the MSF condensing tubes should be developed.

3. The results show that advanced control strategies worked well in controlling nonlinear MSF process. Thus, more work can be carried out to

use such advance control for MSF plants fault diagnosis. Fault diagnosis is very important part in industry and implementation of such technique can have great impact on the reduction of plant operation costs.

4. There are a number of studies in the literature on hybrid integration of a seawater RO unit with an MSF distiller (hybrid MSF/RO). Though, this can improve the performance of MSF and reduce the cost of desalted water, a different configuration can result in different cost reduction outcome. Hence, a superstructure study is required to optimize the best combination structure between RO and MSF unit.

5. Also, pairing MSF plant with a power plant is another way of reducing the cost. A dual purpose plant is the one that supplies heat for the MSF unit and produces electricity for distribution to the electrical grid. Although, this type of combination is considered to be more thermodynamically efficient and economically feasible than a single purpose power generation and water production plant, little information is available in the literature on such simulation studies. Thus, significant work can be done to improve this area.

6. Based on recent studies by (Tanvir and Mujtaba, 2007, Hawaidi and Mujtaba, 2011a, Hawaidi, 2013), it was observed that, for a fixed or variable freshwater demand, winter season require less number of stages than the summer. Therefore, if a plant is designed based on optimum number of stages required in summer, then a new way of designing MSF processes is possible to achieve. This idea requires more investigations to run MSF plant for long period by presenting a novel configuration of MSF process. The new configuration of the MSF process based on optimum number of stages required in summer allows the removal of some stages out of the process in winter for maintenance and operation schedule throughout the year without shutting the plant fully as other seasons require less number of stages.

7.3 Proposal of Novel MSF Configuration for Future Work

The typical configuration of MSF plants, whether MSF-OT or MSF-BR, is almost unchanged since first introduced in the 1950s. This is due to avoiding any risk of failure with new designs or configurations. However, with the availability of powerful computer software, it is possible to design new MSF configuration through simulation studies.

In recent years, several studies have focused on the development of new design of MSF for better performance and low cost. Mussati et al. (2003) presented different configuration of the MSF where the inlet and outlet of distillate, brine and the feed streams have been redesigned to minimize the total annual cost for a given water production. Al-Hamahmy et al. (2016) studied the effect of extracting part of the cooling brine from the water boxes and re-injected it directly to the flash chambers. The extracted part would not pass through the brine heater or high temperature stages and thus less surface area was required for the brine heater.

In MSF process, the production of vapour decreases with the decrease in the brine temperature across the stages. In the first few stages, where the temperature is high, the release of the vapour is higher than in the last stages where the temperature decreases. Thus, maintaining the flash chamber temperature as high as possible may result in higher production of vapour and consequently the water production.

A novel configuration of MSF is proposed for future work to allow the outlet brine from the brine heater to be distributed equally or proportionally to all stages in parallel. This can be done by two scenarios as shown in Figures 7.1 and 7.2. In Figure 7.1, the outlet brine is distributed for all stages so the flash chambers of the plant are connected in parallel while the cooling water tubes at the top are connected in series. This case will benefit from the elimination of the orifice between the stages and thus simple stage design with pipe in and pipe out can be manufactured. The second scenario is shown in Figure 7.2 where the outlet brine is distributed to number of sections and each section contains 3 stages. In

this case, the cooling water tubes for all stages are connected in series while the sections, which contain three flash chambers connected in series, are connected in parallel.

In the first scenario, all the stages will be at highest possible temperature while in the second scenario, every three stages will be at maximum allowable temperature and thus, more vapour production is expected from both scenario. Moreover, the brine discharge will be at higher temperature than the conventional MSF process and hence its energy can be recovered to heat the intake seawater or used elsewhere where extra heat is required. In addition to the expected increase in the reduction rate, the layout of the MSF plant can be configured better. In the conventional MSF plants, the layout of the stages is controlled by the brine flow direction resulting in a long 'train'. However, in these two scenarios, whether single stages or every three stages connected in parallel, the layout of the plant can be rearranged and thus plant area could be better utilised. This study is under investigation and the results will be presented in the near future.
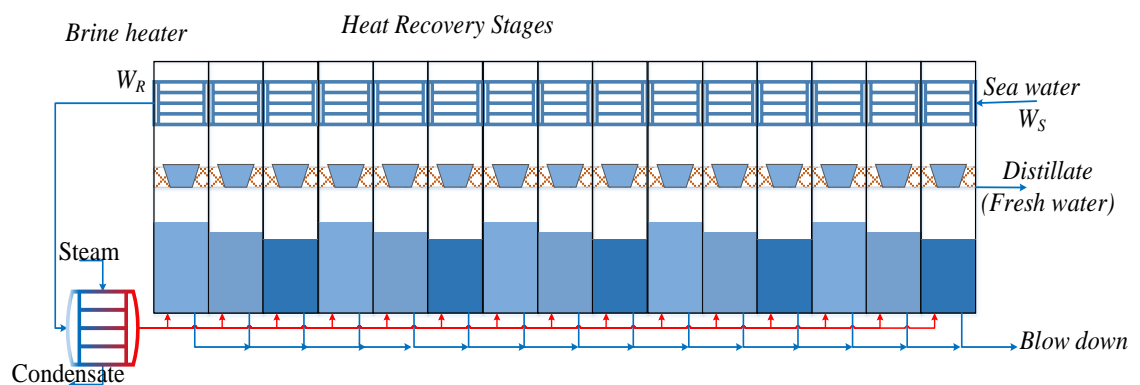
Figure 7.1: Single stage brine distributed
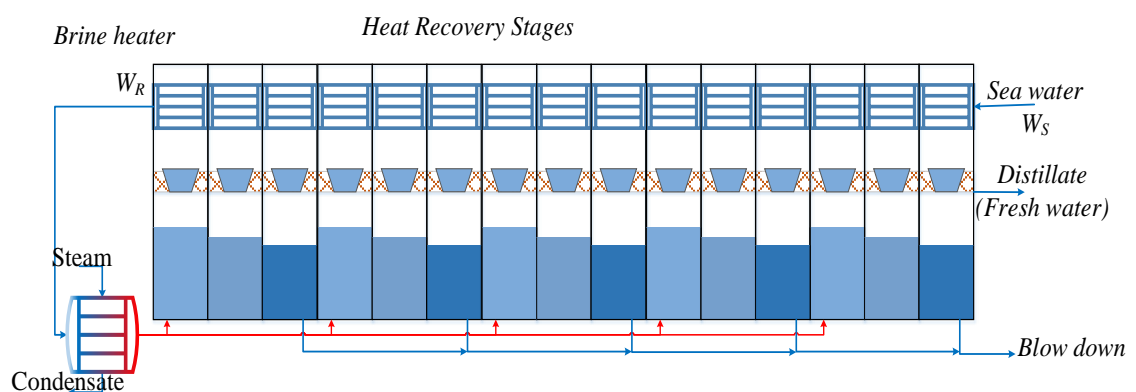
Figure 7.2: Single section brine distributed

<u>REFERENCES</u>

Abdel-Jabbar, N. M., Qiblawey, H. M., Mjalli, F. S. & Ettouney, H. 2007. Simulation of large capacity MSF brine circulation plants. *Desalination,* 204**,** 501-514.

Abdul-Wahab, S. A., Elkamel, A., Al-Weshahi, M. A. & Al Yahmadi, A. S. 2007. Troubleshooting the brine heater of the MSF plant using a fuzzy logic-based expert system. *Desalination,* 217**,** 100-117.

Abdul-Wahab, S. A., Reddy, K. V., Al-Weshahi, M. A., Al-Hatmi, S. & Tajeldin, Y. M. 2012. Development of a steady-state mathematical model for multistage flash (MSF) desalination plant. *International Journal of Energy Research,* 36**,** 710-723.

Abduljawad, M. & Ezzeghni, U. 2010. Optimization of Tajoura MSF desalination plant. *Desalination,* 254**,** 23-28.

Abufayed , A. A. & El-Ghuel, M. K. 2001. Desalination process applications in Libya. *Desalination,* 138**,** 47-53.

Addams, L., Boccaletti, G., Kerlin, M. & Stuchtey, M. 2009. Charting our water future: economic frameworks to inform decision-making. *McKinsey & Company, New York.*

Akbarzadeh, M. R., Kumbla, K. K., Jamshidi, M. & Al-Gobaisi, D. M. K. Evolutionary PID fuzzy control of MSF desalination processes. IDA World Congress on Desalination and Water Reuse, 6-9 October 1997 1997 Madrid, Spain. 35-46.

Al-Ahmad, M. & Aleem, F. A. 1994. Scale formation and fouling problems and their predicted reflection on the performance of desalination plants in Saudi Arabia. *Desalination,* 96**,** 409-419.

Al-Anezi, K. & Hilal, N. 2007. Scale formation in desalination plants: effect of carbon dioxide solubility. *Desalination,* 204**,** 385-402.

Al-Anezi, K., Johnson, D. J. & Hilal, N. 2008. An atomic force microscope study of calcium carbonate adhesion to desalination process equipment: effect of anti-scale agent. *Desalination,* 220**,** 359-370.

Al-bahou, M., Al-Rakaf, Z., Zaki, H. & Ettouney, H. 2007. Desalination experience in Kuwait. *Desalination,* 204**,** 403-415.

Al-Fulaij, H., Cipollina, A., Bogle, D. & Ettouney, H. 2010. Once t hrough m ultistage fl ash d esalination: gPROMS d ynamic and s teady s tate m odeling. *Desalination and Water Treatment,* 18**,** 46-60.

Al-Fulaij, H., Cipollina, A., Ettouney, H. & Bogle, D. 2011. Simulation of stability and dynamic multistage flash desalination. *Desalination,* 281**,** 404-412.

Al-Fulaij, H. F. 2011. *Dynamic modeling of multi stage flash (MSF) desalination plant.* PhD thesis, UCL (University College London).

Al-Gobaisi, D. M. K., Hassan, A., Rao, G. P., Sattar, A., Woldai, A. & Borsani, R. 1994. Towards improved automation for desalination processes, Part I: Advanced control. *Desalination,* 97**,** 469-506.

Al-Hamahmy, M., Fath, H. E. S. & Khanafer, K. 2016. Techno-economical simulation and study of a novel MSF desalination process. *Desalination,* 386**,** 1-12.

Al-Hengari, S., El-Bousiffi, M. & El-Moudir, W. 2007. Libyan Petroleum Institute experience in evaluation ofdesalination plants in the Libyan oil sector. *Desalination,* 206**,** 633-652.

Al-Hengari, S., El-Bousiffi, M. & El-Mudir, W. 2005. Performance analysis of a MSF desalination unit. *Desalination,* 182**,** 73-85.

Al-Karaghouli , A. A. & Kazmerski, L. L. 2011. Renewable Energy Opportunities in Water Desalination. Colorado: National Renewable Energy Laboratory.

Al-Mutaz, I. S., Al-Mojjly, A. A. & Abashar, M. E. Thermal and brine dispersion from coastal MSF desalination plants. 2006 Antalya. MWWD-IEMES.

Al-Mutaz, I. S. & Al-Namlah, A. M. 2004. Characteristics of dual purpose MSF desalination plants. *Desalination,* 166**,** 287-294.

Al-Mutaz, I. S. & Soliman, M. A. 1989. Simulation of MSF desalination plants. *Desalination,* 74**,** 317-326.

Al-Rawajfeh, A. E. 2008. Simultaneous desorption–crystallization of CO_2–$CaCO_3$ in multi-stage flash (MSF) distillers. *Chemical Engineering and Processing: Process Intensification,* 47, 2262-2269.

Al-Rawajfeh, A. E., Al-Garalleh, M., Al-Mazaideh, G., Al-Rawashdeh, B. a. & Khalil, S. 2008. Understanding CaCO3-Mg (OH) 2 scale formation: a semi-empirical mindo-forces study of CO2-H2O system. *Chemical Engineering Communications,* 195, 998-1010.

Al-Rawajfeh, A. E., Fath, H. E. S. & Mabrouk, A. A. 2012. Integrated salts precipitation and nano-filtration as pretreatment of multistage flash desalination system. *Heat Transfer Engineering,* 33, 272-279.

Al-Rawajfeh, A. E., Glade, H. & Ulrich, J. 2003. CO, release in multiple-effect distillers controlled by mass transfer with chemical reaction. *Desalination,* 156, 109-123.

Al-Rawajfeh, A. E., Glade, H. & Ulrich, J. 2005. Scaling in multiple-effect distillers: the role of CO 2 release. *Desalination,* 182, 209-219.

Al-Rawajfeh, A. E., Ihm, S., Varshney, H. & Mabrouk, A. N. 2014. Scale formation model for high top brine temperature multi-stage flash (MSF) desalination plants. *Desalination,* 350, 53-60.

Al-Sahali, M. & Ettouney, H. 2007. Developments in thermal desalination processes: Design, energy, and costing aspects. *Desalination,* 214, 227-240.

Al-Shayji, K. A. 1998. *Modeling, simulation, and optimization of large-scale commercial desalination plants.* PhD Thesis, Virginia Polytechnic Institute and State University.

Al-shayji, K. A., Al-wadyei, S. & Elkamel, A. 2005. Modelling and optimization of a multistage flash desalination process. *Engineering Optimization,* 37, 591-607.

Al-Sofi, M. A.-K. 1999. Fouling phenomena in multi stage flash (MSF) distillers. *Desalination,* 126, 61-76.

Alasfour, F. N. & Abdulrahim, H. K. 2009. Rigorous steady state modeling of MSF-BR desalination system. *Desalination and Water Treatment,* 1**,** 259-276.

Alatiqi, I., Ettouney, H. & El-Dessouky, H. 1999. Process control in water desalination industry: an overview. *Desalination,* 126**,** 15-32.

Alatiqi, I., Ettouney, H., El-Dessouky, H. & Al-Hajri, K. 2004. Measurements of dynamic behavior of a multistage flash water desalination system. *Desalination,* 160**,** 233-251.

Algobaisi, D. M. K., Barakzai, A. S. & Elnashar, A. M. 1991. An overview of modern control strategies for optimizing thermal desalination plants. *Desalination,* 84**,** 3-43.

Ali, E., Alhumaizi, K. & Ajbar, A. 1999. Model reduction and robust control of multi-stage flash (MSF) desalination plants. *Desalination,* 121**,** 65-85.

Ali, J. M., Hoang, N. H., Hussain, M. A. & Dochain, D. 2015. Review and classification of recent observers applied in chemical process systems. *Computers & Chemical Engineering,* 76**,** 27-41.

Altaee, A. & Sharif, A. 2015a. A conceptual NF/RO arrangement design in the pressure vessel for seawater desalination. *Desalination and Water Treatment,* 54**,** 624-636.

Altaee, A. & Sharif, A. 2015b. Performance of Enhanced Forward Osmosis-Reverse Osmosis system Comparing with Conventional Reverse Osmosis System. *Water Efficiency Conference.* Exeter UK.

Altaee, A. & Sharif, A. 2015c. Pressure retarded osmosis: advancement in the process applications for power generation and desalination. *Desalination,* 356**,** 31-46.

AlTaee, A. & Sharif, A. O. 2011. Alternative design to dual stage NF seawater desalination using high rejection brackish water membranes. *Desalination,* 273**,** 391-397.

Aly, N. H. & El-Figi, A. K. 2003. Thermal performance of seawater desalination systems. *Desalination,* 158**,** 127-142.

Aly, N. H. & Marwan, M. A. 1995. Dynamic behavior of MSF desalination plants. *Desalination,* 101**,** 287-293.

Aly, S. E. & Fathalah, K. A mathematical model of a MSF system. In IDA World Congress, 1995 1995. 203-226.

Andritsos, N. 1996. Calcium carbonate deposit formation under isothermal conditions. *Canadian journal of chemical engineering,* 74**,** 911-919.

Arpornwichanop, A., Kittisupakorn, P. & Mujtaba, I. M. 2005. On-line dynamic optimization and control strategy for improving the performance of batch reactors. *Chemical Engineering and Processing: Process Intensification,* 44**,** 101-114.

Augustin, W. & Bohnet, M. 1995. Influence of the ratio of free hydrogen ions on crystallization fouling. *Chemical Engineering and Processing: Process Intensification,* 34**,** 79-85.

Awad, M. M. 2011. *Fouling of heat transfer surfaces*, INTECH Open Access Publisher.

Aziz, N., Hussain, M. A. & Mujtaba, I. M. 2000. Performance of different types of controllers in tracking optimal temperature profiles in batch reactors. *Computers & Chemical Engineering,* 24**,** 1069-1075.

Baig, H., Antar, M. A. & Zubair, S. M. 2011. Performance evaluation of a once-through multi-stage flash distillation system: Impact of brine heater fouling. *Energy Conversion and Management,* 52**,** 1414-1425.

Bandyopadhyay, S. S., Biswas, A. K., Bhattacharyya, D. & Ray, A. K. 2005. *Advances in Separation Processes,* New Delhi, Allied Publisher.

Bansal, B., MÜller-Steinhagen, H. & Chen, X. D. 2001. Comparison of crystallization fouling in plate and double-pipe heat exchangers. *Heat Transfer Engineering,* 22**,** 13-25.

Barba, D., Linzzo, G. & Tagliferri, G. Mathematical model for multiflash desalting plant control. 4th Int. Symp. on Fresh Water from the Sea, Heidelberg, 1973 1973. 153-168.

Bassett, L. & Brinkman, J. T. 2000. *Earth and faith: a book of reflection for action*, UNEP/Earthprint.

Beamer, J. H. & Wilde, D. J. 1971. The simulation and optimization of a single effect multi-stage flash desalination plant. *Desalination,* 9**,** 259-275.

Bennett, A. 2013. 50 th Anniversary: Desalination: 50 years of progress. *Filtration+ Separation,* 50**,** 32-39.

Bodalal, A. S., Abdul_Mounem, S. A. & Salama, H. S. 2010. Dynamic modeling and simulation of MSF desalination plants. *JJMIE,* 4.

Bohnet, M. 1987. Fouling of heat transfer surfaces. *Chemical engineering & technology,* 10**,** 113-125.

Bohnet, M. W. 2005. Crystallization fouling on heat transfer surfaces–25 years research in Braunschweig.

Borsani, R. & Rebagliati, S. 2005. Fundamentals and costing of MSF desalination plants and comparison with other technologies. *Desalination,* 182**,** 29-37.

Boxer, B. & Salah, M. M. 2010. Mediterranean Sea. *Encyclopædia Britannica.* Encyclopædia Britannica, inc. .

Brahim, F., Augustin, W. & Bohnet, M. 2003. Numerical simulation of the fouling process. *International Journal of Thermal Sciences,* 42**,** 323-334.

Bremere, I., Kennedy, M., Stikker, A. & Schippers, J. 2001. How water scarcity will effect the growth in the desalination market in the coming 25 years. *Desalination,* 138**,** 7-15.

Bruggen, B. V. d. & Vandecasteele, C. 2002. Distillation vs. membrane filtration: overview of process evolutions in seawater desalination. *Desalination,* 143**,** 207-218.

Buros, O. K. 2000. *The ABCs of desalting*, International Desalination Association Topsfield, MA.

Calì, G., Fois, E., Lallai, A. & Mura, G. 2008. Optimal design of a hybrid RO/MSF desalination system in a non-OPEC country. *Desalination,* 228**,** 114-127.

Carroll, J. J., Slupsky, J. D. & Mather, A. E. 1991. The solubility of Carbon Dioxide in Water at Low Pressure. *J. Phys. Chem. Ref. Data,* 20**,** 1201-1209.

Coleman, A. K. 1971. Optimization of a single effect, multi-stage flash distillation desalination system. *Desalination,* 9**,** 315-331.

Cooley, H., Gleick, P. H. & Wolff, G. 2006. Desalination: with a Grain of Salt. *Pacific Institute. June.*

Cooper, K. G., Hanlon, L. G., Smart, G. M. & Talbot, R. E. 1983. A model for the fouling of MSF plants based on data from operating units. *Desalination,* 47**,** 37-42.

Cott, B. J. & Macchietto, S. 1989. Temperature control of exothermic batch reactors using generic model control. *Industrial & Engineering Chemistry Research,* 28**,** 1177-1184.

Darwish, M. A. 1991. Thermal analysis of multi-stage flash desalting systems. *Desalination,* 85**,** 59-79.

Darwish, M. A. & Abdulrahim, H. K. 2008. Feed water arrangements in a multi-effect desalting system. *Desalination,* 228**,** 30-54.

Darwish, M. A. & Alsairafi, A. 2004. Technical comparison between TVC/MEB and MSF. *Desalination,* 170**,** 223-239.

Darwish, M. A., El-Refaee, M. M. & Abdel-Jawad, M. 1995. Developments in the multi-stage flash desalting system. *Desalination,* 100**,** 35-64.

David, I., Bogle, L., Cipollina, A. & Micale, G. 2007. Dynamic modeling tools for solar powered desalination process during transient operations. *Solar Desalination for the 21st Century.* Springer.

De Gunzbourg, J. & Larger, D. 1999. Cogeneration applied to very high efficiency thermal seawater desalination plants. *Desalination,* 125**,** 203-208.

Delene, J. G. & Ball, S. J. 1971. Digital computer code for simulating large multistage flash evaporator desaling plant dynamics Oak Ridge National Lab., Tenn.

Dooly, R. & Glater, J. 1972. Alkaline scale formation in boiling sea water brines. *Desalination,* 11**,** 1-16.

DU, X., YU, P. & LUO, D. 2013. Generic Model Control of Dissolved Oxygen Concentration in Sewage System. *Journal of Computational Information Systems,* 9**,** 6.

Eid Al-Rawajfeh, A. 2007. Modeling of alkaline scale formation in falling film horizontal-tube multiple-effect distillers. *Desalination,* 205**,** 124-139.

Ekpo, E. E. & Mujtaba, I. M. 2008. Evaluation of neural networks-based controllers in batch polymerisation of methyl methacrylate. *Neurocomputing,* 71**,** 1401-1412.

El-Dessouky, H., Alatiqi, I. & Ettouney, H. 1998. Process synthesis: the multi-stage flash desalination system. *Desalination,* 115**,** 155-179.

El-Dessouky, H. & Bingulac, S. 1996. Solving equations simulating the steady-state behavior of the multi-stage flash desalination process. *Desalination,* 107**,** 171-193.

El-Dessouky, H., Shaban, H. I. & Al-Ramadan, H. 1995. Steady-state analysis of multi-stage flash desalination process. *Desalination,* 103**,** 271-287.

El-Dessouky, H. T. & Ettouney, H. M. 2002. *Fundamentals of salt water desalination,* Amesterdam, Elsevier Science.

El-Dessouky, H. T., Ettouney, H. M. & Al-Roumi, Y. 1999. Multi-stage flash desalination: present and future outlook. *Chemical Engineering Journal,* 73**,** 173-190.

El-Dessouky, H. T. & Khalifa, T. A. 1985. Scale formation and its effect on the performance of once through MSF plant. *Desalination,* 55**,** 199-217.

El-Mudir, W., El-Bousiffi, M. & Al-Hengari, S. 2004. Performance evaluation of a small size TVC desalination plant. *Desalination,* 165**,** 269-279.

El Din, A. M. S., El-Dahshan, M. E. & Mohammed, R. A. 2002. Inhibition of the thermal decomposition of HCO 3− A novel approach to the problem of alkaline scale formation in seawater desalination plants. *Desalination,* 142**,** 151-159.

El Din, A. M. S. & Mohammed, R. A. 1989. The problem of alkaline scale formation from a study on Arabian Gulf water. *Desalination,* 71**,** 313-324.

Elhassadi, A. 2008. Horizons and future of water desalination in Libya. *Desalination,* 220**,** 115-122.

ElMoudir, W., ElBousiffi, M. & Al-Hengari, S. 2008. Process modelling in desalination plant operations. *Desalination,* 222**,** 431-440.

Energy, U. R. 2012. Water Desalination Using Renewable Energy.

Ettouney, H. M., El-Dessouky, H. T., Faibish, R. S. & Gowin, P. Economics of thermal and membrane desalination processes. 2002. Chem. Engng Prog.

Fahiminia, F., Watkinson, A. P. & Epstein, N. 2007. Early events in the precipitation fouling of calcium sulphate dihydrate under sensible heating conditions. *The Canadian Journal of Chemical Engineering,* 85**,** 679-691.

Falcetta, M. F. & Sciubba, E. 1999. Transient simulation of a real multi-stage flashing desalination process. *Desalination,* 122**,** 263-269.

Fiorenza, G., Sharma, V. K. & Braccio, G. 2003. Techno-economic evaluation of a solar powered water desalination plant. *Energy Conversion and Management,* 44**,** 2217-2240.

Fiorini, P. & Sciubba, E. 2005. Thermoeconomic analysis of a MSF desalination plant. *Desalination,* 182**,** 39-51.

Freyer, D. & Voigt, W. 2003. Crystallization and phase stability of CaSO4 and CaSO4–based salts. *Monatshefte für Chemie/Chemical Monthly,* 134**,** 693-719.

Fritzmann, C., Löwenberg, J., Wintgens, T. & Melin, T. 2007. State-of-the-art of reverse osmosis desalination. *Desalination,* 216**,** 1-76.

Fry, A. & Martin, R. 2005. Water facts and trends. *World Business Council for Sustainable Development,* 16.

Fu, Y. & Liu, X. 2015. Nonlinear dynamic behaviors and control based on simulation of high-purity heat integrated air separation column. *ISA transactions,* 55**,** 145-153.

Furuki, A., Hamanaka, K., Tatsumoto, M. & Inohara, S. 1985. Automatic control system of MSF process (ACSODE®). *Desalination,* 55**,** 77-89.

Gambier, A. & Badreddin, E. 2004. Dynamic modelling of MSF plants for automatic control and simulation purposes: a survey. *Desalination,* 166**,** 191-204.

Gambier, A., Fertig, M. & Badreddin, E. Hybrid modelling for supervisory control purposes for the brine heater of a multi stage flash desalination plant. Proceedings of the American Control Conference, 2002 2002 Anchorage. 5060-5065.

Garcia-Rodriguez, L. 2003. Renewable energy applications in desalination: state of the art. *Solar Energy,* 75**,** 381-393.

Gazit, E. & Hasson, D. 1975. Scale deposition from an evaporating falling film. *Desalination,* 17**,** 339-351.

Genthner, K., Gregorzewski, A. & Seifert, A. 1993. The effects and limitations issued by non-condensible gases in sea water distillers. *Desalination,* 93**,** 207-234.

Genthner, K. & Seifert, A. 1991. A calculation method for condensers in multi-stage evaporators with non-condensable gases. *Desalination,* 81**,** 349-366.

Ghaffour, N., Missimer, T. M. & Amy, G. L. 2013. Technical review and evaluation of the economics of water desalination: Current and future challenges for better water supply sustainability. *Desalination,* 309**,** 197-207.

Ghasem, N. M., Hussain, M. A. & Mujtaba, I. M. 2003. Control of the Industrial Gas Phase Polyethylene Fluidized Bed Reactor Using Generic Model Control (GMC). *Advances in Petrochemicals and Polymers in the New Millennium.* Thailand.

Gill, J. S. 1999. A novel inhibitor for scale control in water desalination. *Desalination,* 124**,** 43-50.

Glade, H. & Al-Rawajfeh, A. E. 2008. Modeling of CO2 release and the carbonate system in multiple-effect distillers. *Desalination,* 222**,** 605-625.

Glade, H., Meyer, J.-H. & Will, S. 2005. The release of CO 2 in MSF and ME distillers and its use for the recarbonation of the distillate: a comparison. *Desalination,* 182**,** 99-110.

Glade, H. & Ulrich, J. 2003. Influence of solution composition on the formation of crystalline scales. *Chemical engineering & technology,* 26**,** 277-281.

Glueck, A. R. & Bradshaw, R. W. A mathematical model for a multistage flash distillation plant. Proc. 3rd Int. Symp. on Fresh Water from the Sea, 1970 1970. 95-108.

Greenleea, L. F., Lawler, D. F., Freeman, B. D., Marrot, B. & Moulin, P. 2009. Reverse osmosis desalination: Water sources, technology, and today's challenges. *Desalination,* 43**,** 2317-2348.

Hamed, O. A. 2005a. Overview of hybrid desalination systems—current status and future prospects. *Desalination,* 186**,** 207-214.

Hamed, O. A. 2005b. Overview of hybrid desalination systems — current status and future prospects. *Desalination,* 186**,** 207-214.

Hamed, O. A. & Al-Otaibi, H. A. 2010. Prospects of operation of MSF desalination plants at high TBT and low antiscalant dosing rate. *Desalination,* 256**,** 181-189.

Hamed, O. A., Al-Sofi, M. A. K., Imam, M., Mustafa, G. M., Bamardouf, K. & Al-Washmi, H. 2001. Simulation of multistage flash desalination process. *Desalination,* 134**,** 195-203.

Hamed, O. A., Al-Sofi, M. A. K., Imam, M., Mustafa, G. M., Mardouf, K. B. & Al-Washmi, H. 2000. Thermal performance of multi-stage flash distillation plants in Saudi Arabia. *Desalination,* 128**,** 281-292.

Hamed, O. A., Al-Sofi, M. A. K., Mustafa, G. M. & Dalvi, A. G. 1999. The performance of different anti-scalants in multi-stage flash distillers. *Desalination,* 123**,** 185-194.

Hamed, O. A., Al-Sofi, M. A. K., Mustafa, G. M., Imam, M., Ba-Mardouf, K. & Al-Washmi, H. Modeling and simulation of multistage flash distillation process. Proceedings of the 4th SWCC Acquired Experience Conference, Riyadh, 2004.

Hamed, O. A., Al-Washmi, H. A. & Al-Otaibi, H. A. 2006. Thermoeconomic analysis of a power/water cogeneration plant. *Energy,* 31**,** 2699-2709.

Hamed, O. A., Hassan, A. M., Al-Shail, K. & Farooque, M. A. 2009. Performance analysis of a trihybrid NF/RO/MSF desalination plant. *Desalination and Water Treatment,* 1**,** 215-222.

Hasson, D., Avriel, M., Resnick, W., Rozenman, T. & Windreich, S. 1968. Mechanism of calcium carbonate scale deposition on heat-transfer surfaces. *Industrial & Engineering Chemistry Fundamentals,* 7**,** 59-65.

Hasson, D., Sherman, H. & Biton, M. 1978. Prediction of Calcium Carbonate Scaling Rates. Proceedings of 6th International Symposium Fresh Water from the Sea, 1978. 193-199.

Hawaidi, E. A. & Mujtaba, I. M. Sensitivity of brine heater fouling on optimization of operation parameters of MSF desalination process using PROMS. In the 20th European Symposium on Computer Aided Chemical Engineering-ESCAPE20, 2010a. 1787-1792.

Hawaidi, E. A. & Mujtaba, I. M. 2011a. Freshwater production by MSF desalination process: Coping with variable demand by flexible design and operation. *Comput. Aided Chem. Eng,* 29**,** 1180-1184.

Hawaidi, E. A. M. 2013. *Simulation, optimisation and flexible scheduling of MSF desalination process under fouling.* PhD thesis, University of Bradford.

Hawaidi, E. A. M. & Mujtaba, I. M. 2010b. Simulation and optimization of MSF desalination process for fixed freshwater demand: Impact of brine heater fouling. *Chemical Engineering Journal,* 165**,** 545-553.

Hawaidi, E. A. M. & Mujtaba, I. M. 2011b. Meeting Variable Freshwater Demand by Flexible Design and Operation of the Multistage Flash Desalination Process. *Industrial & Engineering Chemistry Research,* 50**,** 10604-10614.

Helal, A. M. 2003. Uprating of Umm Al Nar East 4–6 MSF desalination plants. *Desalination,* 159**,** 43-60.

Helal, A. M. 2004. Once-through and brine recirculation MSF design - a comparative study. *Desalination,* 171**,** 33-60.

Helal, A. M. 2005. Once-through and brine recirculation MSF designs—a comparative study. *Desalination,* 171**,** 33-60.

Helal, A. M., Al-Jafri, A. & Al-Yafeai, A. 2012. Enhancement of existing MSF plant productivity through design modification and change of operating conditions. *Desalination,* 307**,** 76-86.

Helal, A. M., El-Nashar, A. M., Al-Katheeri, E. & Al-Malek, S. 2003. Optimal design of hybrid RO/MSF desalination plants Part I: Modeling and algorithms. *Desalination,* 154**,** 43-66.

Helal, A. M., El-Nashar, A. M., Al-Katheeri, E. S. & Al-Malek, S. A. 2004a. Optimal design of hybrid RO/MSF desalination plants Part II: Results and discussion. *Desalination,* 160**,** 13-27.

Helal, A. M., El-Nashar, A. M., Al-Katheeri, E. S. & Al-Maler, S. A. 2004b. Optimal design of hybrid RO/MSF desalination plants Part III: Sensitivity analysis. *Desalination,* 169**,** 43-60.

Helal, A. M., Medani, M. S., Soliman, M. A. & Flower, J. R. 1986. A tridiagonal matrix model for multistage flash desalination plants. *Computers & chemical engineering,* 10**,** 327-342.

Helal, A. M. & Odeh, M. 2004. The once-through MSF design. Feasibility for future large capacity desalination plants. *Desalination,* 166**,** 25-39.

Helalizadeh, A., Müller-Steinhagen, H. & Jamialahmadi, M. 2000. Mixed salt crystallisation fouling. *Chemical Engineering and Processing: Process Intensification,* 39**,** 29-43.

Helalizadeh, A., Müller-Steinhagen, H. & Jamialahmadi, M. 2005. Mathematical modelling of mixed salt precipitation during convective heat transfer and sub-cooled flow boiling. *Chemical engineering science,* 60**,** 5078-5088.

Hinrichsen, D., Robey, B. & Upadhyay, U. D. 1998. Solutions for a water-short world. *Population Reports. Series M: Special Topics***,** 1-31.

Höfling, V., Augustin, W. & Bohnet, M. 2003. Crystallization fouling of the aqueous two-component system CaSO 4/CaCO 3.

Husain, A., Hassan, A., Al-Gobaisi, D. M. K., Al-Radif, A., Woldai, A. & Sommariva, C. 1993. Modelling, simulation, optimization and control of multistage flashing (MSF) desalination plants Part I: Modelling and simulation. *Desalination,* 92**,** 21-41.

Husain, A., Woldai, A., Alradif, A., Kesou, A., Borsani, R., Sultan, H. & Deshpandey, P. B. 1994. Modeling and simulation of a multistage flash (MSF) desalination plant. *Desalination,* 97**,** 555-586.

Hyflux. 2013. Water for All: Conserve, Value, Enjoy. Available: http://hyflux.listedcompany.com/newsroom/20130918_190104_600_614 7CE41D66B86FA48257BE900286DFC.1.pdf.

Ismail, A. 1998. Fuzzy model reference learning control of multi-stage flash desalination plants. *Desalination,* 116**,** 157-164.

Ismail, A. & AbuKhousa, E. Fuzzy TBT control of multi-stage flash desalination plants. Proceedings of the 1996 IEEE International Conference on Control Applications, September 15-18 1996 New York. 241-246.

Jamshidi, M., AkbarzadehT, M. R. & Kumbla, K. 1996. *Design and implementation of fuzzy controllers for complex systems - Case study: A water desalination plant,* 64849 Monterrey N L, Instituto Tecnologico Y Estudios Superiores Monterry.

Kamesh, R., Reddy, P. S. & Rani, K. Y. 2014. Comparative Study of Different Cascade Control Configurations for a Multiproduct Semibatch Polymerization Reactor. *Industrial & Engineering Chemistry Research,* 53**,** 14735-14754.

Karacan, S., Hapoğlu, H. & Alpbaz, M. 2007. Multivariable system identification and generic model control of a laboratory scale packed distillation column. *Applied Thermal Engineering,* 27**,** 1017-1028.

Karagiannis, I. C. & Soldatos, P. G. 2008. Water desalination cost literature: review and assessment. *Desalination,* 223**,** 448-456.

Kathel, P. & Jana, A. K. 2010. Dynamic simulation and nonlinear control of a rigorous batch reactive distillation. *ISA Trans,* 49**,** 130-7.

Kazi, S. N. 2012. *Fouling and fouling mitigation on heat exchanger surfaces*, INTECH Open Access Publisher.

Kern, D. Q. & Seaton, R. E. 1959. Surface fouling: how to calculate limits. *Chem. Eng. Prog,* 55**,** 71-73.

Kershman, S. A. 2001. 25 years of experience in operating thermal desalination plants. *Desalination,* 136**,** 141-145.

Khawaji, A. D., Kutubkhanah, I. K. & Wie, J.-M. 2008. Advances in seawater desalination technologies. *Desalination,* 221**,** 47-69.

Kuwairi, A. Water mining: the great man-made river, Libya. Proceedings of the Institution of Civil Engineers-Civil Engineering, 2006 2006. Thomas Telford Ltd, 39-43.

Lee, P. L. & Sullivan, G. R. 1988. Generic model control (GMC). *Computers & Chemical Engineering,* 12**,** 573-580.

Li, D., Yang, N., Niu, R., Qiu, H. & Xi, Y. 2012. FPGA based QDMC control for reverse-osmosis water desalination system. *Desalination,* 285**,** 83-90.

Lior, N., El-Nashar, A. & Sommariva, C. 2012. Advanced Instrumentation, Measurement, Control, and Automation (IMCA) in Multistage Flash (MSF) and Reverse-Osmosis (RO) Water Desalination. *Advances in Water Desalination***,** 453-658.

Loeb, S. & Sourirajan, S. 1963. Sea Water Deminaralization by Means of an Osmotic Membrane. *Advances in Chemistry Series,* 38**,** 117-132.

Mabrouk, A.-N. A. 2013. Techno-economic analysis of tube bundle orientation for high capacity brine recycle MSF desalination plants. *Desalination,* 320**,** 24-32.

Malayeri, M. R. & Müller-Steinhagen, H. 2007. An overview of fouling mechanisms, prediction and mitigation strategies for thermal desalination plants. Citeseer.

Mandil, M. A. & Ghafour, E. E. A. 1970. Optimization of multi-stage flash evaporation plants. *Chemical Engineering Science,* 25**,** 611-621.

Maniar, V. M. & Deshpande, P. B. 1996. Advanced controls for multi-stage flash (MSF) desalination plant optimization. *Journal of process control,* 6**,** 49-66.

Marcovecchio, M., Mussati, S., Scenna, N. & Aguirre, P. 2009. Hybrid Desalination Systems: Alternative Designs of Thermal and Membrane Processes. *Computer Aided Chemical Engineering,* 27**,** 1011-1016.

Marcovecchio, M. G., Mussati, S. F., Aguirre, P. A. & Nicolás, J. 2005. Optimization of hybrid desalination processes including multi stage flash and reverse osmosis systems. *Desalination,* 182**,** 111-122.

Marshall, W. L. & Slusher, R. 1968. Aqueous systems at high temperature. Solubility to 200. degree. of calcium sulfate and its hydrates in sea water and saline water concentrates, and temperature-concentration limits. *Journal of Chemical & Engineering Data,* 13**,** 83-93.

Mayere, A. 2011. Solar powered desalination.

Mazzotti, M., Rosso, M., Beltramini, A. & Morbidelli, M. 2000. Dynamic modeling of multistage flash desalination plants. *Desalination,* 127**,** 207-218.

Miller, S., Shemer, H. & Semiat, R. 2015. Energy and environmental issues in desalination. *Desalination,* 366**,** 2-8.

Misdan, N., Lau, W. J. & Ismail, A. F. 2012. Seawater Reverse Osmosis (SWRO) desalination by thin-film composite membrane—Current development, challenges and future prospects. *Desalination,* 287**,** 228-237.

Morton, A. J., Callister, I. K. & Wade, N. M. 1996. Environmental impacts of seawater distillation and reverse osmosis processes. *Desalination,* 108**,** 1-10.

Mubarak, A. 1998. A kinetic model for scale formation in MSF desalination plants. Effect of antiscalants. *Desalination,* 120**,** 33-39.

Mucci, A. 1983. The solubility of calcite and aragonite in seawater at various salinities and temperatures, and one atmosphere total pressure. *American Journal of Science,* 283**,** 780-799.

Mujtaba, I. M. 2008. Keynote Lecture. *CAPE FORUM.* Thessaloniki, Greece.

Mujtaba, I. M. 2010. Modeling Multistage Flash Desalination Process–Current Status and Future Development. *In:* GEORGIADIS, M. C., BANGA, J. R.

& PISTIKOPOULOS, E. N. (eds.) *Process Systems Engineering: Dynamic Process Modeling, Volume 7.* Weinheim, Germany: Wiley Online Library.

Mujtaba, I. M., Aziz, N. & Hussain, M. A. 2006. Neural Network Based Modelling and Control in Batch Reactor. *Chemical Engineering Research and Design,* 84**,** 635-644.

Müller-Steinhagen, H. M. & Branch, C. A. 1988. Influence of thermal boundary conditions on calcium carbonate fouling in double pipe heat exchangers: Einfluβ der thermischen Randbedingungen auf die Ablagerung von CaCO3 in Doppelrohrwärmeübertragern. *Chemical Engineering and Processing: Process Intensification,* 24**,** 65-73.

Mussati, S. F., Aguirre, P. A. & Scenna, N. J. 2003. Novel configuration for a multistage flash-mixer desalination system. *Industrial & engineering chemistry research,* 42**,** 4828-4839.

Mussati, S. F., Aguirre, P. A. & Scenna, N. J. 2004. Improving the efficiency of the MSF once through (MSF-OT) and MSF-mixer (MSF-M) evaporators. *Desalination,* 166**,** 141-151.

Mwaba, M. G., Golriz, M. R. & Gu, J. 2006. A semi-empirical correlation for crystallization fouling on heat exchange surfaces. *Applied Thermal Engineering,* 26**,** 440-447.

Myasnikov, S. K., Chipryakova, A. P. & Kulov, N. N. 2013. Kinetics, energy characteristics, and intensification of crystallization processes in chemical precipitation of hardness ions. *Theoretical Foundations of Chemical Engineering,* 47**,** 505-523.

Najibi, S. H., Müller-Steinhagen, H. & Jamialahmadi, M. 1997. Calcium sulphate scale formation during subcooled flow boiling. *Chemical Engineering Science,* 52**,** 1265-1284.

Olafsson, T. F., Jamshidi, M., Titli, A. & Al-Gobaisi, D. 1999. Fuzzy Control of Brine Heater Process in Water Desalination Plants. *Intelligent Automation & Soft Computing,* 5**,** 111-128.

Olderøy, M. Ø., Xie, M., Strand, B. L., Flaten, E. M., Sikorski, P. & Andreassen, J.-P. 2009. Growth and nucleation of calcium carbonate vaterite crystals in presence of alginate. *Crystal Growth & Design,* 9**,** 5176-5183.

Omar, A. M. 1983. Simulation of MSF desalination plants. *Desalination,* 45**,** 65-76.

Pääkkönen, T. M., Riihimäki, M., Puhakka, E., Muurinen, E., Simonson, C. J. & Keiski, R. L. Crystallization fouling of CaCO 3—effect of bulk precipitation on mass deposition on the heat transfer surface. 2009 2009.

Pääkkönen, T. M., Riihimäki, M., Simonson, C. J., Muurinen, E. & Keiski, R. L. 2012. Crystallization fouling of CaCO 3–analysis of experimental thermal resistance and its uncertainty. *International Journal of Heat and Mass Transfer,* 55**,** 6927-6937.

Pääkkönen, T. M., Riihimäki, M., Simonson, C. J., Muurinen, E. & Keiski, R. L. 2015. Modeling CaCO 3 crystallization fouling on a heat exchanger surface–Definition of fouling layer properties and model parameters. *International Journal of Heat and Mass Transfer,* 83**,** 84-98.

Partridge, E. P. & White, A. H. 1929. The solubility of calcium sulfate from 0 to 200. *Journal of the American Chemical Society,* 51**,** 360-370.

Patel, S. & Finan, M. A. 1999. New antifoulants for deposit control in MSF and MED plants. *Desalination,* 124**,** 63-74.

Peyghambarzadeh, S. M., Vatani, A. & Jamialahmadi, M. 2012. Application of asymptotic model for the prediction of fouling rate of calcium sulfate under subcooled flow boiling. *Applied Thermal Engineering,* 39**,** 105-113.

Plummer, L. N. & Busenberg, E. 1982. The solubilities of calcite, aragonite and vaterite in CO 2-H 2 O solutions between 0 and 90 C, and an evaluation of the aqueous model for the system CaCO 3-CO 2-H 2 O. *Geochimica et Cosmochimica Acta,* 46**,** 1011-1040.

Porrazzo, R., Cipollina, A., Galluzzo, M. & Micale, G. 2013. A neural network-based optimizing control system for a seawater-desalination solar-powered membrane distillation unit. *Computers & Chemical Engineering,* 54**,** 79-96.

Prüss-Üstün, A. & Corvalán, C. 2006. Preventing disease through healthy environments. *Towards an estimate of the environmental burden of disease. Geneva: World Health Organization.*

Rautenbach, R. & Buchel, H. G. 1979. Modular program for design and simulation of desalination plants. *Desalination,* 31**,** 85.

Reddy, K. V. & Ghaffour, N. 2007. Overview of the cost of desalinated water and costing methodologies. *Desalination,* 205**,** 340-353.

Reddy, K. V., Husain, A., Woldai, A. & Al-Gopaisi, D. M. K. Dynamic modelling of the MSF desalination process. Proc. IDA and WRPC World Congress on Desalination and Water Treatment, 1995 1995a Abu Dhabi. 227-242.

Reddy, K. V., Husain, A., Woldai, A., Nabi, S. M. & Kurdali, A. Holdup and interstage orifice flow model for an MSF desalination plant. Proceedings of the IDA World Congress on Desalination and Water Sciences, 1995 1995b. 179-197.

Rimawi, M. A., Ettouney, H. M. & Aly, G. S. 1989. Transient model of multistage flash desalination. *Desalination,* 74**,** 327-338.

Rosso, M., Beltramini, A., Mazzotti, M. & Morbidelli, M. 1997. Modeling multistage flash desalination plants. *Desalination,* 108**,** 365-374.

Roudi-Fahimi, F., Creel, L. & De Souza, R.-M. 2002. Finding the balance: Population and water scarcity in the Middle East and North Africa. *Population Reference Bureau Policy Brief***,** 1-8.

Said, S., Mujtaba, I. M. & Emtir, M. Effect of Fouling Factors on the Optimisation of MSF Desalination Process for Fixed Water Demand Using gPROMS. Proceeding of the 9th International Conference on Computational Management, 18-20 April 2012 London, UK.

Said, S. A., Mujtaba, I. M. & Emtir, M. 2010. Modelling and simulation of the effect of non-condensable gases on heat transfer in the MSF desalination plants using gPROMS software. *Computer Aided Chemical Engineering,* 28**,** 25-30.

Said, S. A. R. 2013. *MSF process modelling, simulation and optimisation: impact of non-condensable gases and fouling factor on design and operation.* PhD thesis, University of Bradford.

Salem, O. M. 1992. The great manmade river project: A partial solution to Libya's future water supply. *International Journal of Water Resources Development,* 8**,** 270-278.

Segev, R., Hasson, D. & Semiat, R. 2012. Rigorous modeling of the kinetics of calcium carbonate deposit formation. *AIChE Journal,* 58**,** 1222-1229.

Seifert, A. & Genthner, K. 1991. A model for stagewise calculation of non-condensable gases in multi-stage evaporators. *Desalination,* 81**,** 333-347.

Semiat, R. & Galperin, Y. 2001. Effect of non-condensable gases on heat transfer in the tower MED seawater desalination plant. *Desalination,* 140**,** 27-46.

Shams El Din, A. M., El-Dahshan, M. E. & Mohammed, R. A. 2005. Scale formation in flash chambers of high-temperature MSF distillers. *Desalination,* 177**,** 241-258.

Shams El Din, A. M. & Mohammed, R. A. 1994. Brine and scale chemistry in MSF distillers. *Desalination,* 99**,** 73-111.

Sharif, A. O. Will Reverse Osmosis Replace Thermal Desalination in GCC Region. Qatar Foundation Annual Research Conference Proceedings, March 2016 Qater: HBKU Press. EEPP2725.

Sheikholeslami, R. 2000. Calcium sulfate fouling-precipitation or particulate: a proposed composite model. *Heat Transfer Engineering,* 21**,** 24-33.

Shivayyanamath, S. & Tewari, P. K. 2003. Simulation of start-up characteristics of multi-stage flash desalination plants. *Desalination,* 155**,** 277-286.

Singh, R. 2008. Sustainable fuel cell integrated membrane desalination systems. *Desalination,* 227**,** 14-33.

Skiborowski, M., Mhamdi, A., Kraemer, K. & Marquardt, W. 2012. Model-based structural optimization of seawater desalination plants. *Desalination,* 292**,** 30-44.

Slesarenko, V. N., Dobrzansky, V. G. & Slesarenko, V. V. 2003. The account of heat exchange features when modelling scale formation at distillation plants. *Desalination,* 152**,** 229-236.

Smith, B. R. & Sweett, F. 1971. The crystallization of calcium sulfate dihydrate. *Journal of Colloid and Interface Science,* 37**,** 612-618.

Soliman, M. A. 1981. A mathematical model for multistage flash desalination plants. *Journal of Engineering Sciences,* 7**,** 143-150.

Sousa, R., Lopes, G. P., Pinto, G. A., Almeida, P. I. F. & Giordano, R. C. 2004. GMC-fuzzy control of pH during enzymatic hydrolysis of cheese whey proteins. *Computers & Chemical Engineering,* 28**,** 1661-1672.

Sowgath, M. T. 2007. *Neural Network based hybrid modelling and MINLP based optimisation of MSF desalination process within gPROMS.* PhD Thesis, The University of Bradford.

Sowgath, M. T. & Mujtaba, I. M. 2015. Meeting the Fixed Water Demand of MSF Desalination using Scheduling in gPROMS. *Chemical Engineering Transactions,* 45**,** 6.

Sung-Tsuen, L. & Nancollas, G. H. 1973. The crystallization of magnesium hydroxide. *Desalination,* 12**,** 75-84.

Taborek, J., Aoki, T., Ritter, R. B., Palen, J. W. & Knudsen, J. G. 1972. Predictive methods for fouling behavior. *Chemical Engineering Progress, VOL 68, NO 7, P 69-78, JULY 1972. 17 Fig, 9 Ref.*

Tanvir, M. S. & Mujtaba, I. M. 2006a. Modelling and simulation of MSF desalination process using gPROMS and neural network based physical property correlation. *Computer Aided Chemical Engineering,* 21**,** 315.

Tanvir, M. S. & Mujtaba, I. M. 2006b. Neural network based correlations for estimating temperature elevation for seawater in MSF desalination process. *Desalination,* 195**,** 251-272.

Tanvir, M. S. & Mujtaba, I. M. Simulation of MSF Desalination Process for Fixed Water Demand using gPROMS and Neural Network based Temperature Elevation Correlation. International Water Conference, 12-14 June 2006c Porto, Portugal. Elsevier, 300-308.

Tanvir, M. S. & Mujtaba, I. M. 2007. Optimisation of MSF desalination process for fixed water demand using gPROMS. *Computer Aided Chemical Engineering,* 24**,** 763.

Tanvir, M. S. & Mujtaba, I. M. 2008. Optimisation of design and operation of MSF desalination process using MINLP technique in gPROMS. *Desalination,* 222**,** 419-430.

Tarifa, E. E., Humana, D., Franco, S. & Scenna, N. J. 2004. A new method to process algebraic equation systems used to model a MSF desalination plant. *Desalination,* 166**,** 113-121.

Tarifa, E. E. & Scenna, N. J. 2001. A dynamic simulator for MSF plants. *Desalination,* 138**,** 349-364.

Tayyebi, S. & Alishiri, M. 2014. The control of MSF desalination plants based on inverse model control by neural network. *Desalination,* 333**,** 92-100.

Thomas, P. J., Bhattacharyya, S., Patra, A. & Rao, G. P. 1998. Steady state and dynamic simulation of multi-stage flash desalination plants: A case study. *Computers & chemical engineering,* 22**,** 1515-1529.

Tian, L., Guo, J., Tang, Y. & Cao, L. 2005. A historical opportunity: economic competitiveness of seawater desalination project between nuclear and fossil fuel while the world oil price over $50 per boe—part A: MSF. *Desalination,* 183**,** 317-325.

Tiwari, G. N., Singh, H. N. & Tripathi, R. 2003. Present status of solar distillation. *Solar energy,* 75**,** 367-373.

UN 2015. World Population Prospects: The 2015 Revision, Key Findings and Advance Tables. NewYork.

UN, W. 2007. Coping with water scarcity: challenge of the twenty-first century. *Prepared for World Water Day*.

UNEP. 2001. Desalination by Distillation. Available: http://www.unep.or.jp/ietc/publications/techpublications/techpub-8c/distill.asp [Accessed Feb 1].

Vega, A., Diez, F. & Alvarez, J. M. 1995. Programmed cooling control of a batch crystallizer. *Computers & chemical engineering,* 19**,** 471-476.

Wangnick, K. How incorrectly determined physical and constructional properties in the seawater and brine regimes influence the design and size of an MSF desalination plant–stimulus for further thoughts. Proceedings of the IDA World congress on desalination and water science, 1995 1995. 201-218.

Wheida, E. & Verhoeven, R. 2007. The role of "virtual water" in the water resources management of the Libyan Jamahiriya. *Desalination,* 205**,** 312-316.

Wildebrand, C., Glade, H., Will, S., Essig, M., Rieger, J., Büchner, K.-H. & Brodt, G. 2007. Effects of process parameters and anti-scalants on scale formation in horizontal tube falling film evaporators. *Desalination,* 204**,** 448-463.

Winter, T., Pannell, D. J. & McCann, L. M. J. The Economics of Desalination and It's Potential Application to Australia. In 2002 Conference (46th), February 13-15, 2002, Canberra, 2002 Canberra. Australian Agricultural and Resource Economics Society.

Yokoyama, K., Ikenaga, Y., Inoue, S. & Yamamoto, T. 1977. Analysis of start-up characteristics of commercial MSF plant. *Desalination,* 22**,** 395-401.

Younos, T. & Tulou, K. E. 2005. Overview of desalination techniques. *Journal of Contemporary Water Research & Education,* 132**,** 3-10.

Zak, G. M. 2012. Thermal desalination: structural optimization and integration in clean power and water.

Zhang, F., Xiao, J. & Chen, X. D. 2015. Towards predictive modeling of crystallization fouling: A pseudo-dynamic approach. *Food and Bioproducts Processing,* 93**,** 188-196.

Zhao, X. & Chen, X. D. 2013. A critical review of basic crystallography to salt crystallization fouling in heat exchangers. *Heat Transfer Engineering,* 34**,** 719-732.

Zhong, S. & Mucci, A. 1989. Calcite and aragonite precipitation from seawater solutions of various salinities: Precipitation rates and overgrowth compositions. *Chemical Geology,* 78**,** 283-299.

List of publications

Journal Papers

1. Alsadaie, S. M. & Mujtaba, I. M. 2016. Generic Model Control (GMC) in Multistage Flash (MSF) Desalination. Journal of Process Control, 44, 92-105.

2. Alsadaie, S. M. & Mujtaba, I. M. 2017. Dynamic Modelling of Heat Exchanger Fouling in Multistage Flash (MSF) Desalination. 76, 27-42.

3. Alsadaie, S. M., Salem, I. & Mujtaba, I. M. 2017. Development and validation of dynamic model of multistage flash desalination: A case study of Ras Lanuf MSF plant. (Submitted is under preparation).

4. Alsadaie, S. M., Al-Obaidi, M. A., Tanvir, S. & Mujtaba, I. M. 2017. Super Structure Design of Hybrid RO/MSF desalination plants: Simulation and Optimization. (Submitted is under preparation).

Conference papers

1. Alsadaie, S. M. & Mujtaba, I. M. 2014. Modelling and Simulation of MSF Desalination Plant: The Effect of Venting System Design for Non-Condensable Gases. CHEMICAL ENGINEERING, 39.

2. Alsadaie, S., Zanil, M. F. b., Hussain, A. & Mujtaba, I. M. 2016. Development of Hybrid Fuzzy-GMC Control System for MSF Desalination Process. In Proceeding of the 26th European Symposium on Computer Aided Process Engineering - ESCAPE 26. Portoroz, Slovenia.

3. Alsadaie, S. & Mujtaba, I. M. 2017. Crystallization of Calcium Carbonate and Magnesium Hydroxide in Once-through Multistage Flash (MSF-OT). Accepted paper to be presented in the 27th European Symposium on Computer Aided Process Engineering - ESCAPE 27. Barcelona, Spain

4. Alsadaie, S., Tanvir, S. & Mujtaba, I. M. 2017. Plant wide fault Detection of MSF Process using Statistical Method. (Submitted is under preparation).

APPENDIX A

PHYSICAL PROPERTIES CORRELATIONS

Water Density

The density correlation for seawater is given by El-Dessouky and Ettouney (2002) and it is as following:

$$\rho = 10^3 \times (A_1 F_1 + A_2 F_2 + A_3 F_3 + A_4 F_4)$$

where

A_1 = 4.032219 G_1 + 0.115313 G_2 + 3.26 x10^{-4} G_3

A_2 = - 0.108199 G_1 + 1.571 x 10^{-3} G_2 - 4.23 x10^{-4} G_3

A_3 = - 0.012247 G_1 + 1.74 x10^{-3} G_2 – 9 x10^{-6} G_3

A_4 = 6.92 x10^{-4} G_1 - 8.7 x10^{-5} G_2 - 5.3 x10^{-5} G_3

F_1 = 0.5, F_2 = A, F_3 = 2 x A^2 - 1, F_4 = 4 xA^3 - 3 x A

A = ((2)(T) - 200)/160

G_1 = 0.5, G_2 = B, G_3 = 2 x B^2 – 1

B = ((2)(X)/1000-150)/150

In the above equations ρ is the seawater density in kg/m^3, X is the seawater salinity in ppm, and T is the seawater temperature in ^{o}C. This correlation is valid over the following ranges: 0 < X < 160000 ppm and 10 < T < 180 ^{o}C.

Vapour/ Gas Density

The density correlation for vapour and gas is given by El-Dessouky and Ettouney (2002) and it is as following:

$$\rho_V = \frac{P}{R \times T_V} \times \frac{1}{\left[\left(\frac{(1-Y)}{H_2O.MW}\right) + \left(\frac{Y}{CO_2.MW}\right)\right] \times 1000}$$

Where ρ_V is the vapour density in kg/m^3, P the vapour pressure in Pa, R the universal gas constant, T_V the vapour temperature in ^{o}C, Y the non-condensable gas mass fraction in vapour phase, $H_2O.MW$ the water molecular weight, $CO_2.MW$ the carbon dioxide molecular weight.

Heat Capacity of Seawater

The specific heat of seawater correlation at constant pressure is given by El-Dessouky and Ettouney (2002) as following

$$C_p = (A + BT + CT^2 + DT^3) \times 10^{-3}$$

The variables A, B, C and D are evaluated as a function of the water salinity

A = 4206.8 - 6.6197 X + 1.2288 x10⁻² X²

B = -1.1262 + 5.4178 x10⁻² X - 2.2719 x10⁻⁴ X²

C = 1.2026 x10⁻² - 5.3566 x10⁻⁴ X + 1.8906 x10⁻⁶ X²

D = 6.8777 x l0⁻⁷ + 1.517 x10⁻⁶ X - 4.4268 x10⁻⁹ X²

where *Cp* in kJ/kg °C, *T* in °C, and *X* is the water salinity in gm/kg. The above correlation is valid over salinity and temperature ranges of 20000 ≤ *X* ≤ 160000 ppm and 20 ≤ *T* ≤ 180 °C, respectively.

Latent Heat of Vapour

The correlation for latent heat of water evaporation is given by El-Dessouky and Ettouney (2002) as following

$$\lambda = 2501.897149 - 2.407064037\text{T} + 1.192217 \times 10^{-3}T^2 - 1.5863 \times 10^{-5}T^3$$

where *T* is the saturation temperature in °C and λ is the latent heat in kJ/kg**.**

Seawater Dynamic Viscosity

The correlation for the dynamic viscosity of seawater is given by El-Dessouky and Ettouney (2002) as following

$$\mu = (\mu_W)(\mu_R) \times 10^{-3}$$

where

$$Ln(\mu_W) = -3.79418 + 604.129/(139.18 + T)$$

$$\mu_R = 1 + A.X + B.X^2$$

A = 1.474 x10⁻³ + 1.5 x10⁻⁵ T - 3.927 x10⁻⁸ T²

B = 1.0734 x10⁻⁵ - 8.5 x10⁻⁸T + 2.23 x10⁻¹⁰ T²

In the above equations μ in kg/m s, T in °C, and X in gm/kg. The above correlation is valid over the following ranges $0 \leq X \leq 130$ gm/kg and $10 \leq T \leq 180$ °C.

Boiling Point Elevation (BPE)

The correlation for the boiling point elevation of seawater is given by El-Dessouky and Ettouney (2002) and it is accurate within salinity ranges $1 \leq X \leq 16\%$ and temperature $10 \leq T \leq 180$°C.

$$BPE = A.X + B.X^2 + C.X^3$$

With

$A = (8.325 \ x10^{-2} + 1.883 \ x10^{-4} \ T + 4.02 \ x10^{-6} \ T^2)$

$B = (-7.625 \ x10^{-4} + 9.02 \ x10^{-5} \ T - 5.2 \ x10^{-7} \ T^2)$

$C = (1.522 \ x10^{-4} - 3 \ x10^{-6} \ T - 3 \ x10^{-8} \ T^2)$

where T is the temperature in °C and X is the salt weight percentage.

Non-Equilibrium Allowance (NEA)

There are different correlations in the literature to estimate the Non-equilibrium allowance, however, the one used in this work is reported by Helal et al. (1986). The following equations give values for NEA as a function of the brine temperature, brine height, the brine flow rate per unit length of the chamber width, and the stage temperature drop:

$$NEA = 195 \times (h_b)^{1.1} \times (SL_{st} \times 10^{-3})^{0.5} / [(\Delta T_B)^{0.25} \times (T_V)^{2.5}]$$

where

$$SL_{st} = \frac{B_{in}}{W_{st}}$$

In the above equations, ΔT_B and ΔT_D are stage temperature drop for brine and distillate in °F respectively, h_b is height of the brine in (in), SL_{st} chamber load which is defined as brine flow rate per unit length of chamber width in *lb/ft.hr*.

Temperature Losses Through Demister *(ΔT_{Dem})*

The temperature drop due to demister can be obtained using equation reported by Helal et al. (1986) as following:

$$\Delta T_{Dem} = [EXP(1.885 - 0.02063 \times T_D)]/1.8$$

where ΔT_{Dem} is the demister temperature drop in ^{o}C, T_D is the distillate temperature in ^{o}F.

Saturated Pressure of Water Vapour Containing Gases

As reported by Al-Fulaij (2011), the saturation pressure can be estimated using Antoine's equation. This equation is used to evaluate the pressure drop between stages and through demister.

$$LOG\, P(1 - Ymole) = A - \left(\frac{B}{T_V + C}\right)$$

with

Y_{mole} is the NCGs mole fraction in the vapour phase

A is Antoine's equation coefficient = 23.2256

B is Antoine's equation coefficient = 3835.18

C is Antoine's equation coefficient = 45.343

Where *P* is in Pa and *T_V* is in K

Seawater Thermal Conductivity (KB)

The seawater thermal conductivity is given by El-Dessouky and Ettouney (2002):

$$Log_{10}(k_B) = Log_{10}(240 + 2 \times 10^{-4} \times X_B) +$$

$$0.434 \left(2.3 - \frac{343.5 + 3.7 \times 10^{-2} \times X_B}{T + 273.15}\right)\left(1 - \frac{T + 273.15}{647.3 \times 3 \times 10^{-2} \times X_B}\right)^{1/3}$$

To calculate the thermal conductivity of condensate (k_L), the same previous equation is used with zero salt concentration.

Overall Heat Transfer Coefficient (Uo)

There are several correlations available in literature to evaluate the overall heat transfer coefficient. The value of the overall heat transfer coefficient varies depending on the fouling resistance and inside and outside surface conditions of the tubes. Thus, to consider various resistances, the following equation that reported by El-Dessouky et al. (1999) is used in this work.

$$\frac{1}{U_o} = \left(\frac{d_o}{h_i d_i}\right) + \left(R_{f,i}\frac{d_o}{d_i}\right) + \left(\frac{d_o}{2k_t}\right)Ln\left(\frac{d_o}{d_i}\right) + R_{f,o} + \left(\frac{1}{h_o}\right)$$

Where d is the tube diameter in m, R_f, the fouling resistance in m²°C/kW, k_t the tube material thermal conductivity in kW/m°C, h the heat transfer coefficient in kW/m²°C, and the subscripts o and i refer to the outer and inner tube surface respectively.

The brine side heat transfer coefficient (internal) is calculated from the equation reported by El-Dessouky and Ettouney (2002).

$$h_i = \left(3293.5 + T_F(84.24 - 0.1714T_F) - X_R(8.471 + 0.1161X_R + 0.2716T_F)\right)$$
$$/\left(\left(\frac{d_i}{0.017272}\right)^{0.2}\right)((0.656B_{vel})^{0.8})\left(\frac{d_i}{d_o}\right)$$

Where T_F is the cooling brine temperature in °C, X_R is salt concentration in weight percent and B_{vel} is the cooling brine velocity in m/s.

For the vapour side (external), the heat transfer coefficient is calculated using the following equation as cited by El-Dessouky and Bingulac (1996)

$$h_o = 0.725 \times \left[\frac{gk_L^3\rho_L(\rho_L - \rho_v)\lambda}{\mu d_o(T_D - T_w)}\right]^{0.25} \times C_1 \times C_2$$

Where T_D and T_w are the condensate and the tube wall temperatures in °C, respectively and g is the gravitational acceleration in m/s². C_1 and C_2 represent the correction factors for the number of tubes in vertical direction and NCGs, respectively and are given by the following equations:

$$C_1 = 1.23795 + 0.353808N - 0.0017035N^2$$

$$C_2 = 1.0 - 34.313(Y) + 1226.8(Y)^2 - 14923(Y)^3$$

Where Y is mass fraction of the accumulated non-condensable gases in the stage and N the number of tube rows in the vertical direction and depends on the tube bundle geometry and the total number of tubes, N_t. In the case of rectangular pitch, the following equation can be used to determine N:

$$N = 0.564\sqrt{N_t}$$

$$N_t = \frac{4W_R}{\pi d_i^2 \rho_B v_b}$$

APPENDIX B

Azzour desalination plant data (*Source: Alasfour and Abdulrahim (2009)*)

Stage Design Specification

	Heat Recovery Section	Heat Rejection Section
No. of stages	21	3
Heat transfer area	77206 m^2	9444 m^2
No. of tubes/stage	1451	1588
Tube size		
Inner diameter		
Outer diameter	41.4 mm	31.8 mm
	43.8 mm	34.2 mm
Dimension		
Height	8.34 m	8.34 m
Width	17.66 m	17.66 m
Length	3.998 m	3.998 m

Brine Heater Design Specification

No. of stages	**1**
Fluids	
Shell side	Heating steam
Tube side	Recycle brine
Heat transfer area	3544 m^2
No. of tubes/stage	1367
Tube size	
Inner diameter	41.36 mm
Outer diameter	43.80 mm
Length	18991 mm

Appendix C

Degree of Freedom Analysis

In any model analysis, the degree of the freedom is the first and main step that has to be conducted before starting the simulation. It is defined as the difference between the number of the equations and the number of the variables.

Degree of freedom = number of variables – number of equations

$$\text{Degree of freedom} \begin{cases} \leq \text{-1} & \text{The problem is overspecified.} \\ = 0 & \text{The problem is well established.} \\ \geq 1 & \text{The problem is underspecified.} \end{cases}$$

Here, the analysis of the degree of the freedom is conducted in two steps. A single stage balance as lower level and overall plant balance as higher level. As mentioned in chapter three, the single stage is divided into four compartments with interacting material and thermal streams.
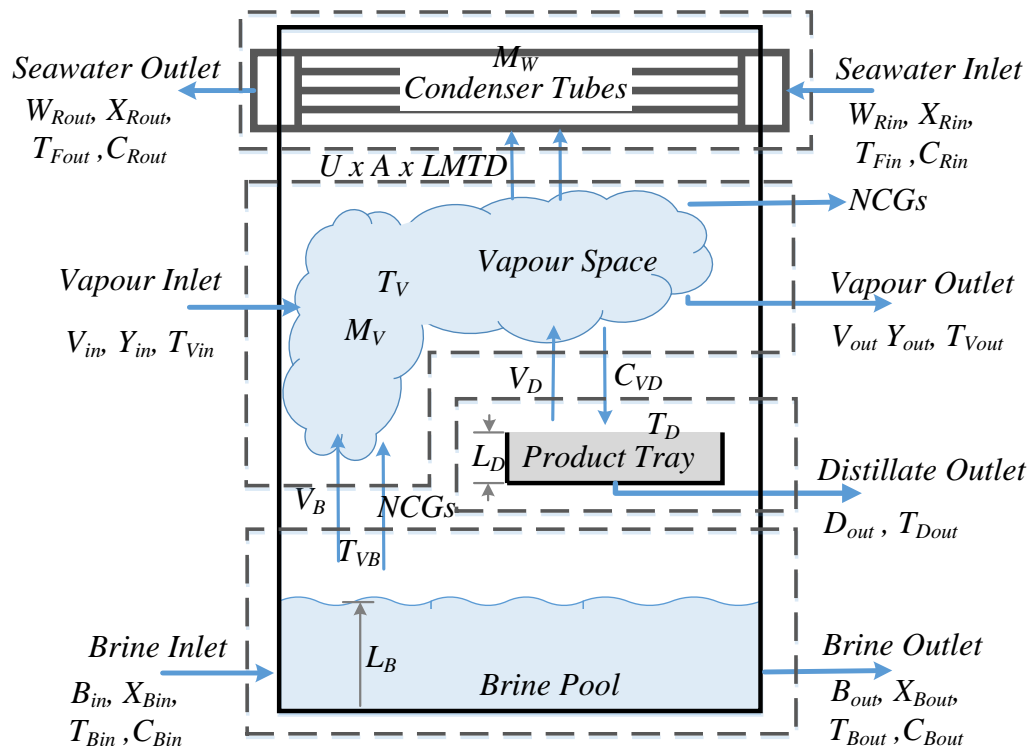
It is assumed that the conditions of streams flowing into the compartment are known by fixed values or calculated from the interacted streams while the exiting streams are unknown. Moreover, the masses are lumped at the exit conditions

thus, for example, T_V is the same as T_{Vout} and T_D is the same as T_{Dout}. Apart from physical properties and geometry dimensions, the number of variables for four different parts are shown in the above figure.

Lower level.

As it can be seen, the above figure indicates the followings:

- Eight unknown variables for the brine pool,
- Five unknown variables for the vapour space,
- Four unknown variables for the distillate tray, and
- Five unknown variables for the condenser tubes.

Higher level.

The last stage should be treated differently due to the makeup and recycle streams and hence these two variables should be included in the higher level. Though these two variables are fixed and thus they are excluded from our list, the salt (X_{rec}) and gas (C_{rec}) concentrations of the recycle brine have to be calculate. Finally, the rejected seawater, the performance ratio and the total capacity are also considered as the last three variables. Hence, the following are considered unknown variables involve in higher level:

- Two unknown variables for the recycle stream,
- Six unknown variables for the brine heater, and
- Three unknown variables for overall balance.

In total, there are 33 variables as listed in table 1.

Table 1: List of the possible variables

Lower Lever	
B_{out}, X_{Bout}, T_{Bout}, C_{Bout}, V_B, NCGs, T_{VB}, L_B, V_{out}, Y_{out}, T_{Vout}, C_{VD}, M_V, D_{out}, T_{Dout}, V_D, L_D, T_{Fout}, W_{Rout}, X_{Rout}, C_{Rout} and M_W	22
Higher Level	
X_{rec}, C_{rec}, W_{steam}, TBT, W_{HBout}, X_{HBout}, C_{BHout}, M_{BH}, W_{CW}, PR, and D_{total}	11
Total	**33**

Since the inlet variables are considered to be known and excluded from the variables list, hence 33 equations are required to solve for the above mentioned variables. Table 2 shows the list of the available variables.

Table 2: Dynamic model equations

$\rho_B \times A_P \times \frac{dL_B}{dt} = B_{in} - B_{out} - V_B - NCGs$	1
$\rho_B \times A_P \times L_B \times \frac{dX_{Bout}}{dt} = B_{in} \times X_{Bin} - X_{Bout}(B_{in} - V_B - NCGs)$	2
$\rho_B \times A_P \times L_B \frac{dC_{Bout}}{dt} = B_{in} \times C_{Bin} - C_{Bout}(B_{in} - V_B) - NCGs(1 - C_{Bout})$	3
$NCGs = B_{out}(C_{Bout} - C_{Be})\gamma$	4
$\rho_B \times A_P \times L_B \frac{dH_{Bout}}{dt} = B_{in}(H_{Bin} - H_{Bout}) - V_B(H_{VB} - H_{Bout})$ $-NCGs(H_{NCGs} - H_{Bout})$	5
$T_B = T_{VB} + BPE + NEA$	6
$B_{out} = C_d \times W_{st} \times H_g \times \sqrt{(2\rho_b(P_j - P_{j+1}) + g\rho_B(L_{B,j} - L_{B,j+1}))}$	7
$T_V = T_{VB} - \Delta T_{DEM}$	8
$\frac{dM_V}{dt} = V_B + V_{in} + V_D + NCGs - C_{VD} - V_{out}$	9
$M_V \frac{dY_{out}}{dt} = V_{in} \times Y_{in} + NCGs(1 - Y_{out}) - Y_{out}(V_{in} + V_B + V_D - C_{VD})$	10
$\frac{dM_V H_{Vout}}{dt} = (V_B \times H_{VB}) + (NCGs \times H_{NCGs}) + (V_{in} \times (1 - Y_{in}) \times H_{Vin})$ $+ (V_{in} \times Y_{in} \times H_{NCGsin}) + (V_D \times H_{Vout}) - (C_{VD} \times H_{VD}) -$ $(V_{out} \times Y_{out} \times H_{NCGsout}) - (V_{out} \times (1 - Y_{out}) \times H_{Vout} - (U \times A_S \times LMTD)$	11
$M_V = \rho_V \times V_v$	12
$V_{out} = k_V \times \sqrt{\rho_V(P_j - P_{j+1})}$	13
$\rho_D \times A_D \times \frac{dL_D}{dt} = C_{VD} - V_D - D_{out}$	14
$\rho_D \times A_D \times L_D \times \frac{dH_{Dout}}{dt} = C_{VD}(H_{VD} - H_{Dout}) - V_D(H_{Vout} - H_{Dout})$	15
$V_D \times H_{Vout} = C_{VD} \times (H_{VD} - H_{Dout})$	16

$D_{out} = C_C \times A_{pipe} \times \sqrt{(2\rho_D(P_j - P_{j+1}) + g\rho_D(L_{D,j} - L_{D,j+1}))}$	17
$M_W = \rho_w \times V_{tubes}$	18
$M_W \times \frac{dH_{Wout}}{dt} = W_{Rin}(H_{Win} - H_{Wout}) + (V_B \times H_{VB}) + (NCGs \times H_{NCGs}) + (V_{in} \times (1 - Y_{in}) \times H_{Vin}) + (V_{in} \times Y_{in} \times H_{NCGsin}) + (V_D \times H_{Vout}) - (C_{VD} \times H_{VD}) - (V_{out} \times Y_{out} \times H_{NCGsout}) - (V_{out} \times (1 - Y_{out}) \times H_{Vout}$	19
$W_{Rout} = W_{Rin}$	20
$X_{Rout} = X_{Rin}$	21
$C_{Rout} = C_{Rin}$	22
$Rec \times X_{Rec} + X_{Bout}(F_{last} - D_{Total}) = F_{Last} \times X_{Fout} + X_{Bout}(Rec - D_{Total})$	23
$Rec \times C_{Rec} + C_{Bout}(F_{last} - D_{Total}) = F_{Last} \times C_{Fout} + C_{Bout}(Rec - D_{Total})$	24
$M_{BH} \times \frac{dH_{BHout}}{dt} = W_{BHin}(H_{BHin} - H_{BHout}) + U_{BH} \times A_{BH} \times LMTD_{BH}$	25
$W_{STEAM} \times \lambda_{STEAM} = U_{BH} \times A_{BH} \times LMTD_{BH}$	26
$W_{BHout} = W_{BHin}$	27
$X_{BHout} = X_{BHin}$	28
$C_{BHout} = C_{BHin}$	29
$M_{BH} = \rho_B \times V_{BH}$	30
$W_{CW} = W_{Rout} - F_{last}$	31
$Performance\ ratio\ (PR) = \frac{D_{total}}{W_{steam}}$	32
$D_{total} = \sum_{j=1}^{N} D_{out(j)}$	**33**

Degree of freedom = 33 - 33 = 0   *The problem is well established*

The above equation is only for a plant with single stage. Thus, for whole plant with N number of stages, the total number of equation and variables are:

Number of equations = 22N+11

Number of variables = 22N+11

It is important to mention that the inlet conditions of the intake seawater are excluded and are not considered as mentioned earlier.

In table 2, others variables appears in the equations and they have to be calculated or given a value. These variables present the physical properties of the streams and geometric dimensions of the plant. These are listed in Table 3.

Table 3: Physical and geometric variables

Variables	
ρ_B, A_P, γ, C_{Be}, H_{Bin}, H_{Bout}, H_{VB}, H_{NCGs}, BPE, NEA, T_{DEM}, H_{Vin}, H_{Vout}, H_{VD}, $H_{NCGsout}$, LMTD, A_S, U, ρ_V, V_v, ρ_D, A_D, C_d, C_C, K_v, W_{st}, H_g, P, g, A_{pipe}, H_{Dout}, H_{Win}, H_{Wout}, ρ_W, V_{tube}, H_{BHin}, H_{BHout}, $\lambda steam$, U_{BH}, A_{BH}, $LMTD_{BH}$ and V_{BH}.	42
Differential variables	
$\frac{dL_B}{dt}$, $\frac{dX_{Bout}}{dt}$, $\frac{dC_{Bout}}{dt}$, $\frac{dH_{Bout}}{dt}$, $\frac{dy_{out}}{dt}$, $\frac{dH_{Vout}}{dt}$, $\frac{dM_V}{dt}$, $\frac{dL_D}{dt}$, $\frac{dH_{Dout}}{dt}$, $\frac{dH_{Wout}}{dt}$, $\frac{dH_{BHout}}{dt}$	11
and independent variable t.	1
Total	**54**

To solve for the above 54 variables, the user has to give them values or define equations to solve them. Table 4 presents the available equations to solve for the Table 3 variables:

Table 4: physical properties equations.

$\rho = 10^3 \times (A_1F_1 + A_2F_2 + A_3F_3 + A_4F_4)$	3
$\rho_V = \frac{P}{R \times T_V} \times \frac{1}{\left[\left(\frac{(1-Y_{out})}{H_2O.MW}\right) + \left(\frac{Y_{out}}{CO_2.MW}\right)\right] \times 1000}$	1
$H_V = 2501.689845 + 1.806916 \times T + 5.0877 \times 10^{-4} \times T^2 - 1.122 \times 10^{-5} \times T^3$	3
$H_D = -0.033635 + 4.207557 \times T - 6.2 \times 10^{-4} \times T^2 + 4.45937 \times 10^{-6} \times T^3$	2
$H_{NCGs} = Cp_{Gas} \times (T - T_{ref})$	2

$H = Cp \times (T - T_{ref})$ *for seawater or brine*	6
$\lambda_{steam} = 2501.897149 - 2.407064037T + 1.192217 \times 10^{-3}T^2 - 1.5863 \times 10^{-5}T^3$	1
$BPE = A \times X_{Bout} + B \times X_{Bout}^2 + C \times X_{Bout}^3$	1
$NEA = 195 \times (L_B)^{1.1} \times (SL_{st} \times 10^{-3})^{0.5}/[(\Delta T_B)^{0.25} \times (T_V)^{2.5}]$	1
$\Delta T_{Dem} = [EXP(1.885 - 0.02063 \times T_D)]/1.8$	1
$LOG\ P(1 - Y_{out}) = A - \left(\frac{B}{T_V + C}\right)$	1
$A_{pipe} = $ *Cross section area of th distillate pipe discharge*	1
$A = W_{st} \times Ls$	2
surface area $A = N_t \times \pi \times d_o \times L_t$	2
$V = N_t \times \frac{\pi \times d^2}{4} \times L_t$ *for* V_{tubes} *and* V_{BH}	2
$V_v = A_p \times (h_s - L_B - L_D) - V_{tubes}$	1
$LMTD = \frac{\Delta T_1 - \Delta T_2)}{\ln\left[\frac{\Delta T_1}{\Delta T_2}\right]}$	2
$\frac{1}{U_o} = \left(\frac{d_o}{h_i d_i}\right) + \left(R_{f,i}\frac{d_o}{d_i}\right) + \left(\frac{d_o}{2k_t}\right)Ln\left(\frac{d_o}{d_i}\right) + R_{f,o} + \left(\frac{1}{h_o}\right)$	2
$C_e \times He = Y_{out} \times P$	1
Total	35

Degree of freedom $= 54 - 35 = 19$ *The problem is underspecified*

The problem is underspecified and thus 19 more variables have to be specified.

At time (t) = 0, the 11 differential variables are assigned. Thus, out of 19, there are only 7 variables to be specified. These are (γ, C_d, C_c, K_v, W_{st}, H_g, g).

Degree of freedom $= 54 - 54 = 0$ *The problem is well established*

However, other more variables are appeared in Table 4 and thus they have to be specified or defined by equations.